

# Best-Effort Communication Improves Performance and Scales Robustly on Conventional Hardware

Matthew Andres Moreno

*Computer Science and Engineering*

*Michigan State University*

mmore500@msu.edu

<https://orcid.org/0000-0003-4726-4479>

Charles Ofria

*Computer Science and Engineering*

*Michigan State University*

<https://orcid.org/0000-0003-2924-1732>

**Abstract**—Exponential advances in HPC hardware enables profound scientific and industrial innovation, but performance overhead from synchronization and error recovery has become increasingly challenging. “Best-effort” approaches that improve efficiency by relaxing guarantees of correctness and determinism have emerged as a promising remedy. Here, we test the performance and scalability of fully-asynchronous, best-effort communication on existing, commercially-available HPC hardware.

A first set of experiments tested whether best-effort communication strategies can benefit performance compared to the traditional perfect communication model. At high CPU counts, best-effort communication improved both the number of computational steps executed per unit time and the solution quality achieved within a fixed-duration run window. Computation-heavy benchmark workloads yielded the strongest scaling efficiency, achieving at 64 processes 92% the update-rate of single-process execution. We observed a relative speedup of up to  $7.8\times$  under communication-heavy workloads.

Under the best-effort model, characterizing the distribution of quality of service across processing components and over time is critical to understanding the actual computation being performed. Additionally, a complete picture of scalability under the best-effort model requires analysis of how such quality of service fares at scale. To answer these questions, we designed and measured a suite of quality of service metrics: simulation update period, message latency, message delivery failure rate, and message delivery coagulation. Under a lower communication-intensity benchmark parameterization, we found that median values for all quality of service metrics were stable when scaling from 64 to 256 process. Under maximal communication intensity, we found only minor — and, in most cases, nil — degradation in median quality of service.

In an additional set of experiments, we tested the effect of an apparently faulty compute node on performance and quality of service. Despite extreme quality of service degradation among that node and its clique, median performance and quality of service remained stable.

We used the Conduit C++ library for best-effort communication to perform reported experiments. Development of this library stemmed from a practical need for an general-purpose, prepackaged framework for best-effort communication. We hope that free availability of this library, which includes built-in tools to measure quality of service metrics, can facilitate broader incorporation of best-effort communication into HPC applications.

rapidly and enable profound scientific and industrial innovations (Gagliardi et al., 2019). These advances in hardware capacity and economy afford great opportunity, but also pose a serious challenge: developing approaches to effectively harness it. As HPC systems scale, it becomes increasingly difficult to write software that makes efficient use of available hardware and also provides reproducible results (or even near-perfectly reproducible results — i.e., up to effects from floating point non-transitivity) consistent with models of computation as being performed a reliable digital machine (Heroux, 2014).

The bulk synchronous parallel (BSP) model, which is prevalent among HPC applications (Dongarra et al., 2014), illustrates the challenge. This model segments fragments of computation into sequential global supersteps, with fragments at superstep  $i$  depending only on data from strictly preceding fragments  $< i$ , often just  $i - 1$ . Computational fragments are assigned across a pool of available processing components. The BSP model assumes perfectly reliable messaging: all dispatched messages between computational fragments are faithfully delivered. In practice, realizing this assumption introduces overhead costs: secondary acknowledgment messages to confirm delivery and mechanisms to dispatch potential resends as the need arises. Global synchronization occurs between supersteps, with computational fragments held until their preceding superstep has completed (Valiant, 1990). This ensures that computational fragments will have at hand every single expected input, including those required from fragments located on other processing elements, before proceeding. So, supersteps only turn over once the entire pool of processing components have completed their work for that superstep. Put another way, all processing components stall until the most laggardly component catches up. In a game of double dutch with several jumpers, this would be like slowing the tempo to whoever is most slow-footed each particular turn of the rope.

Heterogeneous computational fragments, with some easy to process and others much slower, would result in poor efficiency under a naive approach where each processing element handled just one fragment. Some processing elements with easy tasks would finish early then idle while more difficult tasks carry on. To counteract such load imbalances, programmers can allow for “parallel slack” by ensuring computational fragments greatly outnumber processing elements or

## I. INTRODUCTION

The parallel and distributed processing capacity of high-performance computing (HPC) clusters continues to grow

even performing dynamic load balancing at runtime (Valiant, 1990).

Unfortunately, hardware factors on the underlying processing elements ensure that inherent global superstep jitter will persist: memory access time varies due to cache effects, message delivery time varies due to network conditions, extra processing due to error detection and recovery, delays due to unfavorable process scheduling by the operating system, etc. (Dongarra et al., 2014). Power management concerns on future machines will likely introduce even more variability (Gropp and Snir, 2013). Worse yet, as we work with more and more processes, the expected magnitude of the worst-sampled jitter grows and grows — and in lockstep with it, our expected superstep duration. In the double dutch analogy, with enough jumpers, at almost every turn of the rope someone will need to stop and tie their shoe. The global synchronization operations underpinning the BSP model further hinder its scalability. Irrespective of time to complete computational fragments within a superstep, the cost of performing a global synchronization operation increases with processor count (Dongarra et al., 2014).

Efforts to recover scalability by relaxing superstep synchronization fall under two banners. The first approach, termed “Relaxed Bulk-Synchronous Programming” (rBSP), hides latency by performing collective operations asynchronously, essentially allowing useful computation to be performed at the same time as synchronization primitives for a single superstep percolate through the collective (Heroux, 2014). So, the time cost required to perform that synchronization can be discounted, up to the time taken up by computational work at one superstep. Likewise, individual processes experiencing heavier workloads or performance degradation due to hardware factors can fall behind by up to a single superstep without slowing the entire collective. However, this approach cannot mask synchronization costs or cumulative performance degradation exceeding a single superstep’s duration. The second approach, termed relaxed barrier synchronization, forgoes global synchronization entirely (Kim et al., 1998). Instead, computational fragments at superstep  $i$  only wait on expected inputs from the subset of superstep  $i - 1$  fragments that they directly interact with. Imagine a double-dutch routine where each jumper exchanges patty cakes with both neighboring jumpers at every turn of the rope. Relaxed barrier synchronization would dispense entirely with the rope. Instead, players would be free to proceed to their next round of patty cakes as soon as they had successfully patty-caked both neighbors. With  $n$  players, player 0 could conceivably advance  $n$  rounds ahead of player  $n - 1$  (each player would be one round ahead of their right neighbor). Assuming fragment interactions form a graph structure that persists across supersteps, in the general case before causing the entire collective to slow an individual fragment can fall behind at most a number of supersteps equal to the graph diameter (Gamell et al., 2015). Even though this approach can shield the collective from most one-off performance degradations of a single fragment (especially in large-diameter cases), persistently laggard hardware

or extreme one-off degradations will ultimately still hobble efficiency. Dynamic task scheduling and migration aim to address this shortcoming, redistributing work in order to “catch up” delinquent fragments (Acun et al., 2014). With our double-dutch analogy, we could think of this something like a team coach temporarily benching a jumper who skinned their knee and instructing the other jumpers to pick up their roles in the routine.

In addition to concerns over efficiency, resiliency poses another inexorable problem to massive HPC systems. In small scales, it can suffice to assume that failures occur negligibly, with any that do transpire likely to cause an (acceptably rare) global interruption or failure. At large scales, however, software crashes and hardware failures become the rule rather than the exception (Dongarra et al., 2014) — running a simulation to completion could even require so many retries as to be practically infeasible. A typical contemporary approach to improve resiliency is checkpointing: the system periodically records global state then, when a failure arises, progress is rolled back to the most recent global known-good state and runtime restarts (Hursey et al., 2007). Global checkpoint-based recovery is expensive, especially at scale due to overhead associated with regularly recording global state, losing progress since the most recent checkpoint, and actually performing a global teardown and restart procedure. In fact, at large enough scales global recovery durations could conceivably exceed mean time between failures, making any forward simulation progress all but impossible (Dongarra et al., 2014). The local failure, local recovery (LFLR) paradigm eschews global recovery by maintaining persistent state on a process-wise basis and providing a recovery function to initialize a step-in replacement process (Heroux, 2014; Teranishi and Heroux, 2014). In practice, such an approach can require keeping running logs of all messaging traffic in order to replay them for the benefit of any potential step-in replacement (Chakravorty and Kale, 2004). Returning once more to the double dutch analogy, LFLR would transpire as something like a handful teammates pulling a stricken teammate aside to catch them up after an amnesia attack (rather than starting the entire team’s routine back at the top of the current track). The intervening jumpers would have to remind the stricken teammate of a previously recorded position then discreetly re-feign some of their moves that the stricken teammate had cued off of between that recorded position and the amnesia episode.

The possibility of multiple simultaneous failure (perhaps, for example, of dozens of processes resident on a single node) poses an even more difficult, although not insurmountable, challenge for LFLR that would likely necessitate even greater overhead. One approach involves pairing up with a remote “buddy” process. The “buddy” hangs to the focal process’ snapshots and is carbon-copied on all of that process’ messages in order to ensure an independently survivable log. Unfortunately, this could potentially require forwarding all messaging traffic between simulation elements coresident on the focal process to its buddy, dragging inter-node communication into some otherwise trivial simulation operations

(Chakravorty and Kalé, 2007). Efforts to ensure resiliency beyond single-node failures currently appear unnecessary (Ni, 2016, p. 12). Even though LFLR saves the cost of global spin-down and spin-up, all processes will potentially have to wait for work lost since the last checkpoint to be recomputed, although in some cases this could be helped along by tapping idle hardware to take over delinquent work from the failed process and help catch it up (Dongarra et al., 2014).

Still more insidious to the reliable digital machine model, though, are soft errors — events where corruption of data in memory occurs, usually do to environmental interference (i.e., “cosmic rays”) (Karnik and Hazucha, 2004). Further miniaturization and voltage reduction, which are assumed as a likely vehicle for continuing advances in hardware efficiency and performance, could conceivably worsen susceptibility to such errors (Dongarra et al., 2014; Kajmakovic et al., 2020). What makes soft errors so dangerous is their potential undetectability. Unlike typical hardware or software failures, which result in an explicit, observable outcome (i.e., an error code, an exception, or even just a crash), soft errors can transpire silently and lead to incorrect computational results without leaving anyone the wiser. Luckily, soft errors occur rarely enough to be largely neglected in most single-processor applications (except the most safety-critical settings); however, at scale soft errors occur at a non-trivial rate (Scoles, 2018; Sridharan et al., 2015). Redundancy (be it duplicated hardware components or error correction codes) can reduce the rate of uncorrected (or at least undetected) soft errors, although at a non-trivial cost (Sridharan et al., 2015; Vankeirsbilck et al., 2015). In some application domains with symmetries or conservation principles, the rate of soft errors (or, at least, silent soft errors) could be also reduced through so-called “skeptical” assertions at runtime (Dongarra et al., 2014), although this too comes at a cost.

Even if soft errors can be effectively eradicated — or at least suppressed to a point of inconsequentiality — the nondeterministic mechanics of fault recovery and dynamic task scheduling could conceivably make guaranteeing bitwise reproducibility at exascale effectively impossible, or at least an unreasonable engineering choice (Dongarra et al., 2014). However, the assumption of the reliable digital machine model remains near-universal within parallel and distributed algorithm design (Chakradhar and Raghunathan, 2010). Be it just costly or simply a practical impossibility, the worsening burden of synchronization, fault recovery, and error correction begs the question of whether it is viable to maintain, or even to strive to maintain, the reliable digital machine model at scale. Indeed, software and hardware that relaxes guarantees of correctness and determinism — a so-called “best-effort model” — have been shown to improve speed (Chakrapani et al., 2008), energy efficiency (Bocquet et al., 2018; Chakrapani et al., 2008), and scalability (Meng et al., 2009). Discussion around “approximate computing” overlaps significantly with “best-effort computing,” although focusing more heavily on using algorithm design to shirk non-essential computation (i.e., reducing floating point precision, inexact memoization,

etc.) (Mittal, 2016). As technology advances, computing is becoming more distributed and we are colliding with physical limits for speed and reliability. Massively distributed systems are becoming inevitable, and indeed if we are to truly achieve “indefinite scalability” (Ackley and Cannon, 2011) we must shift from guaranteed accuracy to best-effort methods that operate asynchronously and degrade gracefully under hardware failure.

The suitability of the best-effort model varies from application to application. Some domains are clear cut in favor of the reliable digital machine model — for example, due to regulatory issues (Dongarra et al., 2014). However, a subset of HPC applications can tolerate — or even harness — occasionally flawed or even fundamentally nondeterministic computation (Chakradhar and Raghunathan, 2010). Various approximation algorithms or heuristics fall into this category, with notable work being done on best-effort stochastic gradient descent for artificial neural network applications (Dean et al., 2012; Niu et al., 2011; Noel and Osindero, 2014; Rhodes et al., 2020; Zhao et al., 2019). Best-effort, real-time computing approaches have also been used in some artificial life models (Ray, 1995). Likewise, algorithms relying on pseudo-stochastic methods that tend to exploit noise (rather than destabilize due to it) also make good candidates (Chakradhar and Raghunathan, 2010; Chakrapani et al., 2008). Real-time control systems that cannot afford to pause or retry, by necessity, fall into the best-effort category (Rahmati et al., 2011; Rhodes et al., 2020).

This work distills best-effort communication from the larger issue of best-effort computing, paying it special attention and generally preterming the larger issue. Specifically, we investigate the implications of relaxing synchronization and message delivery requirements. Under this model, the runtime strives to minimize message latency and loss, but guarantees elimination of neither. Instead, processes continue their compute work unimpeded and incorporate communication from collaborating processes as it happens to become available. We still assume that messages, if and when they are delivered, retain contentual integrity.

We see best-effort communication as a particularly fruitful target for investigation. Firstly, synchronization constitutes the root cause of many contemporary scaling bottlenecks, well below the mark of thousands or millions of cores where runtime failures and soft errors become critical considerations. Secondly, future HPC hardware is expected to provide more heterogeneous, more variable (i.e., due to power management), and generally lower (relative to compute) communication bandwidth (Acun et al., 2014; Gropp and Snir, 2013); a best-effort approach suits these challenges. A best-effort communication model presents the possibility of runtime adaptation to effectively utilize available resources given the particular ratio of compute and communication capability at any one moment in any one rack.

Complex biological organisms exhibit characteristic best-effort properties: trillions of cells interact asynchronously while overcoming all but the most extreme failures in a noisy world. As such, bio-inspired algorithms present strong

potential to benefit from best-effort communication strategies. For example, evolutionary algorithms commonly use guided stochastic methods (i.e., selection and mutation operators) resulting in a search process that does not guarantee optimality, but typically produces a diverse range of high-quality results. Indeed, island model genetic algorithms are easy to parallelize and have been shown to perform well with asynchronous migration (Izzo et al., 2009). Likewise, artificial life simulations commonly rely on a bottom-up approach and seek to model life-as-it-could-be evolving in a noisy environment akin to the natural world, yet distinct from it (Bonabeau and Theraulaz, 1994). Although perfect reproducibility and observability have uniquely enabled digital evolution experiments to ask and answer otherwise intractable questions (Bundy et al., 2021; Covert et al., 2013; Dolson et al., 2020; Dolson and Ofria, 2017; Fortuna et al., 2019; Goldsby et al., 2014; Grabowski et al., 2013; Lenski et al., 2003; Pontes et al., 2020; Zaman et al., 2011), the reliable digital machine model is not strictly necessary for all such work. Issues of distributed and parallel computing are of special interest within the the artificial life subdomain of open-ended evolution (OEE) (Ackley and Small, 2014), which studies long-term dynamics of evolutionary systems in order to understand factors that affect potential to generate ongoing novelty (Taylor et al., 2016). Recent evidence suggests that the generative potential of at least some model systems are — at least in part — meaningfully constrained by available compute resources (Channon, 2019).

Much exciting work on best-effort computing has incorporated bespoke experimental hardware (Ackley and Williams, 2011; Chakrapani et al., 2008; Chippa et al., 2014; Cho et al., 2012; Rhodes et al., 2020). However, here, we focus on exploring best-effort communication among parallel and distributed elements within existing, commercially-available hardware. Existing software libraries, though, do not explicitly expose a convenient best-effort communication interface for such work. As such, best-effort approaches remain rare in production software and efforts to study best-effort communication must make use of a combination of limited existing support and the development of new software tools.

The Message Passing Interface (MPI) standard (Gropp et al., 1996) represents the mainstay for high-performance computing applications. This standard exposes communication primitives directly to the end user. MPI’s nonblocking communication primitives, in particular, are sufficient to program distributed computations with relaxed synchronization requirements. Although its explicit, the imperative nature of the MPI protocols enables precise control over execution; unfortunately it also poses significant expense in terms of programmability. This cost manifests in terms of reduced programmer productivity and software quality, while increasing domain knowledge requirements and the effort required to tune for performance due to program brittleness (Gu and Becchi, 2019; Tang et al., 2014).

In response to programmability concerns, many frameworks have arisen to offer useful parallel and distributed programming abstractions. Task-based frameworks such as Charm++

(Kale and Krishnan, 1993), Legion (Bauer et al., 2012), Cilk (Blumofe et al., 1996), and Threading Building Blocks (TBB) (Reinders, 2007) describe the dependency relationships among computational tasks and associated data and relies on an associated runtime to automatically schedule and manage execution. These frameworks assume a deterministic relationship between tasks. In a similar vein, programming languages and extensions like Unified Parallel C (UPC) (El-Ghazawi and Smith, 2006) and Chapel (Chamberlain et al., 2007) rely on programmers to direct execution, but equips them with powerful abstractions, such as global shared memory. However, Chapel’s memory model explicitly forbids data races and UPC ultimately relies on a barrier model for data transfer.

To bridge these shortcomings, we employ a new software framework, the Conduit C++ Library for Best-Effort High Performance Computing (Moreno et al., 2021). The Conduit library provides tools to perform best-effort communication in a flexible, intuitive interface and uniform inter-operation of serial, parallel, and distributed modalities. Although Conduit currently implements distributed functionality via MPI intrinsics, in future work we will explore lower-level protocols like InfiniBand Unreliable Datagrams (Kashyap, 2006; Koop et al., 2007).

Here, we present a set of on-hardware experiments to empirically characterize Conduit’s best-effort communication model. In order to survey across workload profiles, we tested performance under both a communication-intensive graph coloring solver and a compute-intensive artificial life simulation.

First, we determine whether best-effort communication strategies can benefit performance compared to the traditional perfect communication model. We considered two measures of performance: computational steps executed per unit time and solution quality achieved within a fixed-duration run window.

We compare the best-effort and perfect-computation strategies across processor counts, expecting to see the marginal benefit from best-effort communication increase at higher processor counts. We focus on weak scaling, growing overall problem size proportional to processor count. Put another way, we hold problem size per processor constant.<sup>1</sup> This approach prevents interference from shifts in processes’ workload profiles in observation of the effects of scaling up processor count.

To survey across hardware configurations, we tested scaling CPU count via threading on a single node and scaling CPU count via multiprocessing with each process assigned to a distinct node. In addition to a fully best-effort mode and a perfect communication mode, we also tested two intermediate, partially synchronized modes: one where the processor pool completed a global barrier (i.e., they aligned at a synchronization point) at predetermined, rigidly scheduled timepoints and another where global barriers occurred on a rolling basis spaced out by fixed-length delays from the end of the last

<sup>1</sup>As opposed to strong scaling, where the problem size is held fixed while processor count increases.



synchronization.<sup>2</sup>

Second, we sought to more closely characterize variability in message dispatch, transmission, and delivery under the best-effort model. Unlike perfect communication, real-time volatility affects the outcome of computation under the best-effort model. Because real-time processing speed degradations and message latency or loss alters inputs to simulation elements, characterizing the distribution of these phenomena across processing components and over time is critical to understanding the actual computation being performed. For example, consistently faster execution or lower messaging latency for some subset of processing elements could violate uniformity or symmetry assumptions within a simulation. It is even possible to imagine reciprocal interactions between real-time best-effort dynamics and simulation state. In the case of a positive feedback loop, the magnitude of effects might become extreme. For example, in artificial life scenarios, agents may evolve strategies that selectively increase messaging traffic so as to encumber neighboring processing elements or even cause important messages to be dropped.

We monitor five aspects of real-time behavior, which we refer to as quality of service metrics (Karakus and Durreisi, 2017),

- wall-time simulation update rate (“simstep period”),
- simulation-time message latency,
- wall-time message latency,
- steadiness of message inflow (“delivery clumpiness”), and
- delivery failure rate.

In an initial set of experiments, we use the graph coloring problem to test this suite of quality of service metrics across runtime conditions expected to strongly influence them. We compare

- increasing compute workload per simulation update step,
- within-node versus between-node process placement, and
- multithreading versus multiprocessing.

We perform these experiments using a graph coloring solver configured to maximize communication relative to computation (i.e., just one simulation element per CPU) in order to maximize sensitivity of quality of service to the runtime manipulations.

Finally, we extend our understanding of performance scaling from the preceding experiments by analyzing how each quality of service metric fares as problem size and processor count grow together, a “weak scaling” experiment. This analysis would detect a scenario where raw performance remains stable under weak scaling, but quality of service (and, therefore, potentially quality of computation) degrades.

## II. METHODS

We performed two benchmarks to compare the performance of Conduit’s best-effort approach to a traditional synchronous model. We tested our benchmarks across both a multithread,

shared-memory context and a distributed, multinode context. In each hardware context, we assessed performance on two algorithmic contexts: a communication-intensive distributed graph coloring problem (Section II-B) and a compute-intensive digital evolution simulation (Section II-A). The latter benchmark — presented in Section II-A — grew out of the original work developing the Conduit library to support large-scale experimental systems to study open-ended evolution. The former benchmark — presented in Section II-B — complements the first by providing a clear definition of solution quality. Metrics to define solution quality in the open-ended digital evolution context remain a topic of active research.

### A. Digital Evolution Benchmark

The digital evolution benchmark runs the DISHTINY (Distributed Hierarchical Transitions in Individuality) artificial life framework. This system is designed to study major transitions in evolution, events where lower-level organisms unite to form a self-replicating entity. The evolution of multicellularity and eusociality exemplify such transitions. Previous work with DISHTINY has explored methods for selecting traits characteristic of multicellularity such as reproductive division of labor, resource sharing within kin groups, resource investment in offspring, and adaptive apoptosis (Moreno and Ofria, 2019).

DISHTINY simulates a fixed-size toroidal grid populated by digital cells. Cells can sense attributes of their immediate neighbors, can communicate with those neighbors through arbitrary message passing, and can interact with neighboring cells cooperatively through resource sharing or competitively through antagonistic competition to spawn daughter cells into limited space. This cell behavior is controlled by SignalGP event-driven linear genetic programs (Lalejini and Ofria, 2018). Full details of the DISHTINY simulation are available in (Moreno and Ofria, 2022).

We use Conduit-based messaging channels to manage all interactions between neighboring cells. Conduit models messaging channels as independent objects. However, support is provided for behind-the-scenes consolidation of communication along these channels between pairs of processes. Pooling joins together exactly one message per messaging channel to create a fixed-size consolidated message. Aggregation joins together arbitrarily many messages per channel to create a variable-size consolidated message.

During a computational update, each cell advances its internal state and pushes information about its current state to neighbor cells. Several independent messaging layers handle disparate aspects of cell-cell interaction, including

- Cell spawn messages, which contain variable-length genomes (seeded at 100 12-byte instructions with a hard cap of 1000 instructions). These are handled every 16 updates and use Conduit’s built-in aggregation support for inter-process transfer.
- Resource transfer messages, consisting of a 4-byte float value. These are handled every update and use Conduit’s built-in pooling support for inter-process transfer.

<sup>2</sup>Our motivation for these intermediate synchronization modes was interest in the effect of clearing any potentially-unbounded accumulation of message backlogs on laggard processes.

- Cell-cell communication messages, consisting of arbitrarily many 20-byte packets dispatched by genetic program execution. These are handled every 16 updates and use Conduit’s built-in aggregation support for inter-process transfer.
- Environmental state messages, consisting of a 216-byte struct of data. These are handled every 8 updates and use conduit’s built-in pooling support for inter-process transfer.
- Multicellular kin-group size detection messages, consisting of a 16-byte bitstring. These are handled every update and use Conduit’s built-in pooling support for inter-process transfer.

Implementing all cell-cell interaction via Conduit-based messaging channels allows the simulation to be parallelized down to the granularity, potentially, of individual cells. These messaging channels allow cells to communicate using the same interface whether they are placed within the same thread, across different threads, or across different processes. However, in practice, for this benchmarking we assign 3600 cells to each thread or process. Because all cell-cell interactions occur via Conduit-based messaging channels, logically-neighboring cells can interact fully whether or not they are located on the same thread or process (albeit with potential irregularities due to best-effort limitations). An alternate approach to evolving large populations might be an island model, where Conduit-based messaging channels would be used solely to exchange genomes between otherwise independent populations (Bennett III et al., 1999). However, we chose to instead parallelize DISHTINY as a unified spatial realm in order to enable parent-offspring interaction and leave the door open for future work with multicells that exceed the scope of an individual thread or process.

### B. Graph Coloring Benchmark

The graph coloring benchmark employs a graph coloring algorithm designed for distributed WLAN channel selection (Leith et al., 2012). In this algorithm, nodes begin by randomly choosing a color. Each computational update, nodes test for any neighbor with the same color. If and only if a conflicting neighbor is detected, nodes randomly select another color. The probability of selecting each possible color is stored in array associated with each node. Before selecting a new color, the stored probability of selecting the current (conflicting) color is decreased by a multiplicative factor  $1 - b$ . We used  $b = 0.1$ , as suggested by Leith et al. Tandem adjustments increase the probability of selecting all other channels. Regardless of whether their color changed, nodes always transmit their current color to their neighbor.

Our benchmarks focus on weak scalability, using a fixed problem size of 2048 graph nodes per thread or process. These nodes were arranged in a two-dimensional grid topology where each node had three possible colors and four neighbors. We implement the algorithm with a single Conduit communication layer carrying graph color as an unsigned integer. We used Conduit’s built-in pooling feature to consolidate

Mode	Description
0	Barrier sync every update
1	Rolling barrier sync
2	Fixed barrier sync
3	No barrier sync
4	No inter-cpu communication

TABLE I: Asynchronicity modes used for benchmarking experiments, arranged from most to least synchronized.

color information into a single MPI message between pairs of communicating processes each update. We performed five replicates, each with a five second simulation runtime. Solution error was measured as the number of graph color conflicts remaining at the end of the benchmark.

### C. Asynchronicity Modes

For both benchmarks, we compared performance across a spectrum of synchronization settings, which we term “asynchronicity modes” (Table I). Asynchronicity mode 0 represents traditional fully-synchronous methodology. Under this treatment, full barrier synchronization was performed between each computational update. Asynchronicity mode 3 represents fully asynchronous methodology. Under this treatment, individual threads or processes performed computational updates freely, incorporating input from other threads or processes on a fully best-effort basis.

During early development of the library, we discovered episodes where unprocessed messages built up faster than they could be processed — even if they were being skipped over to only get the latest message. In some instances, this strongly degraded quality of service or even caused runtime instability. We switched to MPI communication primitives that could consume many backlogged messages per call and increased buffer size to address these issues, but remained interested in the possibility of partial synchronization to clear potential message backlogs. So, we included two partially-synchronized treatments: asynchronicity modes 1 and 2.

In asynchronicity mode 1, threads and processes alternated between performing computational updates for a fixed-time duration and executing a global barrier synchronization. For the graph coloring benchmark, work was performed in 10ms chunks. For the digital evolution benchmark, which is more computationally intensive, work was performed in 100ms chunks. In asynchronicity mode 2, threads and processes executed global barrier synchronizations at predetermined time points based on the UTC clock.

Finally, asynchronicity mode 4 disables all inter-thread and inter-process communication, including barrier synchronization. We included this mode to isolate the impact on performance of communication between threads and processes from other factors potentially affecting performance, such as cache crowding. In this run mode for the graph coloring benchmark, all calls send messages between processes or threads were skipped (except after the benchmark concluded, when assessing solution quality). Because of its larger footprint, incorporating logic into the digital evolution simulation

to disable all inter-thread and inter-process messaging was impractical. Instead, we launched multiple instances of the simulation as fully-independent processes and measured performance of each.

#### D. Quality of Service Metrics

The best-effort communication model eschews effort to insulate computation from real-time message delivery dynamics. Because these dynamics are difficult to predict *a priori* and can bias computation, thorough, empirical runtime measurements are necessary to understand results of such computation. To this end, we developed a suite of quality of service metrics. Figure 1 provides space-time diagrams illustrating the metrics presented in this section.

For the purposes of these metrics, we assume that simulations proceed in an iterative fashion with alternating compute and communication phases. For short, we refer to a single compute-communication cycle as a “simstep.” We derive formulas for metrics in terms of independent observations preceding and succeeding a “snapshot” window, during which the simulation and any associated best-effort communication proceeds unimpeded. Snapshot observations are taken at one minute intervals over the course of each of our a replicate experiments. The following section, II-E, details the experimental apparatus used to generate quality of service metrics reported in this work.

1) *Simstep Period*: We calculate the amount of wall-time elapsed per simulation update cycle (“Simstep Period”) during a snapshot window as

$$\frac{\text{update count after} - \text{update count before}}{\text{walltime after} - \text{walltime before}}.$$

Figure 1d compares a scenario with low simstep period to a scenario with a higher simstep period.

2) *Simstep Latency*: This metric reports the number of simulation iterations that elapse between message dispatch and message delivery. Figure 1c compares a scenario with low latency to a scenario with a higher latency.

To prevent interfering effects of imperfect clock synchronization, we estimate one-way wall-time latency from a round-trip measure. As part of our instrumentation, each simulation element maintains an independent zero-initialized “touch counter” for each neighbor simulation element it communicates with. Dispatched messages are bundled with the current value touch counter associated with the target element. Every message received sets the corresponding touch counter to  $1 + \text{bundled touch count}$ . In this manner, the touch counter increments by two for each successful round trip completed. (Because simulation elements are arranged as a toroidal mesh in all experiments, interaction between simulation elements is always reciprocal.)

We therefore calculate one-way latency during a snapshot window as,

$$\frac{\text{update count after} - \text{update count before}}{\min(\text{touch count after} - \text{touch count before}, 1)}.$$

Note that, in the case where no touches elapse, we bound our latency measure to snapshot duration.

3) *Wall-time Latency*: Wall-time latency is closely related to simstep latency, simply denominating in elapsed real time instead of elapsed simulation steps. To calculate wall-time latency we apply a conversion to simstep latency based on simstep period,

$$\text{simstep latency} \times \text{simstep period}.$$

This metric directly tells the real-time performance of message transmission. Although it directly follows from the interaction between simstep period and wall-time latency, it complements simstep latency’s convenient interpretation in terms of potential simulation mechanics (e.g., simulation elements tending to see data from two updates ago versus from ten).

In addition to simstep latency, Figure 1c is also representative of wall-time latency — simply interpreting the  $y$  axis in terms of wall-time instead of elapsed simulation updates.

4) *Delivery Failure Rate*: Delivery failure rate measures the fraction of messages sent that are dropped. The only condition where messages are dropped is when a send buffer fills. (Under the existing MPI-based implementation, messages that queue on the send buffer are guaranteed for delivery.) So, we can calculate

$$\frac{\text{successful send count after} - \text{successful send count before}}{\text{attempted send count after} - \text{attempted send count before}}.$$

5) *Delivery Clumpiness*: Delivery clumpiness quantifies the extent to which message arrival is consolidated to a subset of message pull attempts. That is, the extent to which independently dispatched messages arrive in batches rather than as an even stream.

If messages all arrive in independent pull attempts, then clumpiness will be zero. At the point where the pigeon-hole principle applies (i.e.,  $\text{num arriving messages} \geq \text{num pull attempts}$ ), clumpiness will also be zero so long as every pull attempt is laden. If all messages arrive during a single pull attempt, then clumpiness will approach 1.

We formulate clumpiness as the compliment of steadiness. (Reporting clumpiness provides a lower-is-better interpretation consistent with the rest of the quality of service metrics.) Steadiness, in turn, stems from three component statistics,

$$\begin{aligned} \text{num laden pulls elapsed} &= \text{laden pull count after} \\ &\quad - \text{laden pull count before} \\ \text{num messages received} &= \text{message count after} \\ &\quad - \text{message count before} \\ \text{num pulls attempted} &= \text{pull attempt count after} \\ &\quad - \text{pull attempt count before.} \end{aligned}$$

Here, we refer to pull attempts that successfully retrieve a message as “laden.”

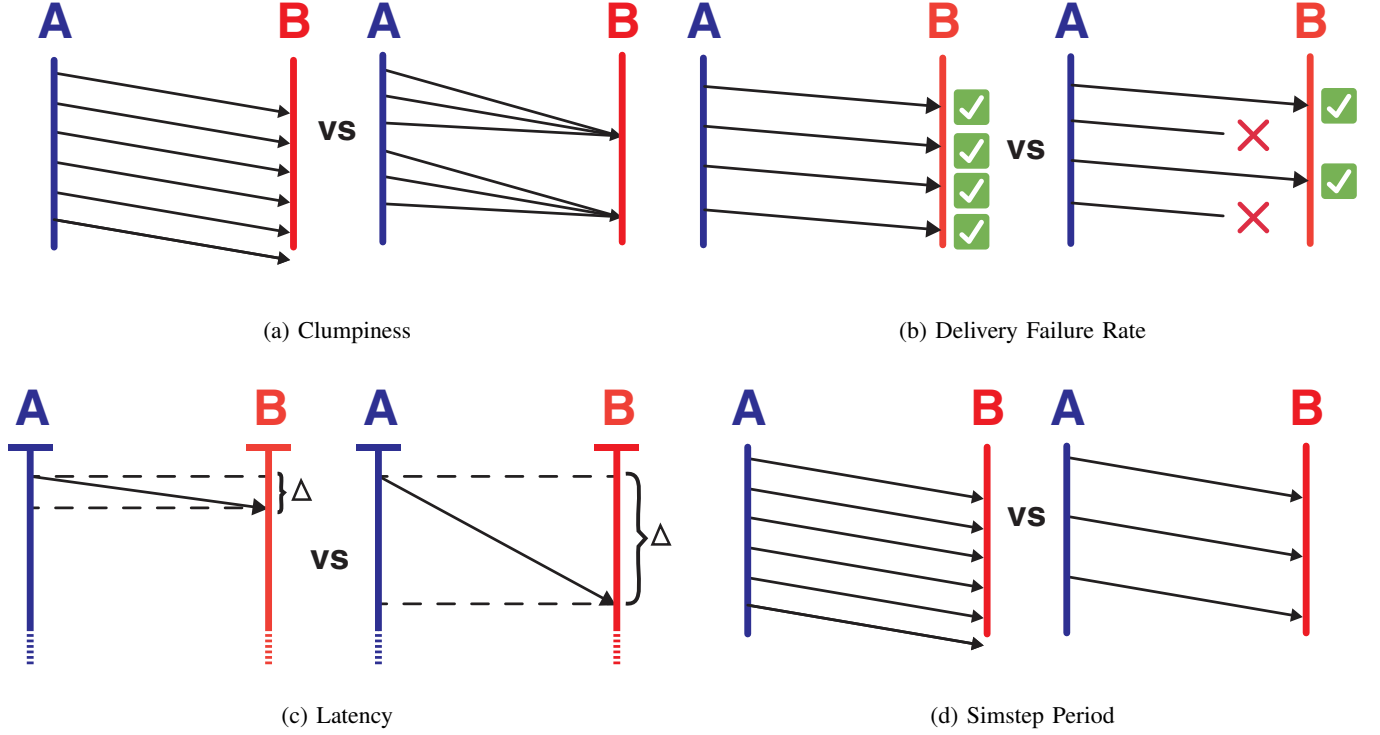


Fig. 1: Quality of service metrics. Each illustration is a space-time diagram, with  $A$  and  $B$  representing independent processes. The vertical axis depicts the passage of time, from top to bottom. Solid black arrows represent message delivery. The left panel of each metric’s diagram depicts a scenario with a lower (“better”) value for that metric compared to the right panel, which depicts a higher (“worse”) value for that metric.

We combine num messages received and num pulls attempted to derive,

$$\text{num opportunities for laden pulls} = \min \left( \text{num messages received}, \text{num pulls attempted} \right).$$

Then, to calculate steadiness,

$$\frac{\text{num laden pulls elapsed}}{\text{num opportunities for laden pulls}}.$$

Delivery clumpiness follows as  $1 - \text{steadiness}$ . Figure 1a compares a scenario with low clumpiness to a scenario with higher clumpiness.

#### E. Quality of Service Experiments

Quality of service experiments executed the graph coloring algorithm described in Section II-B. In order to maximize communication intensity, only one graph vertex was assigned per CPU. Ten experimental replicates were performed for each condition surveyed. Slightly over five minutes of runtime was afforded to each replicate. Over five minutes of runtime, snapshot observations were taken at one minute intervals. The first snapshot observation was taken one minute after the beginning of runtime.

Snapshot observations lasted one second, with the graph coloring algorithm running fully unhampered during the entire

snapshot. This was accomplished by collecting and recording data via a separate thread. That thread collected and recorded a first tranche of snapshot data, spin waited for one second, and then recorded a second tranche. Because the underlying system runs in real-time while being observed, state changes can occur during data collection (somewhat akin to photographic motion blur). Therefore, violations of intuitive invariants — like strictly non-negative delivery failure rates — occur in some cases. However, the magnitude of such violations is generally minor. Further, because data collection procedures were consistent across treatments, statistical comparisons between treatments nevertheless remain sound.

Snapshots were performed independently for each process at each timepoint. So, for example, for two processes over the five minute window of a single replicate ten snapshots were collected. For statistical tests comparing treatments, snapshots were aggregated by replicate by both mean and median. For each quality of service statistic we estimate mean — which captures effects of extreme-magnitude outliers — and median — which more better represents typicality — across these window samples. Statistical comparisons across treatment conditions are performed via regression. We use ordinary least squares regression to analyze means (Geladi and Kowalski, 1986) and quantile regression to analyze medians (Koenker and Hallock, 2001). For comparisons between dichotomous,

categorical treatment conditions, one condition is coded as 0 and the other as 1. In the case of ordinary least squares regression, this boils down to an independent  $t$ -test. Although quantile regression on categorical predictors is not precisely equivalent to a direct test on medians between two groups (i.e., Mood’s median test), there is precedent for this approach (Konstantopoulos et al., 2019; Petscher and Logan, 2014).

Most statistics reported here can be calculated just as well in terms of incoming or outgoing messages. That is, most statistics can be generated via data from instrumentation attached to message “inlets” or data from instrumentation attached to message “outlets” with no obvious reason to prefer one over the other. As “inlet-” and “outlet-” derived statistics are nearly identical in all cases, we simply report the mean over these two measurements.

#### F. Code, Data, and Reproducibility

1) *Benchmarking Experiments*: Benchmarking experiments were performed on Michigan State University’s High Performance Computing Center, a cluster of hundreds of heterogeneous x86 nodes linked with InfiniBand interconnects. For multithread experiments, benchmarks for each thread count were collected from the same node. For multiprocess experiments, each process was assigned to a distinct node in order to ensure results were representative of performance in a distributed context. All multiprocess benchmarks were recorded from the same collection of nodes. Hostnames are recorded for each benchmark data point. For an exact accounting of hardware architectures used, these hostnames can be crossreferenced with a table included with the data that summarizes the cluster’s node configurations.

Code for the distributed graph coloring benchmark is available at <https://github.com/mm500/conduit> under `demos/channel_selection`. Code for the digital evolution simulation benchmark is available at <https://github.com/mm500/dishtiny>. Exact versions of software used are recorded with each benchmark data point. Data is available via the Open Science Framework at <https://osf.io/7jkgp/> (Foster and Deardorff, 2017). Notebook code for all reported statistics and data visualizations is available at <https://hopth.ru/ci>.

2) *Quality of Service Experiments*: Quality of service experiments were carried out on Michigan State University’s High Performance Computing Center `lac` cluster, consisting of 28-core Intel(R) Xeon(R) CPU E5-2680 v4 2.40GHz nodes. All statistical comparisons are performed between observations from the same job allocation. (Except in the case where intranode and internode configurations were compared, where experiments were performed on separate allocations using comparable nodes on the same cluster.)

Benchmarking experiments described in Section II-F1 used a send/receive buffer size of 2. However, due to the high communication intensity of the graph coloring problem with just one simulation element per CPU, quality of service experiments required a larger buffer size of 64 to maintain runtime stability. In early work developing the Conduit library, we discovered that real-time messaging channels can

enter a destabilizing positive feedback spiral when incoming messages take longer to handle (e.g., skip past or read) than sending messages. Under such conditions, when a process exchanging messages from a partner process experiences a delay it sends fewer messages to that partner process. Due to fewer incoming messages, the partner process can update more rapidly, increasing incoming message load on the delayed process. This effect can snowball the partnership intended for even, two-way message exchange into effectively a unilateral producer-consumer relationship where (potentially unbounded) work piles up on the consumer. To interrupt such a scenario, we use the bulk message pull call `MPI_Testsome` to ensure fast message consumption under backlogged conditions. So, receiver workload remains closer to constant under high traffic situations (instead of having to pull messages down one-by-one). Larger receive buffer size, as configured for the quality of service experiments, increases the effectiveness of the bulk message consumption countermeasure.

Code for the distributed graph coloring benchmark is available at <https://github.com/mm500/conduit> under `demos/channel_selection`. Exact versions of software used are recorded with each benchmark data point. Data is available via the Open Science Framework at <https://osf.io/72k5n/> (Foster and Deardorff, 2017). Notebook code for all reported statistics is available at <https://hopth.ru/cj>.

### III. RESULTS AND DISCUSSION

Sections III-A and III-B compare execution performance under the best-effort communication versus the perfect communication models. In particular, both sections investigate how the impact of best-effort communication on performance relates to CPU count scale. Section III-A covers multithreading and Section III-B covers multiprocessing.

The following sections investigate how system configuration affects quality of service. Specifically, these sections cover the impact of

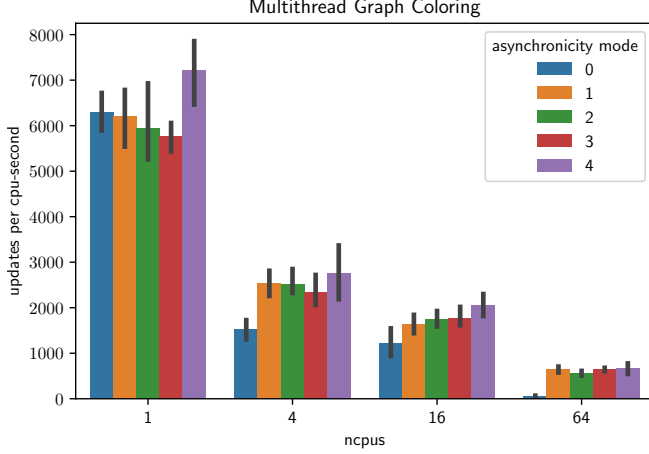
- increasing compute workload per simulation update step (Section III-C),
- within-node versus between-node process placement (Section III-D), and
- multithreading versus multiprocessing (Section III-E).

Section III-F tests how quality of service changes with CPU count. This analysis fleshes out the performance-centric picture of best-effort scalability established in Sections III-A and III-B.

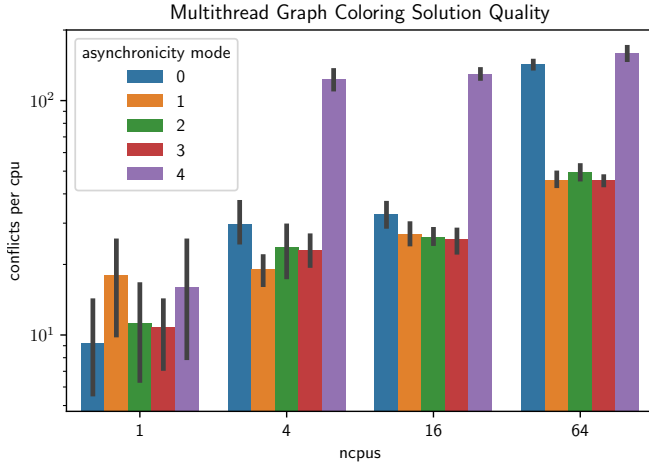
Section III-G tests how inclusion of an apparently faulty node (i.e., that provided exceptionally poor quality of service) affects global quality of service. This experiment provides insight into the robustness of best-effort approaches to single-point failure.

#### A. Performance: Multithread Benchmarks

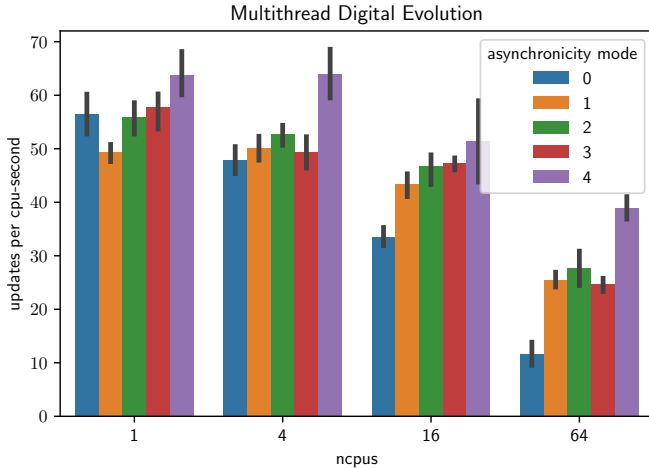
We first tested how performance on the graph coloring and digital evolution benchmarks fared when increasing thread count on a single hardware node.



(a) Graph coloring per-thread update rate. Higher is better.



(b) Graph coloring solution conflicts. Lower is better.



(c) Digital evolution per-thread update rate. Higher is better.

Fig. 2: Multithread benchmark results. Bars represent bootstrapped 95% confidence intervals.

Figure 2a presents per-CPU algorithm update rate for the graph coloring benchmark at 1, 4, 16, and 64 threads. Update rate performance decreased with increasing multithreading across all asynchronicity modes. This performance degradation was rather severe — per-CPU update rate decreased by 61% between 1 and 4 threads and by about another 75% between 4 and 64 threads. Surprisingly, this issue appears largely unrelated to inter-thread communication, as it was also observed in asynchronicity mode 4, where all interthread communication is disabled. Perhaps per-CPU update rate degradation under threading was induced by strain on a limited system resource like memory cache or access to the system clock (which was used to control run timing).

Nevertheless, we were able to observe significantly better performance of best-effort asynchronicity modes 1, 2, and 3 at high thread counts. At 64 threads, these run modes significantly outperformed the fully-synchronized mode 0 ( $p < 0.05$ , non-overlapping 95% confidence intervals). Likewise, as shown in Figure 2b, best-effort asynchronicity modes were able to deliver significantly better graph coloring solutions within the allotted compute time than the fully-synchronized mode 0 ( $p < 0.05$ , non-overlapping 95% confidence intervals).

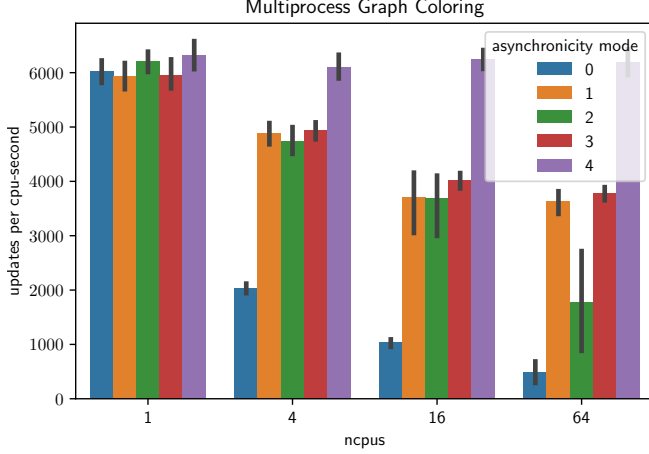
Figure 2c shows per-CPU algorithm update rate for the digital evolution benchmark at 1, 4, 16, and 64 threads. Similarly to the graph coloring benchmark, update rate performance decreased with increasing multithreading across all asynchronicity modes — including mode 4, which eschews inter-thread communication. Even without communication between threads, with 64 threads each thread performed updates at only 61% the rate of a lone thread. At 64 threads, best-effort asynchronicity modes 1, 2, and 3 exhibit about 43% the update-rate performance of a lone thread. Although best-effort inter-thread communication only exhibits half the update-rate performance of completely decoupled execution at 64 threads, this update-rate performance is roughly  $2.1\times$  that of the fully-synchronous mode 0. Indeed, best-effort modes significantly outperform the fully-synchronous mode on the digital evolution benchmark at both 16 and 64 threads ( $p < 0.05$ , non-overlapping 95% confidence intervals).

#### B. Performance: Multiprocess Benchmarks

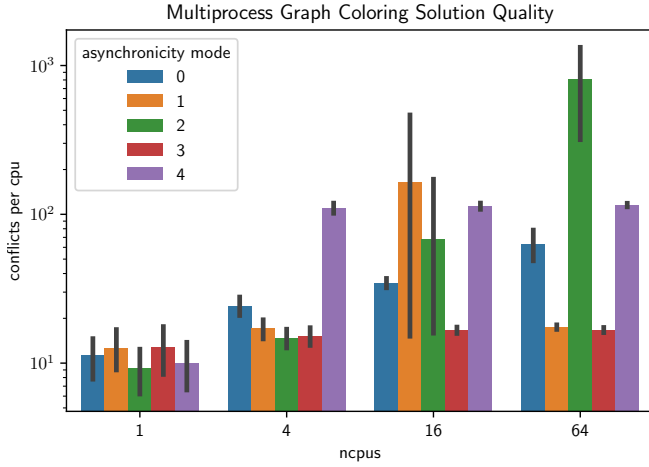
Next, we tested how performance on the graph coloring and digital evolution benchmarks fared when scaling with fully independent processes located on different hardware nodes.

Figure 3a shows per-CPU algorithm update rate for the graph coloring benchmark at 1, 4, 16, and 64 processes. Unlike the multithreaded benchmark, multiprocess graph coloring exhibits consistent update-rate performance across process counts under asynchronicity mode 4, where inter-CPU communication is entirely disabled. This matches the unsurprising expectation that, indeed, with comparable hardware a single process should exhibit the same mean performance as any number of completely decoupled processes.

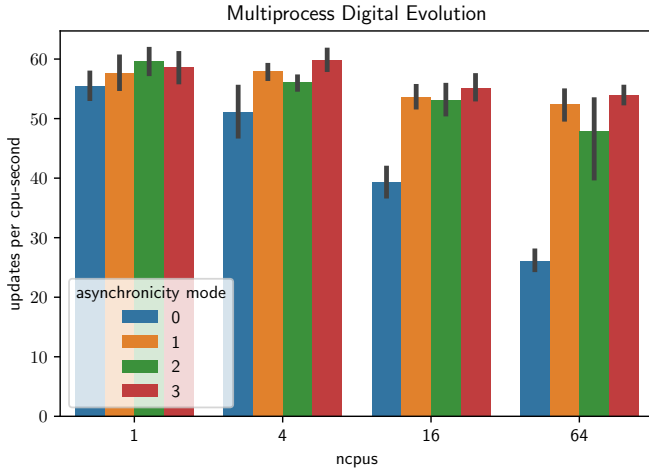
At 64 processes, best-effort asynchronicity mode 3 with the graph coloring benchmark exhibits about 63% the update-rate performance of single-process execution. This represents a



(a) Graph coloring per-process update rate. Higher is better.



(b) Graph coloring solution conflicts. Lower is better.



(c) Digital evolution per-process update rate. Higher is better.

Fig. 3: Multiprocess benchmark results. Bars represent bootstrapped 95% confidence intervals.

7.8 $\times$  speedup compared to fully-synchronous mode 0. Indeed, best-effort mode 3 enables significantly better per-CPU update rates at 4, 16, and 64 processes ( $p < 0.05$ , non-overlapping 95% confidence intervals).

Likewise, shown in Figure 3b, best-effort asynchronicity mode 3 yields significantly better graph-coloring results within the allotted time at 4, 16, and 64 processes ( $p < 0.05$ , non-overlapping 95% confidence intervals). Interestingly, partial-synchronization modes 1 and 2 exhibited highly inconsistent solution quality performance at 16 and 64 process count benchmarks. Fixed-timepoint barrier sync (mode 2) had particularly poor performance at 64 processes (note the log-scale axis). We suspect this was caused by a race condition where workers would assign sync points to different fixed points different based on slightly different startup times (i.e., process 0 syncs at seconds 0, 1, 2... while process 1 syncs at seconds 1, 2, 3..).

Figure 3c presents per-CPU algorithm update rate for the digital evolution benchmark at 1, 4, 16, and 64 processes. Relative performance fares well at high process counts under this relatively computation-heavy workload. With 64 processes, fully best-effort simulation retains about 92% the update rate performance of single-process simulation. This represents a 2.1 $\times$  speedup compared to the fully-synchronous run mode 0. Best-effort mode 3 significantly outperforms the per-CPU update rate of fully-synchronous mode 0 at process counts 16 and 64 ( $p < 0.05$ , non-overlapping 95% confidence intervals).

### C. Quality of Service: Computation vs. Communication

Having shown performance benefits of best-effort communication on the graph coloring and digital evolution benchmarks in Sections III-A and III-B, we next seek to more fully characterize the best-effort approach using a holistic suite of proposed quality of service metrics.

This section evaluates how a simulation's ratio of communication intensity to computational work affects these quality of service metrics. The graph coloring benchmark serves as our experimental model.

For this experiment, arbitrary compute work (detached from the underlying algorithm) was added to the simulation update process. We used a call to the `std::mt19937` random number engine as a unit of compute work. In microbenchmarks, we found that one work unit consumed about 35ns of walltime and 21ns of compute time. We performed 5 treatments, adding 0, 64, 4 096, 262 144, or 16 777 216 units of compute work to the update process. For each treatment, measurements were made on a pair of processes split across different nodes.

1) *Simstep Period*: Unsurprisingly, we found a direct relationship between per-update computational workload and the walltime required per computational update.

Supplementary Figures 32 and 34 depict the distribution of walltime per computational update across snapshots. Once added compute work supersedes the light compute work already associated with the graph coloring algorithm update step (at around 64 work units), simstep period scales in direct proportion with compute work.



Indeed, we found a significant positive relationship between both mean and median simstep period and added compute work (Supplementary Figures 40 and 42). At 0 units of added compute work, mean and median simstep period was 14.7  $\mu$ s. At 16 777 216 units of added compute work, mean simstep period was 611ms and median simstep period was 507ms. This largest workload brushes against instrumentation limitations, accounting for more than half the one second snapshot window. Supplementary Tables XVIII and XIX detail numerical results of these regressions.

2) *Simstep Latency*: Unsurprisingly, again, we observed a negative relationship between the number of simulation steps elapsed during message transit and added computational work. Put simply, longer update steps provide more time for messages to transit.

Supplementary Figures 33 and 29 show the distribution of simstep latency across compute workloads. With no added compute work, messages take between 20 and 100 simulation steps to transit (mean: 48.0 updates; median: 42.5 updates). At maximum compute work per update, messages arrive at a median 1.00 update latency.

Regression analysis confirms a significant negative relationship between both mean and median log simstep latency and log added compute work (Supplementary Figures 41 and 37). Supplementary Tables XVIII and XIX detail numerical results of these regressions.

3) *Walltime Latency*: Effects of compute work on walltime latency highlight an important caveat in interpretation of this metric: sensitivity in measuring walltime latency is limited by the simulation update pace. If a message is dispatched while its recipient is busy, the soonest it can be received will be when that recipient completes the computational phase of its update. Then, a full computational update will elapse before touch count propagates in a return message. So, even approaching instantaneous message delivery, a lower floor of  $\approx 1.5\times$  simstep period should be expected for the walltime latency measure. It should be noted, however, that distinctions in latency below the simulation update rate largely lack practical significance with respect to simulation outcomes.

For 0, 64, and 4 096 work units, walltime latency measures  $\approx 1$  ms (means: 708  $\mu$ s, 788  $\mu$ s, 902  $\mu$ s; medians: 622  $\mu$ s, 640  $\mu$ s, 738  $\mu$ s). At higher computational loads, simstep period surpasses 1ms. At 262 144 work units, simulation update time reaches  $\approx 8$ ms and, correspondingly, measured walltime latency registers slightly more than 50% longer at  $\approx 13$ ms (mean: 13.2ms, median 13.1ms). So, true latency likely falls well below simulation update time. At the highest computational workload, measured walltime latency stretches to the full one second snapshot window.

Supplementary Figures 28 and 30 show the distribution of walltime latency across computational workloads. Supplementary Figures 36 and 38 summarize regression between walltime latency and added compute work. Supplementary Tables XVIII and XIX detail numerical results of those regressions.

4) *Delivery Clumpiness*: We observed a significant negative relationship between computation workload and delivery

clumpiness.

At low computational intensity, we observed clumpiness greater than 0.95, meaning that fewer than 5% of pull requests were laden with fresh messages (at 0 compute work mean: 0.96, median 0.96). However, at high computational intensity clumpiness reached 0, indicating that messages arrived as a steady stream (at 16 777 216 compute work mean: 0.00, median 0.00). Presumably, the reduction in clumpiness is due to increased real-time separation between dispatched messages.

Supplementary Figure 31 shows the effect of computational workload on the distribution of observed clumpinesses. We found a significant negative relationship between both mean and median clumpiness and computational intensity. Supplementary Figure 39 visualizes these regressions and Supplementary Tables XVIII and XIX provide numerical details.

5) *Delivery Failure Rate*: We did not observe any delivery failures across all replicates and all compute workloads. So, compute workload had no observable effect on delivery reliability.

Supplementary Figure 35 shows the distribution of delivery failure rates across computation workloads and Supplementary Figure 43 shows regressions of delivery failure rate against computational workload. See Supplementary Tables XVIII and XIX for numerical details.

#### D. Quality of Service: Intranode vs. Internode

This section tests the effect of process assignment on best-effort quality of service, comparing multi-node and single-node assignments. The graph coloring benchmark again serves as our experimental substrate.

For this experiment, processes were either assigned to the same node or were assigned to different nodes. In both cases, we used two processes.

1) *Simstep Period*: Simstep period was significantly slower under internode conditions than under intranode conditions.

When processes shared the same node, simstep period was around 9  $\mu$ s (mean: 9.06  $\mu$ s; median: 9.08  $\mu$ s). Under internode conditions, simstep period was around 14  $\mu$ s (mean: 14.5  $\mu$ s; median: 14.4  $\mu$ s). Supplementary Figures 48 and 50 depict the distribution of walltime per computational update across intranode and internode conditions.

This result presumably attributes to an increased walltime cost for calls to the MPI implementation backing internode communication compared to the MPI implementation backing intranode communication. Although this effect is clearly detectable, its magnitude is modest given the minimal computational intensity of the simulation update step — only  $\approx 56\%$  more expensive than intranode dispatch.

Both mean and median simstep period increased significantly under internode conditions. (Supplementary Figures 56 and 58 visualize these regressions and Supplementary Tables XX and XXI detail numerical results.)

2) *Simstep Latency*: Significantly more simulation updates transpired during message transmission under internode conditions compared to intranode conditions.



Supplementary Figures 49 and 45 compares the distributions of simstep latency across these conditions. Simstep latency was around 1 update for intranode communication (mean: 1.00 updates; median 0.75 updates) and around 40 updates for internode communication (mean: 41.6 updates; median: 37.4 updates).

Regression analysis confirms the significant effect of process placement on simstep latency (Supplementary Figures 57 and 53). Supplementary Tables XX and XXI detail numerical results of these regressions.

3) *Walltime Latency*: Significantly more walltime elapsed during message transmission under internode conditions compared to intranode conditions.

Walltime latency was less than 10  $\mu$ s for intranode communication (mean: 7.70  $\mu$ s; median: 6.94  $\mu$ s). Internode communication had approximately 50 $\times$  greater walltime latency, at around 500  $\mu$ s (mean: 600  $\mu$ s; median: 551  $\mu$ s).

Supplementary Figures 44 and 46 show the distributions of walltime latency for intra- and inter-node communication. Regression analysis confirmed a significant increase in walltime latency under inter-node communication (Supplementary Figures 52, 54; Supplementary Tables XX and XXI).

4) *Delivery Clumpiness*: Delivery clumpiness was minimal under intranode communication and very high under internode communication.

Under intranode conditions, we observed a mean clumpiness value of 0.014 and a median of 0.002. Under internode conditions, we observed mean and median clumpiness values of 0.96. Supplementary Figures 47 and 47 show the distributions of clumpiness for intra- and inter-node communication. Regression analysis confirmed a significant increase in clumpiness under inter-node communication (Supplementary Figures 55, 55; Supplementary Tables XX and XXI).

5) *Delivery Failure Rate*: Somewhat counterintuitively, a significantly higher proportion of deliveries failed for intranode communication than for internode communication.

We observed a delivery failure rate of around 0.3 for intranode communication (mean: 0.33; median: 0.30) and no delivery failures for internode communication (mean: 0.00; median: 0.00). In some intranode snapshot windows, we observed a delivery failure rate as high as 0.8. Supplementary Figures 47 and 47 show the distributions of delivery failure rate for intra- and inter-node communication.

Because of Conduit's current MPI-based implementation, messages only drop when the underlying send buffer fills; queued messages are guaranteed for delivery. Slower simstep period under internode allocation could improve stability of the send buffer due to more time, on average, between send attempts. Underlying buffering or consolidation by the MPI backend for internode communication might also play a role by allowing data to be moved out of the userspace send buffer more promptly.

Regression analysis confirmed a significant increase in delivery failure under intra-node communication (Supplementary Figures 55, 55; Supplementary Tables XX and XXI).

## E. Quality of Service: Multithreading vs. Multiprocessing

This section compares best-effort quality of service under multithreading and multiprocessing schemes. We hold hardware configuration constant by restricting multiprocessing to cores a single hardware node, as is the case for multithreading. However, inter-process communication occurred via MPI calls while inter-thread communication occurred via shared memory access mediated by a C++ `std::mutex`.

Experiments again applied the graph coloring benchmark. Both treatments used a single pair of CPUs.

1) *Simstep Period*: Multithreading enabled faster simulation update turnover than multiprocessing.

Under multithreading, simstep period was around 5  $\mu$ s (mean: 4.60  $\mu$ s; median: 4.64  $\mu$ s). Simstep period for multiprocessing was around 9  $\mu$ s (mean: 9.00  $\mu$ s; median: 9.04  $\mu$ s). Supplementary Figures 64 and 66 depict the distribution of walltime per computational update for both multiprocessing and multithreading. This result falls in line with expectations that interaction via shared memory incurs lower overhead than via MPI calls.

Regression analysis showed that both mean and median simstep period were significantly slower under multiprocessing compared to multithreading. (Supplementary Figures 72 and 74 visualize these regressions and Supplementary Tables XXII and XXIII detail numerical results.)

2) *Walltime Latency*: No significant difference in walltime latency was detected between multiprocessing and multithreading.

In the median case, walltime latency was approximately 5  $\mu$ s for multithreading and 8  $\mu$ s for multiprocessing. However, a pair of extreme outliers among snapshot windows — with walltime latencies of approximately 12ms — drove multithreading walltime latency much higher in the mean case, to 451  $\mu$ s. In the median case, multiprocessing walltime latency was 8.56  $\mu$ s.

Cache invalidation or mutex contention provide possible explanations for the observed episodes of extreme multithreading latency, although magnitude on the order of milliseconds for such effects is surprising. Multithreading appears to provide marginally lower latency service in the median case, but at the cost of vulnerability to extreme high-latency disruptions.

Supplementary Figures 60 and 62 show the distributions of walltime latency for multithread and multiprocess runs. Regression analysis did not detect any significant difference in walltime latency between multithreading and multiprocessing (Supplementary Figures 68, 70; Supplementary Tables XXII and XXIII).

3) *Simstep Latency*: No significant difference in simstep latency was detected between multiprocessing and multithreading.

In the median case, multiprocessing offered marginally lower simstep latency than multithreading. Median simstep latency was 0.84 updates under multiprocessing and 1.10 updates under multithreading. However, just as for walltime latency, extreme magnitude outliers ( $\approx$  2000 simsteps)

boosted mean simstep latency for multithreading. Mean simstep latency was 0.94 updates under multiprocessing and 78.0 updates under multithreading. Supplementary Figures 65 and 61 compare the distributions of simstep latency across these conditions.

Direct measurements of simstep period and walltime latency suggest that faster simstep period, rather than slower walltime latency, explain the marginally higher simstep latency under multithreading.

Regression analysis detected no significant effect of threading versus processing on simstep latency in both the mean and median cases (Supplementary Figures 73 and 69). Supplementary Tables XXII and XXIII detail numerical results of these regressions.

4) *Delivery Clumpiness*: Multithreading exhibited higher median clumpiness and greater variance in clumpiness than multiprocessing.

Under multithreading, clumpiness was nearly 1 within some snapshot windows and less than 0.1 within others. Under multiprocessing, clumpiness was consistently less than 0.1. Supplementary Figures 63 and 63 show the distributions of clumpiness under both multiprocessing and multithreading. Multithreading median clumpiness was 0.54. Multiprocessing median clumpiness was 0.03. Multithreading and multiprocessing mean clumpinesses were 0.56 and 0.03, respectively.

Regression analysis confirmed a significantly greater clumpiness under both multithreading compared to multiprocessing (Supplementary Figures 71, 71; Supplementary Tables XXII and XXIII).

5) *Delivery Failure Rate*: We observed a higher proportion of deliveries fail for multiprocessing than for multithreading. (This is as expected; the multithread implementation directly wrote updates to a piece of shared memory, so there was no send buffer to backlog and induce message drops.)

Multiprocessing exhibited both mean and median delivery failure rate of 0.38. In individual multiprocessing snapshot windows, we observed a delivery failure rates ranging from less than 0.1 to as high as 0.7. We observed no multithreaded delivery failures. Supplementary Figures 63 and 63 show the distributions of delivery failure rate for multithreading and multiprocessing.

Regression analysis confirmed a significant increase in delivery failure under multiprocessing (Supplementary Figures 71, 71; Supplementary Tables XXII and XXIII).

#### F. Quality of Service: Weak Scaling

Sections III-B and III-A showed how best-effort communication could improve application performance, particularly when scaling up processor count. Multiprocess performance scales well under the best-effort approach, with overlapping performance estimate intervals for 16 and 64 processor counts on both surveyed benchmark problems.

This section aims to flesh out a more holistic picture of the effects of increasing processor count on best-effort computation by considering a comprehensive suite of quality of service metrics. Our particular interest is in which, if any,

aspects of quality of service degrade under larger processing pools.

To address these questions, we performed weak scaling experiments on 16, 64, and 256 processes using the graph coloring benchmark. To broaden the survey, we tested scaling with different numbers of processors allocated per node and different numbers of simulation elements assigned per processor.

For the first variable, we tested scaling on allocations with each processor hosted on an independent node and allocations where each node hosted an average of four processors. This allowed us to examine how quality of service fared in homogeneous network conditions, where all communication between processes was inter-node, compared to heterogeneous conditions, where some inter-process communication was inter-node and some was intra-node.

For the second variable, we tested with 2048 simulation elements (“simels”) per processor (consistent with the benchmarking experiments performed in Sections III-B and III-A) and just one simulation element per processor. This allowed us to vary the amount of computational work performed per process.

1) *Simstep Period*: Supplementary Figures 13 and 15 survey the distributions of simstep periods observed within snapshot windows. Across process counts, simstep period registers around 80  $\mu$ s with one simel per CPU and around 200  $\mu$ s with 2048 simels per CPU. However, on heterogeneous allocations (4 CPUs per node) this metric is more variable between snapshots. Outlier observations range up to around 10ms with 2048 simels per CPU. With 1 simel per CPU, outlying values fell upwards of 100ms.

We performed an ordinary least squares (OLS) regression to test how mean simstep period changed with processor count. In all cases except one simel per CPU with four CPUs per node, mean simstep period increased significantly with processor count from 16 to 64 to 256 CPUs. However, from 64 to 256 processors mean simstep period only increased significantly with one simel per CPU per node. Between 64 and 256 processes, mean simstep period actually decreased significantly for runs with 2048 simels per CPU. Figure 4 and Supplementary Figure 21 visualize reported OLS regressions. Supplementary Tables VI and VIII provide numerical details on reported OLS regressions.

Median simstep period exhibited the same relationships with processor count, tested with quartile regression. Supplementary Figures 26 and 27 visualize corresponding quartile regressions. Supplementary Tables XIV and XVI report numerical details on those quartile regressions.

Except for the extreme case of one simel per CPU and one CPU per node, simstep period quality of service is stable in scaling from 64 to 256 processes.

2) *Walltime Latency*: Walltime latency sits at around 500  $\mu$ s for one-simel runs and around 2ms for 2048-simel runs. However, variability is greater for heterogeneous (four CPUs per node) allocations. Extreme outliers of up to almost 100ms inlet/2s outlet occur in four CPUs per node, one-simel runs.

In 256 process, 2048-simel, one CPU per node runs, outliers of more than 10s occur. Supplementary Figures 9 and 11 show the distribution of walltime latencies observed across run conditions.

We performed OLS regressions to test how mean walltime latency changed with processor count. Over 16, 64, and 256 processes, mean walltime latency increased significantly with processor count only with 2048 simels per CPU. Between 64 and 256 processes, mean walltime latency increased significantly with processor count only for one CPU per node with 2048 simels per CPU. Supplementary Figures 17 and Figure 19 show these regressions. Supplementary Tables II and IV provide numerical details.

Next, we performed quantile regressions to test how processor count affected median walltime latency. Over 16, 64, and 256 processes, median walltime latency increased significantly only with 4 CPUs per node and 2048 simels per CPU. Over 64 and 256 processes, there was no significant relationship between processor count and median walltime latency under any condition. Figure 5 and Supplementary Figure 24 show regression results. Supplementary Tables X and XII provide numerical details.

3) *Simstep Latency*: Simstep latency sits around 7 updates for runs with one simel per CPU and around 1.2 updates for runs with 2048 simels per CPU. For runs with one simel per CPU, outlier snapshot windows reach up to 50 updates under homogeneous allocations and up to almost 100 updates under heterogeneous allocations. The 2048 simels per CPU, one CPU per node, 256 process condition exhibited outliers of up to almost 8000 update simstep latency. Supplementary Figures 14 and 10 show the distribution of simstep latencies observed across run conditions.

Over 16, 64, and 256 processes, mean simstep latency increased with process count only under 1 CPU per node, 2048 simel per CPU conditions. The same was true over just 64 to 256 processes. Supplementary Figures 20 and 18 show the OLS regressions performed, with Supplementary Tables VII and III providing numerical details.

For median simstep latency, however, there was no condition where latency increased significantly with process count. Figure 6 and Supplementary Figure 23 show the quantile regressions performed, with Supplementary Tables XV and XI providing numerical details.

4) *Delivery Clumpiness*: For one-simel-per-CPU runs, median delivery clumpiness registered between 0.8 and 0.6. On 2048-simel-per-CPU runs, median delivery clumpiness was lower at around 0.4. Supplementary Figure 12 shows the distribution of delivery clumpiness values observed across run conditions.

Using OLS regression, we found no evidence of mean clumpiness worsening with increased process count. In fact, over 16, 64, and 256 processes clumpiness significantly decreased with process count in all conditions except four CPUs per node with 2048 simels per CPU. Figure 7 and Supplementary Table V detail regressions performed to test the relationship between mean clumpiness and process count.

Median delivery clumpiness exhibited the same relationships with processor count, tested with quartile regression. Supplementary Figure 25 and Supplementary Table XIII detail regressions between median clumpiness and process count.

5) *Delivery Failure Rate*: Typical delivery failure rate was near zero, except with one simel per CPU and four CPUs per node where median delivery failure rate was approximately 0.1. However, outlier delivery failure rates of up to 0.7 were observed with 1 CPU per node, 2048 simels per CPU, and 256 processes. Outlier delivery failure rates of up to 0.2 were observed with 4 CPUs per node, 2048 simels per CPU, and 256 processes. Supplementary Figure 16 shows the distribution of delivery failure rates observed across run conditions.

Mean delivery failure rate increased significantly between 64 and 256 processes with 1 CPU per node and 2048 simels per CPU as well as with 4 CPUs per node and 1 simel per CPU. However, the median delivery failure rate only increased significantly with processor count with 4 CPUs per node and 1 simel per CPU.

Supplementary Figure 22 and Supplementary Table IX detail the OLS regression testing mean delivery failure rate against processor count. Figure 8 and Supplementary Table XVII detail the quantile regression testing median delivery failure rate against processor count.

#### G. Quality of Service: Faulty Hardware

The extreme magnitude of outliers for metrics reported in Section III-F prompted further investigation of the conditions under which these outliers arose. Closer inspection revealed that the most extreme outliers were all associated with snapshots on a single node: lac-417.

So, we acquired two separate 256 process allocations on the lac cluster: one including lac-417 and one excluding lac-417.

Supplementary Figures 80, 82, 81, 77, 76, 78, 79, and 83 compare the distributions of quality of service metrics between allocations with and without lac-417. Extreme outliers are present exclusively in the lac-417 allocation for walltime latency, simstep latency, and delivery failure rate. Otherwise, the metrics' distributions across snapshots are very similar between allocations.

Supplementary Figures 88, 90, 89, 85, 84, 86, 87, 87, and 91 chart OLS and quantile regressions of quality of service metrics on job composition. Mean walltime latency, simstep latency, and delivery failure rate are all significantly greater with lac-417. Surprisingly, mean simstep period is significantly longer without lac-417.

However, there is no significant difference in median value for any quality of service metric between allocations including or excluding lac-417. This stability of metric medians within allocations containing lac-417 — which have significantly different means due to outlier values induced by the presence of lac-417 — demonstrates how the best-effort system maintains overall quality of service stability despite defective or degraded components.

Supplementary Tables XXIV and XXV provide numerical details on regressions reported above.

#### IV. CONCLUSION

The fundamental motivation for best-effort communication is efficient scalability. Our results confirm that best-effort communication can fulfill on this goal.

We found that the best-effort approach significantly increases performance at high CPU count. This finding was consistent across the communication-intensive graph coloring benchmark and the computation-intensive digital evolution benchmark. The computation-heavy digital evolution benchmark yielded the strongest scaling efficiency, achieving at 64 processes 92% the update-rate of single-process execution. We observed the greatest relative speedup under distributed communication-heavy workloads — about  $7.8\times$  on the graph coloring benchmark. In the case of the graph coloring benchmark, we found that best-effort communication can help achieve tangibly better solution quality within a fixed time constraint.

Because real-time volatility affects the outcome of computation under the best-effort model, raw execution speed performance does not suffice to fully understand the consequences of the best-effort communication model. In order to characterize the real-time dynamics under the best-effort model, we designed and measured a suite of quality of service metrics: simstep period, simstep latency, wall-time latency, delivery failure rate, and delivery clumpiness.

We performed several experiments to validate and characterize these metrics. Comparing quality of service between multithreading and multiprocessing, we found that multithreading had lower runtime overhead cost but that multiprocessing reduced delivery erraticity, curbing especially extreme poor quality of service outlier events. We found better quality of service, especially with respect to latency, for processes occupying the same node. Finally, varying the ratio of computational work to communication, we found lower communication intensity associated with less volatile quality of service.

In order for best-effort communication to succeed in facilitating scale-up, median quality of service must stabilize with increasing CPU count. Put another way, best-effort communication cannot succeed at scale if communication quality tends toward complete degradation. In Section III-F, we used weak scaling experiments to test the effect of scale-up on quality of service at 8, 64, and 256 processes. Under a lower communication-intensity task parameterization, we found that all median quality of service metrics were stable when scaling from 64 to 256 process. Under maximal communication intensity, we found in one case that median simstep period degraded from around  $80\mu\text{s}$  to around  $85\mu\text{s}$ . In another case, median message delivery failure rate increased from around 7% to around 9%. Such minor — and, in most cases, nil — degradation in median quality of service despite maximal communication intensity bodes well for the viability of best-effort communication at scale.

Resilience is a second major motivating factor for best-effort computing. In another promising result, we found that the presence of an apparently faulty compute node did not

degrade median performance or quality of service. Despite extreme quality of service degradation measured among that node and its clique, collective performance and quality of service remained steady. In effect, the best-effort approach successfully decoupled global performance from the worst performer. Such so-called “straggler effects” plague traditional approaches to large-scale high-performance computing (Aktaş and Soljanin, 2019), so avoiding them is a major boon.

Development of the Conduit library stemmed from a practical need for an abstract, prepackaged best-effort communication interface to support our digital evolution research. Because real-time effects are fundamentally application-dependent and arise without any explicit in-program specification (and therefore may be unanticipated) it is important to be able to perform such quality of service profiling case-by-case in applications of best-effort communication. The instrumentation used in these experiments is written as wrappers around the library’s `Inlet` and `Outlet` classes that may be enabled via compile-time configuration switch. This makes data generation for quality of service analysis trivial to perform in any system built with the Conduit library. We hope that making this library and quality of service metrics available to the community can reduce domain expertise and programmability barriers to taking advantage of the best-effort communication model to efficiently leverage burgeoning parallel and distributed computing power.

In future work, it may be of interest to design systems that monitor and proactively react to real-time quality of service conditions. For example, imposing a variable cost for cell-cell messaging to agents based on traffic levels or increasing per-update resource generation rates for agents on slow-running nodes. We are eager to investigate how Conduit’s best-effort communication model scales on much larger process counts on the order of thousands of cores.

#### ACKNOWLEDGMENT

Thanks to Santiago Rodriguez Papa for contributing graphics illustrating quality of service metrics. This research was supported in part by NSF grants DEB-1655715 and DBI-0939454 as well as by Michigan State University through the computational resources provided by the Institute for Cyber-Enabled Research. This material is based upon work supported by the National Science Foundation Graduate Research Fellowship under Grant No. DGE-1424871. Any opinions, findings, and conclusions or recommendations expressed in this material are those of the author(s) and do not necessarily reflect the views of the National Science Foundation.

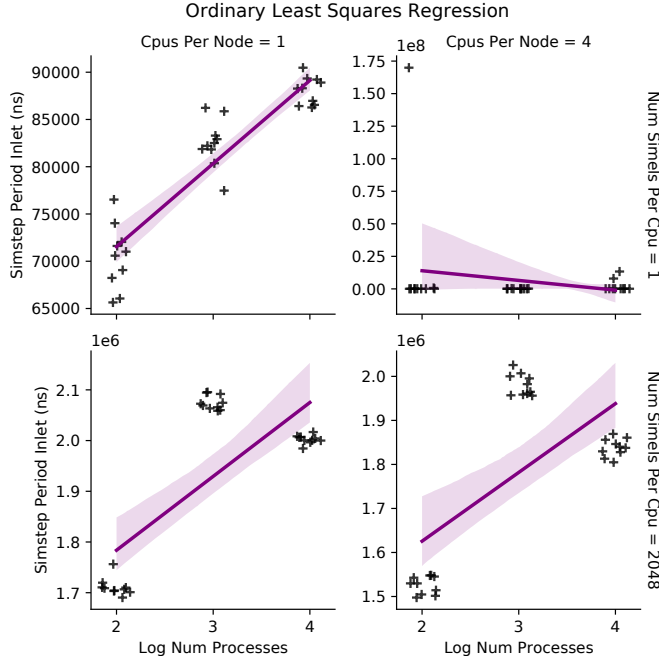
#### REFERENCES

- Ackley, D. and Small, T. (2014). Indefinitely scalable computing= artificial life engineering. In *ALIFE 14: The Fourteenth International Conference on the Synthesis and Simulation of Living Systems*, pages 606–613. MIT Press.
- Ackley, D. H. and Cannon, D. C. (2011). Pursue robust indefinite scalability. In *Proceedings of the 13th USENIX Conference on Hot Topics in Operating Systems*, HotOS’13, page 8, USA. USENIX Association.

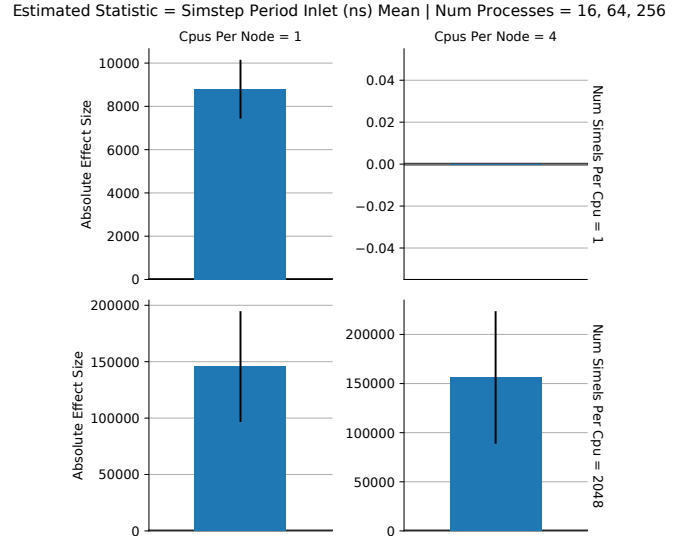
- Ackley, D. H. and Williams, L. R. (2011). Homeostatic architectures for robust spatial computing. In *2011 Fifth IEEE Conference on Self-Adaptive and Self-Organizing Systems Workshops*, pages 91–96. IEEE.
- Acun, B., Gupta, A., Jain, N., Langer, A., Menon, H., Mikida, E., Ni, X., Robson, M., Sun, Y., Totoni, E., et al. (2014). Parallel programming with migratable objects: Charm++ in practice. In *SC'14: Proceedings of the International Conference for High Performance Computing, Networking, Storage and Analysis*, pages 647–658. IEEE.
- Aktaş, M. F. and Soljanin, E. (2019). Straggler mitigation at scale. *IEEE/ACM Transactions on Networking*, 27(6):2266–2279.
- Bauer, M., Treichler, S., Slaughter, E., and Aiken, A. (2012). Legion: Expressing locality and independence with logical regions. In *SC'12: Proceedings of the International Conference on High Performance Computing, Networking, Storage and Analysis*, pages 1–11. IEEE.
- Bennett III, F. H., Koza, J. R., Shipman, J., and Stiffelman, O. (1999). Building a parallel computer system for \$18,000 that performs a half peta-flop per day. In *Proceedings of the 1st Annual Conference on Genetic and Evolutionary Computation-Volume 2*, pages 1484–1490.
- Blumofe, R. D., Joerg, C. F., Kuszmaul, B. C., Leiserson, C. E., Randall, K. H., and Zhou, Y. (1996). Cilk: An efficient multithreaded runtime system. *Journal of Parallel and Distributed Computing*, 37(1):55–69.
- Bocquet, M., Hirzlin, T., Klein, J.-O., Nowak, E., Vianello, E., Portal, J.-M., and Querlioz, D. (2018). In-memory and error-immune differential rram implementation of binarized deep neural networks. In *2018 IEEE International Electron Devices Meeting (IEDM)*, pages 20–6. IEEE.
- Bonabeau, E. W. and Theraulaz, G. (1994). Why do we need artificial life? *Artificial Life*, 1(3):303–325.
- Bundy, J., Ofria, C., and Lenski, R. E. (2021). How the footprint of history shapes the evolution of digital organisms. *bioRxiv*.
- Chakradhar, S. T. and Raghunathan, A. (2010). Best-effort computing: Re-thinking parallel software and hardware. In *Design Automation Conference*, pages 865–870. IEEE.
- Chakrapani, L. N., Korkmaz, P., Akgul, B. E., and Palem, K. V. (2008). Probabilistic system-on-a-chip architectures. *ACM Transactions on Design Automation of Electronic Systems (TODAES)*, 12(3):1–28.
- Chakravorty, S. and Kale, L. V. (2004). A fault tolerant protocol for massively parallel systems. In *18th International Parallel and Distributed Processing Symposium*, page 212. IEEE.
- Chakravorty, S. and Kalé, L. V. (2007). A fault tolerance protocol with fast fault recovery. In *2007 IEEE International Parallel and Distributed Processing Symposium*, pages 1–10. IEEE.
- Chamberlain, B. L., Callahan, D., and Zima, H. P. (2007). Parallel programmability and the chapel language. *The International Journal of High Performance Computing Applications*, 21(3):291–312.
- Channon, A. (2019). Maximum individual complexity is indefinitely scalable in geb. *Artificial Life*, 25(2):134–144.
- Chippa, V. K., Mohapatra, D., Roy, K., Chakradhar, S. T., and Raghunathan, A. (2014). Scalable effort hardware design. *IEEE Transactions on Very Large Scale Integration (VLSI) Systems*, 22(9):2004–2016.
- Cho, H., Leem, L., and Mitra, S. (2012). Ers: Error resilient system architecture for probabilistic applications. *IEEE Transactions on Computer-Aided Design of Integrated Circuits and Systems*, 31(4):546–558.
- Covert, A. W., Lenski, R. E., Wilke, C. O., and Ofria, C. (2013). Experiments on the role of deleterious mutations as stepping stones in adaptive evolution. *Proceedings of the National Academy of Sciences*, 110(34):E3171–E3178.
- Dean, J., Corrado, G., Monga, R., Chen, K., Devin, M., Mao, M., Ranzato, M. a., Senior, A., Tucker, P., Yang, K., Le, Q., and Ng, A. (2012). Large scale distributed deep networks. In Pereira, F., Burges, C. J. C., Bottou, L., and Weinberger, K. Q., editors, *Advances in Neural Information Processing Systems*, volume 25. Curran Associates, Inc.
- Dolson, E., Lalejini, A., Jorgensen, S., and Ofria, C. (2020). Interpreting the tape of life: Ancestry-based analyses provide insights and intuition about evolutionary dynamics. *Artificial Life*, 26(1):58–79.
- Dolson, E. and Ofria, C. (2017). Spatial resource heterogeneity creates local hotspots of evolutionary potential. In *ECAL 2017, the Fourteenth European Conference on Artificial Life*, pages 122–129.
- Dongarra, J., Hittinger, J., Bell, J., Chacon, L., Falgout, R., Heroux, M., Hovland, P., Ng, E., Webster, C., and Wild, S. (2014). Applied mathematics research for exascale computing. Technical report, Lawrence Livermore National Lab.(LLNL).
- El-Ghazawi, T. and Smith, L. (2006). Upc: Unified parallel c. In *Proceedings of the 2006 ACM/IEEE Conference on Supercomputing*, SC '06, page 27–es, New York, NY, USA. Association for Computing Machinery.
- Fortuna, M. A., Barbour, M. A., Zaman, L., Hall, A. R., Buckling, A., and Bascombe, J. (2019). Coevolutionary dynamics shape the structure of bacteria-phage infection networks. *Evolution*, 73(5):1001–1011.
- Foster, E. D. and Deardorff, A. (2017). Open science framework (osf). *Journal of the Medical Library Association*, 105(2):203.
- Gagliardi, F., Moreto, M., Olivieri, M., and Valero, M. (2019). The international race towards exascale in europe. *CCF Transactions on High Performance Computing*, pages 1–11.
- Gamell, M., Teranishi, K., Heroux, M. A., Mayo, J., Kolla, H., Chen, J., and Parashar, M. (2015). Local recovery and failure masking for stencil-based applications at extreme scales. In *SC'15: Proceedings of the International Conference for High Performance Computing, Networking, Storage and Analysis*, pages 1–12. IEEE.
- Geladi, P. and Kowalski, B. R. (1986). Partial least-squares regression: a tutorial. *Analytica Chimica Acta*, 185:1–17.
- Goldsby, H. J., Knoester, D. B., Ofria, C., and Kerr, B. (2014).

- The evolutionary origin of somatic cells under the dirty work hypothesis. *PLoS Biology*, 12(5):e1001858.
- Grabowski, L. M., Bryson, D. M., Dyer, F. C., Pennock, R. T., and Ofria, C. (2013). A case study of the de novo evolution of a complex odometric behavior in digital organisms. *PLoS One*, 8(4):e60466.
- Gropp, W., Lusk, E., Doss, N., and Skjellum, A. (1996). A high-performance, portable implementation of the mpi message passing interface standard. *Parallel Computing*, 22(6):789–828.
- Gropp, W. and Snir, M. (2013). Programming for exascale computers. *Computing in Science & Engineering*, 15(6):27–35.
- Gu, R. and Becchi, M. (2019). A comparative study of parallel programming frameworks for distributed gpu applications. In *Proceedings of the 16th ACM International Conference on Computing Frontiers*, pages 268–273.
- Heroux, M. A. (2014). Toward resilient algorithms and applications. *arXiv preprint arXiv:1402.3809*.
- Hursey, J., Squyres, J. M., Mattox, T. I., and Lumsdaine, A. (2007). The design and implementation of checkpoint/restart process fault tolerance for open mpi. In *2007 IEEE International Parallel and Distributed Processing Symposium*, pages 1–8. IEEE.
- Izzo, D., Rucinski, M., and Ampatzis, C. (2009). Parallel global optimisation meta-heuristics using an asynchronous island-model. In *2009 IEEE Congress on Evolutionary Computation*, pages 2301–2308. IEEE.
- Kajmakovic, A., Diwold, K., Kajtazovic, N., and Zupanc, R. (2020). Challenges in mitigating soft errors in safety-critical systems with cots microprocessors. In *PESARO 2020, The Tenth International Conference on Performance, Safety and Robustness in Complex Systems and Applications*, pages 13–18. IARIA.
- Kale, L. V. and Krishnan, S. (1993). Charm++ a portable concurrent object oriented system based on c++. In *Proceedings of the Eighth Annual Conference on Object-oriented Programming Systems, Languages, and Applications*, pages 91–108.
- Karakus, M. and Durrresi, A. (2017). Quality of service (qos) in software defined networking (sdn): A survey. *Journal of Network and Computer Applications*, 80:200–218.
- Karnik, T. and Hazucha, P. (2004). Characterization of soft errors caused by single event upsets in cmos processes. *IEEE Transactions on Dependable and Secure Computing*, 1(2):128–143.
- Kashyap, V. (2006). Ip over infiniband (ipoib) architecture. *The Internet Society*, 22.
- Kim, J.-S., Ha, S., and Jhon, C. S. (1998). Relaxed barrier synchronization for the bsp model of computation on message-passing architectures. *Information Processing Letters*, 66(5):247–253.
- Koenker, R. and Hallock, K. F. (2001). Quantile regression. *Journal of Economic Perspectives*, 15(4):143–156.
- Konstantopoulos, S., Li, W., Miller, S., and van der Ploeg, A. (2019). Using quantile regression to estimate intervention effects beyond the mean. *Educational and Psychological Measurement*, 79(5):883–910.
- Koop, M. J., Sur, S., Gao, Q., and Panda, D. K. (2007). High performance mpi design using unreliable datagram for ultra-scale infiniband clusters. In *Proceedings of the 21st Annual International Conference on Supercomputing*, pages 180–189.
- Lalejini, A. and Ofria, C. (2018). Evolving event-driven programs with signalgp. In *Proceedings of the Genetic and Evolutionary Computation Conference*, pages 1135–1142.
- Leith, D. J., Clifford, P., Badarla, V., and Malone, D. (2012). Wlan channel selection without communication. *Computer Networks*, 56(4):1424–1441.
- Lenski, R. E., Ofria, C., Pennock, R. T., and Adami, C. (2003). The evolutionary origin of complex features. *Nature*, 423(6936):139–144.
- Meng, J., Chakradhar, S., and Raghunathan, A. (2009). Best-effort parallel execution framework for recognition and mining applications. In *2009 IEEE International Symposium on Parallel & Distributed Processing*, pages 1–12. IEEE.
- Mittal, S. (2016). A survey of techniques for approximate computing. *ACM Computing Surveys (CSUR)*, 48(4):1–33.
- Moreno, M. A. and Ofria, C. (2019). Toward open-ended fraternal transitions in individuality. *Artificial Life*, 25(2):117–133.
- Moreno, M. A. and Ofria, C. (2022). Exploring evolved multicellular life histories in a open-ended digital evolution system. *Frontiers in Ecology and Evolution*, 10.
- Moreno, M. A., Papa, S. R., and Ofria, C. (2021). Conduit: A c++ library for best-effort high performance computing. In *Proceedings of the Genetic and Evolutionary Computation Conference Companion, GECCO '21*, page 1795–1800, New York, NY, USA. Association for Computing Machinery.
- Ni, X. (2016). *Mitigation of failures in high performance computing via runtime techniques*. PhD thesis, University of Illinois.
- Niu, F., Recht, B., Re, C., and Wright, S. J. (2011). Hogwild! a lock-free approach to parallelizing stochastic gradient descent. In *Proceedings of the 24th International Conference on Neural Information Processing Systems*, pages 693–701.
- Noel, C. and Osindero, S. (2014). Dogwild!-distributed hogwild for cpu & gpu. In *NIPS Workshop on Distributed Machine Learning and Matrix Computations*, pages 693–701.
- Petscher, Y. and Logan, J. A. (2014). Quantile regression in the study of developmental sciences. *Child Development*, 85(3):861–881.
- Pontes, A. C., Mobley, R. B., Ofria, C., Adami, C., and Dyer, F. C. (2020). The evolutionary origin of associative learning. *The American Naturalist*, 195(1):E1–E19.
- Rahmati, D., Murali, S., Benini, L., Angiolini, F., De Micheli, G., and Sarbazi-Azad, H. (2011). Computing accurate performance bounds for best effort networks-on-chip. *IEEE Transactions on Computers*, 62(3):452–467.
- Ray, T. (1995). A proposal to create a network-wide bio-

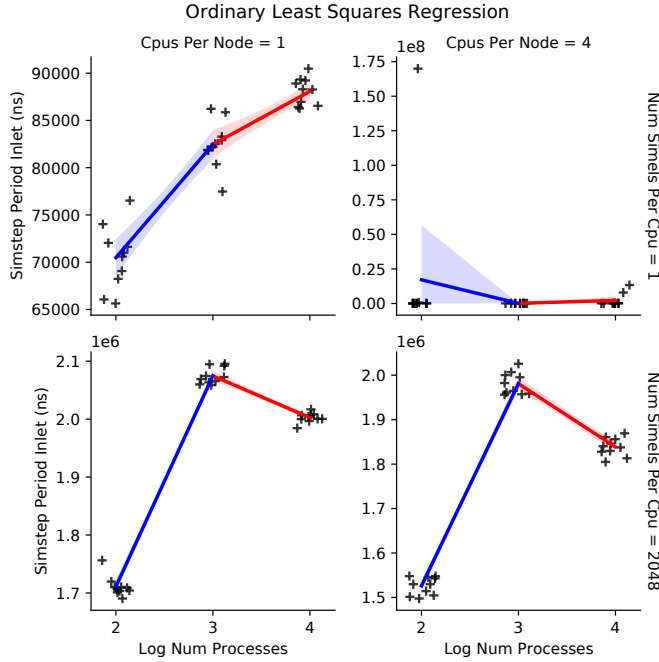
- diversity reserve for digital organisms. Technical Report TR-H-133, ATR.
- Reinders, J. (2007). *Intel threading building blocks: outfitting C++ for multi-core processor parallelism*. " O'Reilly Media, Inc."
- Rhodes, O., Peres, L., Rowley, A. G., Gait, A., Plana, L. A., Brenninkmeijer, C., and Furber, S. B. (2020). Real-time cortical simulation on neuromorphic hardware. *Philosophical Transactions of the Royal Society A*, 378(2164):20190160.
- Scoles, S. (2018). Cosmic ray showers crash supercomputers. here's what to do about it. *Wired*.
- Sridharan, V., DeBardeleben, N., Blanchard, S., Ferreira, K. B., Stearley, J., Shalf, J., and Gurumurthi, S. (2015). Memory errors in modern systems: The good, the bad, and the ugly. *ACM SIGARCH Computer Architecture News*, 43(1):297–310.
- Tang, C., Bouteiller, A., Herault, T., Venkata, M. G., and Bosilca, G. (2014). From mpi to openshmem: Porting lammmps. In *Workshop on OpenSHMEM and Related Technologies*, pages 121–137. Springer.
- Taylor, T., Bedau, M., Channon, A., Ackley, D., Banzhaf, W., Beslon, G., Dolson, E., Froese, T., Hickinbotham, S., Ikegami, T., et al. (2016). Open-ended evolution: Perspectives from the oee workshop in york. *Artificial Life*, 22(3):408–423.
- Teranishi, K. and Heroux, M. A. (2014). Toward local failure local recovery resilience model using mpi-ulfm. In *Proceedings of the 21st European MPI Users' Group Meeting*, pages 51–56.
- Valiant, L. G. (1990). A bridging model for parallel computation. *Communications of the ACM*, 33(8):103–111.
- Vankeirsbilck, J., Hallez, H., and Boydens, J. (2015). Soft error protection in safety critical embedded applications: An overview. In *2015 10th International Conference on P2P, Parallel, Grid, Cloud and Internet Computing (3PGCIC)*, pages 605–610. IEEE.
- Zaman, L., Devangam, S., and Ofria, C. (2011). Rapid host-parasite coevolution drives the production and maintenance of diversity in digital organisms. In *Proceedings of the 13th Annual Conference on Genetic and Evolutionary Computation*, pages 219–226.
- Zhao, X., Papagelis, M., An, A., Chen, B. X., Liu, J., and Hu, Y. (2019). Elastic bulk synchronous parallel model for distributed deep learning. In *2019 IEEE International Conference on Data Mining (ICDM)*, pages 1504–1509. IEEE.



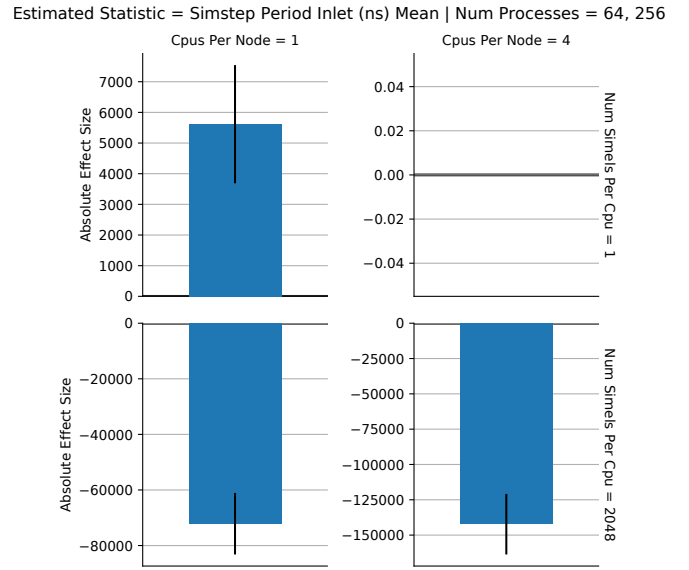
(a) Complete ordinary least squares regression plot. Observations are means per replicate.



(b) Estimated regression coefficient for complete regression. Zero corresponds to no effect.



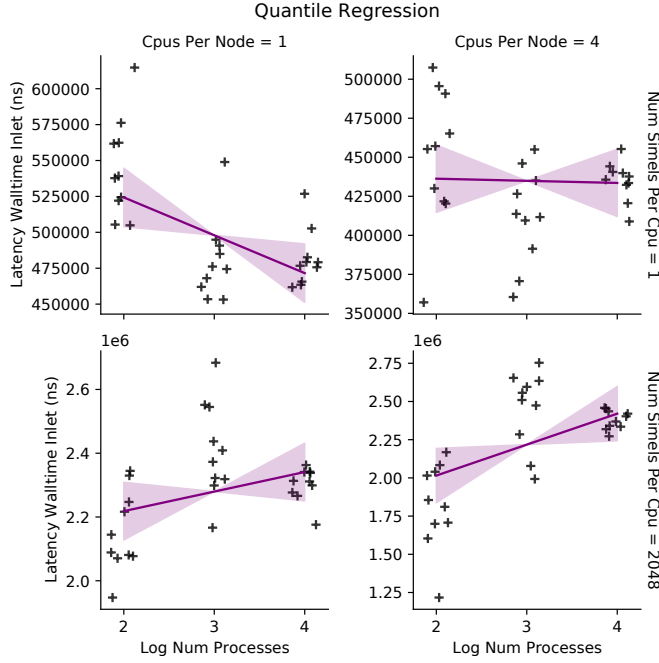
(c) Piecewise ordinary least squares regression plot. Observations are means per replicate.



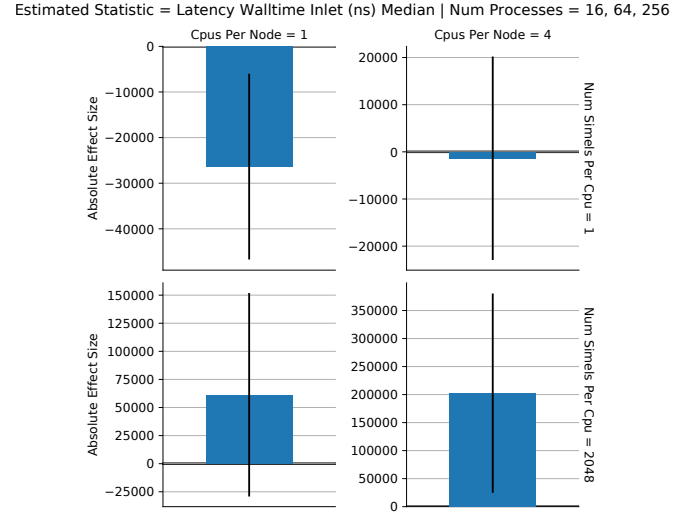
(d) Estimated regression coefficient for rightmost partial regression. Zero corresponds to no effect.

Fig. 4: Ordinary least squares regressions of Simstep Period Inlet (ns) against log processor count for weak scaling experiment (Section III-F). Lower is better. Top row shows complete regression and bottom row shows piecewise regression. Ordinary least squares regression estimates relationship between independent variable and mean of response variable. Error bands and bars are 95% confidence intervals. Note that log is base 4, so processor counts correspond to 16, 64, and 256.

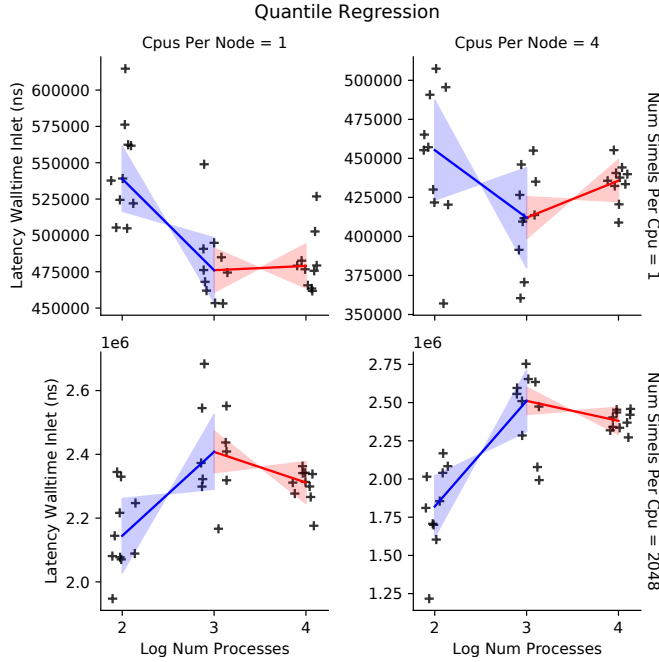




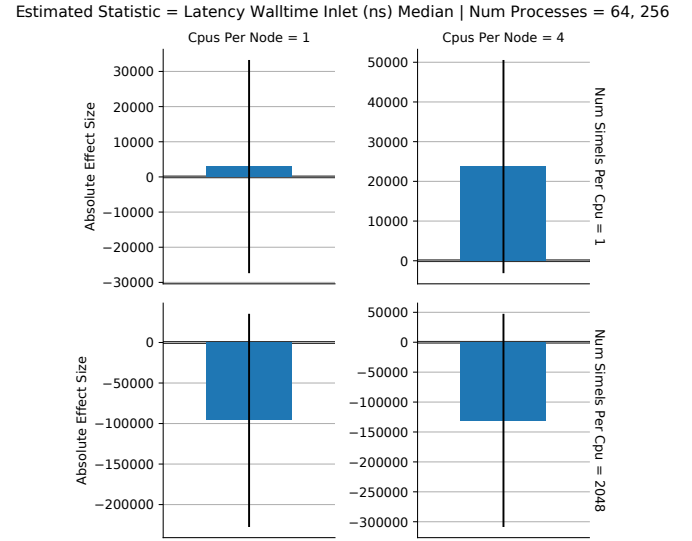
(a) Complete quantile regression plot. Observations are medians per replicate.



(b) Estimated regression coefficient for ordinary least squares regression. Zero corresponds to no effect.

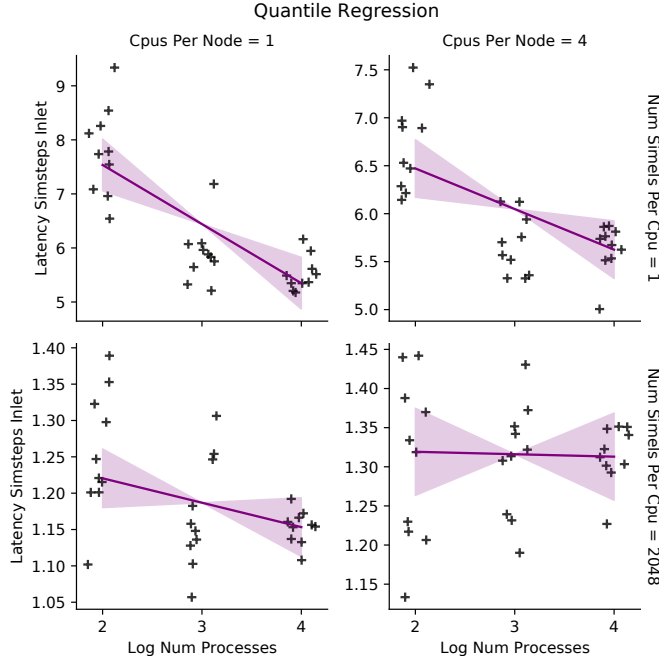


(c) Piecewise quantile regression plot. Observations are medians per replicate.

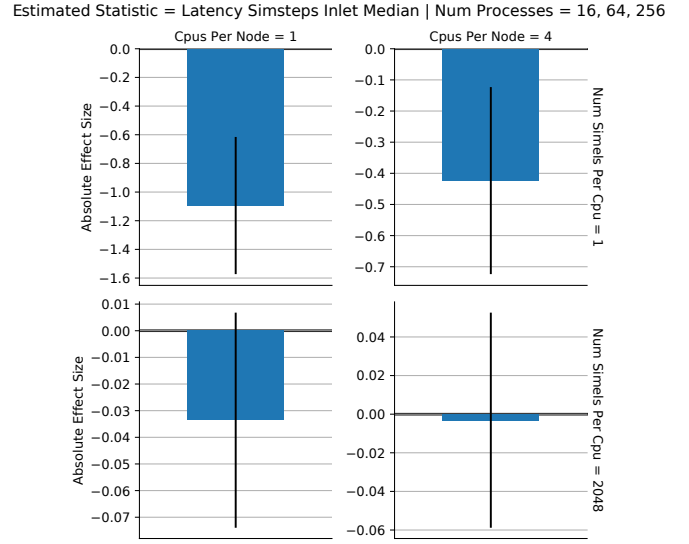


(d) Estimated regression coefficient for rightmost partial regression. Zero corresponds to no effect.

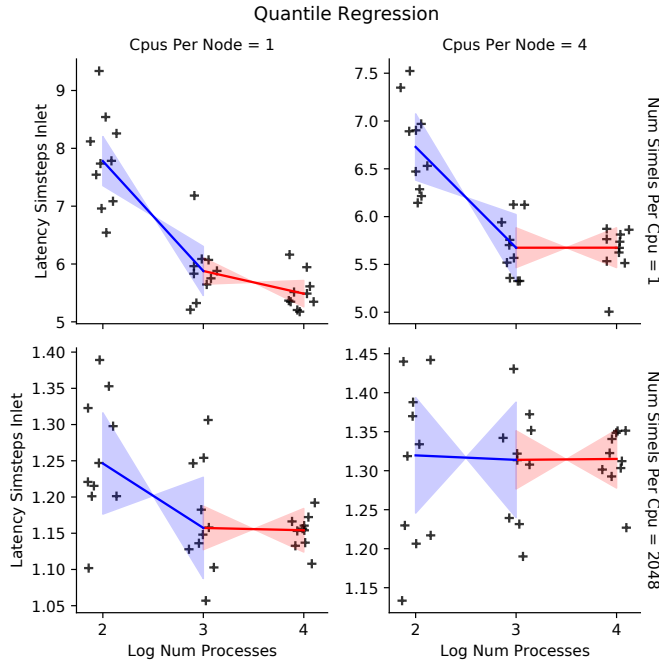
Fig. 5: Quantile Regressions of Latency Walltime Inlet (ns) against log processor count for weak scaling experiment (Section III-F). Lower is better. Top row shows complete regression and bottom row shows piecewise regression. Quantile regression estimates relationship between independent variable and median of response variable. Note that log is base 4, so processor counts correspond to 16, 64, and 256.



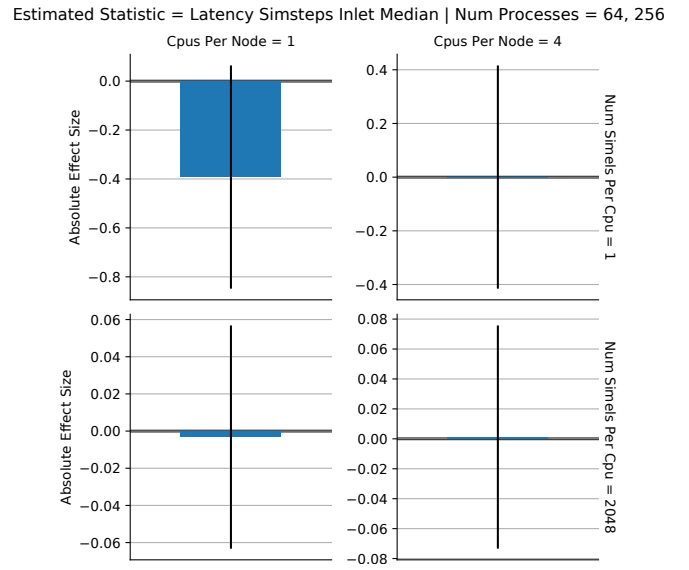
(a) Complete quantile regression plot. Observations are medians per replicate.



(b) Estimated regression coefficient for ordinary least squares regression. Zero corresponds to no effect.

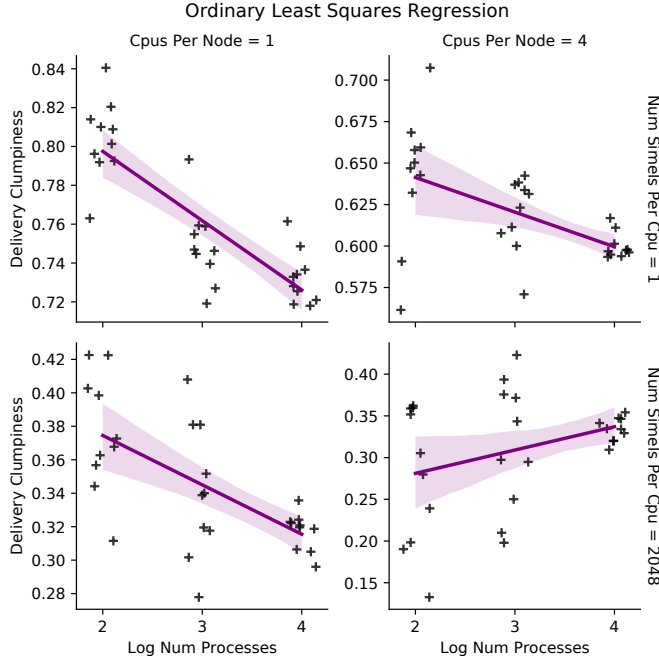


(c) Piecewise quantile regression plot. Observations are medians per replicate.

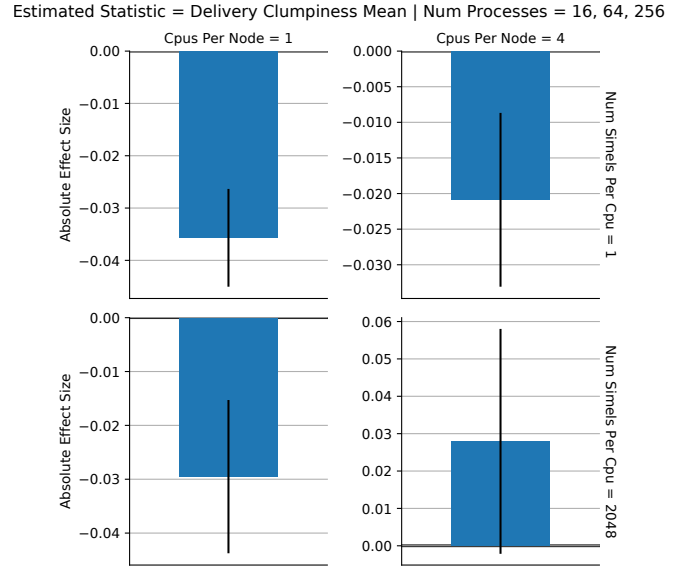


(d) Estimated regression coefficient for rightmost partial regression. Zero corresponds to no effect.

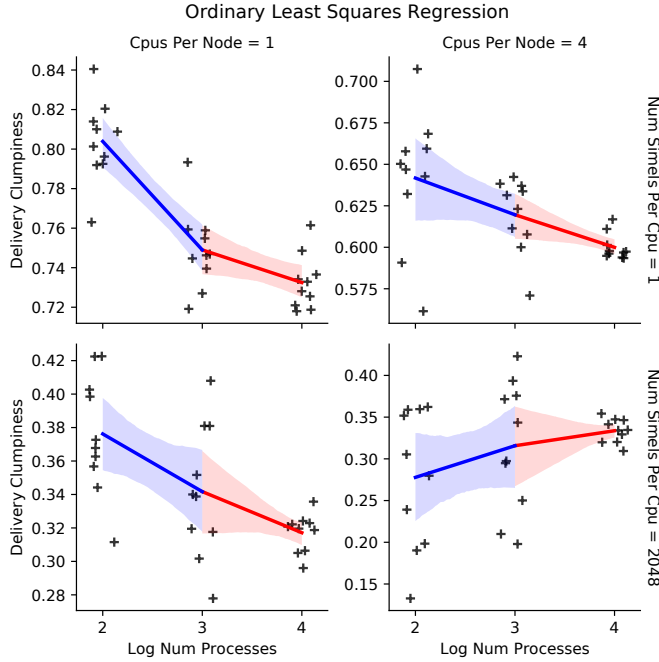
Fig. 6: Quantile Regressions of Latency Simsteps Inlet against log processor count for weak scaling experiment (Section III-F). Lower is better. Top row shows complete regression and bottom row shows piecewise regression. Quantile regression estimates relationship between independent variable and median of response variable. Note that log is base 4, so processor counts correspond to 16, 64, and 256.



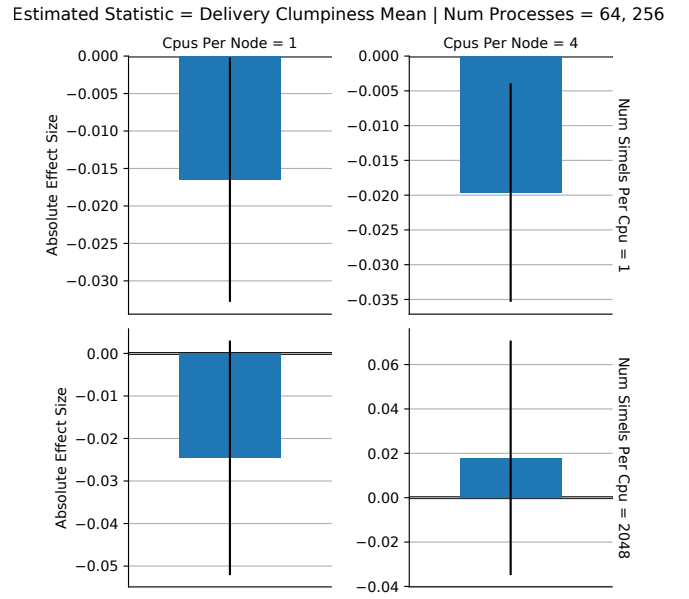
(a) Complete ordinary least squares regression plot. Observations are means per replicate.



(b) Estimated regression coefficient for complete regression. Zero corresponds to no effect.

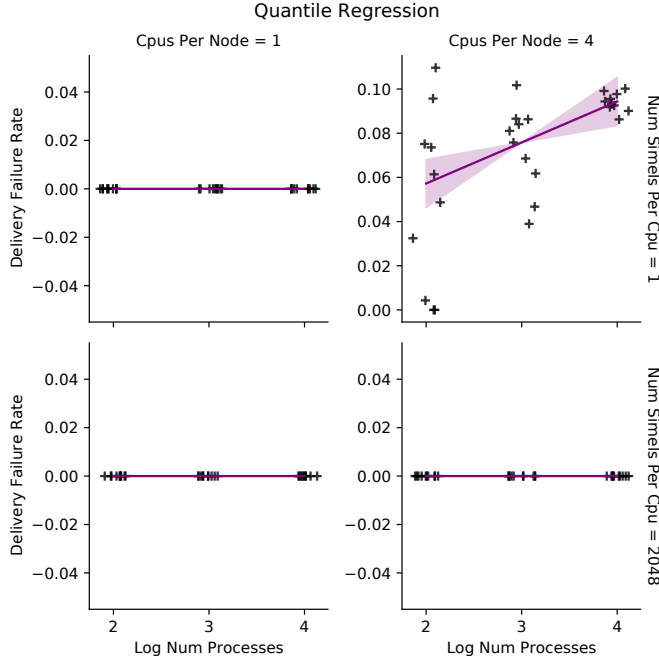


(c) Piecewise ordinary least squares regression plot. Observations are means per replicate.

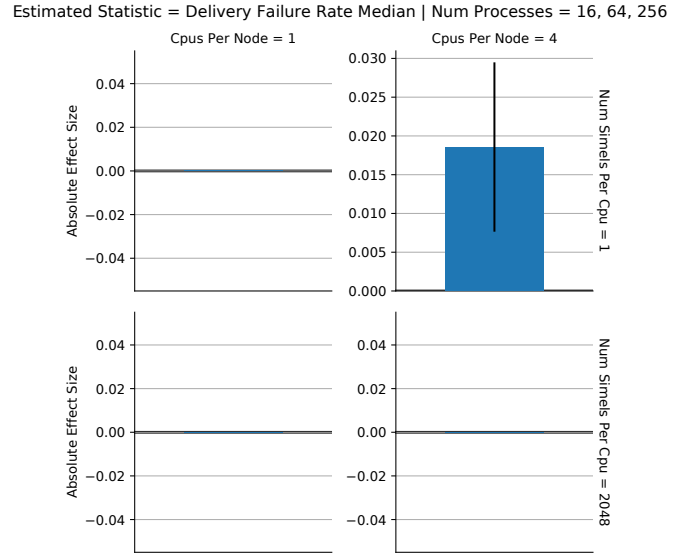


(d) Estimated regression coefficient for rightmost partial regression. Zero corresponds to no effect.

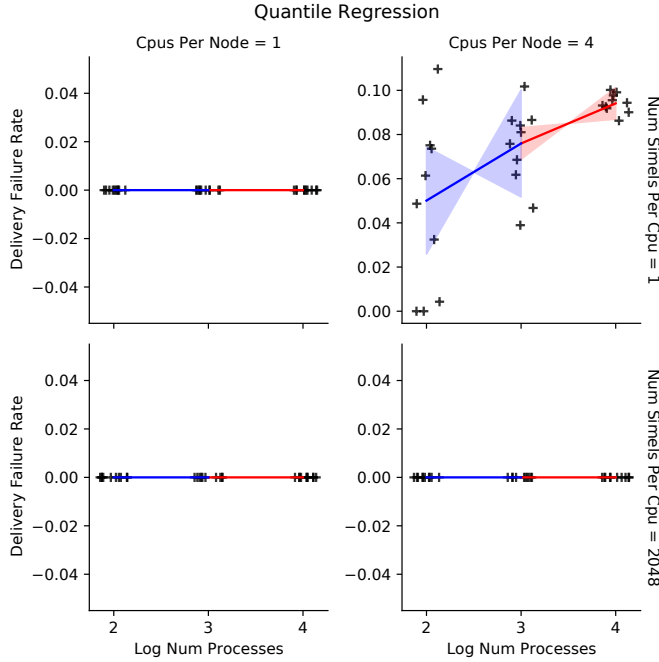
Fig. 7: Ordinary least squares regressions of Delivery Clumpiness against log processor count for weak scaling experiment (Section III-F). Lower is better. Top row shows complete regression and bottom row shows piecewise regression. Ordinary least squares regression estimates relationship between independent variable and mean of response variable. Error bands and bars are 95% confidence intervals. Note that log is base 4, so processor counts correspond to 16, 64, and 256.



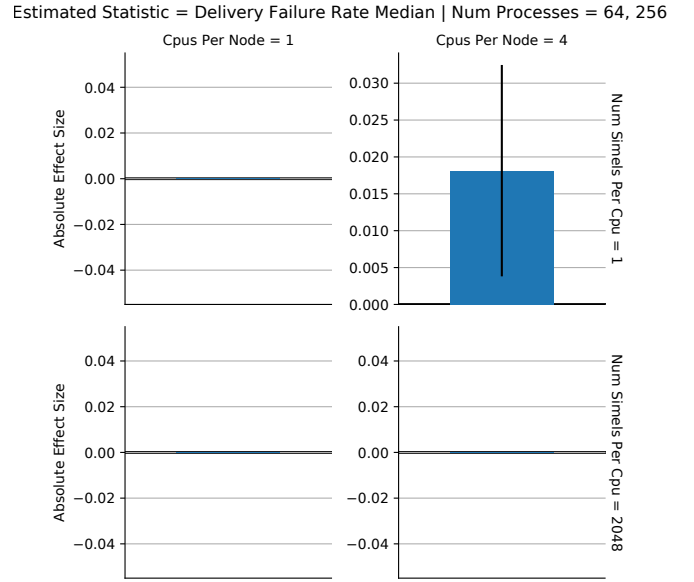
(a) Complete quantile regression plot. Observations are medians per replicate.



(b) Estimated regression coefficient for ordinary least squares regression. Zero corresponds to no effect.



(c) Piecewise quantile regression plot. Observations are medians per replicate.



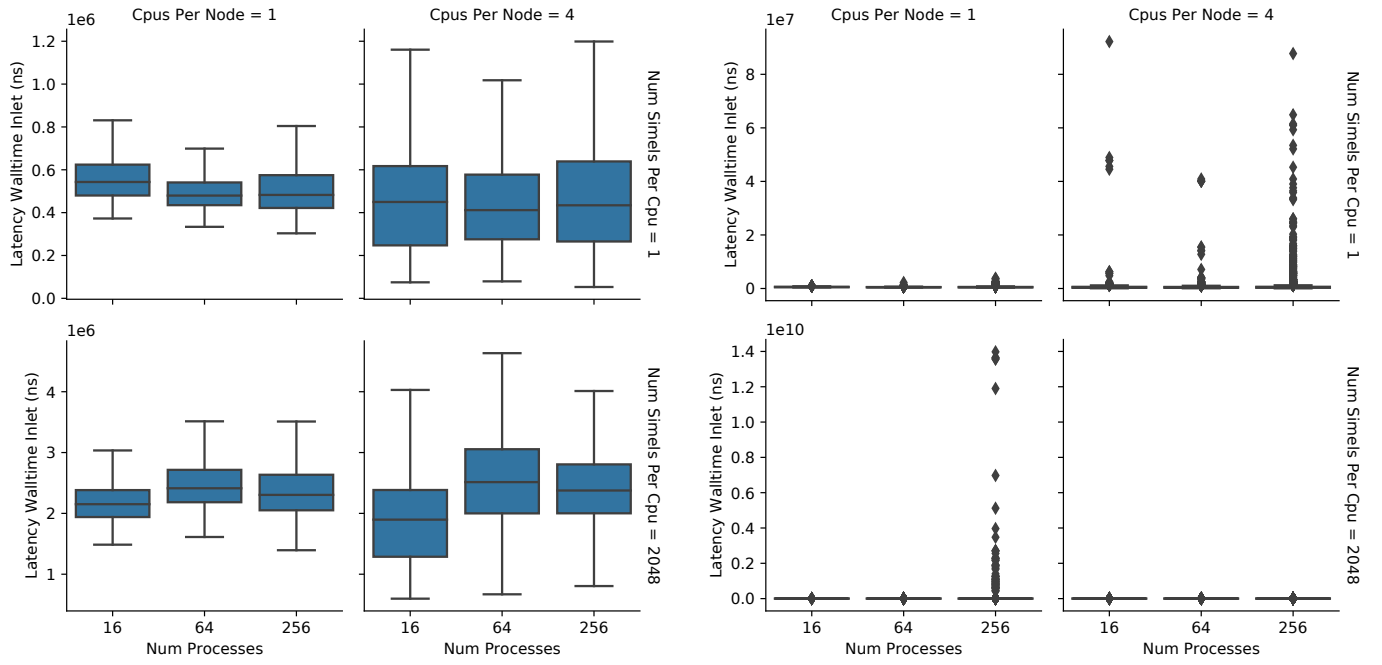
(d) Estimated regression coefficient for rightmost partial regression. Zero corresponds to no effect.

Fig. 8: Quantile Regressions of Delivery Failure Rate against log processor count for weak scaling experiment (Section III-F). Lower is better. Top row shows complete regression and bottom row shows piecewise regression. Quantile regression estimates relationship between independent variable and median of response variable. Note that log is base 4, so processor counts correspond to 16, 64, and 256.

## V. SUPPLEMENTAL MATERIALS

### A. *Weak Scaling*

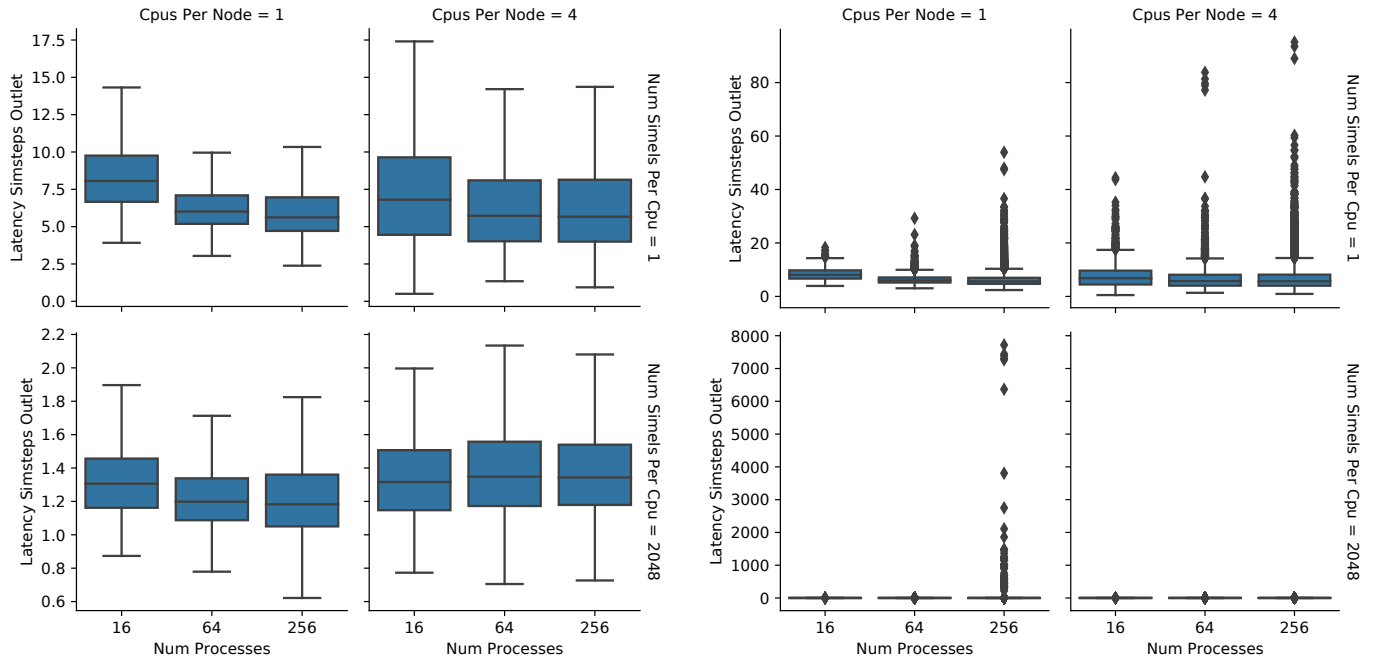
This section provides full results from weak scaling experiments discussed in III-F.



(a) Distribution of Latency Walltime Inlet (ns) for each snapshot, without outliers.

(b) Distribution of Latency Walltime Inlet (ns) for each snapshot, with outliers.

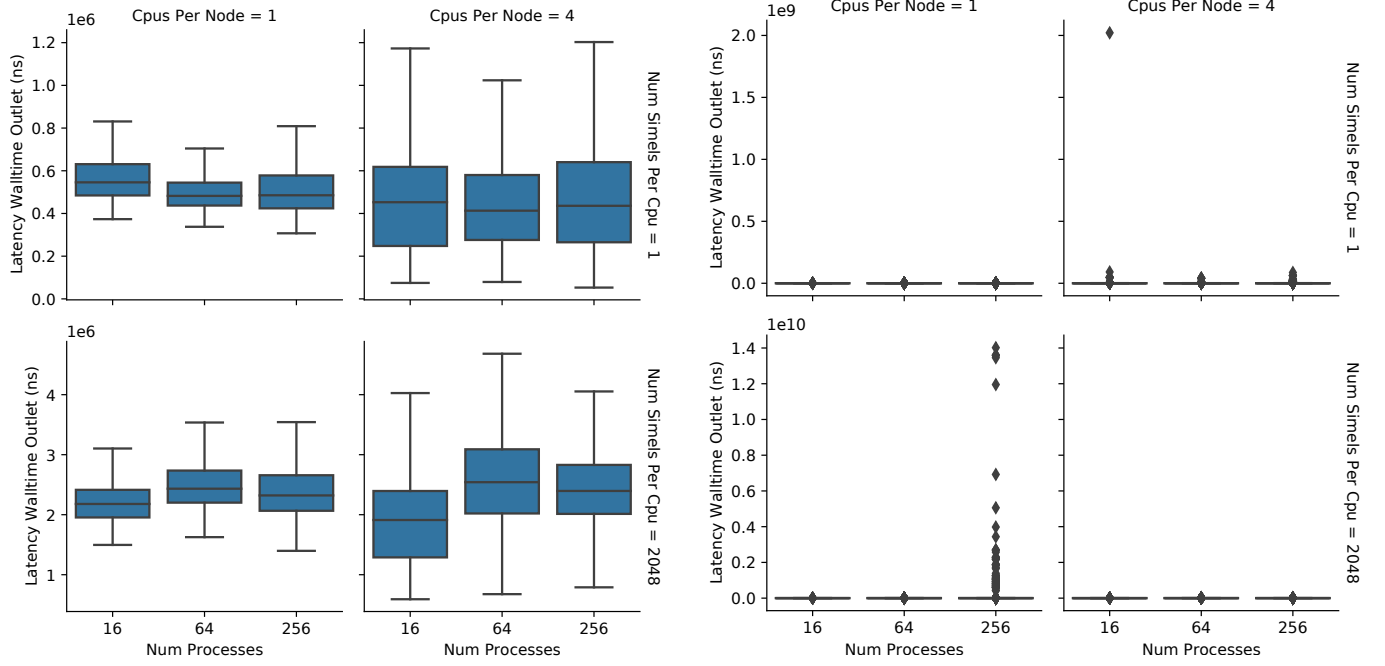
Fig. 9: Distribution of Latency Walltime Inlet (ns) for individual snapshot measurements for weak scaling experiment (Section III-F). Lower is better.



(a) Distribution of Latency Simsteps Outlet for each snapshot, without outliers.

(b) Distribution of Latency Simsteps Outlet for each snapshot, with outliers.

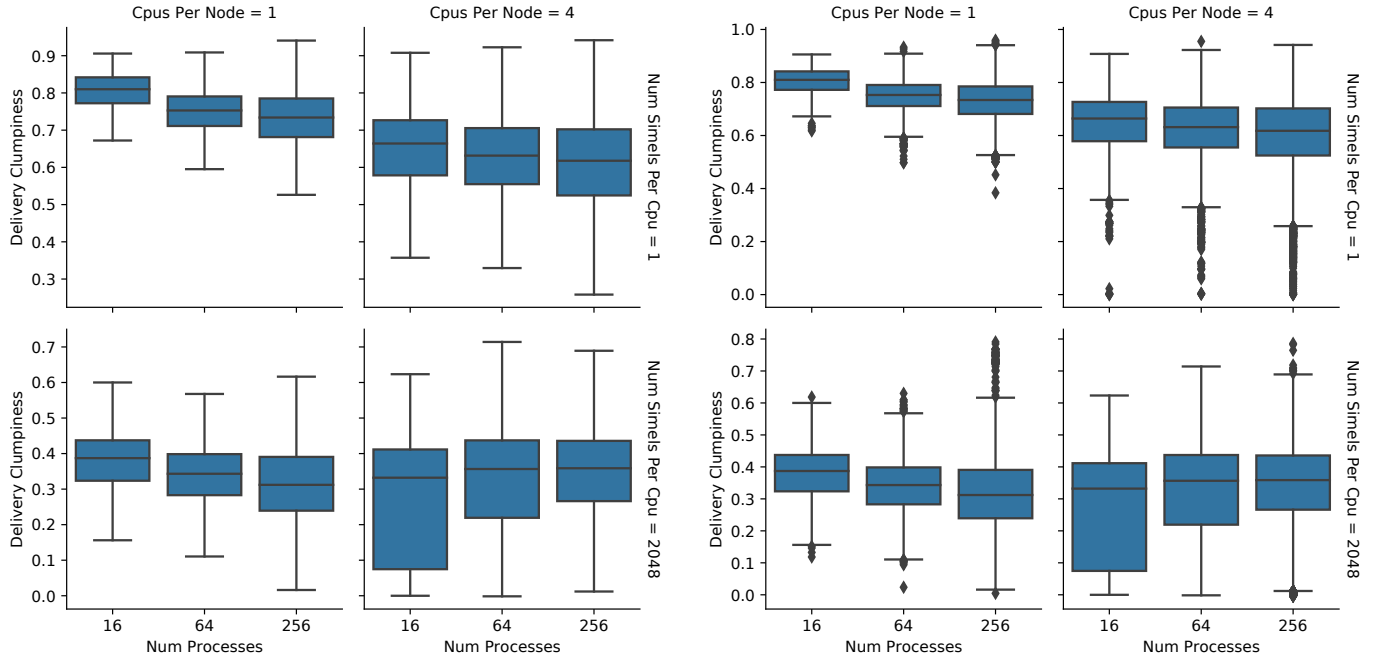
Fig. 10: Distribution of Latency Simsteps Outlet for individual snapshot measurements for weak scaling experiment (Section III-F). Lower is better.



(a) Distribution of Latency Walltime Outlet (ns) for each snapshot, without outliers.

(b) Distribution of Latency Walltime Outlet (ns) for each snapshot, with outliers.

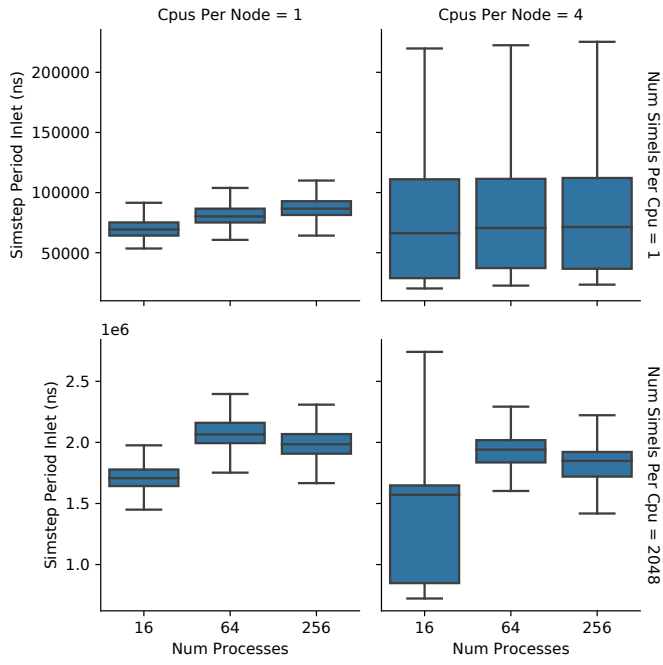
Fig. 11: Distribution of Latency Walltime Outlet (ns) for individual snapshot measurements for weak scaling experiment (Section III-F). Lower is better.



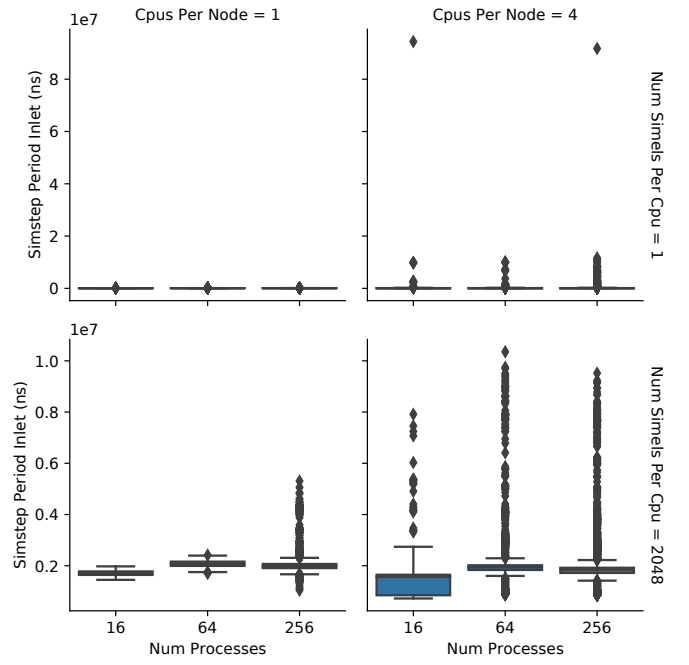
(a) Distribution of Delivery Clumpiness for each snapshot, without outliers.

(b) Distribution of Delivery Clumpiness for each snapshot, with outliers.

Fig. 12: Distribution of Delivery Clumpiness for individual snapshot measurements for weak scaling experiment (Section III-F). Lower is better.

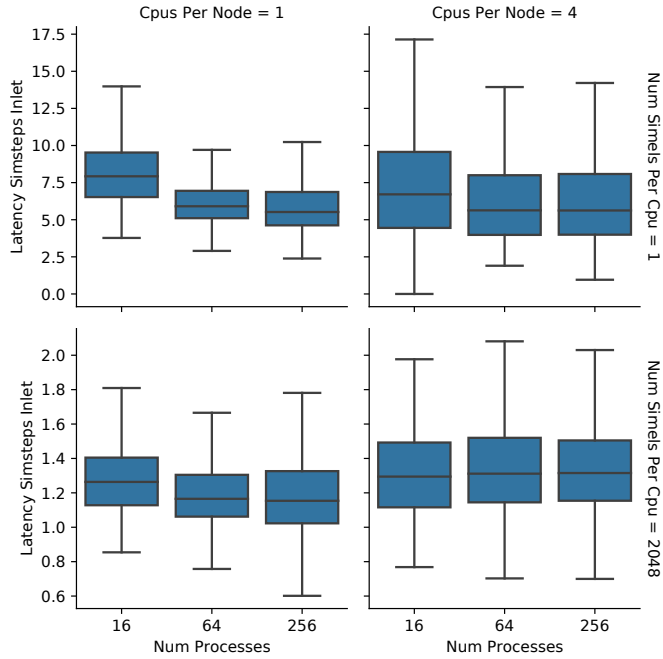


(a) Distribution of Simstep Period Inlet (ns) for each snapshot, without outliers.

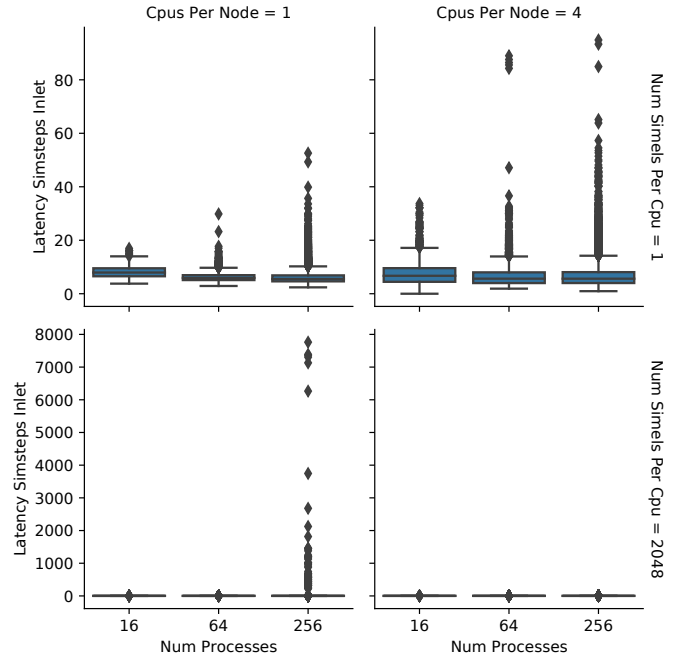


(b) Distribution of Simstep Period Inlet (ns) for each snapshot, with outliers.

Fig. 13: Distribution of Simstep Period Inlet (ns) for individual snapshot measurements for weak scaling experiment (Section III-F). Lower is better.



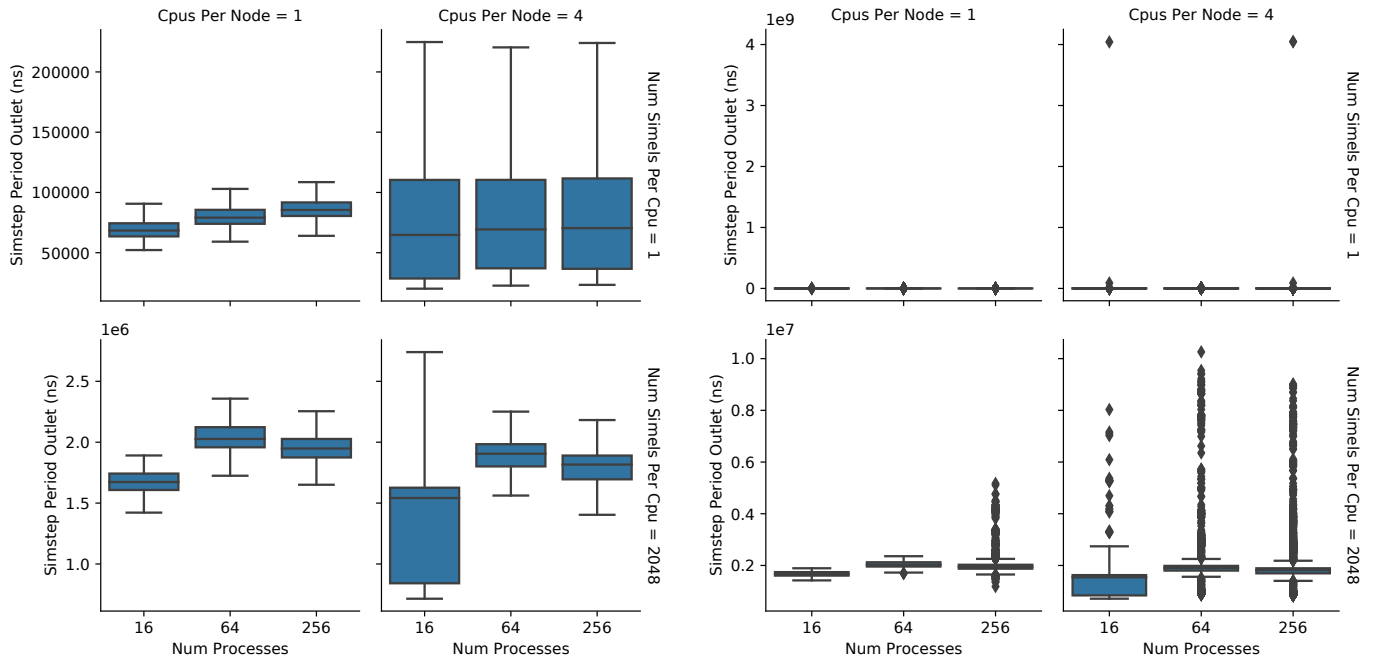
(a) Distribution of Latency Simsteps Inlet for each snapshot, without outliers.



(b) Distribution of Latency Simsteps Inlet for each snapshot, with outliers.

Fig. 14: Distribution of Latency Simsteps Inlet for individual snapshot measurements for weak scaling experiment (Section III-F). Lower is better.

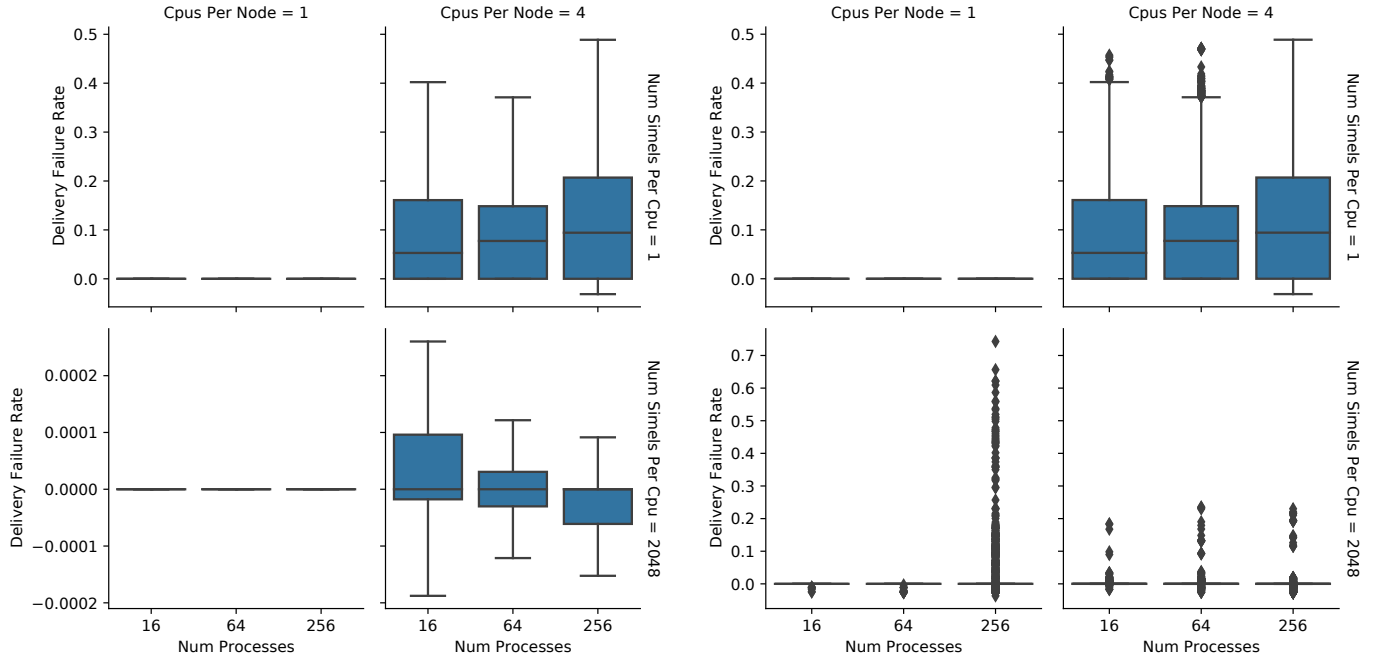




(a) Distribution of Simstep Period Outlet (ns) for each snapshot, without outliers.

(b) Distribution of Simstep Period Outlet (ns) for each snapshot, with outliers.

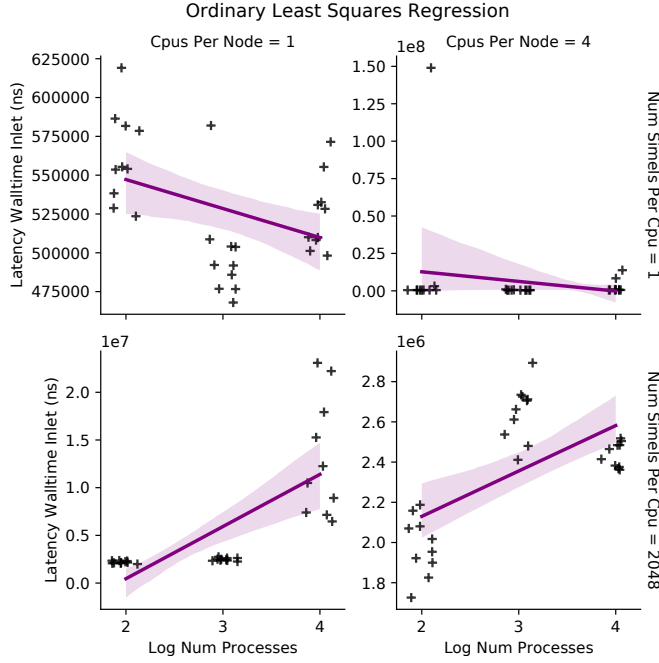
Fig. 15: Distribution of Simstep Period Outlet (ns) for individual snapshot measurements for weak scaling experiment (Section III-F). Lower is better.



(a) Distribution of Delivery Failure Rate for each snapshot, without outliers.

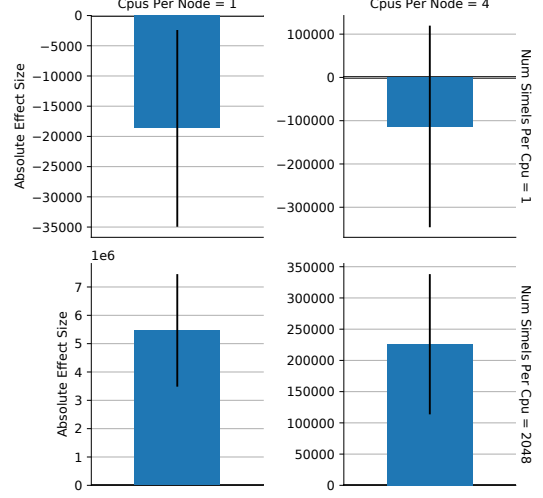
(b) Distribution of Delivery Failure Rate for each snapshot, with outliers.

Fig. 16: Distribution of Delivery Failure Rate for individual snapshot measurements for weak scaling experiment (Section III-F). Lower is better.

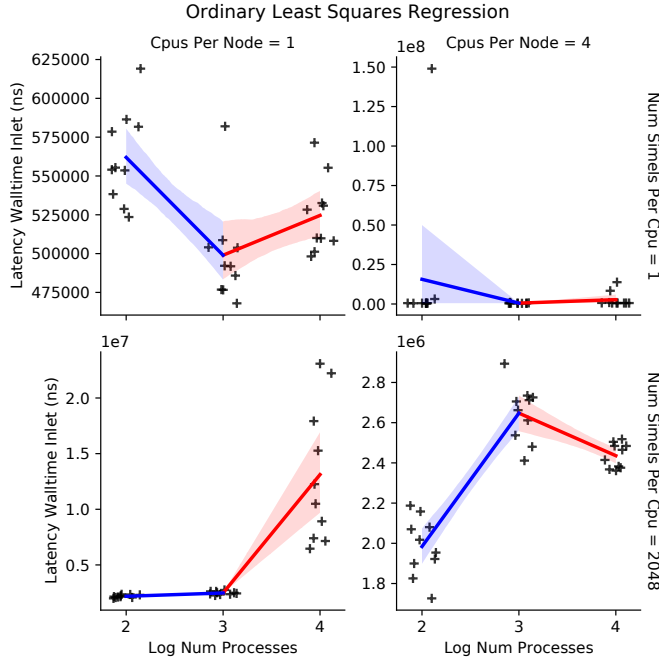


(a) Complete ordinary least squares regression plot. Observations are means per replicate.

Estimated Statistic = Latency Walltime Inlet (ns) Mean | Num Processes = 16, 64, 256

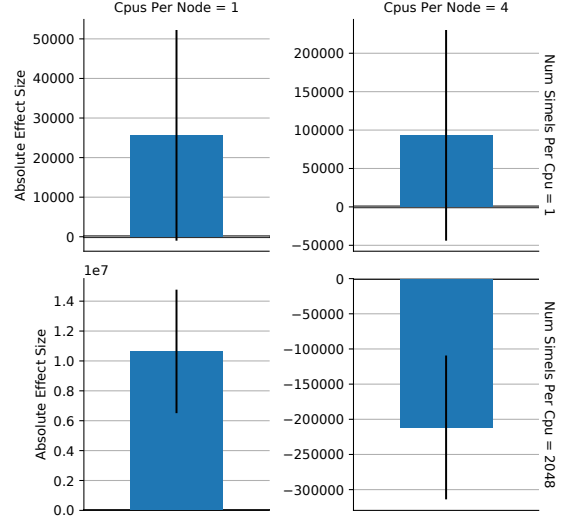


(b) Estimated regression coefficient for complete regression. Zero corresponds to no effect.



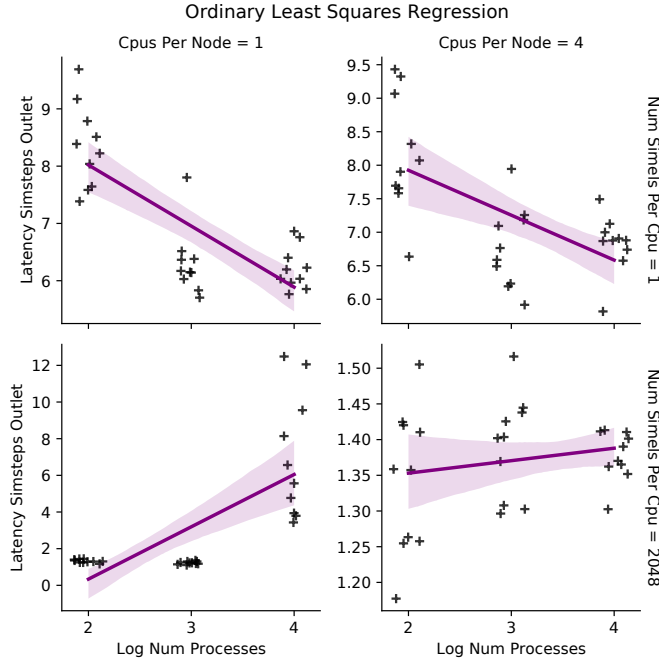
(c) Piecewise ordinary least squares regression plot. Observations are means per replicate.

Estimated Statistic = Latency Walltime Inlet (ns) Mean | Num Processes = 64, 256

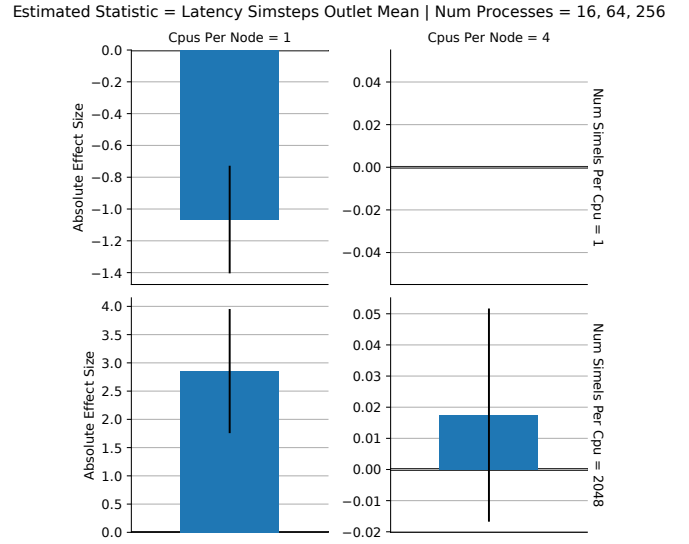


(d) Estimated regression coefficient for rightmost partial regression. Zero corresponds to no effect.

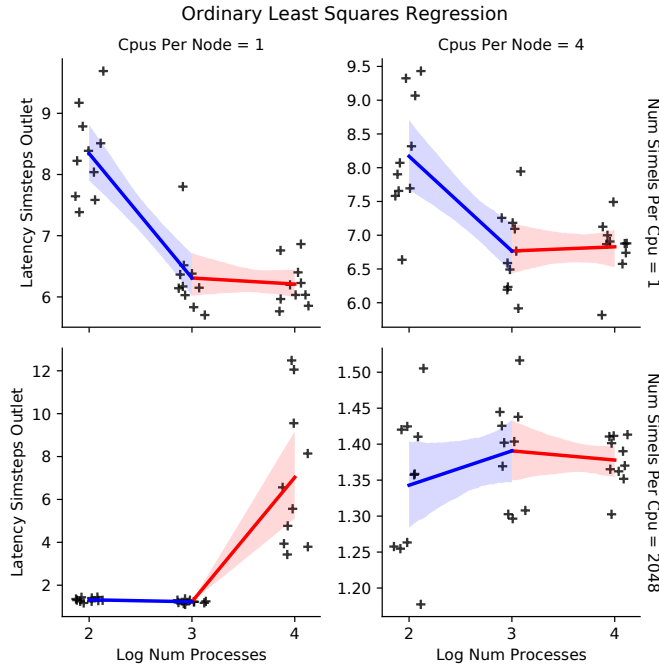
Fig. 17: Ordinary least squares regressions of Latency Walltime Inlet (ns) against log processor count for weak scaling experiment (Section III-F). Lower is better. Top row shows complete regression and bottom row shows piecewise regression. Ordinary least squares regression estimates relationship between independent variable and mean of response variable. Error bands and bars are 95% confidence intervals. Note that log is base 4, so processor counts correspond to 16, 64, and 256.



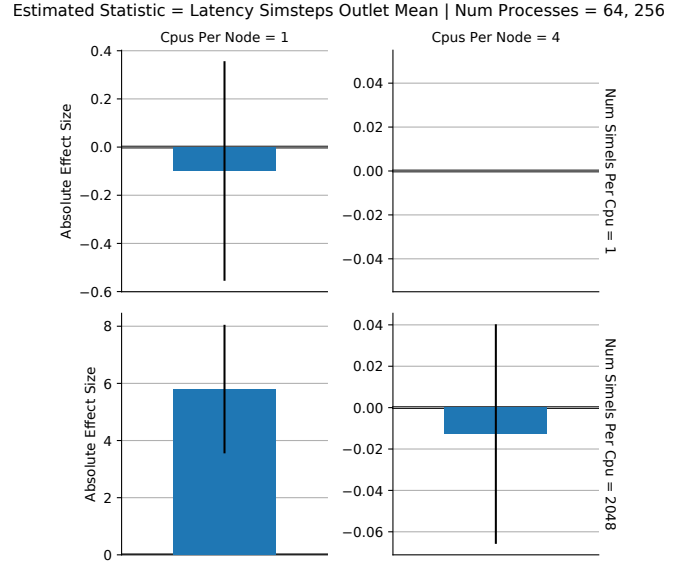
(a) Complete ordinary least squares regression plot. Observations are means per replicate.



(b) Estimated regression coefficient for complete regression. Zero corresponds to no effect.

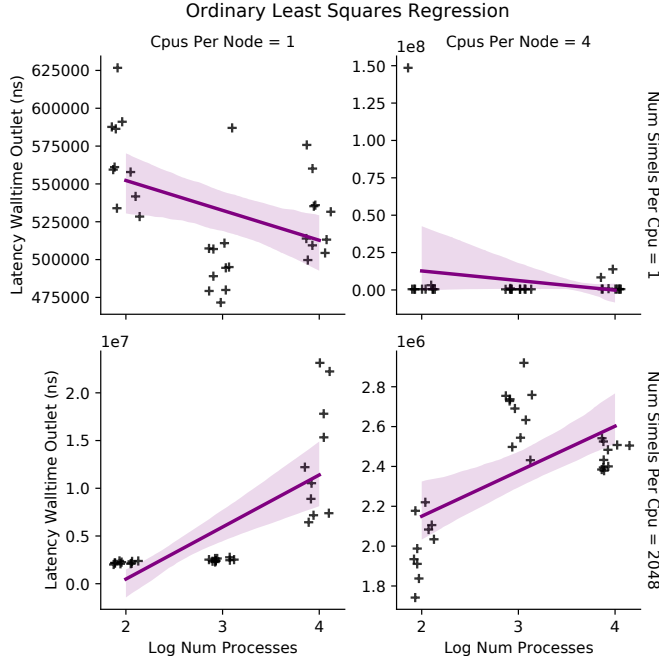


(c) Piecewise ordinary least squares regression plot. Observations are means per replicate.



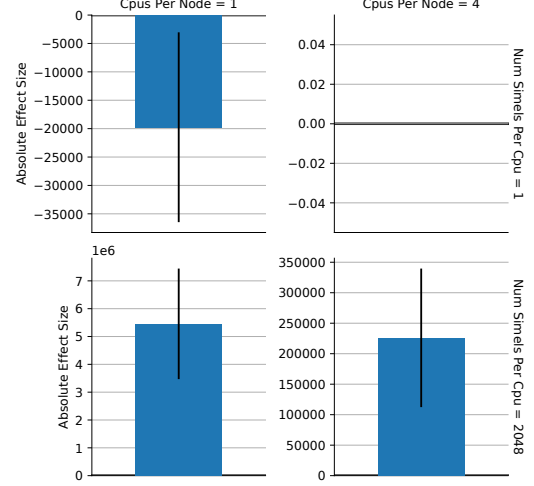
(d) Estimated regression coefficient for rightmost partial regression. Zero corresponds to no effect.

Fig. 18: Ordinary least squares regressions of Latency Simsteps Outlet against log processor count for weak scaling experiment (Section III-F). Lower is better. Top row shows complete regression and bottom row shows piecewise regression. Ordinary least squares regression estimates relationship between independent variable and mean of response variable. Error bands and bars are 95% confidence intervals. Note that log is base 4, so processor counts correspond to 16, 64, and 256.

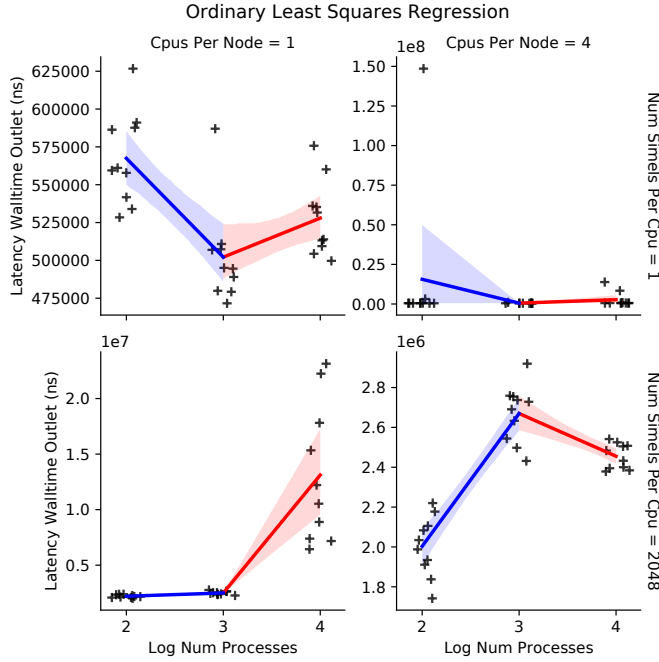


(a) Complete ordinary least squares regression plot. Observations are means per replicate.

Estimated Statistic = Latency Walltime Outlet (ns) Mean | Num Processes = 16, 64, 256

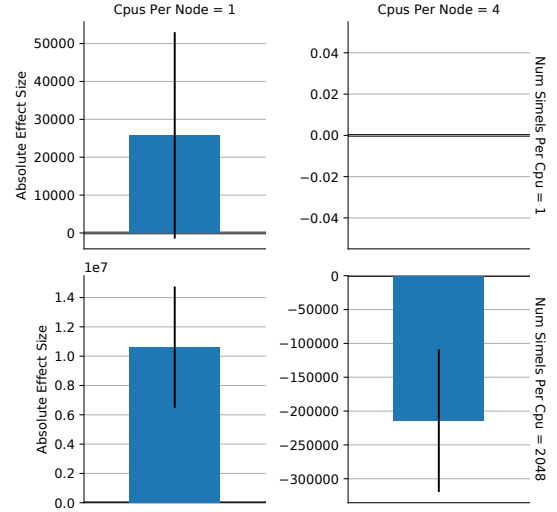


(b) Estimated regression coefficient for complete regression. Zero corresponds to no effect.



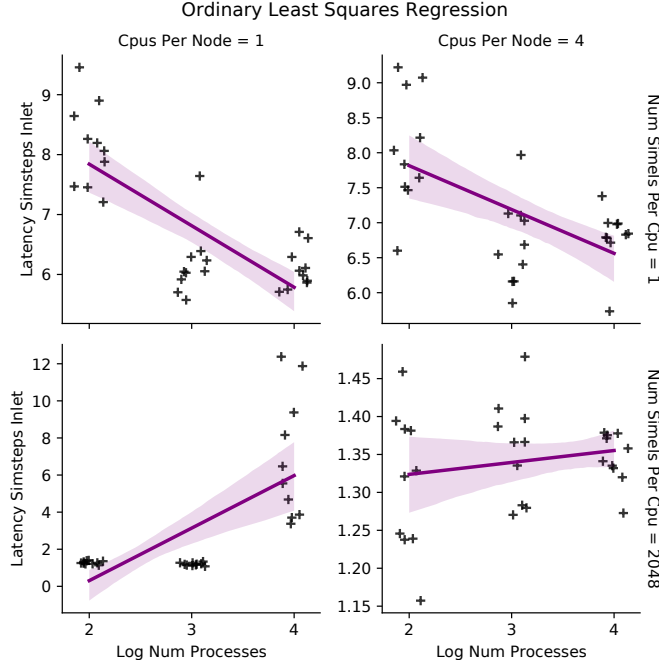
(c) Piecewise ordinary least squares regression plot. Observations are means per replicate.

Estimated Statistic = Latency Walltime Outlet (ns) Mean | Num Processes = 64, 256



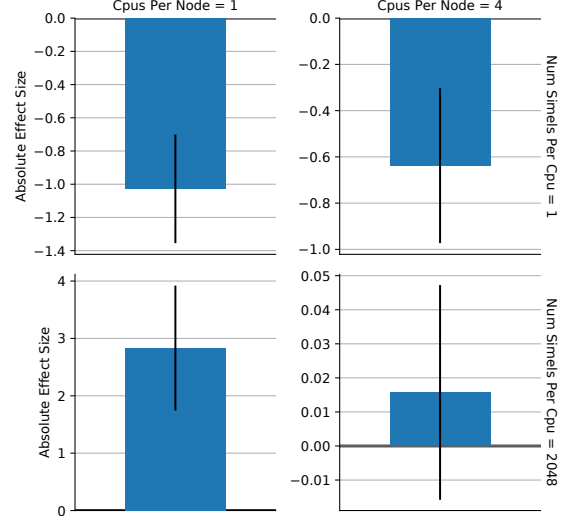
(d) Estimated regression coefficient for rightmost partial regression. Zero corresponds to no effect.

Fig. 19: Ordinary least squares regressions of Latency Walltime Outlet (ns) against log processor count for weak scaling experiment (Section III-F). Lower is better. Top row shows complete regression and bottom row shows piecewise regression. Ordinary least squares regression estimates relationship between independent variable and mean of response variable. Error bands and bars are 95% confidence intervals. Note that log is base 4, so processor counts correspond to 16, 64, and 256.

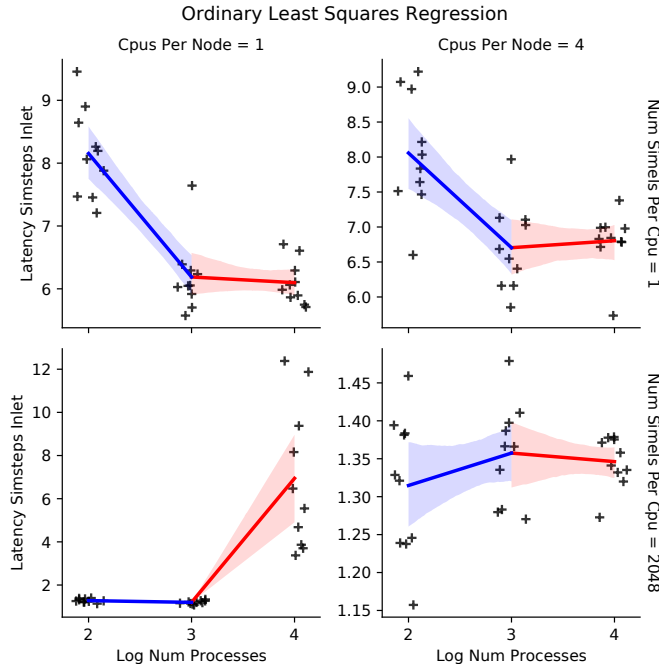


(a) Complete ordinary least squares regression plot. Observations are means per replicate.

Estimated Statistic = Latency Simsteps Inlet Mean | Num Processes = 16, 64, 256

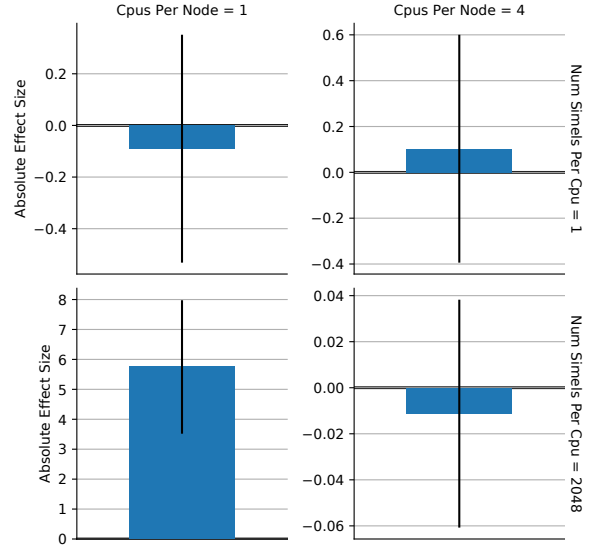


(b) Estimated regression coefficient for complete regression. Zero corresponds to no effect.



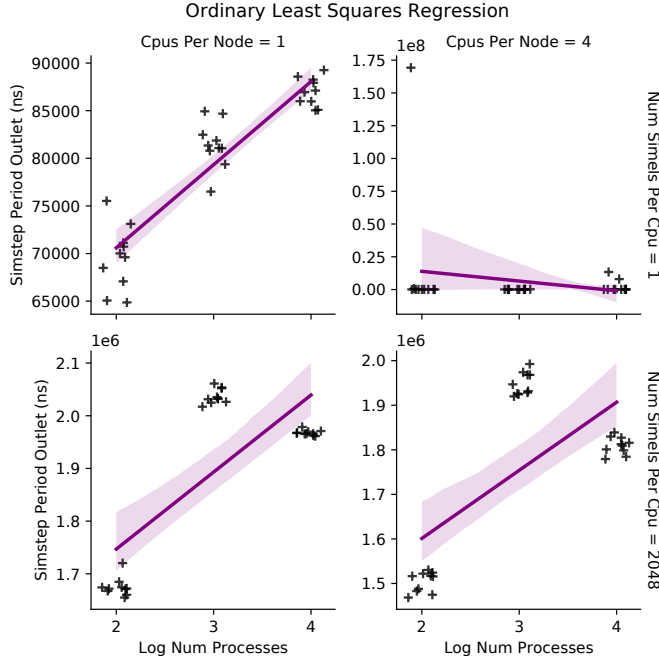
(c) Piecewise ordinary least squares regression plot. Observations are means per replicate.

Estimated Statistic = Latency Simsteps Inlet Mean | Num Processes = 64, 256

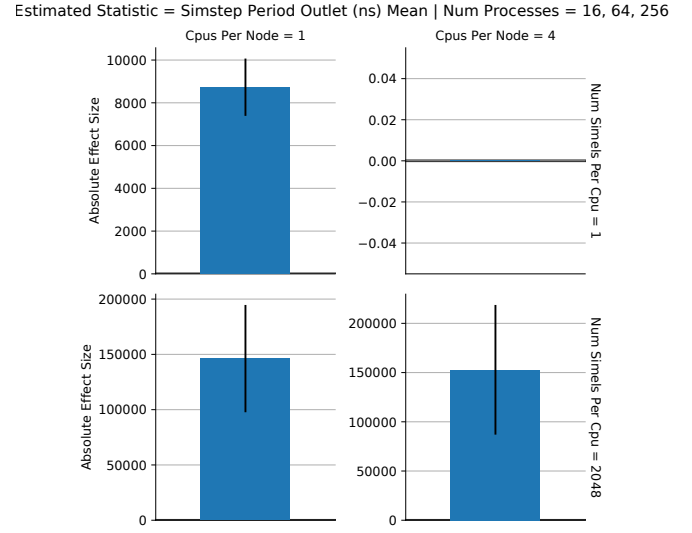


(d) Estimated regression coefficient for rightmost partial regression. Zero corresponds to no effect.

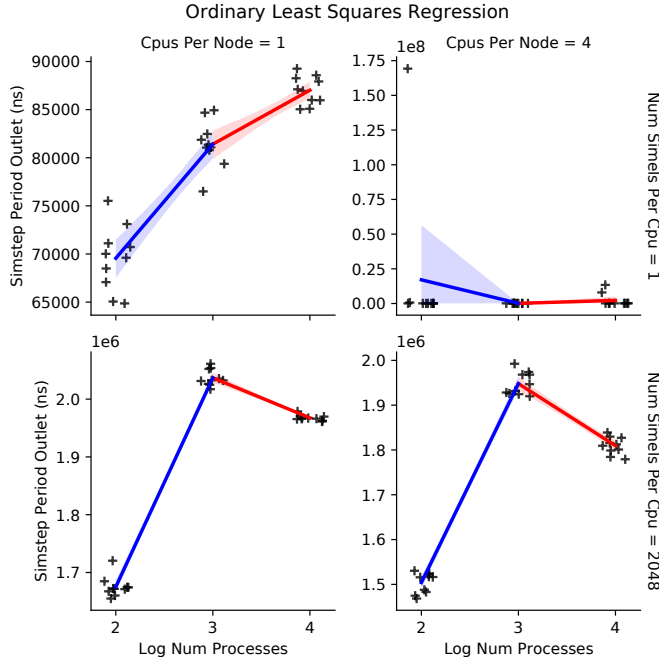
Fig. 20: Ordinary least squares regressions of Latency Simsteps Inlet against log processor count for weak scaling experiment (Section III-F). Lower is better. Top row shows complete regression and bottom row shows piecewise regression. Ordinary least squares regression estimates relationship between independent variable and mean of response variable. Error bands and bars are 95% confidence intervals. Note that log is base 4, so processor counts correspond to 16, 64, and 256.



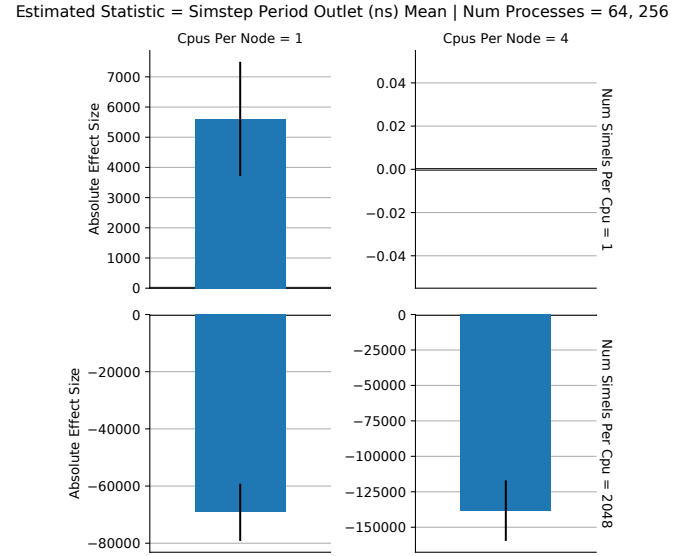
(a) Complete ordinary least squares regression plot. Observations are means per replicate.



(b) Estimated regression coefficient for complete regression. Zero corresponds to no effect.

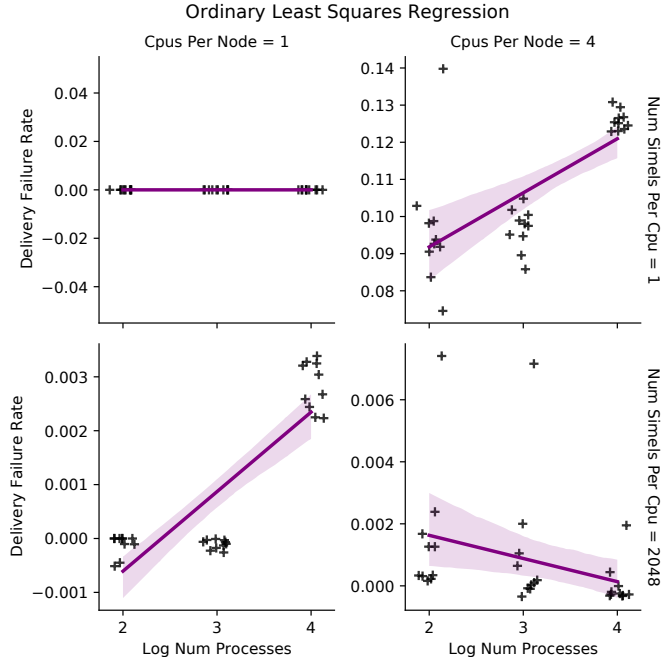


(c) Piecewise ordinary least squares regression plot. Observations are means per replicate.

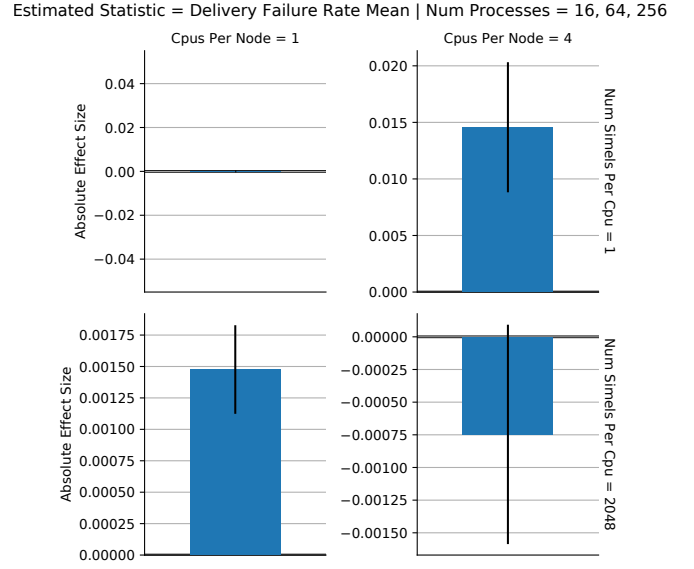


(d) Estimated regression coefficient for rightmost partial regression. Zero corresponds to no effect.

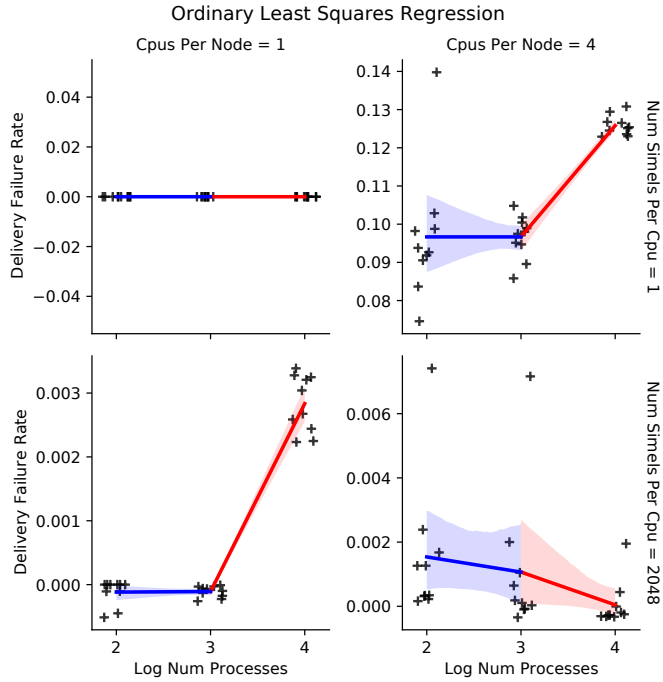
Fig. 21: Ordinary least squares regressions of Simstep Period Outlet (ns) against log processor count for weak scaling experiment (Section III-F). Lower is better. Top row shows complete regression and bottom row shows piecewise regression. Ordinary least squares regression estimates relationship between independent variable and mean of response variable. Error bands and bars are 95% confidence intervals. Note that log is base 4, so processor counts correspond to 16, 64, and 256.



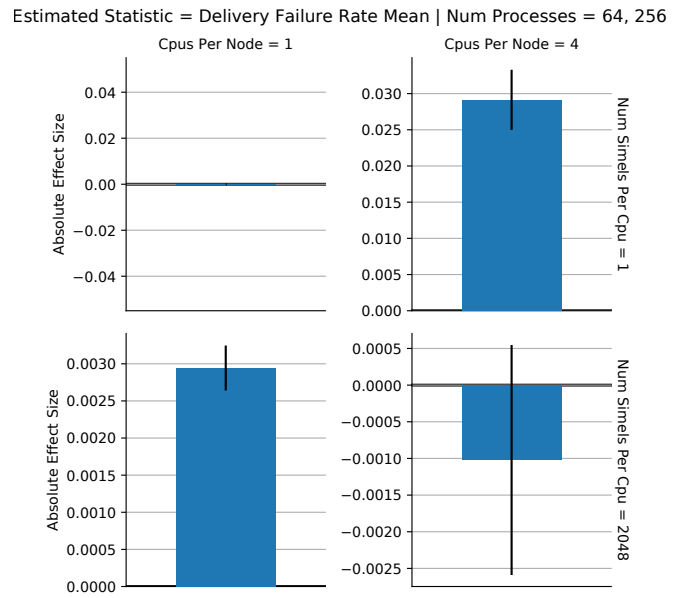
(a) Complete ordinary least squares regression plot. Observations are means per replicate.



(b) Estimated regression coefficient for complete regression. Zero corresponds to no effect.

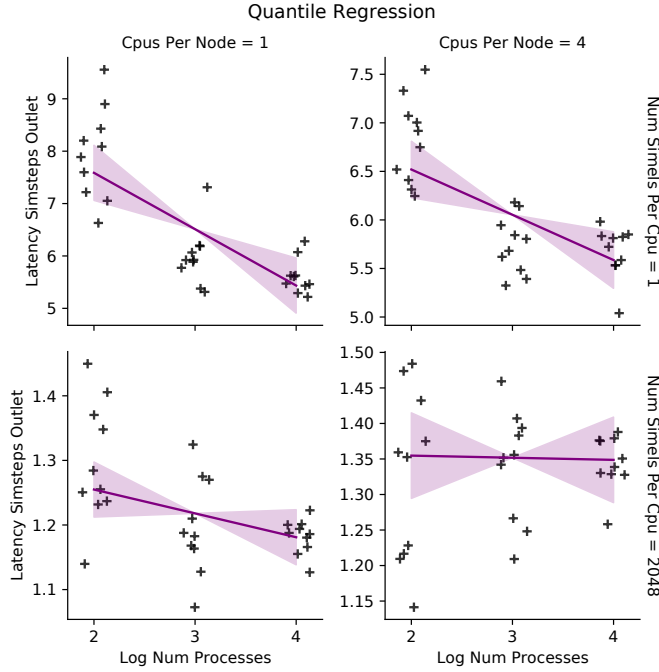


(c) Piecewise ordinary least squares regression plot. Observations are means per replicate.



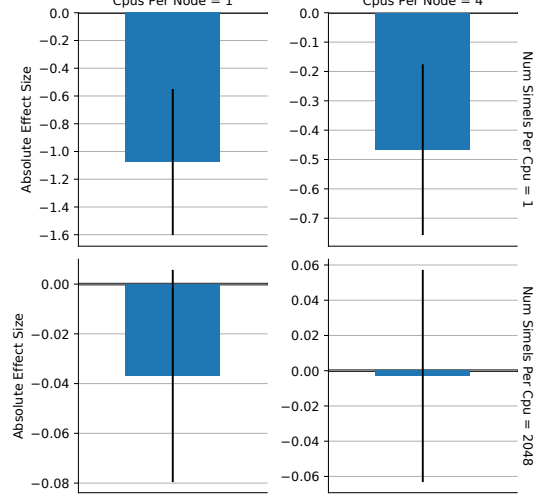
(d) Estimated regression coefficient for rightmost partial regression. Zero corresponds to no effect.

Fig. 22: Ordinary least squares regressions of Delivery Failure Rate against log processor count for weak scaling experiment (Section III-F). Lower is better. Top row shows complete regression and bottom row shows piecewise regression. Ordinary least squares regression estimates relationship between independent variable and mean of response variable. Error bands and bars are 95% confidence intervals. Note that log is base 4, so processor counts correspond to 16, 64, and 256.

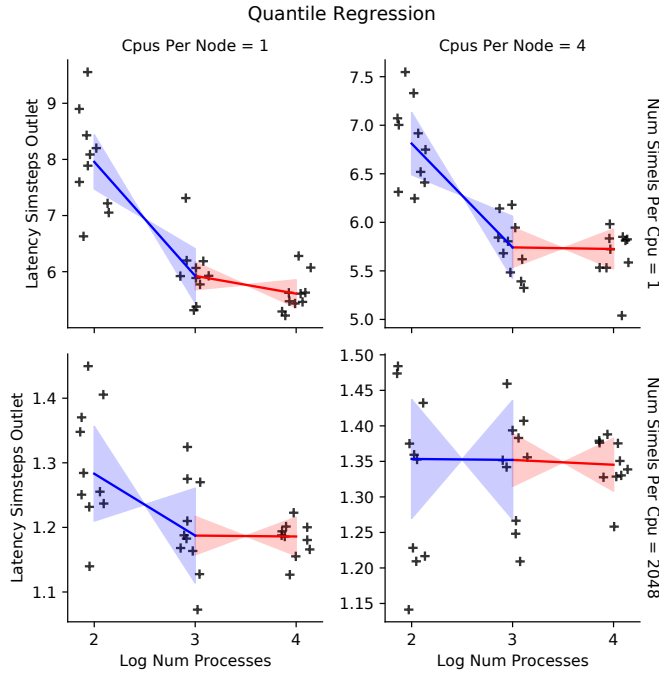


(a) Complete quantile regression plot. Observations are medians per replicate.

Estimated Statistic = Latency Simsteps Outlet Median | Num Processes = 16, 64, 256

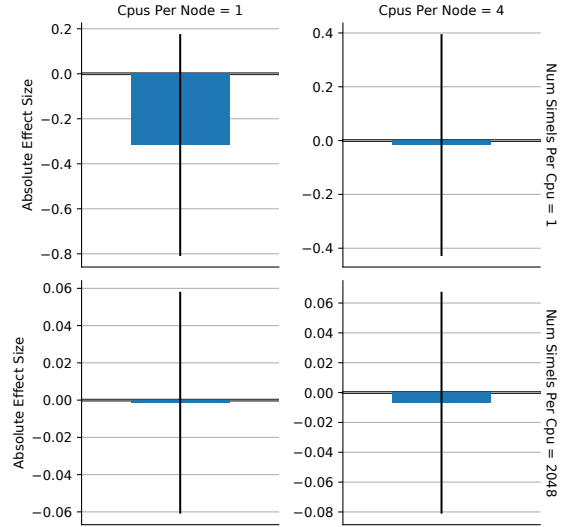


(b) Estimated regression coefficient for ordinary least squares regression. Zero corresponds to no effect.



(c) Piecewise quantile regression plot. Observations are medians per replicate.

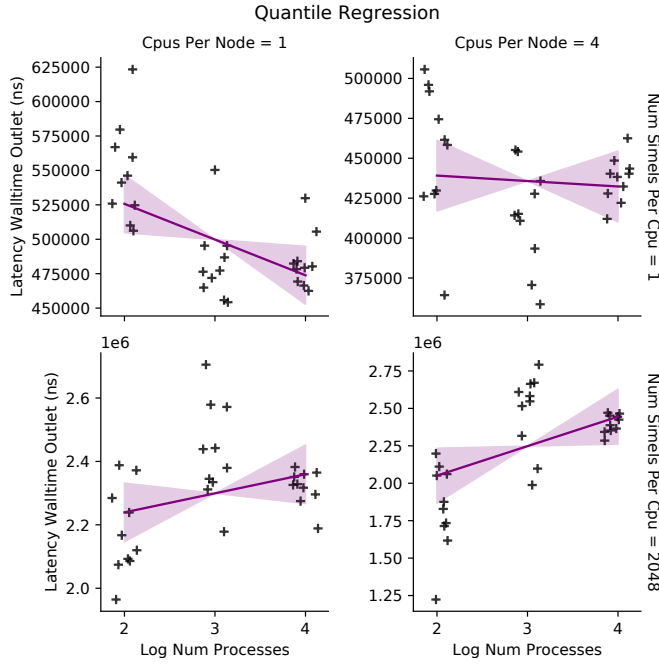
Estimated Statistic = Latency Simsteps Outlet Median | Num Processes = 64, 256



(d) Estimated regression coefficient for rightmost partial regression. Zero corresponds to no effect.

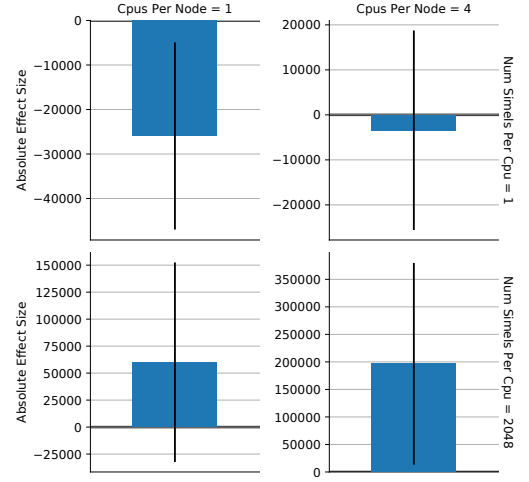
Fig. 23: Quantile Regressions of Latency Simsteps Outlet against log processor count for weak scaling experiment (Section III-F). Lower is better. Top row shows complete regression and bottom row shows piecewise regression. Quantile regression estimates relationship between independent variable and median of response variable. Note that log is base 4, so processor counts correspond to 16, 64, and 256.



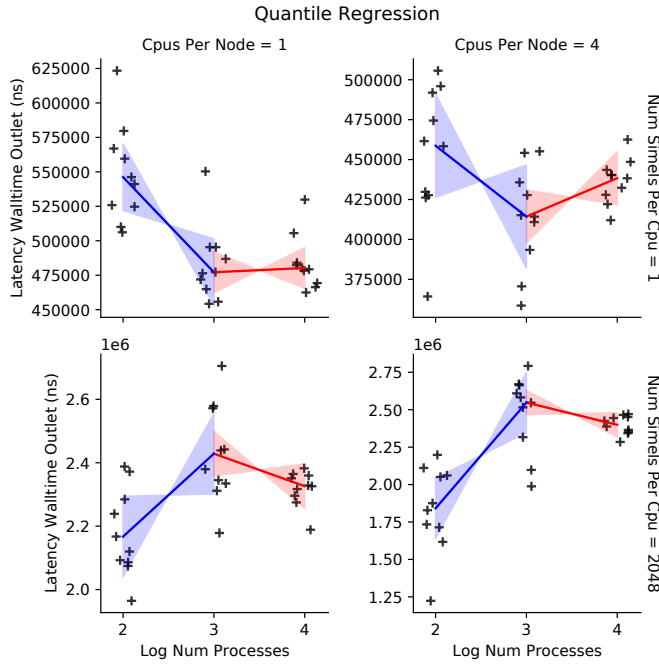


(a) Complete quantile regression plot. Observations are medians per replicate.

Estimated Statistic = Latency Walltime Outlet (ns) Median | Num Processes = 16, 64, 256

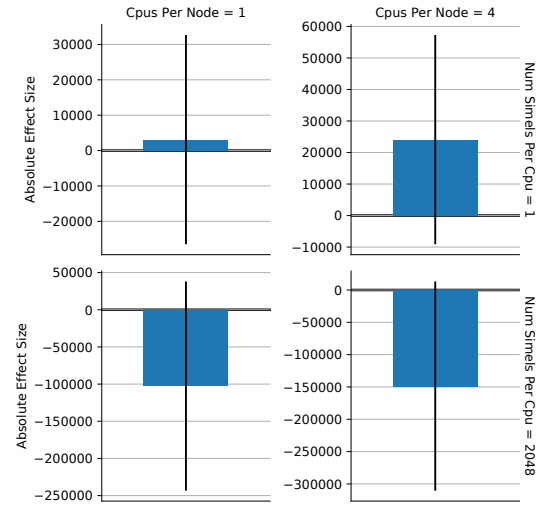


(b) Estimated regression coefficient for ordinary least squares regression. Zero corresponds to no effect.



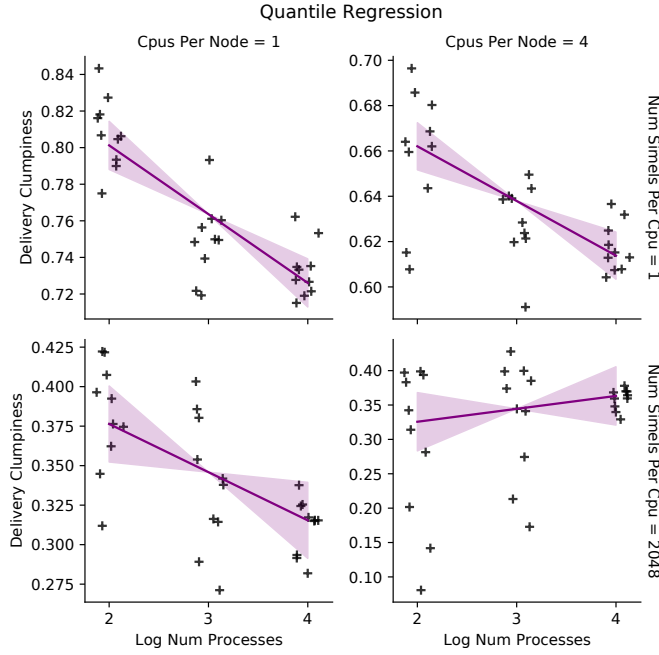
(c) Piecewise quantile regression plot. Observations are medians per replicate.

Estimated Statistic = Latency Walltime Outlet (ns) Median | Num Processes = 64, 256

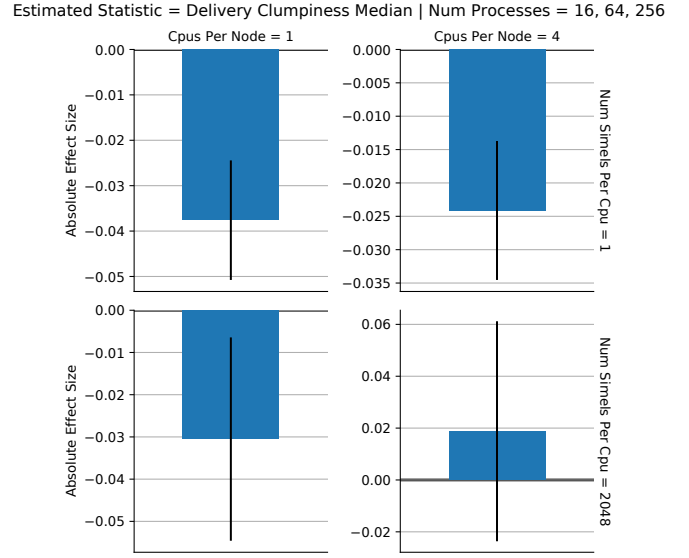


(d) Estimated regression coefficient for rightmost partial regression. Zero corresponds to no effect.

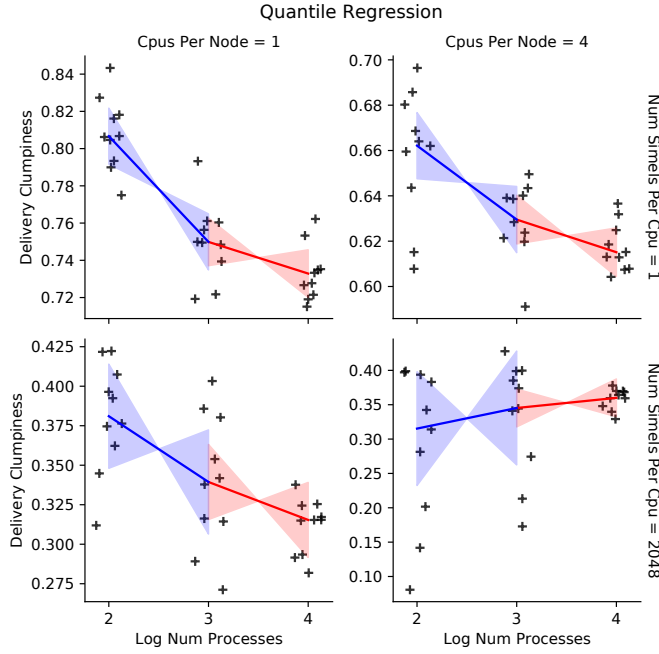
Fig. 24: Quantile Regressions of Latency Walltime Outlet (ns) against log processor count for weak scaling experiment (Section III-F). Lower is better. Top row shows complete regression and bottom row shows piecewise regression. Quantile regression estimates relationship between independent variable and median of response variable. Note that log is base 4, so processor counts correspond to 16, 64, and 256.



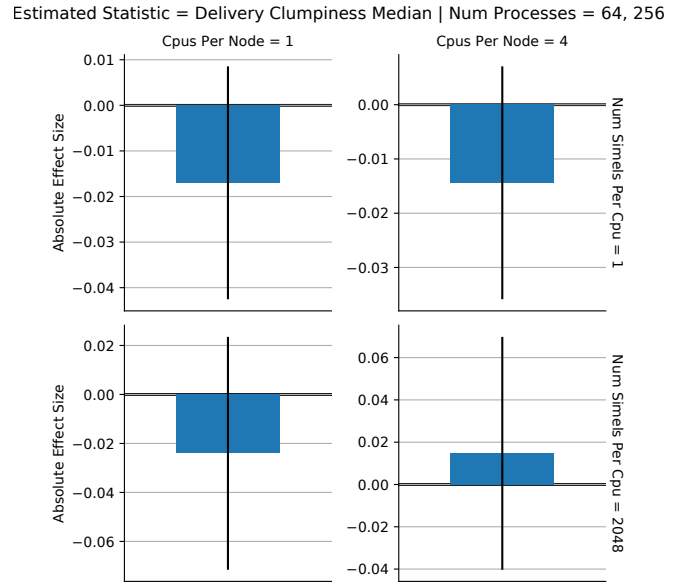
(a) Complete quantile regression plot. Observations are medians per replicate.



(b) Estimated regression coefficient for ordinary least squares regression. Zero corresponds to no effect.

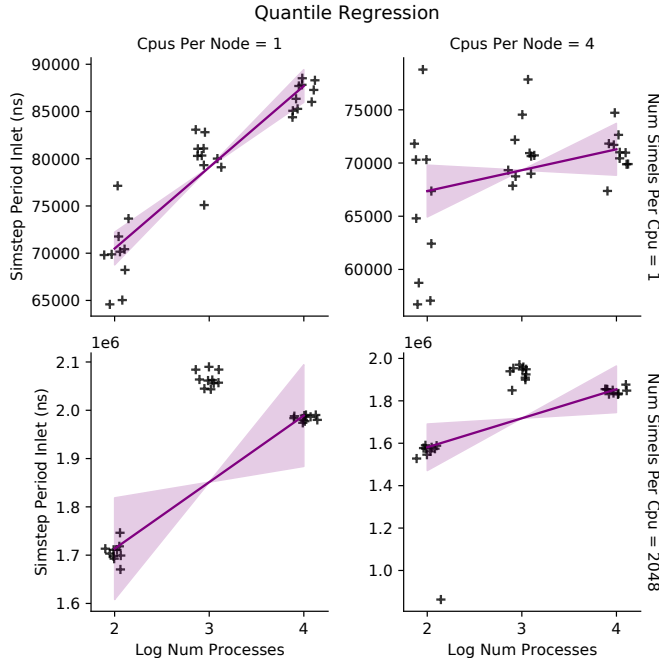


(c) Piecewise quantile regression plot. Observations are medians per replicate.



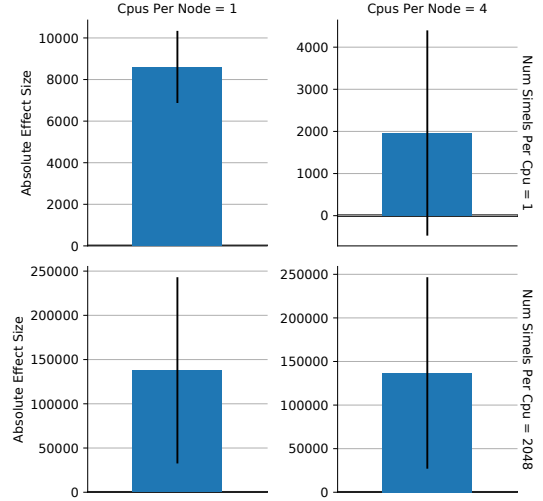
(d) Estimated regression coefficient for rightmost partial regression. Zero corresponds to no effect.

Fig. 25: Quantile Regressions of Delivery Clumpiness against log processor count for weak scaling experiment (Section III-F). Lower is better. Top row shows complete regression and bottom row shows piecewise regression. Quantile regression estimates relationship between independent variable and median of response variable. Note that log is base 4, so processor counts correspond to 16, 64, and 256.

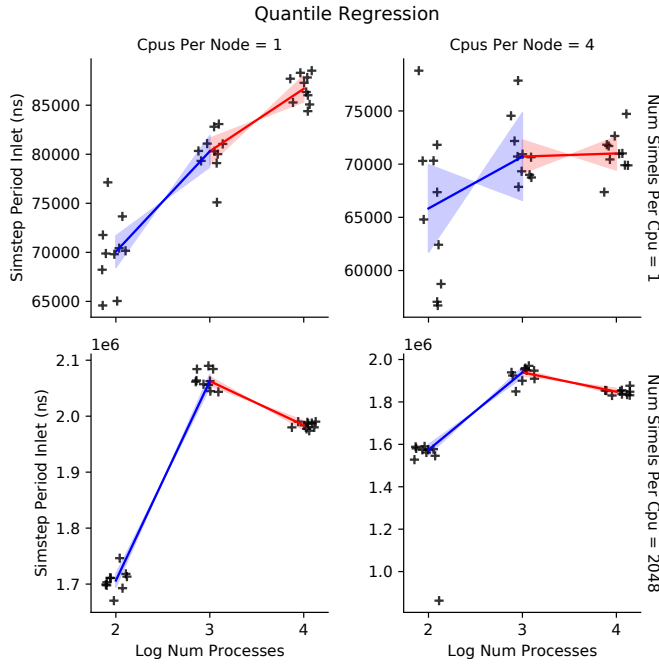


(a) Complete quantile regression plot. Observations are medians per replicate.

Estimated Statistic = Simstep Period Inlet (ns) Median | Num Processes = 16, 64, 256

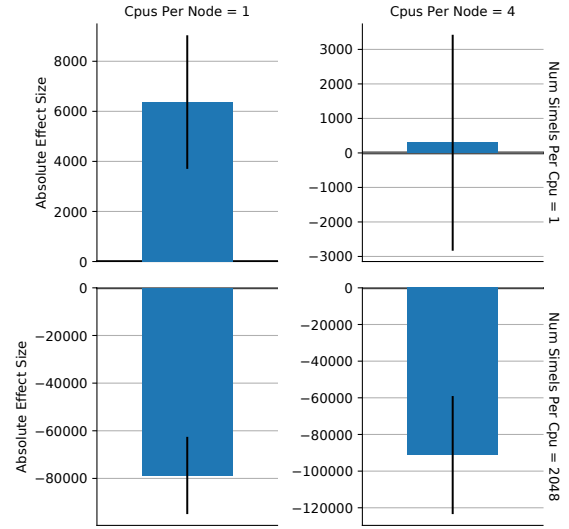


(b) Estimated regression coefficient for ordinary least squares regression. Zero corresponds to no effect.



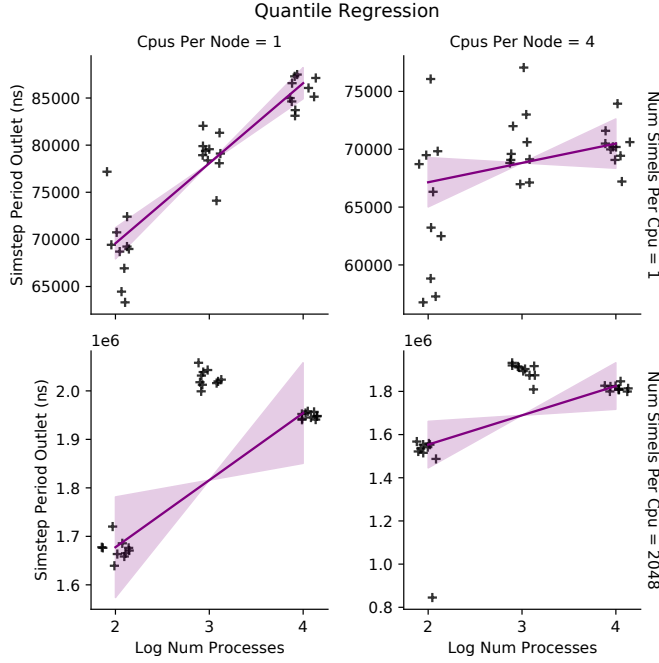
(c) Piecewise quantile regression plot. Observations are medians per replicate.

Estimated Statistic = Simstep Period Inlet (ns) Median | Num Processes = 64, 256



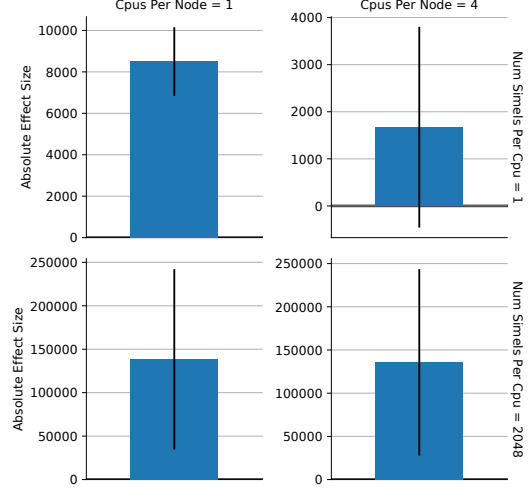
(d) Estimated regression coefficient for rightmost partial regression. Zero corresponds to no effect.

Fig. 26: Quantile Regressions of Simstep Period Inlet (ns) against log processor count for weak scaling experiment (Section III-F). Lower is better. Top row shows complete regression and bottom row shows piecewise regression. Quantile regression estimates relationship between independent variable and median of response variable. Note that log is base 4, so processor counts correspond to 16, 64, and 256.

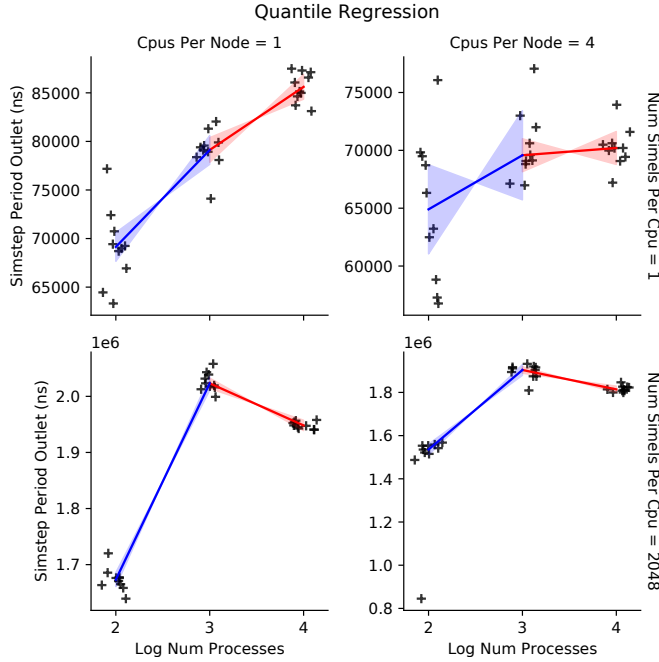


(a) Complete quantile regression plot. Observations are medians per replicate.

Estimated Statistic = Simstep Period Outlet (ns) Median | Num Processes = 16, 64, 256

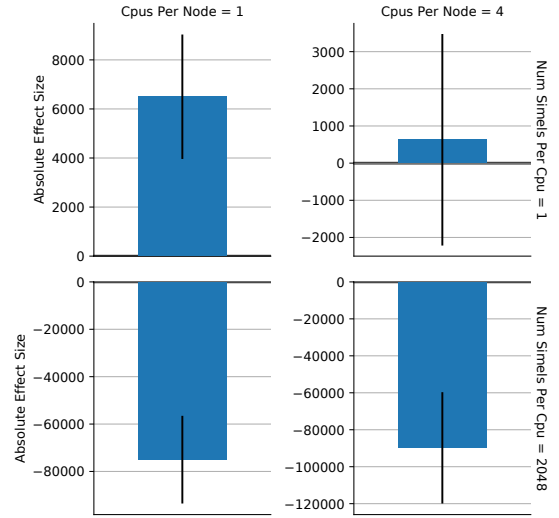


(b) Estimated regression coefficient for ordinary least squares regression. Zero corresponds to no effect.



(c) Piecewise quantile regression plot. Observations are medians per replicate.

Estimated Statistic = Simstep Period Outlet (ns) Median | Num Processes = 64, 256



(d) Estimated regression coefficient for rightmost partial regression. Zero corresponds to no effect.

Fig. 27: Quantile Regressions of Simstep Period Outlet (ns) against log processor count for weak scaling experiment (Section III-F). Lower is better. Top row shows complete regression and bottom row shows piecewise regression. Quantile regression estimates relationship between independent variable and median of response variable. Note that log is base 4, so processor counts correspond to 16, 64, and 256.

TABLE II: Full Ordinary Least Squares Regression results of Latency Walltime Inlet (ns) against against log processor count (Section III-F). Significance level  $p < 0.05$  used. Inf or NaN values may occur due to multicollinearity or due to inf or NaN observations.

Metric	Statistic	Significant Effect Sign	Cpus Per Node	Num SimeIs Per Cpu	Num Processes	Absolute Effect Size	Absolute Effect Size 95% CI Lower Bound	Absolute Effect Size 95% CI Upper Bound	Relative Effect Size	Relative Effect Size 95% CI Lower Bound	Relative Effect Size 95% CI Upper Bound	n	p
Latency Walltime Inlet (ns)	mean	-	1	1	16/64/256	-19 000	-35 000	-2 400	-0.033	-0.062	-0.0043	30	0.026
Latency Walltime Inlet (ns)	mean	+	1	2048	16/64/256	5.5e+06	3.5e+06	7.5e+06	2.5	1.6	3.4	30	4.8e-06
Latency Walltime Inlet (ns)	mean	0	4	1	16/64/256	-110 000	-350 000	120 000	-0.13	-0.4	0.14	30	0.33
Latency Walltime Inlet (ns)	mean	+	4	2048	16/64/256	230 000	110 000	340 000	0.11	0.057	0.17	30	0.0003
Latency Walltime Inlet (ns)	mean	-	1	1	16/64	-63 000	-92 000	-34 000	-0.11	-0.16	-0.061	20	0.00024
Latency Walltime Inlet (ns)	mean	+	1	2048	16/64	300 000	170 000	430 000	0.14	0.077	0.2	20	0.00014
Latency Walltime Inlet (ns)	mean	0	4	1	16/64	-320 000	-900 000	260 000	-0.37	-1	0.3	20	0.26
Latency Walltime Inlet (ns)	mean	+	4	2048	16/64	660 000	530 000	800 000	0.33	0.27	0.4	20	5.5e-09
Latency Walltime Inlet (ns)	mean	0	1	1	64/256	26 000	-990	52 000	0.046	-0.0018	0.093	20	0.058
Latency Walltime Inlet (ns)	mean	+	1	2048	64/256	1.1e+07	6.5e+06	1.5e+07	4.9	3	6.8	20	3.9e-05
Latency Walltime Inlet (ns)	mean	0	4	1	64/256	93 000	-44 000	230 000	0.11	-0.051	0.27	20	0.17
Latency Walltime Inlet (ns)	mean	-	4	2048	64/256	-210 000	-310 000	-110 000	-0.11	-0.16	-0.055	20	0.00039

TABLE III: Full Ordinary Least Squares Regression results of Latency Simsteps Outlet against log processor count (Section III-F). Significance level  $p < 0.05$  used. Inf or NaN values may occur due to multicollinearity or due to inf or NaN observations.

Metric	Statistic	Significant	Effect Sign	Cpus Per Node	Num Simels Per Cpu	Num Processes	Absolute Effect Size			Relative Effect Size			n	p
							Absolute Effect Size	95% CI Lower Bound	95% CI Upper Bound	Relative Effect Size	95% CI Lower Bound	95% CI Upper Bound		
Latency Simsteps Outlet	mean	-	1	1	16/64/256	-1.1	-1.4	-0.73	-0.13	-0.17	-0.087	30	5.5e-07	
Latency Simsteps Outlet	mean	+	1	2048	16/64/256	2.9	1.8	4	2.2	1.3	3	30	1.1e-05	
Latency Simsteps Outlet	mean	NaN	4	1	16/64/256	inf	nan	nan	inf	nan	nan	30	nan	
Latency Simsteps Outlet	mean	0	4	2048	16/64/256	0.017	-0.017	0.052	0.013	-0.012	0.038	30	0.3	
Latency Simsteps Outlet	mean	-	1	1	16/64	-2	-2.7	-1.4	-0.24	-0.32	-0.17	20	1.9e-06	
Latency Simsteps Outlet	mean	-	1	2048	16/64	-0.092	-0.17	-0.013	-0.069	-0.13	-0.0097	20	0.025	
Latency Simsteps Outlet	mean	-	4	1	16/64	-1.4	-2.1	-0.71	-0.17	-0.26	-0.087	20	0.00053	
Latency Simsteps Outlet	mean	0	4	2048	16/64	0.048	-0.035	0.13	0.036	-0.026	0.097	20	0.24	
Latency Simsteps Outlet	mean	0	1	1	64/256	-0.099	-0.56	0.36	-0.012	-0.067	0.043	20	0.65	
Latency Simsteps Outlet	mean	+	1	2048	64/256	5.8	3.6	8	4.4	2.7	6.1	20	3.8e-05	
Latency Simsteps Outlet	mean	NaN	4	1	64/256	inf	nan	nan	inf	nan	nan	20	nan	
Latency Simsteps Outlet	mean	0	4	2048	64/256	-0.013	-0.066	0.04	-0.0095	-0.049	0.03	20	0.62	

TABLE IV: Full Ordinary Least Squares Regression results of Latency Walltime Outlet (ns) against against log processor count (Section III-F). Significance level  $p < 0.05$  used. Inf or NaN values may occur due to multicollinearity or due to inf or NaN observations.

Metric	Statistic	Significant Effect Sign	Cpus Per Node	Num Slices Per Cpu	Num Processes	Absolute Effect Size	Absolute Effect Size	Absolute Effect Size 95% CI Lower Bound	Absolute Effect Size 95% CI Upper Bound	Relative Effect Size	Relative Effect Size 95% CI Lower Bound	Relative Effect Size 95% CI Upper Bound	n	p
							Absolute Effect Size	Relative Effect Size	Relative Effect Size					
Latency Walltime Outlet (ns)	mean	-	1	1	16/64/256	-20 000	-36 000	-3 000	-0.035	-0.064	-0.0054	30	0.022	
Latency Walltime Outlet (ns)	mean	+	1	2048	16/64/256	5.5e+06	3.5e+06	7.4e+06	2.5	1.6	3.4	30	5e-06	
Latency Walltime Outlet (ns)	mean	NaN	4	1	16/64/256	inf	nan	nan	inf	nan	nan	30	nan	
Latency Walltime Outlet (ns)	mean	+	4	2048	16/64/256	230 000	110 000	340 000	0.11	0.056	0.17	30	0.00034	
Latency Walltime Outlet (ns)	mean	-	1	1	16/64	-65 000	-95 000	-36 000	-0.12	-0.17	-0.063	20	0.00021	
Latency Walltime Outlet (ns)	mean	+	1	2048	16/64	290 000	160 000	430 000	0.13	0.073	0.19	20	0.00021	
Latency Walltime Outlet (ns)	mean	0	4	1	16/64	-2.5e+06	-7.2e+06	2.2e+06	-0.82	-2.4	0.73	20	0.28	
Latency Walltime Outlet (ns)	mean	+	4	2048	16/64	670 000	530 000	810 000	0.33	0.26	0.4	20	8e-09	
Latency Walltime Outlet (ns)	mean	0	1	1	64/256	26 000	-1 500	53 000	0.045	-0.0026	0.093	20	0.062	
Latency Walltime Outlet (ns)	mean	+	1	2048	64/256	1.1e+07	6.5e+06	1.5e+07	4.8	2.9	6.7	20	4e-05	
Latency Walltime Outlet (ns)	mean	NaN	4	1	64/256	inf	nan	nan	inf	nan	nan	20	nan	
Latency Walltime Outlet (ns)	mean	-	4	2048	64/256	-210 000	-320 000	-110 000	-0.11	-0.16	-0.054	20	0.00045	

TABLE V: Full Ordinary Least Squares Regression results of Delivery Clumpiness against log processor count (Section III-F). Significance level  $p < 0.05$  used. Inf or NaN values may occur due to multicollinearity or due to inf or NaN observations.

Metric	Statistic	Significant Effect Sign	Cpus Per Node	Num SimeIs Per Cpu	Num Processes	Absolute Effect Size	Absolute Effect Size 95% CI		Relative Effect Size		Relative Effect Size 95% CI		n	p
							Lower Bound	Upper Bound	Lower Bound	Upper Bound	Lower Bound	Upper Bound		
Delivery Clumpiness	mean	-	1	1	16/64/256	-0.036	-0.045	-0.026	-0.044	-0.056	-0.033	30	1.6e-08	
Delivery Clumpiness	mean	-	1	2048	16/64/256	-0.03	-0.044	-0.015	-0.078	-0.12	-0.041	30	0.00021	
Delivery Clumpiness	mean	-	4	1	16/64/256	-0.021	-0.033	-0.0087	-0.033	-0.052	-0.014	30	0.0016	
Delivery Clumpiness	mean	0	4	2048	16/64/256	0.028	-0.0021	0.058	0.1	-0.0077	0.21	30	0.067	
Delivery Clumpiness	mean	-	1	1	16/64	-0.055	-0.074	-0.036	-0.068	-0.092	-0.044	20	1.1e-05	
Delivery Clumpiness	mean	0	1	2048	16/64	-0.034	-0.07	0.001	-0.092	-0.19	0.0027	20	0.056	
Delivery Clumpiness	mean	0	4	1	16/64	-0.022	-0.053	0.0087	-0.034	-0.082	0.013	20	0.15	
Delivery Clumpiness	mean	0	4	2048	16/64	0.038	-0.038	0.11	0.14	-0.14	0.41	20	0.31	
Delivery Clumpiness	mean	-	1	1	64/256	-0.017	-0.033	-0.0002	-0.021	-0.041	-0.00025	20	0.048	
Delivery Clumpiness	mean	0	1	2048	64/256	-0.025	-0.052	0.003	-0.065	-0.14	0.008	20	0.078	
Delivery Clumpiness	mean	-	4	1	64/256	-0.02	-0.035	-0.0039	-0.031	-0.055	-0.0061	20	0.017	
Delivery Clumpiness	mean	0	4	2048	64/256	0.018	-0.035	0.071	0.065	-0.13	0.25	20	0.48	



TABLE VI: Full Ordinary Least Squares Regression results of Simstep Period Inlet (ns) against against log processor count (Section III-F). Significance level  $p < 0.05$  used. Inf or NaN values may occur due to multicollinearity or due to inf or NaN observations.

Metric	Statistic	Significant Effect Sign	Cpus Per Node	Num Simels Per Cpu	Num Processes	Absolute Effect Size	Absolute Effect Size 95% CI Lower Bound	Absolute Effect Size 95% CI Upper Bound	Relative Effect Size	Relative Effect Size 95% CI Lower Bound	Relative Effect Size 95% CI Upper Bound	n	p
Simstep Period Inlet (ns)	mean	+	1	1	16/64/256	8 800	7 400	10 000	0.12	0.11	0.14	30	1.4e-13
Simstep Period Inlet (ns)	mean	+	1	2048	16/64/256	150 000	97 000	190 000	0.085	0.056	0.11	30	1.5e-06
Simstep Period Inlet (ns)	mean	NaN	4	1	16/64/256	nan	nan	nan	nan	nan	nan	30	nan
Simstep Period Inlet (ns)	mean	+	4	2048	16/64/256	160 000	89 000	220 000	0.1	0.058	0.15	30	5.6e-05
Simstep Period Inlet (ns)	mean	+	1	1	16/64	12 000	9 200	15 000	0.17	0.13	0.21	20	4.5e-08
Simstep Period Inlet (ns)	mean	+	1	2048	16/64	360 000	350 000	380 000	0.21	0.2	0.22	20	7e-21
Simstep Period Inlet (ns)	mean	NaN	4	1	16/64	-inf	nan	nan	nan	nan	nan	20	nan
Simstep Period Inlet (ns)	mean	+	4	2048	16/64	450 000	430 000	480 000	0.3	0.28	0.31	20	6.2e-20
Simstep Period Inlet (ns)	mean	+	1	1	64/256	5 600	3 700	7 500	0.08	0.052	0.11	20	8.8e-06
Simstep Period Inlet (ns)	mean	-	1	2048	64/256	-72 000	-83 000	-61 000	-0.042	-0.049	-0.036	20	5.8e-11
Simstep Period Inlet (ns)	mean	NaN	4	1	64/256	inf	nan	nan	nan	nan	nan	20	nan
Simstep Period Inlet (ns)	mean	-	4	2048	64/256	-140 000	-160 000	-120 000	-0.093	-0.11	-0.079	20	4.4e-11

TABLE VII: Full Ordinary Least Squares Regression results of Latency Simsteps Inlet against against log processor count (Section III-F). Significance level  $p < 0.05$  used. Inf or NaN values may occur due to multicollinearity or due to inf or NaN observations.

Metric	Statistic	Significant Effect Sign	Cpus Per Node	Num Simels Per Cpu	Num Processes	Absolute Effect Size	Absolute Effect Size 95% CI Lower Bound	Absolute Effect Size 95% CI Upper Bound	Relative Effect Size	Relative Effect Size 95% CI Lower Bound	Relative Effect Size 95% CI Upper Bound	n	p
Latency Simsteps Inlet	mean	-	1	1	16/64/256	-1	-1.4	-0.7	-0.13	-0.17	-0.086	30	5.7e-07
Latency Simsteps Inlet	mean	+	1	2048	16/64/256	2.8	1.7	3.9	2.2	1.4	3.1	30	1.1e-05
Latency Simsteps Inlet	mean	-	4	1	16/64/256	-0.64	-0.97	-0.3	-0.079	-0.12	-0.037	30	0.00055
Latency Simsteps Inlet	mean	0	4	2048	16/64/256	0.016	-0.016	0.047	0.012	-0.012	0.036	30	0.32
Latency Simsteps Inlet	mean	-	1	1	16/64	-2	-2.6	-1.4	-0.24	-0.31	-0.17	20	2e-06
Latency Simsteps Inlet	mean	-	1	2048	16/64	-0.081	-0.16	-0.0058	-0.064	-0.12	-0.0045	20	0.036
Latency Simsteps Inlet	mean	-	4	1	16/64	-1.4	-2.1	-0.69	-0.17	-0.26	-0.085	20	0.00055
Latency Simsteps Inlet	mean	0	4	2048	16/64	0.043	-0.033	0.12	0.032	-0.025	0.09	20	0.25
Latency Simsteps Inlet	mean	0	1	1	64/256	-0.09	-0.53	0.35	-0.011	-0.065	0.043	20	0.67
Latency Simsteps Inlet	mean	+	1	2048	64/256	5.7	3.5	8	4.5	2.8	6.2	20	3.8e-05
Latency Simsteps Inlet	mean	0	4	1	64/256	0.1	-0.39	0.6	0.013	-0.049	0.074	20	0.67
Latency Simsteps Inlet	mean	0	4	2048	64/256	-0.011	-0.061	0.038	-0.0086	-0.046	0.029	20	0.64

TABLE VIII: Full Ordinary Least Squares Regression results of Simstep Period Outlet (ns) against against log processor count (Section III-F). Significance level  $p < 0.05$  used. Inf or NaN values may occur due to multicollinearity or due to inf or NaN observations.

Metric	Statistic	Significant Effect Sign	Cpus Per Node	Num Simels Per Cpu	Num Processes	Absolute Effect Size	Absolute Effect Size 95% CI Lower Bound	Absolute Effect Size 95% CI Upper Bound	Relative Effect Size	Relative Effect Size 95% CI Lower Bound	Relative Effect Size 95% CI Upper Bound	n	p
Simstep Period Outlet (ns)	mean	+	1	1	16/64/256	8 700	7 400	10 000	0.13	0.11	0.14	30	1.2e-13
Simstep Period Outlet (ns)	mean	+	1	2048	16/64/256	150 000	98 000	190 000	0.087	0.058	0.12	30	1.2e-06
Simstep Period Outlet (ns)	mean	NaN	4	1	16/64/256	nan	nan	nan	nan	nan	nan	30	nan
Simstep Period Outlet (ns)	mean	+	4	2048	16/64/256	150 000	87 000	220 000	0.1	0.058	0.15	30	5.5e-05
Simstep Period Outlet (ns)	mean	+	1	1	16/64	12 000	9 100	15 000	0.17	0.13	0.21	20	4.2e-08
Simstep Period Outlet (ns)	mean	+	1	2048	16/64	360 000	350 000	380 000	0.22	0.21	0.22	20	8.8e-21
Simstep Period Outlet (ns)	mean	NaN	4	1	16/64	-inf	nan	nan	nan	nan	nan	20	nan
Simstep Period Outlet (ns)	mean	+	4	2048	16/64	440 000	420 000	470 000	0.3	0.28	0.31	20	3.4e-19
Simstep Period Outlet (ns)	mean	+	1	1	64/256	5 600	3 700	7 500	0.081	0.053	0.11	20	7.1e-06
Simstep Period Outlet (ns)	mean	-	1	2048	64/256	-69 000	-79 000	-59 000	-0.041	-0.047	-0.035	20	2.2e-11
Simstep Period Outlet (ns)	mean	NaN	4	1	64/256	inf	nan	nan	nan	nan	nan	20	nan
Simstep Period Outlet (ns)	mean	-	4	2048	64/256	-140 000	-160 000	-120 000	-0.092	-0.11	-0.078	20	6.5e-11

TABLE IX: Full Ordinary Least Squares Regression results of Delivery Failure Rate against log processor count (Section III-F). Significance level  $p < 0.05$  used. Inf or NaN values may occur due to multicollinearity or due to inf or NaN observations.

Metric	Statistic	Significant	Cpus Per Node	Num SimeIs Per Cpu	Num Processes	Absolute Effect Size	Absolute Effect Size 95% CI Lower Bound	Absolute Effect Size 95% CI Upper Bound	Relative Effect Size	Relative Effect Size 95% CI Lower Bound	Relative Effect Size 95% CI Upper Bound	n	p
Delivery Failure Rate	mean	NaN	1	1	16/64/256	0	0	0	nan	nan	nan	30	nan
Delivery Failure Rate	mean	+	1	2048	16/64/256	0.0015	0.0011	0.0018	-13	-9.6	-16	30	2.5e-09
Delivery Failure Rate	mean	+	4	1	16/64/256	0.015	0.0088	0.02	0.15	0.091	0.21	30	1.7e-05
Delivery Failure Rate	mean	0	4	2048	16/64/256	-0.00075	-0.0016	9.3e-05	-0.49	-1	0.06	30	0.079
Delivery Failure Rate	mean	NaN	1	1	16/64	0	0	0	nan	nan	nan	20	nan
Delivery Failure Rate	mean	0	1	2048	16/64	8.6e-06	-0.00013	0.00015	-0.073	1.1	-1.3	20	0.9
Delivery Failure Rate	mean	0	4	1	16/64	-5.7e-08	-0.012	0.012	-5.8e-07	-0.12	0.12	20	1
Delivery Failure Rate	mean	0	4	2048	16/64	-0.00047	-0.0026	0.0016	-0.31	-1.7	1.1	20	0.64
Delivery Failure Rate	mean	NaN	1	1	64/256	0	0	0	nan	nan	nan	20	nan
Delivery Failure Rate	mean	+	1	2048	64/256	0.0029	0.0026	0.0032	-25	-23	-28	20	6.7e-14
Delivery Failure Rate	mean	+	4	1	64/256	0.029	0.025	0.033	0.3	0.26	0.34	20	1.7e-11
Delivery Failure Rate	mean	0	4	2048	64/256	-0.001	-0.0026	0.00055	-0.66	-1.7	0.36	20	0.19

TABLE X: Full Quantile Regression results of Latency Walltime Inlet (ns) against against log processor count (Section III-F). Significance level  $p < 0.05$  used. Inf or NaN values may occur due to multicollinearity or due to inf or NaN observations.

Metric	Statistic	Significant Effect Sign	Cpus Per Node	Num Simeles Per Cpu	Num Processes	Absolute Effect Size	Absolute Effect Size 95% CI Lower Bound		Absolute Effect Size 95% CI Upper Bound		Relative Effect Size	Relative Effect Size 95% CI Lower Bound		Relative Effect Size 95% CI Upper Bound		n	p
Latency	Walltime Inlet (ns)	-	1	1	16/64/256	-26 000	-47 000	-6 000	-0.049	-0.087	-0.011	-0.011	30	0.013			
Latency	Walltime Inlet (ns)	0	1	2048	16/64/256	61 000	-29 000	150 000	0.029	-0.014	0.072	0.072	30	0.18			
Latency	Walltime Inlet (ns)	0	4	1	16/64/256	-1 400	-23 000	20 000	-0.003	-0.05	0.044	0.044	30	0.9			
Latency	Walltime Inlet (ns)	+	4	2048	16/64/256	200 000	25 000	380 000	0.11	0.014	0.21	0.21	30	0.027			
Latency	Walltime Inlet (ns)	-	1	1	16/64	-63 000	-110 000	-18 000	-0.12	-0.2	-0.034	-0.034	20	0.0083			
Latency	Walltime Inlet (ns)	+	1	2048	16/64	260 000	30 000	500 000	0.12	0.014	0.23	0.23	20	0.029			
Latency	Walltime Inlet (ns)	0	4	1	16/64	-43 000	-110 000	21 000	-0.095	-0.24	0.046	0.046	20	0.17			
Latency	Walltime Inlet (ns)	+	4	2048	16/64	690 000	290 000	1.1e+06	0.38	0.16	0.6	0.6	20	0.002			
Latency	Walltime Inlet (ns)	0	1	1	64/256	2 900	-27 000	33 000	0.0055	-0.051	0.062	0.062	20	0.84			
Latency	Walltime Inlet (ns)	0	1	2048	64/256	-96 000	-230 000	35 000	-0.045	-0.11	0.017	0.017	20	0.14			
Latency	Walltime Inlet (ns)	0	4	1	64/256	24 000	-3 100	51 000	0.052	-0.0068	0.11	0.11	20	0.08			
Latency	Walltime Inlet (ns)	0	4	2048	64/256	-130 000	-310 000	48 000	-0.071	-0.17	0.026	0.026	20	0.14			

TABLE XI: Full Quantile Regression results of Latency Simsteps Outlet against log processor count (Section III-F). Significance level  $p < 0.05$  used. Inf or NaN values may occur due to multicollinearity or due to inf or NaN observations.

Metric	Statistic	Significant Effect Sign	Cpus Per Node	Num Sims Per Cpu	Num Processes	Absolute Effect Size	Absolute Effect Size 95% CI Lower Bound		Absolute Effect Size 95% CI Upper Bound		Relative Effect Size	Relative Effect Size 95% CI Lower Bound		Relative Effect Size 95% CI Upper Bound		p
							-	0	1	2048		-0.069	0.0045	30	0.00025	
Latency Simsteps	Outlet	median	1	1	16/64/256	95	-1.1	-1.6	-0.55	-0.13	-0.2	-0.069	30	0.00025		
Latency Simsteps	Outlet	median	0	1	2048	16/64/256	-0.037	-0.08	0.0057	-0.029	-0.063	0.0045	30	0.087		
Latency Simsteps	Outlet	median	-	4	1	16/64/256	-0.47	-0.76	-0.18	-0.068	-0.11	-0.026	30	0.0027		
Latency Simsteps	Outlet	median	0	4	2048	16/64/256	-0.003	-0.063	0.057	-0.0022	-0.047	0.042	30	0.92		
Latency Simsteps	Outlet	median	-	1	1	16/64	-2	-3	-1.1	-0.25	-0.38	-0.13	20	0.00033		
Latency Simsteps	Outlet	median	0	1	2048	16/64	-0.096	-0.24	0.051	-0.075	-0.19	0.04	20	0.19		
Latency Simsteps	Outlet	median	-	4	1	16/64	-1.1	-1.7	-0.43	-0.16	-0.25	-0.063	20	0.0025		
Latency Simsteps	Outlet	median	0	4	2048	16/64	-0.0014	-0.17	0.17	-0.001	-0.12	0.12	20	0.99		
Latency Simsteps	Outlet	median	0	1	1	64/256	-0.32	-0.81	0.18	-0.04	-0.1	0.022	20	0.19		
Latency Simsteps	Outlet	median	0	1	2048	64/256	-0.0014	-0.061	0.058	-0.0011	-0.048	0.046	20	0.96		
Latency Simsteps	Outlet	median	0	4	1	64/256	-0.017	-0.43	0.4	-0.0024	-0.063	0.058	20	0.93		
Latency Simsteps	Outlet	median	0	4	2048	64/256	-0.0068	-0.081	0.068	-0.005	-0.06	0.05	20	0.85		

TABLE XII: Full Quantile Regression results of Latency Walltime Outlet (ns) against against log processor count (Section III-F). Significance level  $p < 0.05$  used. Inf or NaN values may occur due to multicollinearity or due to inf or NaN observations.

Metric	Statistic	Significant Effect Sign	Cpus Per Node	Num Slices Per Cpu	Num Processes	Absolute Effect Size	Absolute Effect Size 95% CI Lower Bound	Absolute Effect Size 95% CI Upper Bound	Relative Effect Size	Relative Effect Size 95% CI Lower Bound	Relative Effect Size 95% CI Upper Bound	n	p
Latency Walltime Outlet (ns)	median	-	1	1	16/64/256	-26 000	-47 000	-4 900	-0.048	-0.086	-0.0091	30	0.017
Latency Walltime Outlet (ns)	median	0	1	2048	16/64/256	60 000	-32 000	150 000	0.028	-0.015	0.071	30	0.19
Latency Walltime Outlet (ns)	median	0	4	1	16/64/256	-3 400	-26 000	19 000	-0.0074	-0.056	0.041	30	0.75
Latency Walltime Outlet (ns)	median	+	4	2048	16/64/256	200 000	13 000	380 000	0.11	0.0073	0.21	30	0.036
Latency Walltime Outlet (ns)	median	-	1	1	16/64	-69 000	-120 000	-21 000	-0.13	-0.22	-0.038	20	0.0077
Latency Walltime Outlet (ns)	median	+	1	2048	16/64	260 000	7 700	520 000	0.12	0.0036	0.24	20	0.044
Latency Walltime Outlet (ns)	median	0	4	1	16/64	-44 000	-110 000	20 000	-0.096	-0.24	0.044	20	0.17
Latency Walltime Outlet (ns)	median	+	4	2048	16/64	710 000	300 000	1.1e+06	0.38	0.16	0.6	20	0.0017
Latency Walltime Outlet (ns)	median	0	1	1	64/256	3 100	-26 000	33 000	0.0057	-0.049	0.06	20	0.83
Latency Walltime Outlet (ns)	median	0	1	2048	64/256	-100 000	-240 000	38 000	-0.048	-0.11	0.018	20	0.14
Latency Walltime Outlet (ns)	median	0	4	1	64/256	24 000	-9 100	57 000	0.052	-0.02	0.12	20	0.14
Latency Walltime Outlet (ns)	median	0	4	2048	64/256	-150 000	-310 000	13 000	-0.08	-0.17	0.0072	20	0.07

TABLE XIII: Full Quantile Regression results of Delivery Clumpiness against against log processor count (Section III-F). Significance level  $p < 0.05$  used. Inf or NaN values may occur due to multicollinearity or due to inf or NaN observations.

Metric	Statistic	Significant Effect Sign	Cpus Per Node	Num SineIs Per Cpu	Num Processes	Absolute Effect Size	Absolute Effect Size 95% CI Lower Bound	Absolute Effect Size 95% CI Upper Bound	Relative Effect Size	Relative Effect Size 95% CI Lower Bound	Relative Effect Size 95% CI Upper Bound	n	p
Delivery Clumpiness	median	-	1	1	16/64/256	-0.038	-0.051	-0.024	-0.047	-0.063	-0.03	30	2.7e-06
Delivery Clumpiness	median	-	1	2048	16/64/256	-0.031	-0.055	-0.0064	-0.079	-0.14	-0.017	30	0.015
Delivery Clumpiness	median	-	4	1	16/64/256	-0.024	-0.035	-0.014	-0.036	-0.052	-0.021	30	5.5e-05
Delivery Clumpiness	median	0	4	2048	16/64/256	0.019	-0.024	0.061	0.057	-0.072	0.19	30	0.37
Delivery Clumpiness	median	-	1	1	16/64	-0.057	-0.087	-0.027	-0.07	-0.11	-0.033	20	0.00091
Delivery Clumpiness	median	0	1	2048	16/64	-0.042	-0.11	0.024	-0.11	-0.28	0.063	20	0.2
Delivery Clumpiness	median	-	4	1	16/64	-0.033	-0.062	-0.0034	-0.049	-0.093	-0.0052	20	0.031
Delivery Clumpiness	median	0	4	2048	16/64	0.03	-0.14	0.2	0.091	-0.41	0.6	20	0.71
Delivery Clumpiness	median	0	1	1	64/256	-0.017	-0.043	0.0085	-0.021	-0.053	0.011	20	0.18
Delivery Clumpiness	median	0	1	2048	64/256	-0.024	-0.072	0.024	-0.063	-0.19	0.061	20	0.3
Delivery Clumpiness	median	0	4	1	64/256	-0.014	-0.036	0.0071	-0.022	-0.054	0.011	20	0.18
Delivery Clumpiness	median	0	4	2048	64/256	0.015	-0.04	0.07	0.045	-0.12	0.21	20	0.58



TABLE XIV: Full Quantile Regression results of Simsteps Period Inlet (ns) against against log processor count (Section III-F). Significance level  $p < 0.05$  used. Inf or NaN values may occur due to multicollinearity or due to inf or NaN observations.

Metric	Statistic	Significant Effect Sign	Cpus Per Node	Num Simels Per Cpu	Num Processes	Absolute Effect Size	Absolute Effect Size 95% CI Lower Bound	Absolute Effect Size 95% CI Upper Bound	Relative Effect Size	Relative Effect Size 95% CI Lower Bound	Relative Effect Size 95% CI Upper Bound	n	p
Simstep Period Inlet (ns)	median	+	1	1	16/64/256	8 600	6 900	10 000	0.12	0.098	0.15	30	6.7e-11
Simstep Period Inlet (ns)	median	+	1	2048	16/64/256	140 000	33 000	240 000	0.081	0.019	0.14	30	0.012
Simstep Period Inlet (ns)	median	0	4	1	16/64/256	2 000	-470	4 400	0.03	-0.0072	0.067	30	0.11
Simstep Period Inlet (ns)	median	+	4	2048	16/64/256	140 000	27 000	250 000	0.087	0.017	0.16	30	0.016
Simstep Period Inlet (ns)	median	+	1	1	16/64	10 000	7 000	13 000	0.15	0.1	0.19	20	2.9e-06
Simstep Period Inlet (ns)	median	+	1	2048	16/64	360 000	330 000	380 000	0.21	0.2	0.22	20	2.7e-17
Simstep Period Inlet (ns)	median	0	4	1	16/64	4 900	-3 300	13 000	0.074	-0.051	0.2	20	0.23
Simstep Period Inlet (ns)	median	+	4	2048	16/64	370 000	320 000	410 000	0.23	0.2	0.26	20	6.8e-12
Simstep Period Inlet (ns)	median	+	1	1	64/256	6 400	3 700	9 000	0.091	0.053	0.13	20	9e-05
Simstep Period Inlet (ns)	median	-	1	2048	64/256	-79 000	-95 000	-63 000	-0.046	-0.056	-0.037	20	6.5e-09
Simstep Period Inlet (ns)	median	0	4	1	64/256	300	-2 800	3 400	0.0045	-0.043	0.052	20	0.85
Simstep Period Inlet (ns)	median	-	4	2048	64/256	-91 000	-120 000	-59 000	-0.058	-0.078	-0.037	20	1.2e-05

TABLE XV: Full Quantile Regression results of Latency Simsteps Inlet against against log processor count (Section III-F). Significance level  $p < 0.05$  used. Inf or NaN values may occur due to multicollinearity or due to inf or NaN observations.

Metric	Statistic	Significant Effect Sign	Cpus Per Node	Num Simels Per Cpu	Num Processes	Absolute Effect Size	Absolute Effect Size 95% CI Lower Bound	Absolute Effect Size 95% CI Upper Bound	Relative Effect Size	Relative Effect Size 95% CI Lower Bound	Relative Effect Size 95% CI Upper Bound	n	p
Latency Simsteps Inlet	median	-	1	1	16/64/256	-1.1	-1.6	-0.62	-0.14	-0.2	-0.079	30	6.6e-05
Latency Simsteps Inlet	median	0	1	2048	16/64/256	-0.034	-0.074	0.0068	-0.027	-0.06	0.0055	30	0.1
Latency Simsteps Inlet	median	-	4	1	16/64/256	-0.42	-0.72	-0.12	-0.063	-0.11	-0.018	30	0.0074
Latency Simsteps Inlet	median	0	4	2048	16/64/256	-0.0031	-0.059	0.053	-0.0023	-0.044	0.04	30	0.91
Latency Simsteps Inlet	median	-	1	1	16/64	-1.9	-2.7	-1.1	-0.24	-0.35	-0.14	20	0.00017
Latency Simsteps Inlet	median	0	1	2048	16/64	-0.089	-0.23	0.051	-0.072	-0.19	0.041	20	0.2
Latency Simsteps Inlet	median	-	4	1	16/64	-1.1	-1.7	-0.36	-0.16	-0.26	-0.054	20	0.005
Latency Simsteps Inlet	median	0	4	2048	16/64	-0.0057	-0.15	0.14	-0.0043	-0.12	0.11	20	0.94
Latency Simsteps Inlet	median	0	1	1	64/256	-0.39	-0.85	0.064	-0.051	-0.11	0.0082	20	0.088
Latency Simsteps Inlet	median	0	1	2048	64/256	-0.0032	-0.063	0.057	-0.0026	-0.051	0.046	20	0.91
Latency Simsteps Inlet	median	0	4	1	64/256	0.00035	-0.42	0.42	5.2e-05	-0.062	0.062	20	1
Latency Simsteps Inlet	median	0	4	2048	64/256	0.0012	-0.073	0.076	0.00089	-0.055	0.057	20	0.97

TABLE XVI: Full Quantile Regression results of Simstep Period Outlet (ns) against against log processor count (Section III-F). Significance level  $p < 0.05$  used. Inf or NaN values may occur due to multicollinearity or due to inf or NaN observations.

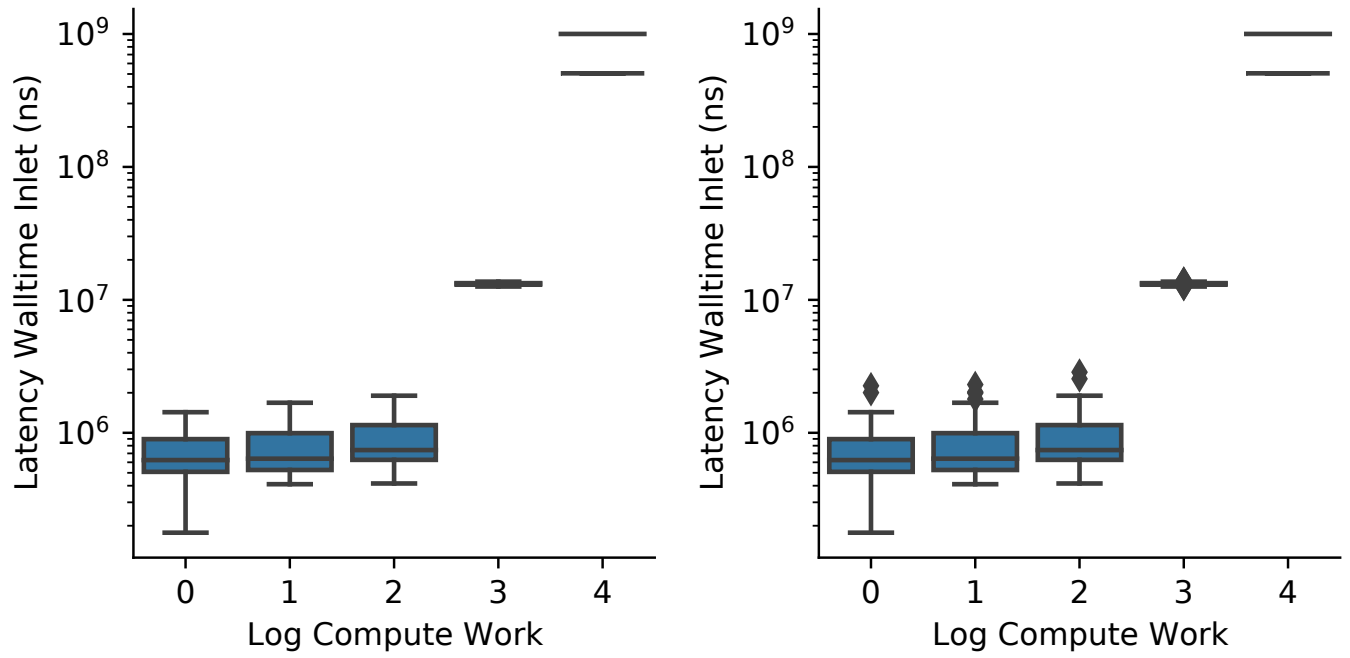
Metric	Statistic	Significant Effect Sign	Cpus Per Node	Num Simels Per Cpu	Num Processes	Absolute Effect Size	Absolute Effect Size 95% CI Lower Bound	Absolute Effect Size 95% CI Upper Bound	Relative Effect Size	Relative Effect Size 95% CI Lower Bound	Relative Effect Size 95% CI Upper Bound	n	p
Simstep Period Outlet (ns)	median	+	1	1	16/64/256	8 500	6 800	10 000	0.12	0.099	0.15	30	3.2e-11
Simstep Period Outlet (ns)	median	+	1	2048	16/64/256	140 000	35 000	240 000	0.083	0.021	0.14	30	0.011
Simstep Period Outlet (ns)	median	0	4	1	16/64/256	1 700	-460	3 800	0.026	-0.0071	0.059	30	0.12
Simstep Period Outlet (ns)	median	+	4	2048	16/64/256	140 000	28 000	240 000	0.088	0.018	0.16	30	0.015
Simstep Period Outlet (ns)	median	+	1	1	16/64	10 000	7 000	13 000	0.14	0.1	0.19	20	1.3e-06
Simstep Period Outlet (ns)	median	+	1	2048	16/64	350 000	330 000	370 000	0.21	0.19	0.22	20	1e-16
Simstep Period Outlet (ns)	median	0	4	1	16/64	4 700	-3 000	12 000	0.072	-0.047	0.19	20	0.22
Simstep Period Outlet (ns)	median	+	4	2048	16/64	370 000	320 000	420 000	0.24	0.21	0.27	20	6.6e-12
Simstep Period Outlet (ns)	median	+	1	1	64/256	6 500	4 000	9 000	0.094	0.057	0.13	20	4.1e-05
Simstep Period Outlet (ns)	median	-	1	2048	64/256	-75 000	-94 000	-57 000	-0.045	-0.056	-0.034	20	9.9e-08
Simstep Period Outlet (ns)	median	0	4	1	64/256	630	-2 200	3 500	0.0097	-0.034	0.054	20	0.65
Simstep Period Outlet (ns)	median	-	4	2048	64/256	-90 000	-120 000	-60 000	-0.058	-0.078	-0.039	20	6.6e-06

TABLE XVII: Full Quantile Regression results of Delivery Failure Rate against log processor count (Section III-F). Significance level  $p < 0.05$  used. Inf or NaN values may occur due to multicollinearity or due to inf or NaN observations.

Metric	Statistic	Significant Effect Sign	Cpus Per Node	Num SimeIs Per Cpu	Num Processes	Absolute Effect Size	Absolute Effect Size 95% CI Lower Bound	Absolute Effect Size 95% CI Upper Bound	Relative Effect Size	Relative Effect Size 95% CI Lower Bound	Relative Effect Size 95% CI Upper Bound	n	p
Delivery Failure Rate	median	NaN	1	1	16/64/256	0	nan	nan	nan	nan	nan	30	nan
Delivery Failure Rate	median	NaN	1	2048	16/64/256	0	nan	nan	nan	nan	nan	30	nan
Delivery Failure Rate	median	+	4	1	16/64/256	0.019	0.0076	0.029	0.34	0.14	0.54	30	0.0016
Delivery Failure Rate	median	NaN	4	2048	16/64/256	0	nan	nan	nan	nan	nan	30	nan
Delivery Failure Rate	median	NaN	1	1	16/64	0	nan	nan	nan	nan	nan	20	nan
Delivery Failure Rate	median	NaN	1	2048	16/64	0	nan	nan	nan	nan	nan	20	nan
Delivery Failure Rate	median	0	4	1	16/64	0.026	-0.023	0.074	0.47	-0.41	1.4	20	0.28
Delivery Failure Rate	median	NaN	4	2048	16/64	0	nan	nan	nan	nan	nan	20	nan
Delivery Failure Rate	median	NaN	1	1	64/256	0	nan	nan	nan	nan	nan	20	nan
Delivery Failure Rate	median	NaN	1	2048	64/256	0	nan	nan	nan	nan	nan	20	nan
Delivery Failure Rate	median	+	4	1	64/256	0.018	0.0038	0.032	0.33	0.069	0.59	20	0.016
Delivery Failure Rate	median	NaN	4	2048	64/256	0	nan	nan	nan	nan	nan	20	nan

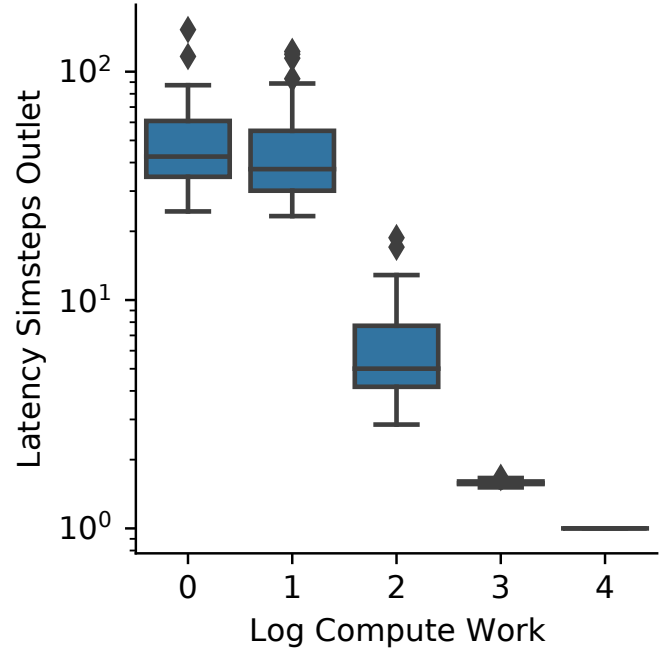
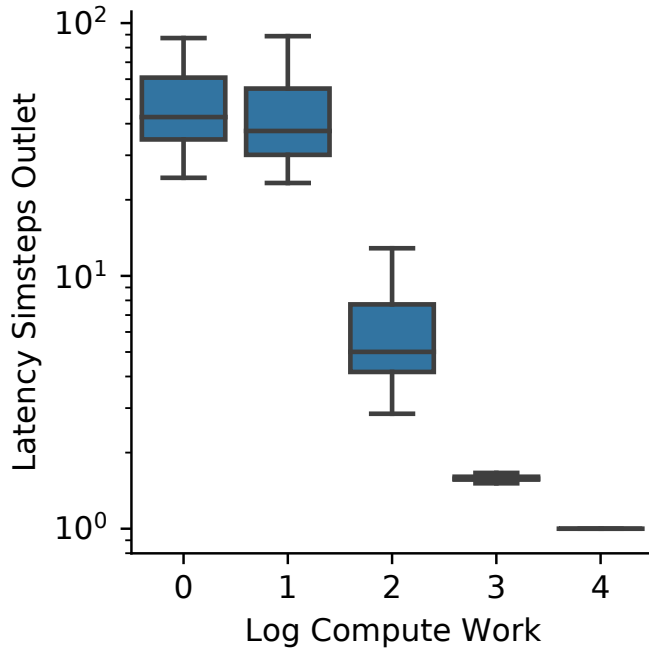
### B. Computation vs. Communication

This section provides full results from computation vs. communication experiments discussed in Section III-C.



(a) Distribution of Latency Walltime Inlet (ns) for each snapshot, (b) Distribution of Latency Walltime Inlet (ns) for each snapshot, with outliers.

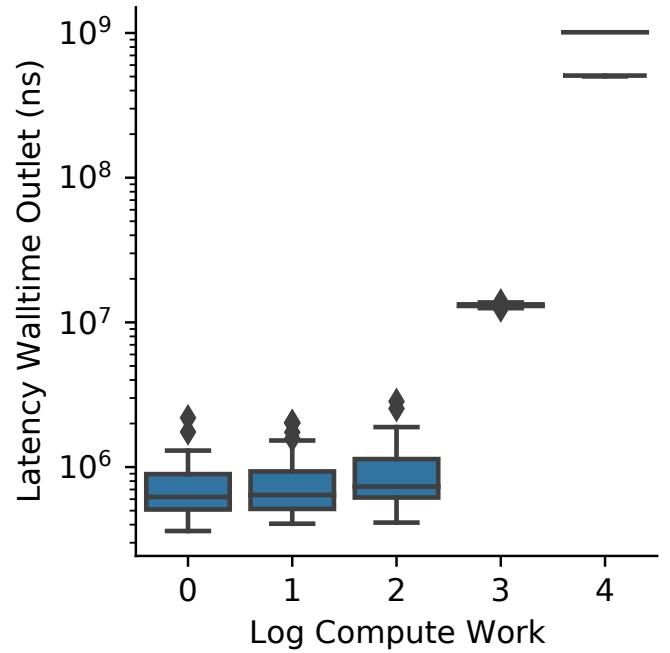
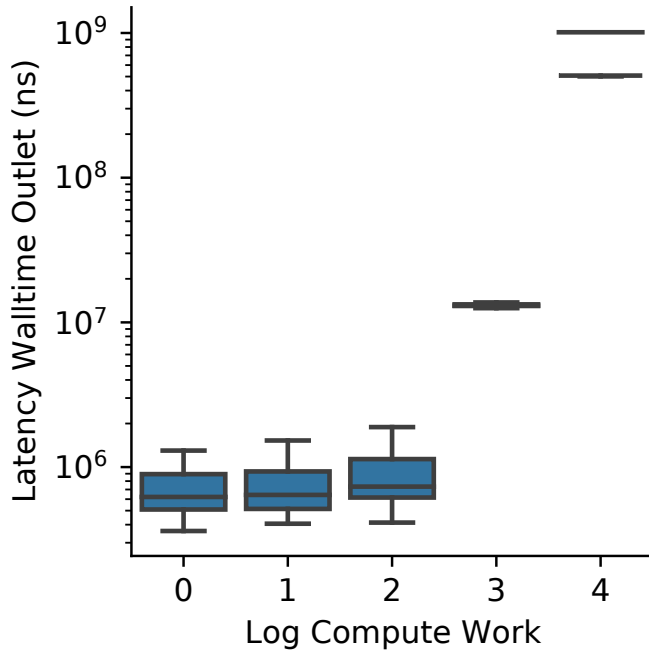
Fig. 28: Distribution of Latency Walltime Inlet (ns) for individual snapshot measurements for computation vs. communication experiment (Section III-C). Lower is better.



(a) Distribution of Latency Simsteps Outlet for each snapshot, without outliers.

(b) Distribution of Latency Simsteps Outlet for each snapshot, with outliers.

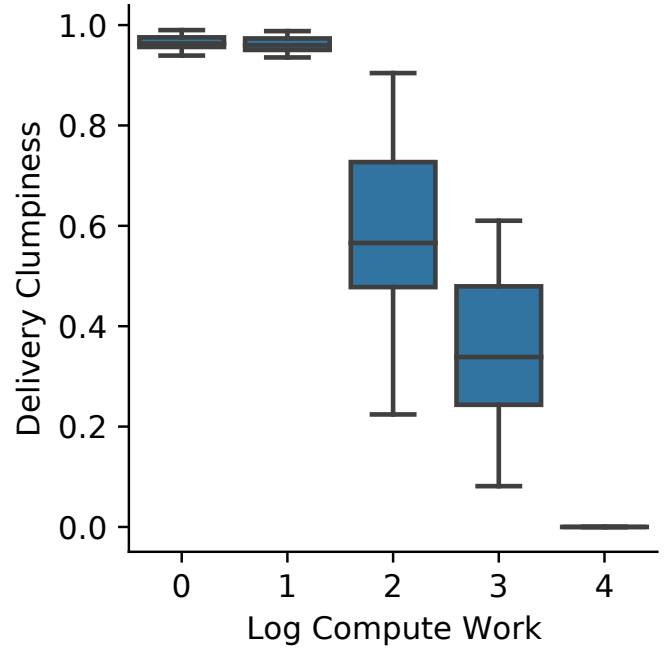
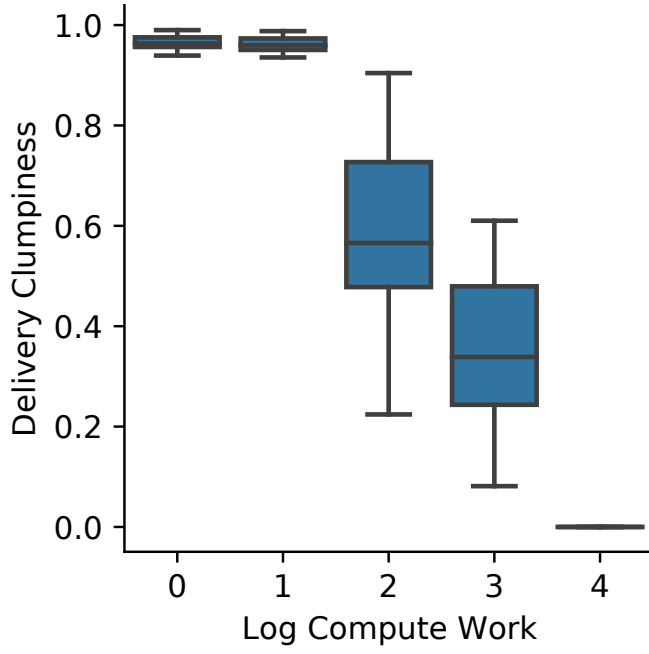
Fig. 29: Distribution of Latency Simsteps Outlet for individual snapshot measurements for computation vs. communication experiment (Section III-C). Lower is better.



(a) Distribution of Latency Walltime Outlet (ns) for each snapshot, without outliers.

(b) Distribution of Latency Walltime Outlet (ns) for each snapshot, with outliers.

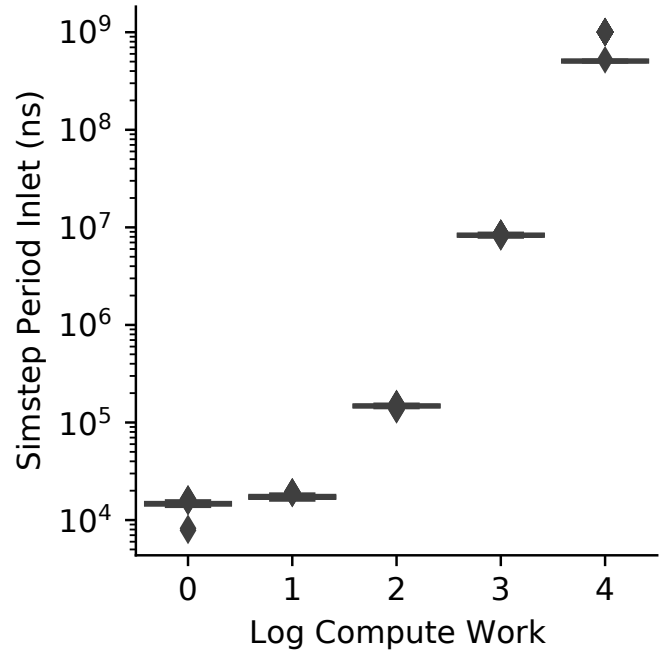
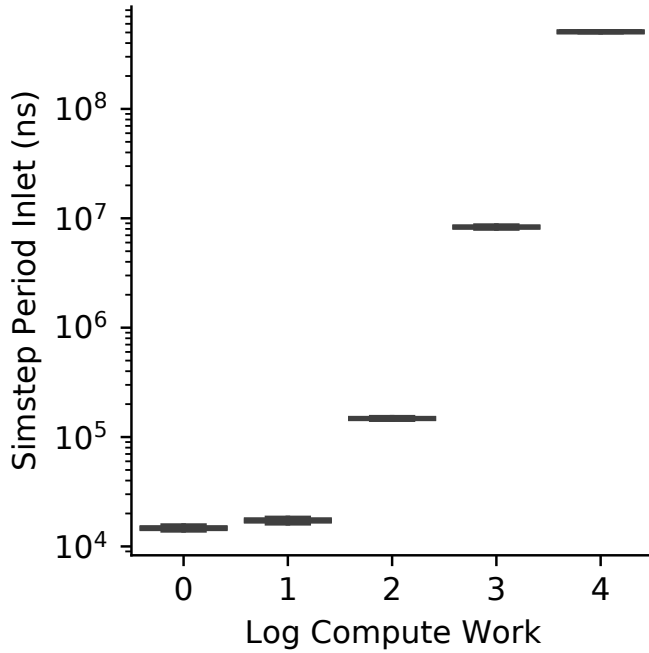
Fig. 30: Distribution of Latency Walltime Outlet (ns) for individual snapshot measurements for computation vs. communication experiment (Section III-C). Lower is better.



(a) Distribution of Delivery Clumpiness for each snapshot, without outliers.

(b) Distribution of Delivery Clumpiness for each snapshot, with outliers.

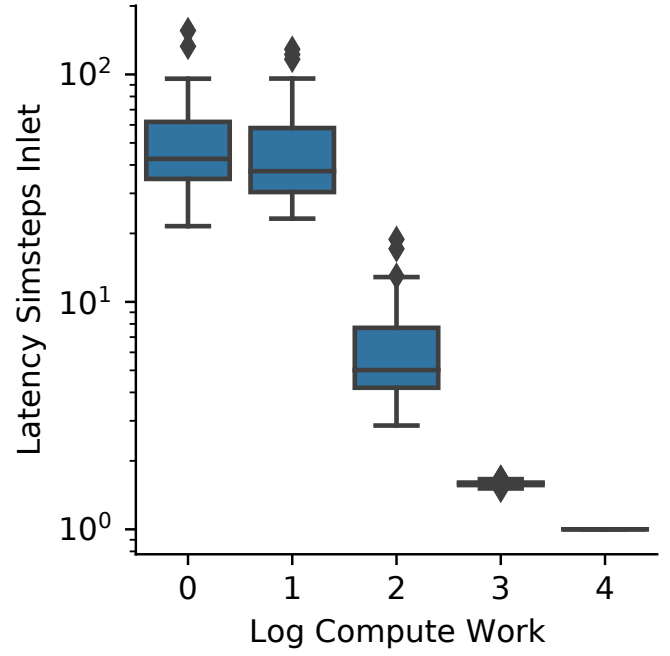
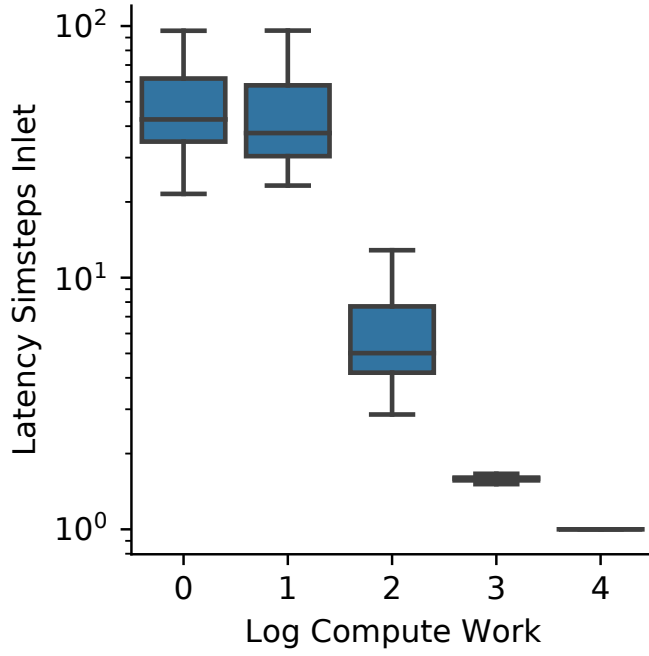
Fig. 31: Distribution of Delivery Clumpiness for individual snapshot measurements for computation vs. communication experiment (Section III-C). Lower is better.



(a) Distribution of Simstep Period Inlet (ns) for each snapshot, without outliers.

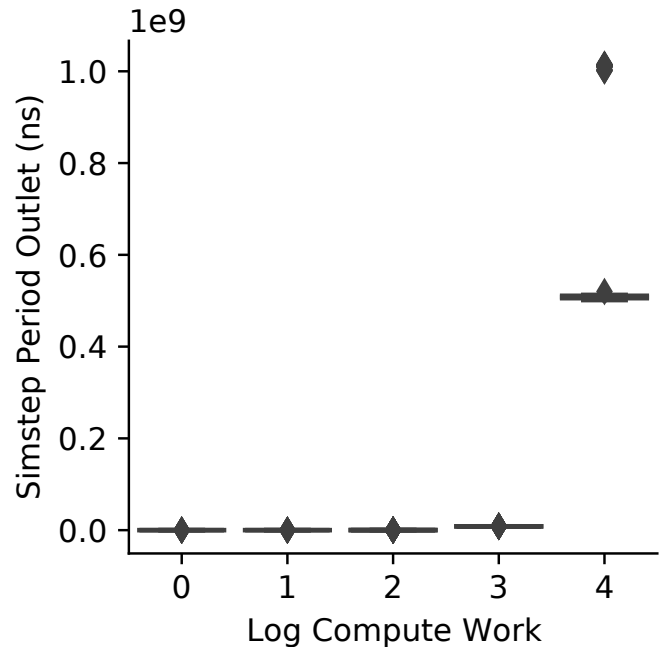
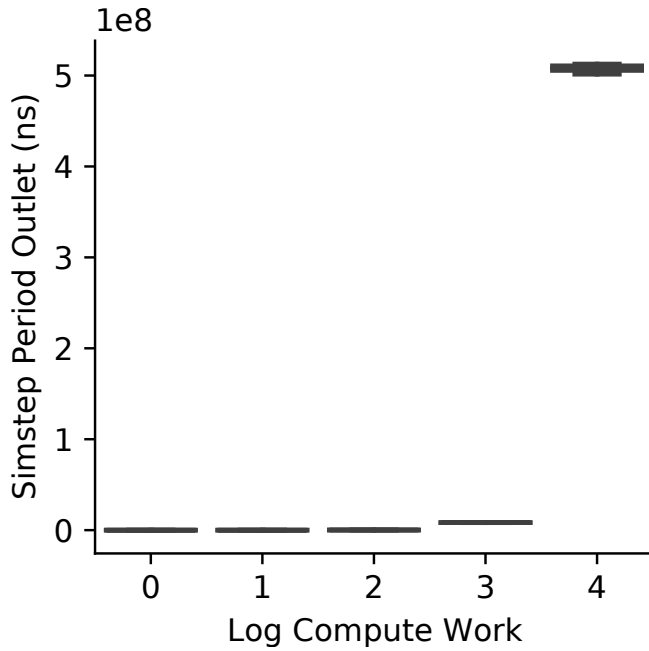
(b) Distribution of Simstep Period Inlet (ns) for each snapshot, with outliers.

Fig. 32: Distribution of Simstep Period Inlet (ns) for individual snapshot measurements for computation vs. communication experiment (Section III-C). Lower is better.



(a) Distribution of Latency Simsteps Inlet for each snapshot, without outliers. (b) Distribution of Latency Simsteps Inlet for each snapshot, with outliers.

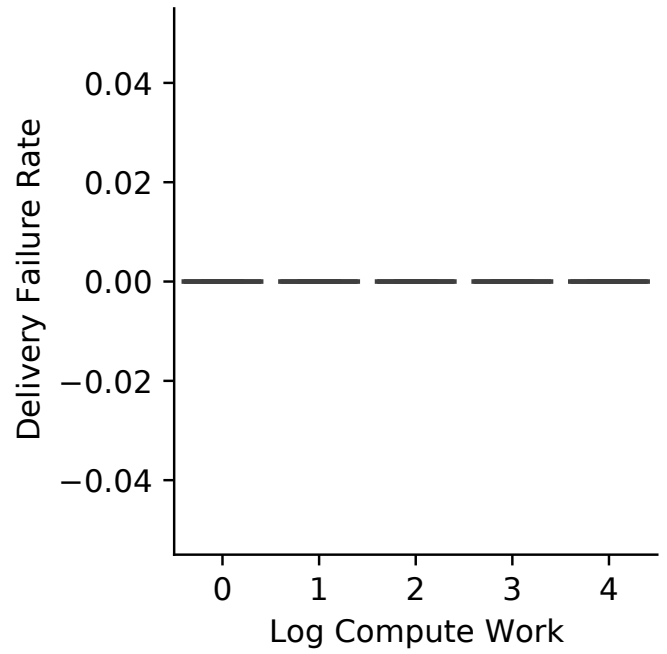
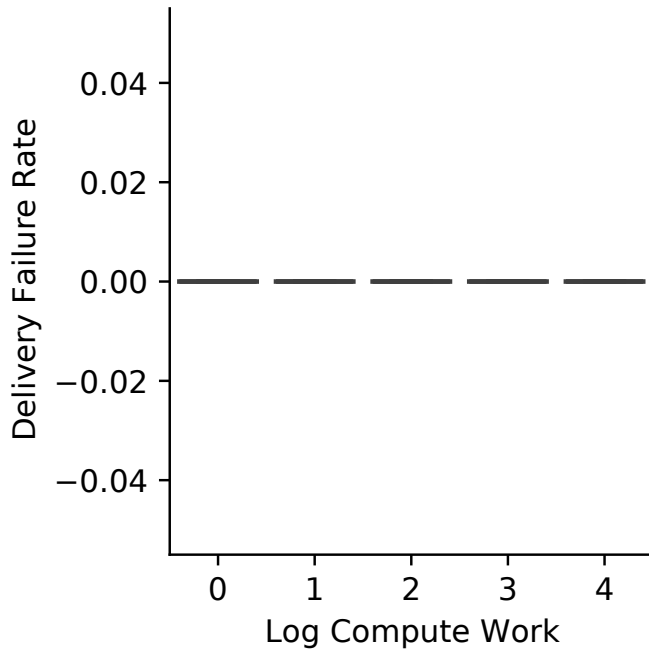
Fig. 33: Distribution of Latency Simsteps Inlet for individual snapshot measurements for computation vs. communication experiment (Section III-C). Lower is better.



(a) Distribution of Simstep Period Outlet (ns) for each snapshot, without outliers. (b) Distribution of Simstep Period Outlet (ns) for each snapshot, with outliers.

Fig. 34: Distribution of Simstep Period Outlet (ns) for individual snapshot measurements for computation vs. communication experiment (Section III-C). Lower is better.



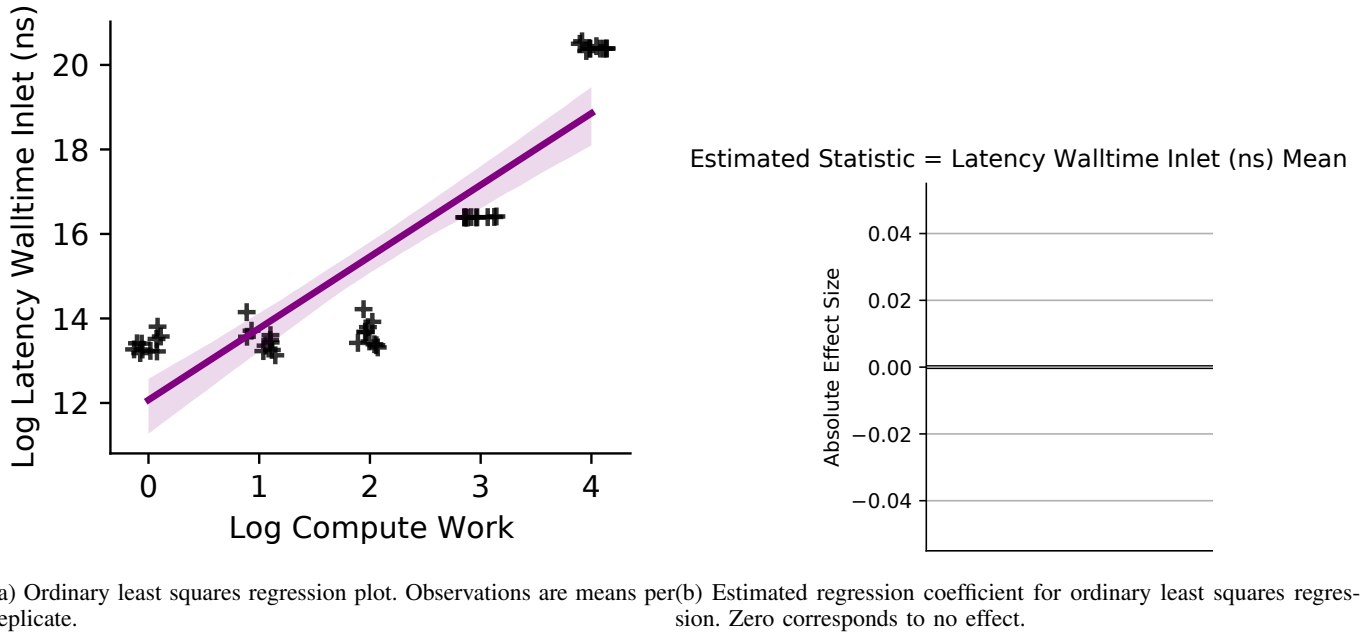


(a) Distribution of Delivery Failure Rate for each snapshot, without outliers.

(b) Distribution of Delivery Failure Rate for each snapshot, with outliers.

Fig. 35: Distribution of Delivery Failure Rate for individual snapshot measurements for computation vs. communication experiment (Section III-C). Lower is better.

## Ordinary Least Squares Regression



## Quantile Regression

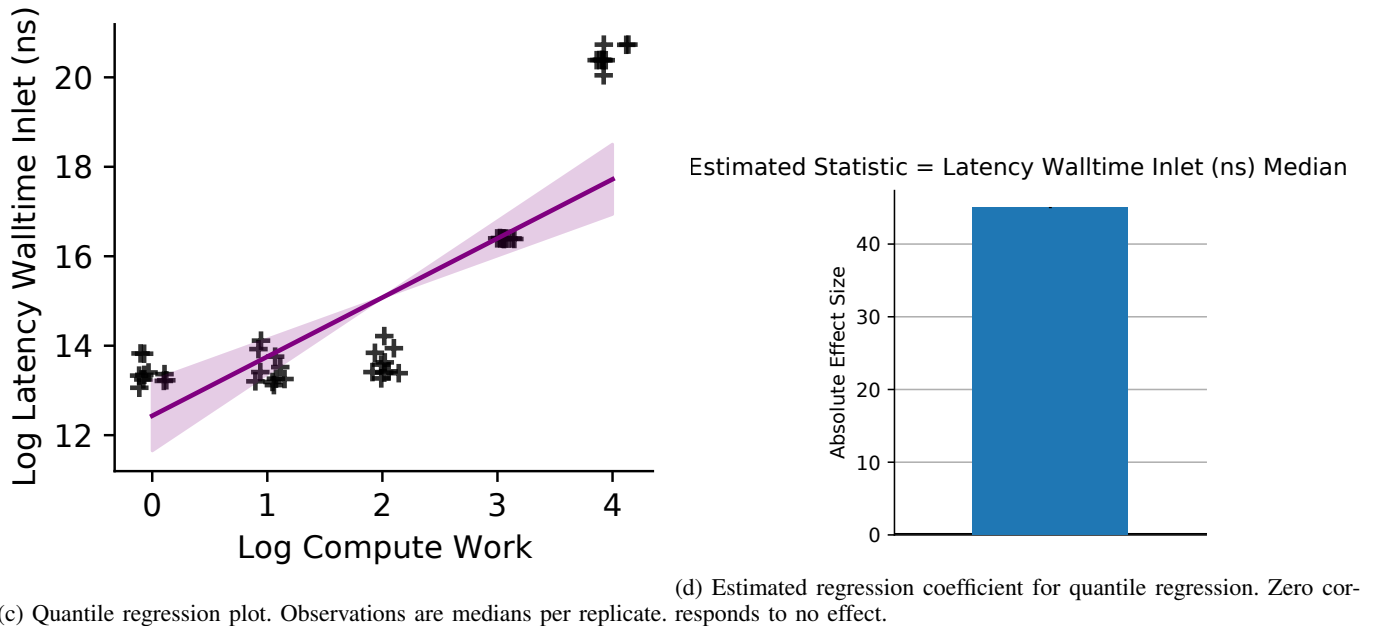
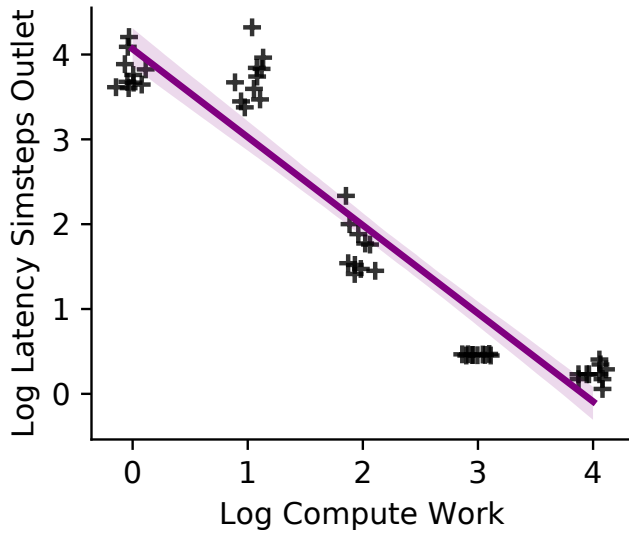
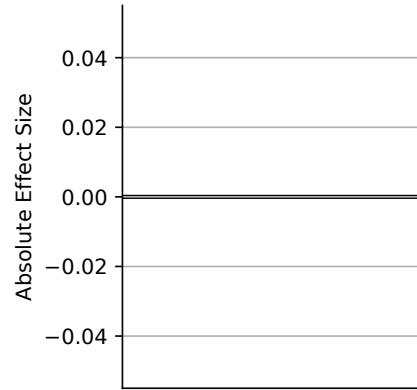


Fig. 36: Regressions of Latency Walltime Inlet (ns) against log computational intensity for computation vs. communication experiment (Section III-C). Lower is better. Ordinary least squares regression (top row) estimates relationship between dependent variable and mean of response variable. Quantile regression (bottom row) estimates relationship between independent variable and median of response variable. Error bands and bars are 95% confidence intervals.

## Ordinary Least Squares Regression

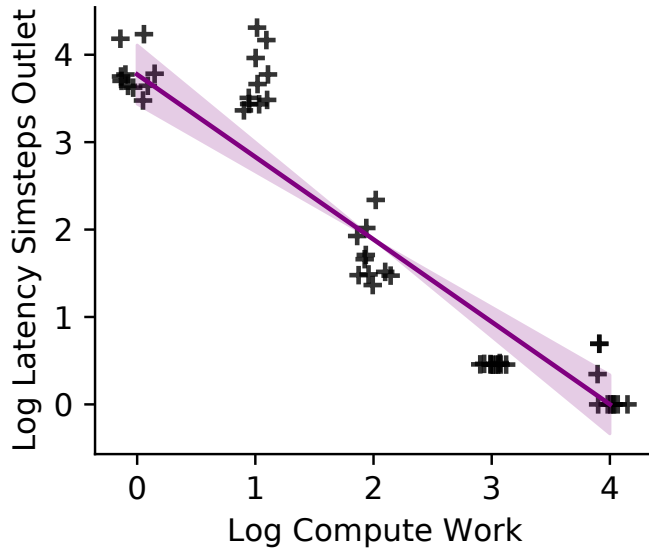


Estimated Statistic = Latency Simsteps Outlet Mean

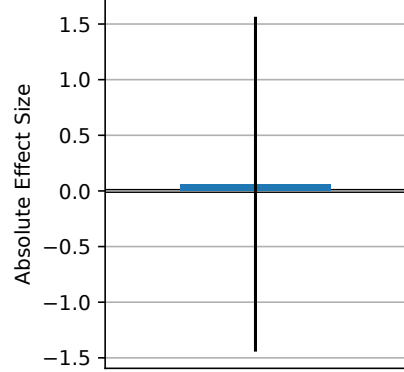


(a) Ordinary least squares regression plot. Observations are means per replicate. (b) Estimated regression coefficient for ordinary least squares regression. Zero corresponds to no effect.

## Quantile Regression



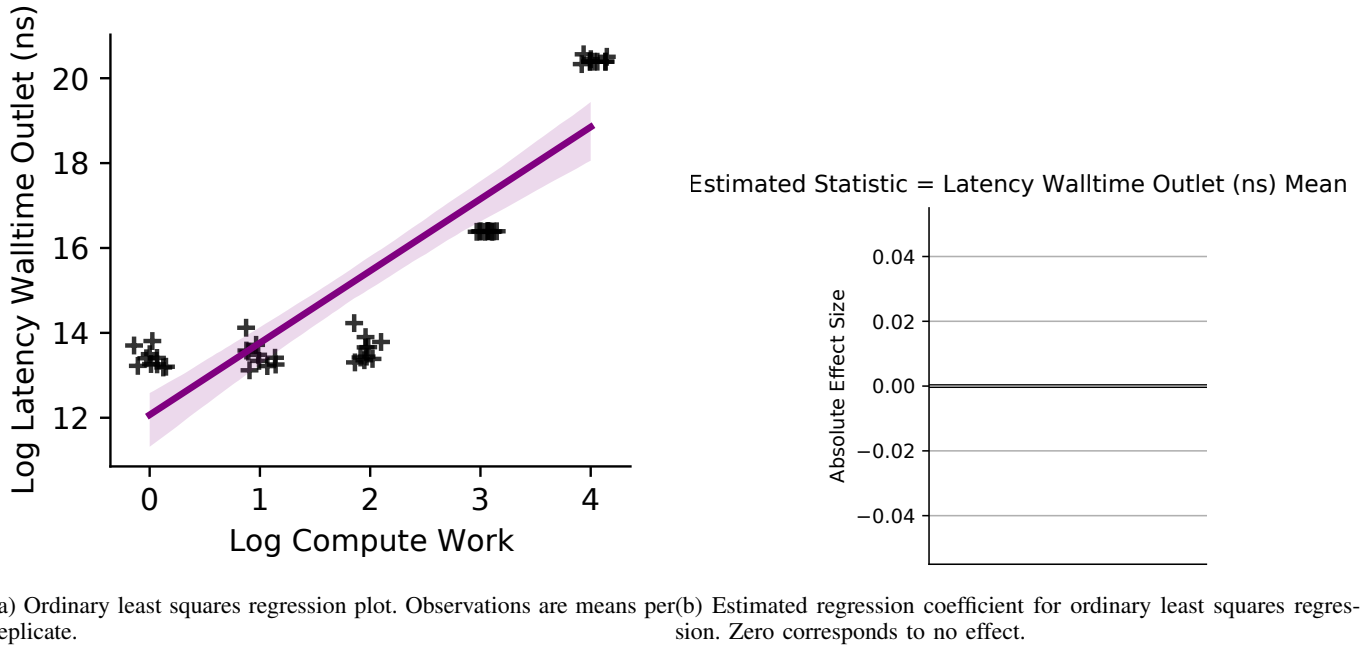
Estimated Statistic = Latency Simsteps Outlet Median



(c) Quantile regression plot. Observations are medians per replicate. (d) Estimated regression coefficient for quantile regression. Zero corresponds to no effect.

Fig. 37: Regressions of Latency Simsteps Outlet against log computational intensity for computation vs. communication experiment (Section III-C). Lower is better. Ordinary least squares regression (top row) estimates relationship between dependent variable and mean of response variable. Quantile regression (bottom row) estimates relationship between independent variable and median of response variable. Error bands and bars are 95% confidence intervals.

## Ordinary Least Squares Regression



## Quantile Regression

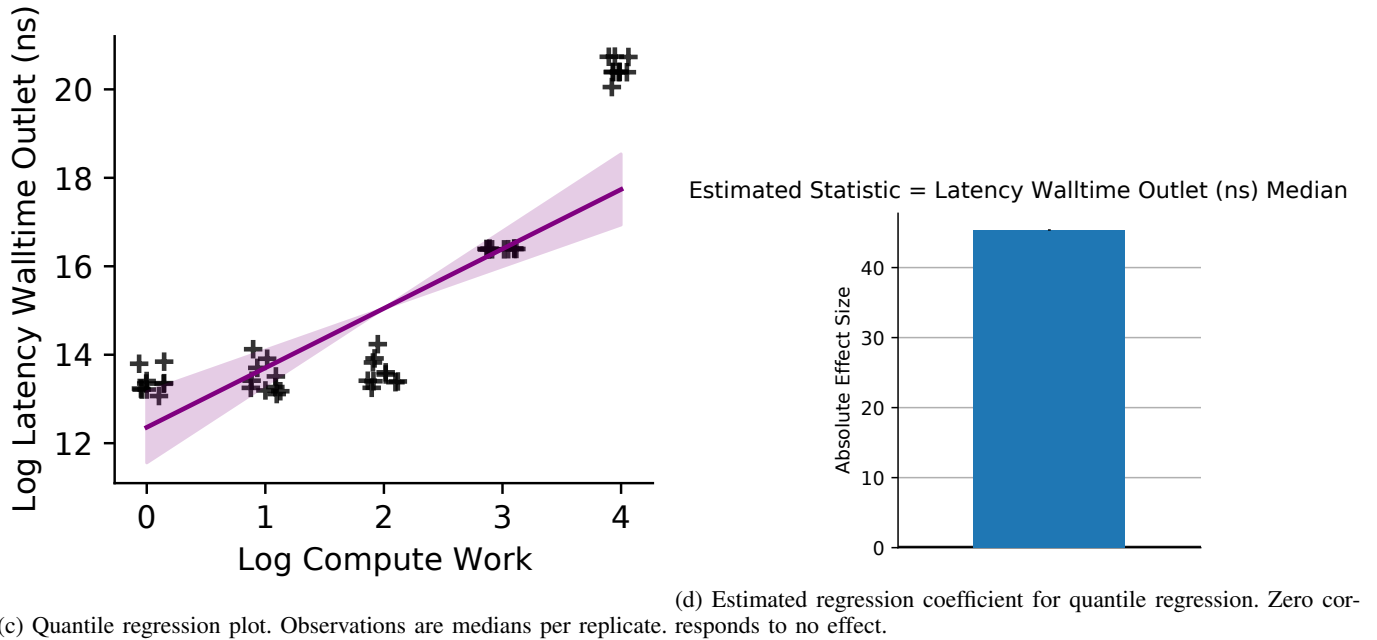
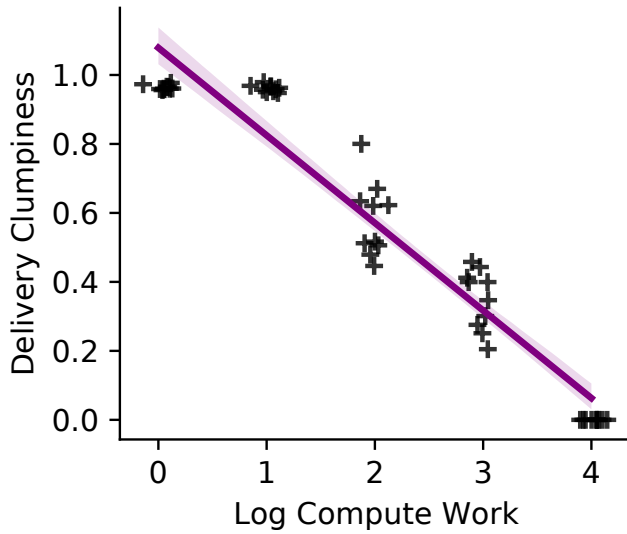


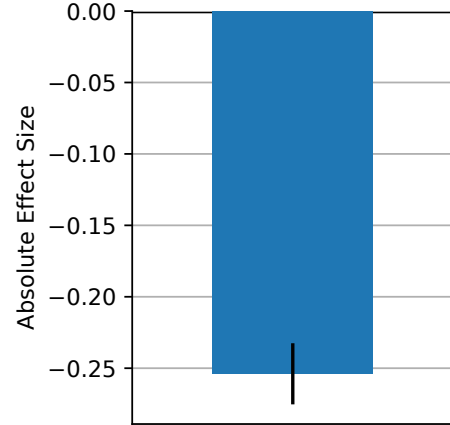
Fig. 38: Regressions of Latency Walltime Outlet (ns) against log computational intensity for computation vs. communication experiment (Section III-C). Lower is better. Ordinary least squares regression (top row) estimates relationship between dependent variable and mean of response variable. Quantile regression (bottom row) estimates relationship between independent variable and median of response variable. Error bands and bars are 95% confidence intervals.

## Ordinary Least Squares Regression



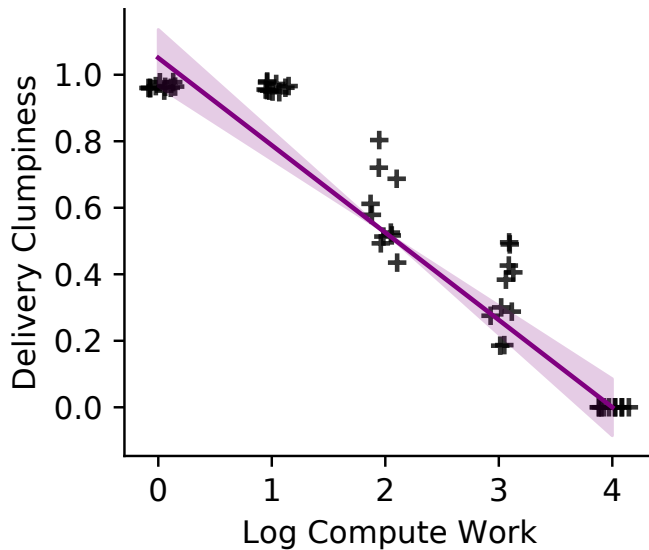
(a) Ordinary least squares regression plot. Observations are means per replicate.

Estimated Statistic = Delivery Clumpiness Mean



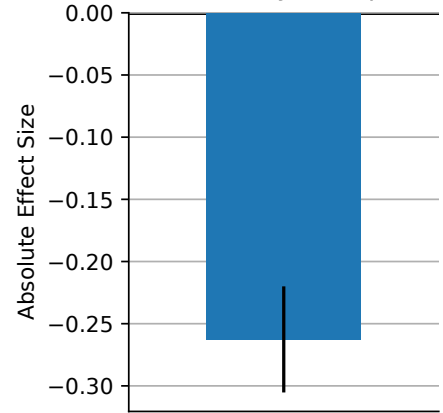
(b) Estimated regression coefficient for ordinary least squares regression. Zero corresponds to no effect.

## Quantile Regression



(c) Quantile regression plot. Observations are medians per replicate.

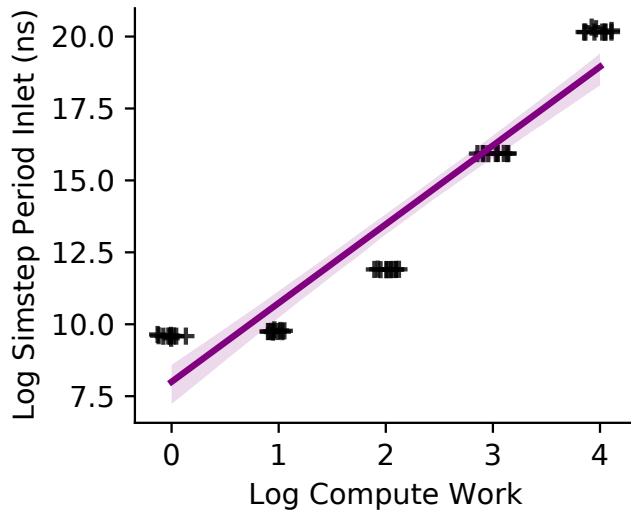
Estimated Statistic = Delivery Clumpiness Median



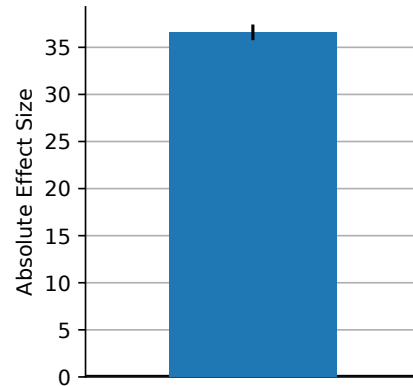
(d) Estimated regression coefficient for quantile regression. Zero corresponds to no effect.

Fig. 39: Regressions of Delivery Clumpiness against log computational intensity for computation vs. communication experiment (Section III-C). Lower is better. Ordinary least squares regression (top row) estimates relationship between dependent variable and mean of response variable. Quantile regression (bottom row) estimates relationship between independent variable and median of response variable. Error bands and bars are 95% confidence intervals.

## Ordinary Least Squares Regression

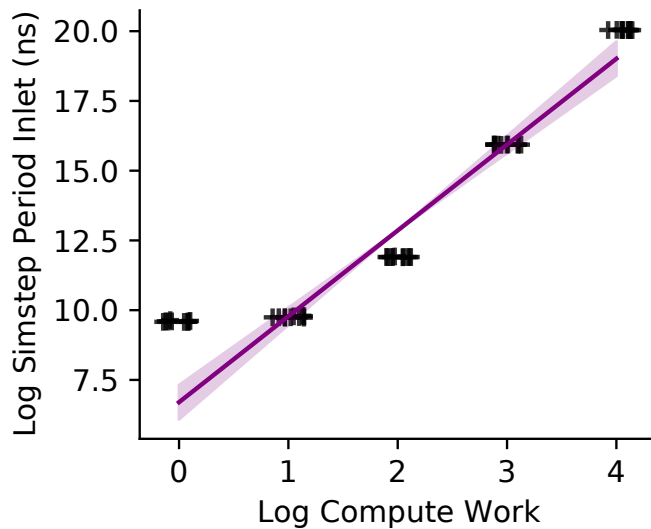


Estimated Statistic = Simstep Period Inlet (ns) Mean

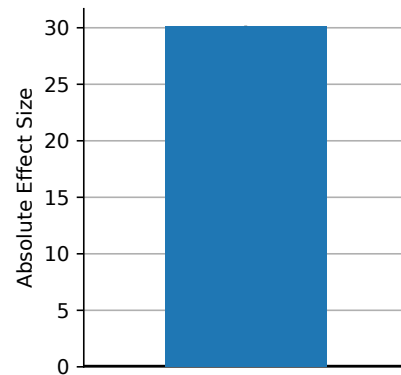


(a) Ordinary least squares regression plot. Observations are means per replicate. (b) Estimated regression coefficient for ordinary least squares regression. Zero corresponds to no effect.

## Quantile Regression



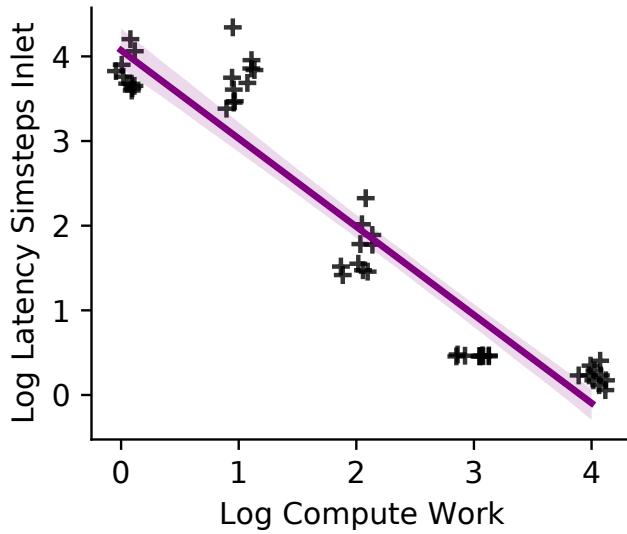
Estimated Statistic = Simstep Period Inlet (ns) Median



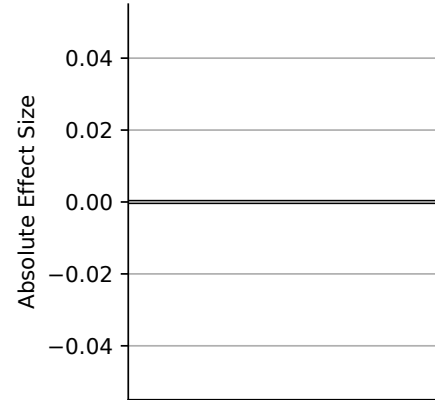
(c) Quantile regression plot. Observations are medians per replicate. (d) Estimated regression coefficient for quantile regression. Zero corresponds to no effect.

Fig. 40: Regressions of Simstep Period Inlet (ns) against log computational intensity for computation vs. communication experiment (Section III-C). Lower is better. Ordinary least squares regression (top row) estimates relationship between dependent variable and mean of response variable. Quantile regression (bottom row) estimates relationship between independent variable and median of response variable. Error bands and bars are 95% confidence intervals.

## Ordinary Least Squares Regression

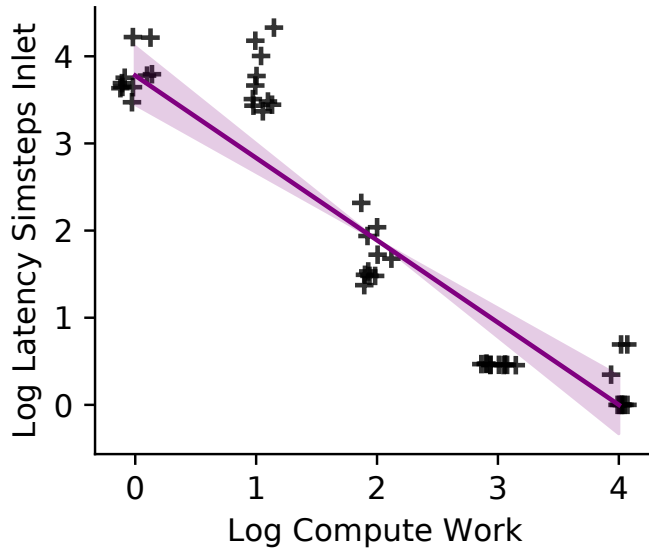


Estimated Statistic = Latency Simsteps Inlet Mean

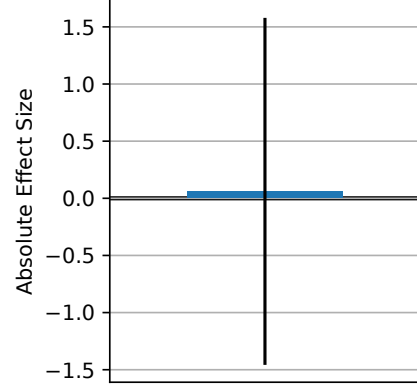


(a) Ordinary least squares regression plot. Observations are means per replicate. (b) Estimated regression coefficient for ordinary least squares regression. Zero corresponds to no effect.

## Quantile Regression



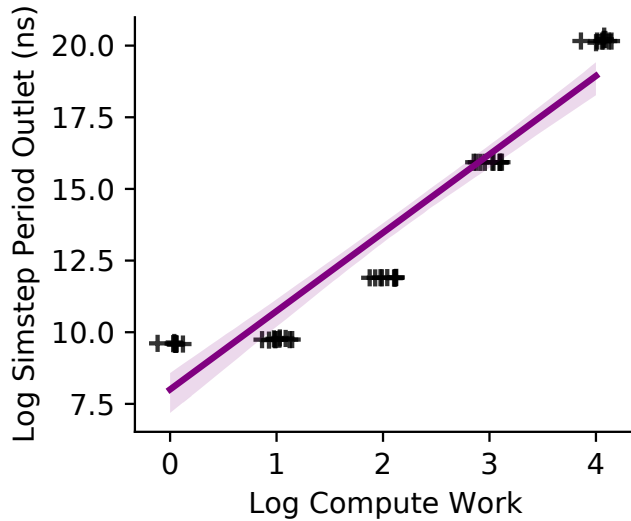
Estimated Statistic  $\tau_{\tau=6}$  = Latency Simsteps Inlet Median



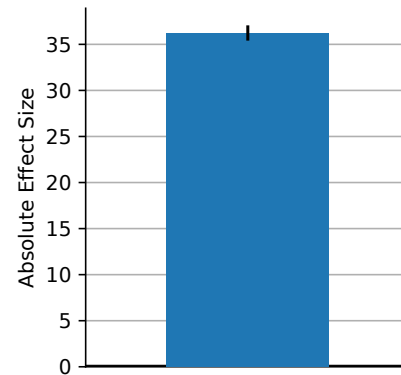
(c) Quantile regression plot. Observations are medians per replicate. (d) Estimated regression coefficient for quantile regression. Zero corresponds to no effect.

Fig. 41: Regressions of Latency Simsteps Inlet against log computational intensity for computation vs. communication experiment (Section III-C). Lower is better. Ordinary least squares regression (top row) estimates relationship between dependent variable and mean of response variable. Quantile regression (bottom row) estimates relationship between independent variable and median of response variable. Error bands and bars are 95% confidence intervals.

## Ordinary Least Squares Regression

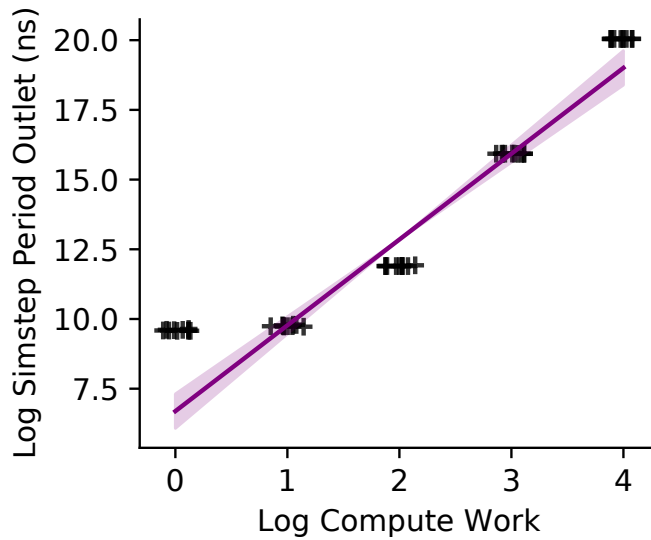


Estimated Statistic = Simstep Period Outlet (ns) Mean

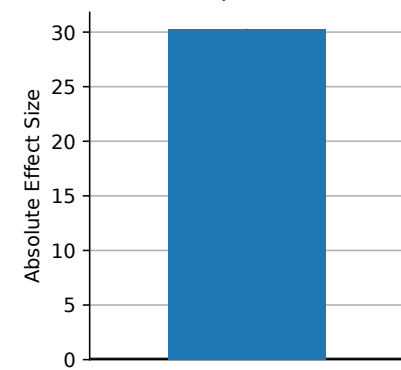


(a) Ordinary least squares regression plot. Observations are means per replicate. (b) Estimated regression coefficient for ordinary least squares regression. Zero corresponds to no effect.

## Quantile Regression



Estimated Statistic = Simstep Period Outlet (ns) Median

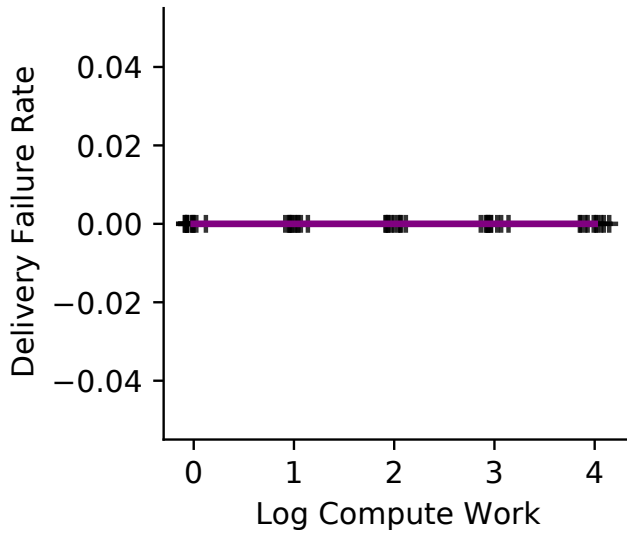


(c) Quantile regression plot. Observations are medians per replicate. (d) Estimated regression coefficient for quantile regression. Zero corresponds to no effect.

Fig. 42: Regressions of Simstep Period Outlet (ns) against log computational intensity for computation vs. communication experiment (Section III-C). Lower is better. Ordinary least squares regression (top row) estimates relationship between dependent variable and mean of response variable. Quantile regression (bottom row) estimates relationship between independent variable and median of response variable. Error bands and bars are 95% confidence intervals.

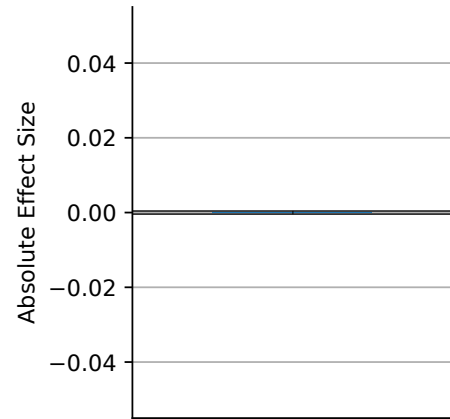


## Ordinary Least Squares Regression



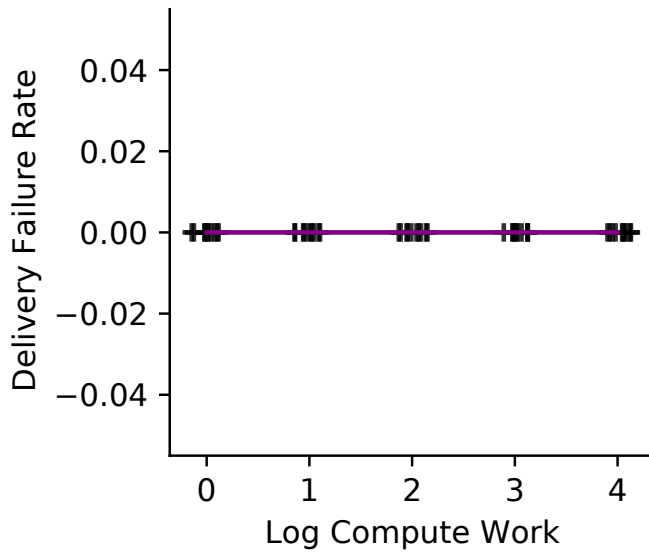
(a) Ordinary least squares regression plot. Observations are means per replicate.

Estimated Statistic = Delivery Failure Rate Mean



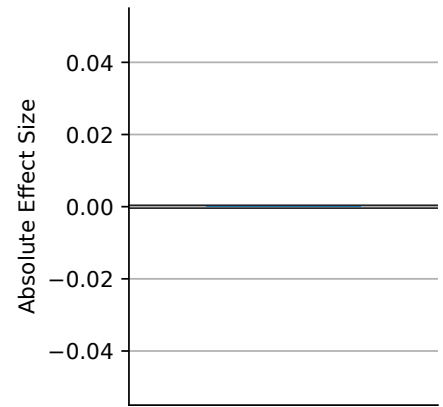
(b) Estimated regression coefficient for ordinary least squares regression. Zero corresponds to no effect.

## Quantile Regression



(c) Quantile regression plot. Observations are medians per replicate.

Estimated Statistic = Delivery Failure Rate Median



(d) Estimated regression coefficient for quantile regression. Zero corresponds to no effect.

Fig. 43: Regressions of Delivery Failure Rate against log computational intensity for computation vs. communication experiment (Section III-C). Lower is better. Ordinary least squares regression (top row) estimates relationship between dependent variable and mean of response variable. Quantile regression (bottom row) estimates relationship between independent variable and median of response variable. Error bands and bars are 95% confidence intervals.

TABLE XVIII: Full Ordinary Least Squares Regression results of quality of service metrics against log computational intensity for computation vs. communication experiment (Section III-C). Significance level  $p < 0.05$  used. Inf or NaN values may occur due to multicollinearity or due to inf or NaN observations.

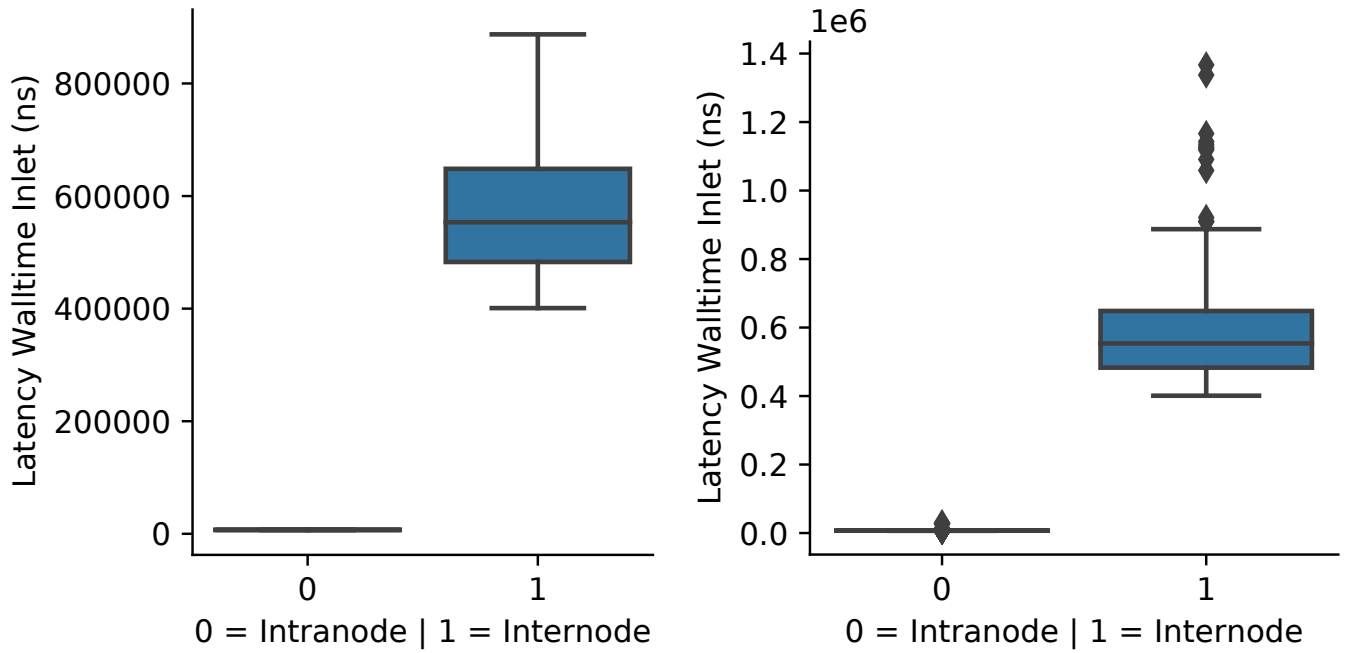
Metric	Statistic	Significant	Effect Sign	Cpus Per Node	Num Simsels Per Cpu	Num Processes	Absolute Effect Size	Absolute Effect Size 95% CI		Relative Effect Size	Relative Effect Size 95% CI		n	p
								Lower Bound	Upper Bound		Lower Bound	Upper Bound		
Latency Walltime Inlet (ns)	mean	NaN	1	1	2	inf	nan	nan	inf	nan	nan	nan	50	nan
Latency Walltime Outlet (ns)	mean	NaN	1	1	2	inf	nan	nan	inf	nan	nan	nan	50	nan
Latency Simsteps Inlet	mean	NaN	1	1	2	inf	nan	nan	inf	nan	nan	nan	50	nan
Latency Simsteps Outlet	mean	NaN	1	1	2	inf	nan	nan	inf	nan	nan	nan	50	nan
Delivery Failure Rate	mean	NaN	1	1	2	0	0	0	nan	nan	nan	nan	50	nan
Delivery Clumpiness	mean	-	1	1	2	-0.25	-0.28	-0.23	-0.26	-0.29	-0.24	50	2.8e-28	
Simstep Period Inlet (ns)	mean	+	1	1	2	37	36	37	0.0025	0.0024	0.0026	50	7.1e-55	
Simstep Period Outlet (ns)	mean	+	1	1	2	36	35	37	0.0025	0.0024	0.0025	50	1.1e-54	

TABLE XIX: Full Quantile Regression results of quality of service metrics against log computational intensity for computation vs. communication experiment (Section III-C). Significance level  $p < 0.05$  used. Inf or NaN values may occur due to multicollinearity or due to inf or NaN observations.

Metric	Statistic	Significant Effect Sign	Cpus Per Node	Num Simels Per Cpu	Num Processes	Absolute Effect Size	Absolute Effect Size 95% CI Lower Bound	Absolute Effect Size 95% CI Upper Bound	Relative Effect Size	Relative Effect Size 95% CI Lower Bound	Relative Effect Size 95% CI Upper Bound	n	p
Latency Walltime Inlet (ns)	median	+	1	1	2	45	45	45	7.2e-05	7.2e-05	7.2e-05	50	5.8e-107
Latency Walltime Outlet (ns)	median	+	1	1	2	45	45	45	7.2e-05	7.2e-05	7.2e-05	50	1.8e-103
Latency Simsteps Inlet	median	0	1	1	2	6.1e-08	-1.5e-06	1.6e-06	7.2e-05	-3.5e-08	3.8e-08	50	0.94
Latency Simsteps Outlet	median	0	1	1	2	6.1e-08	-1.4e-06	1.6e-06	7.2e-05	-3.5e-08	3.7e-08	50	0.94
Delivery Failure Rate	median	NaN	1	1	2	0	nan	nan	nan	nan	nan	50	nan
Delivery Clumpiness	median	-	1	1	2	-0.26	-0.31	-0.22	-0.32	-0.23	-0.23	50	1.5e-16
Simstep Period Inlet (ns)	median	+	1	1	2	30	30	30	0.0021	0.0021	0.0021	50	1.9e-139
Simstep Period Outlet (ns)	median	+	1	1	2	30	30	30	0.0021	0.0021	0.0021	50	1.1e-143

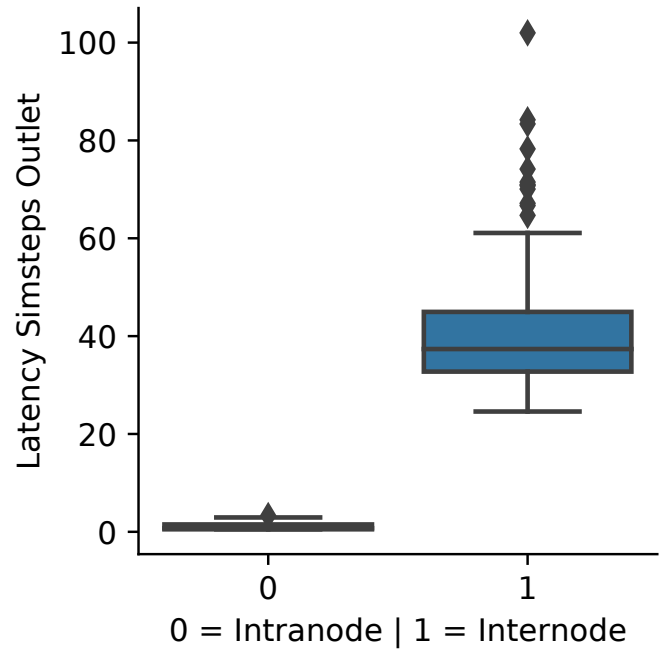
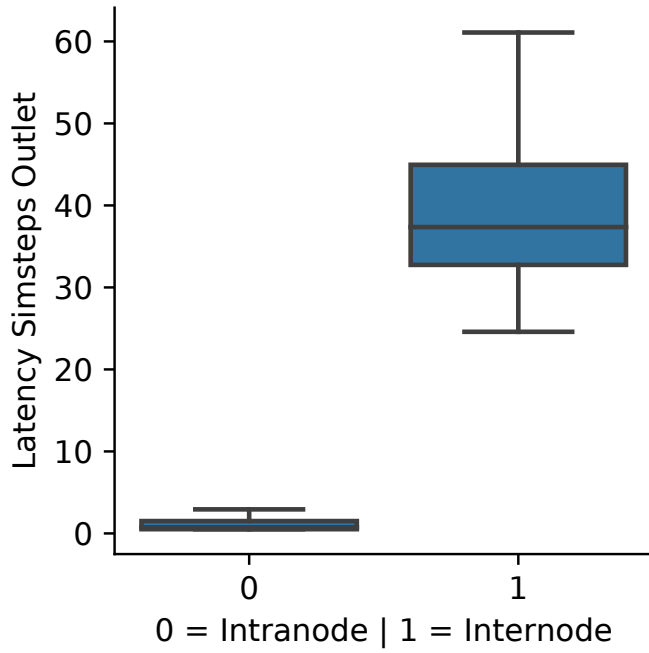
## VI. INTRANODE VS INTERNODE

This section provides full results from intranode vs. internode experiments discussed in Section III-D.



(a) Distribution of Latency Walltime Inlet (ns) for each snapshot, (b) Distribution of Latency Walltime Inlet (ns) for each snapshot, with without outliers.

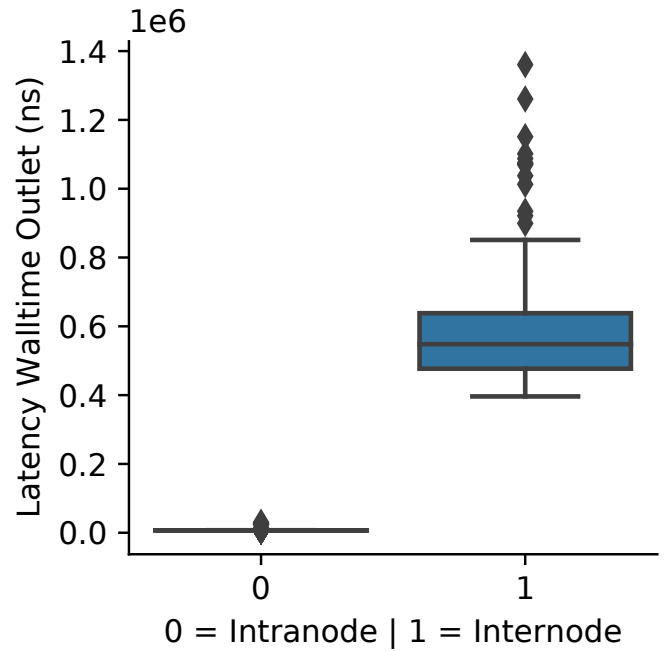
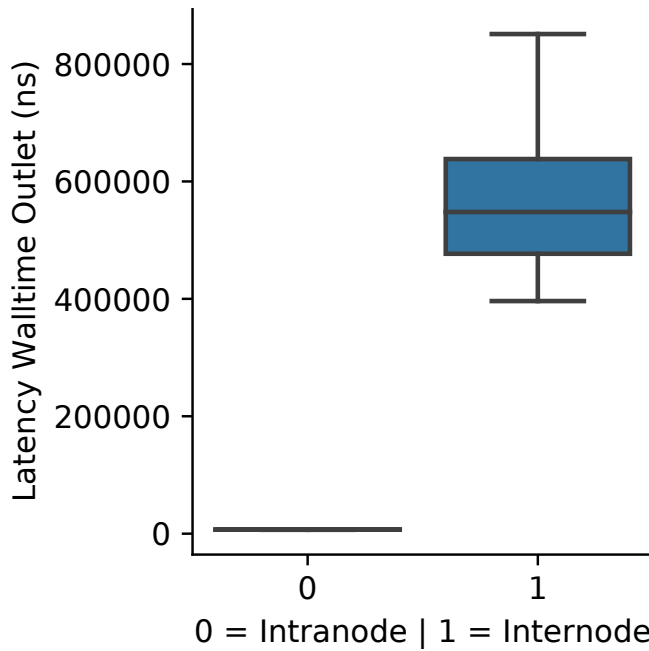
Fig. 44: Distribution of Latency Walltime Inlet (ns) for individual snapshot measurements for intranode vs. internode experiment (Section III-D). Lower is better.



(a) Distribution of Latency Simsteps Outlet for each snapshot, without outliers.

(b) Distribution of Latency Simsteps Outlet for each snapshot, with outliers.

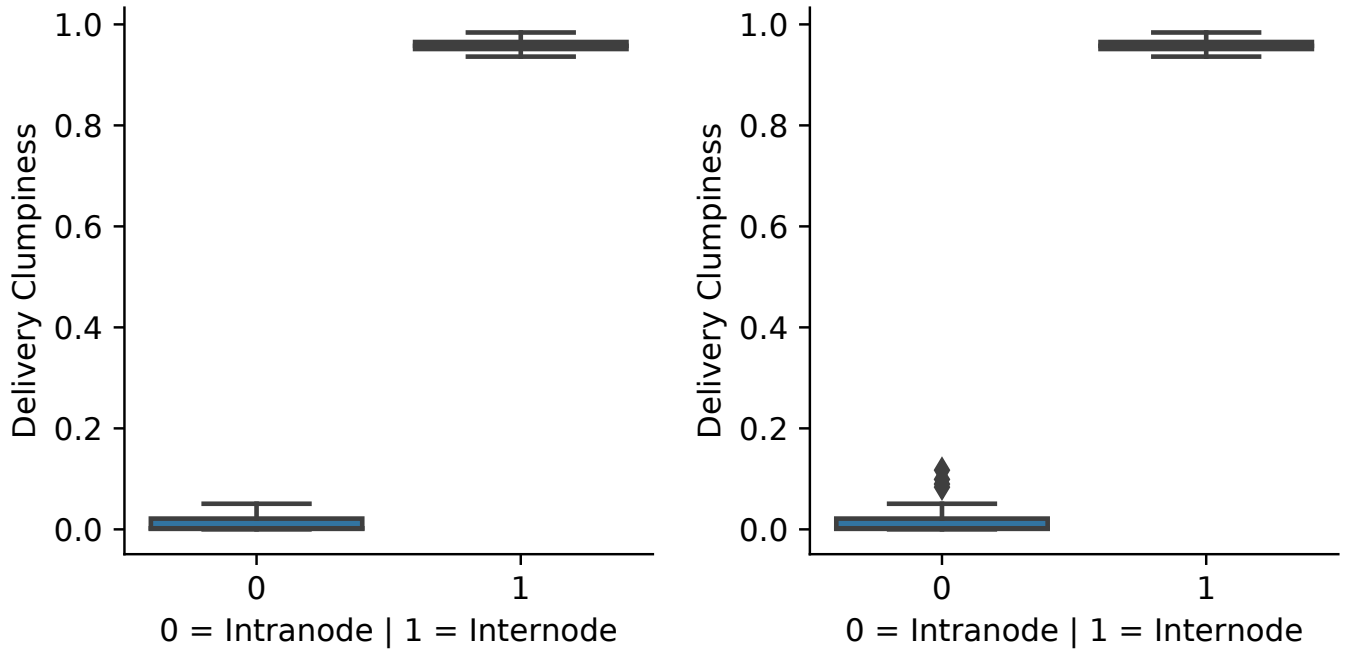
Fig. 45: Distribution of Latency Simsteps Outlet for individual snapshot measurements for intranode vs. internode experiment (Section III-D). Lower is better.



(a) Distribution of Latency Walltime Outlet (ns) for each snapshot, without outliers.

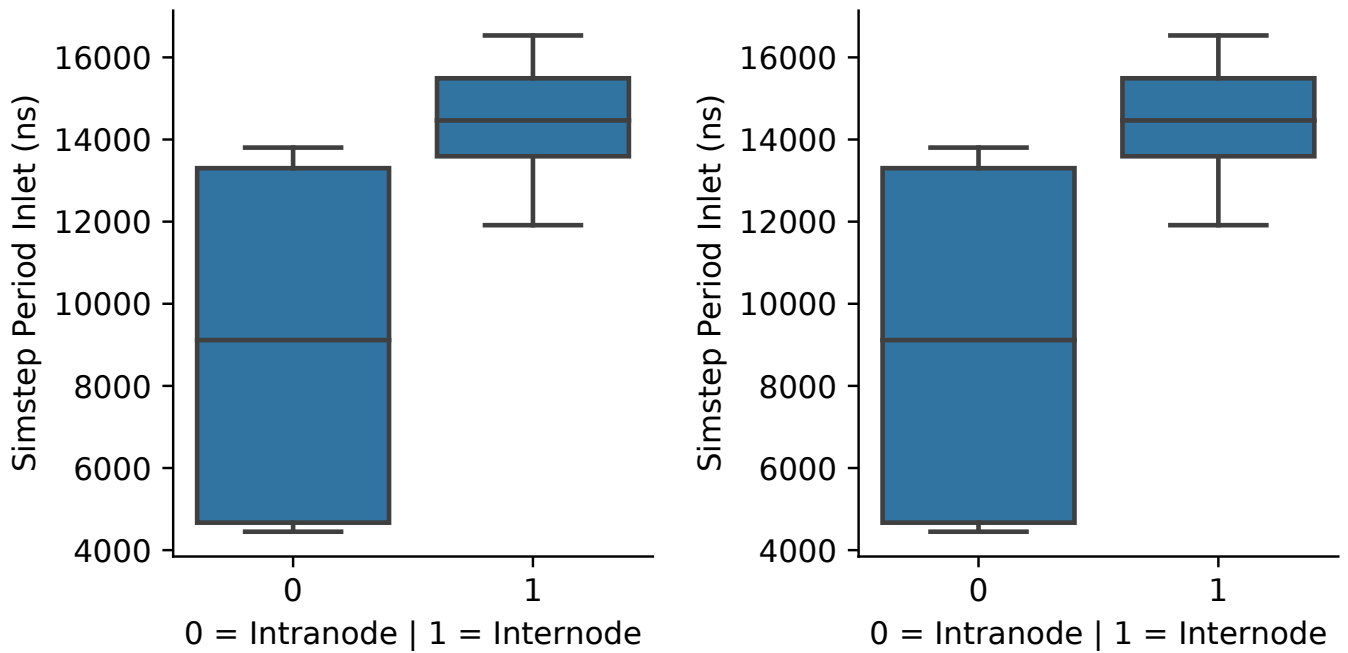
(b) Distribution of Latency Walltime Outlet (ns) for each snapshot, with outliers.

Fig. 46: Distribution of Latency Walltime Outlet (ns) for individual snapshot measurements for intranode vs. internode experiment (Section III-D). Lower is better.



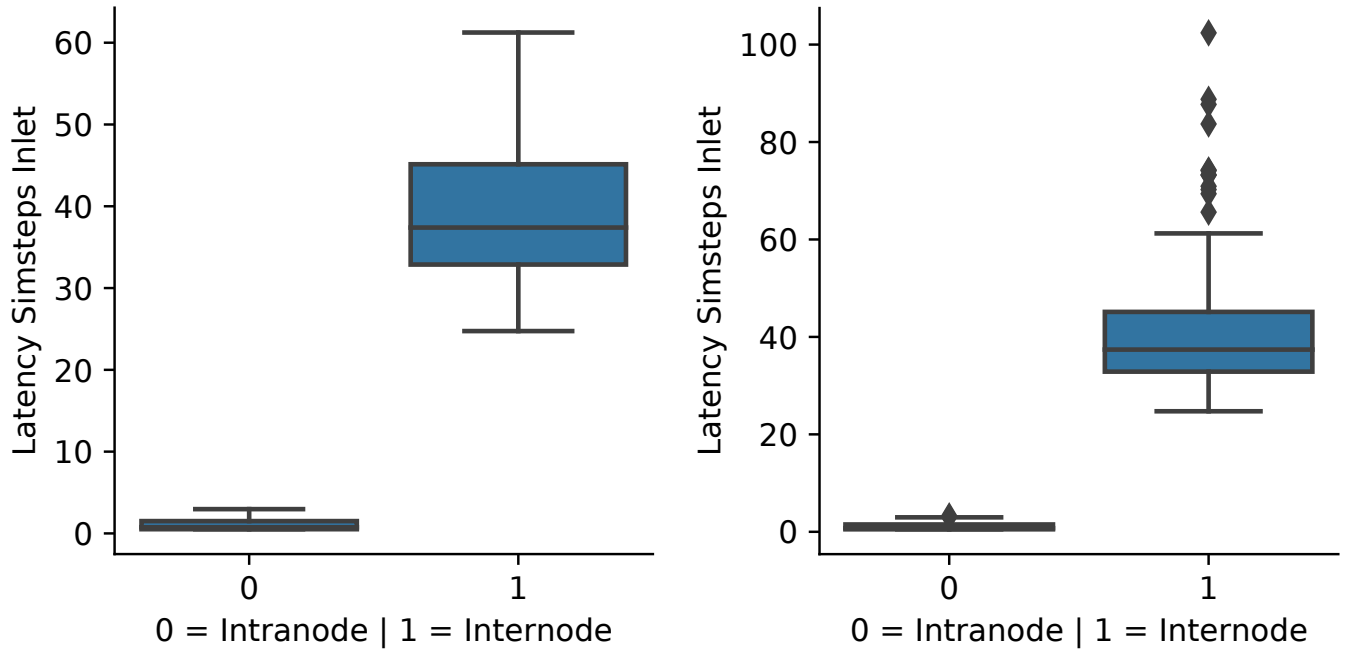
(a) Distribution of Delivery Clumpiness for each snapshot, without outliers. (b) Distribution of Delivery Clumpiness for each snapshot, with outliers.

Fig. 47: Distribution of Delivery Clumpiness for individual snapshot measurements for intranode vs. internode experiment (Section III-D). Lower is better.



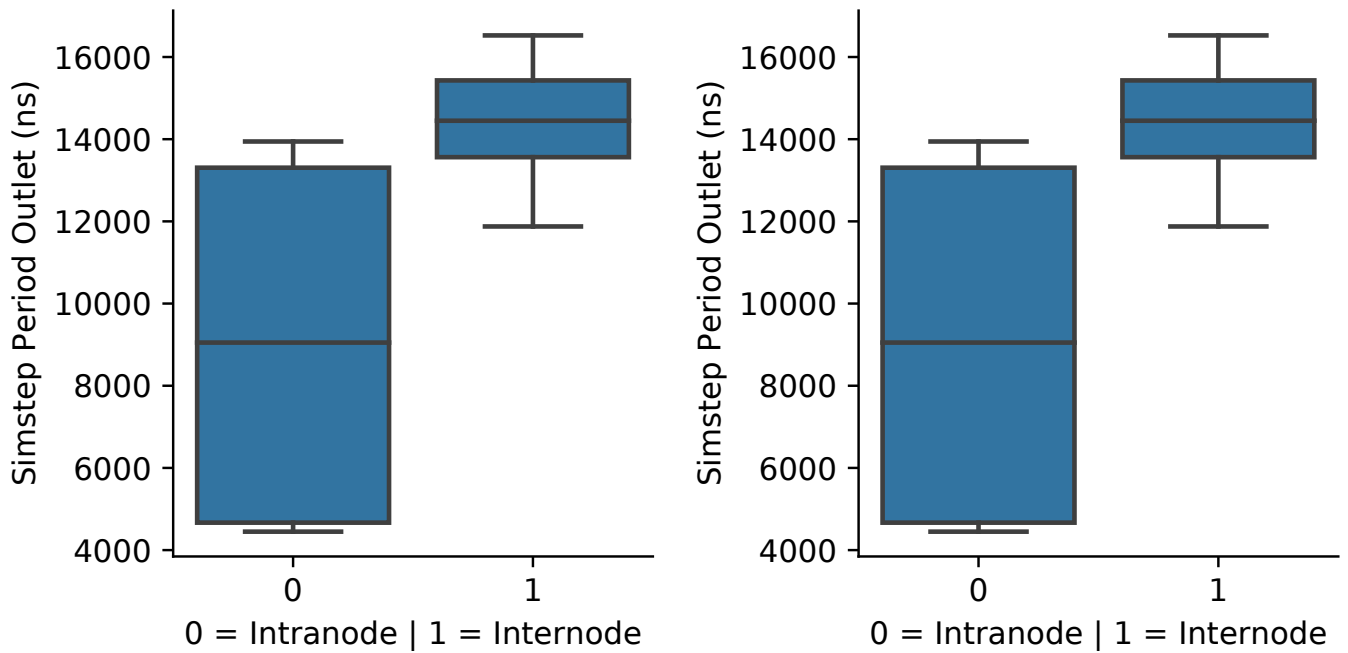
(a) Distribution of Simstep Period Inlet (ns) for each snapshot, without outliers. (b) Distribution of Simstep Period Inlet (ns) for each snapshot, with outliers.

Fig. 48: Distribution of Simstep Period Inlet (ns) for individual snapshot measurements for intranode vs. internode experiment (Section III-D). Lower is better.



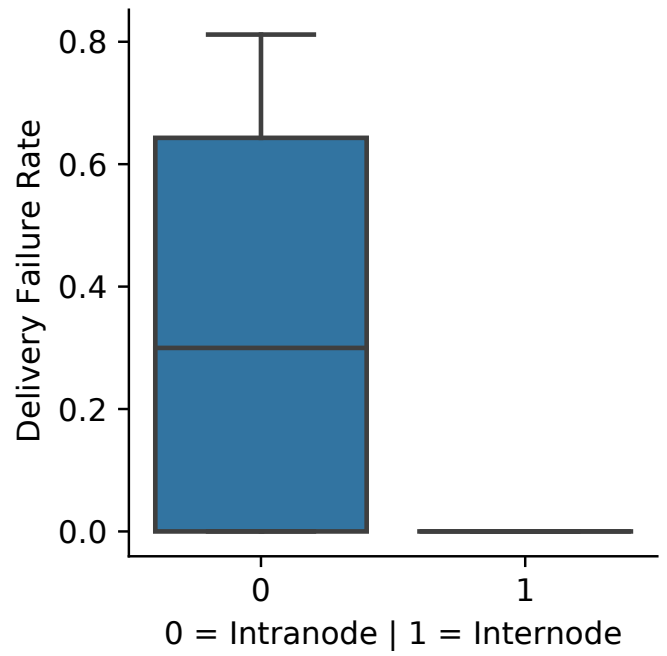
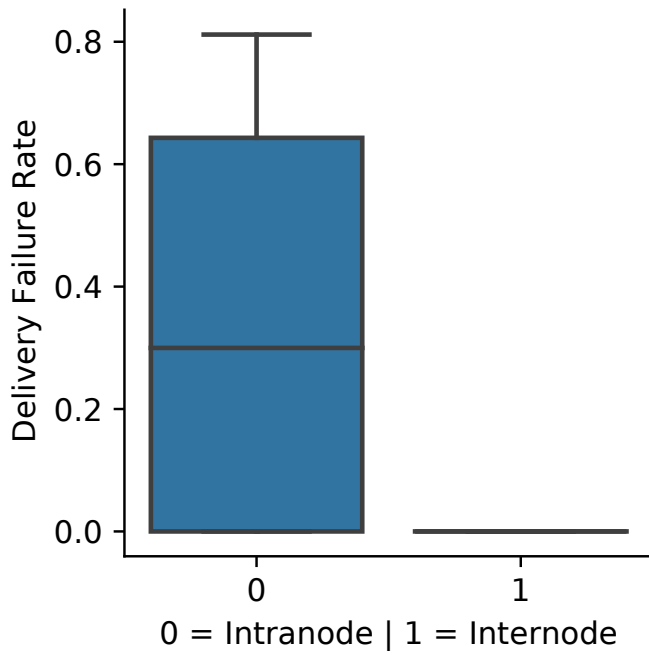
(a) Distribution of Latency Simsteps Inlet for each snapshot, without outliers. (b) Distribution of Latency Simsteps Inlet for each snapshot, with outliers.

Fig. 49: Distribution of Latency Simsteps Inlet for individual snapshot measurements for intranode vs. internode experiment (Section III-D). Lower is better.



(a) Distribution of Simstep Period Outlet (ns) for each snapshot, without outliers. (b) Distribution of Simstep Period Outlet (ns) for each snapshot, with outliers.

Fig. 50: Distribution of Simstep Period Outlet (ns) for individual snapshot measurements for intranode vs. internode experiment (Section III-D). Lower is better.

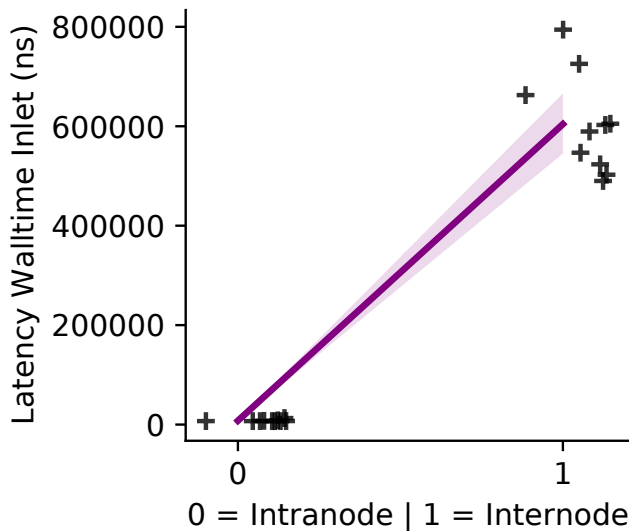


(a) Distribution of Delivery Failure Rate for each snapshot, without outliers. (b) Distribution of Delivery Failure Rate for each snapshot, with outliers.

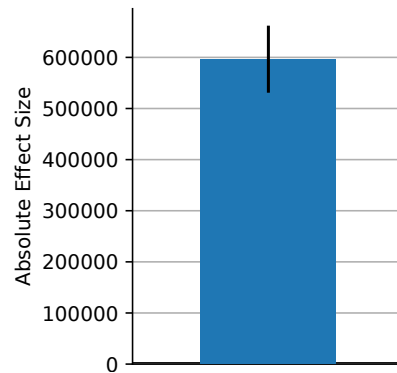
Fig. 51: Distribution of Delivery Failure Rate for individual snapshot measurements for intranode vs. internode experiment (Section III-D). Lower is better.



## Ordinary Least Squares Regression

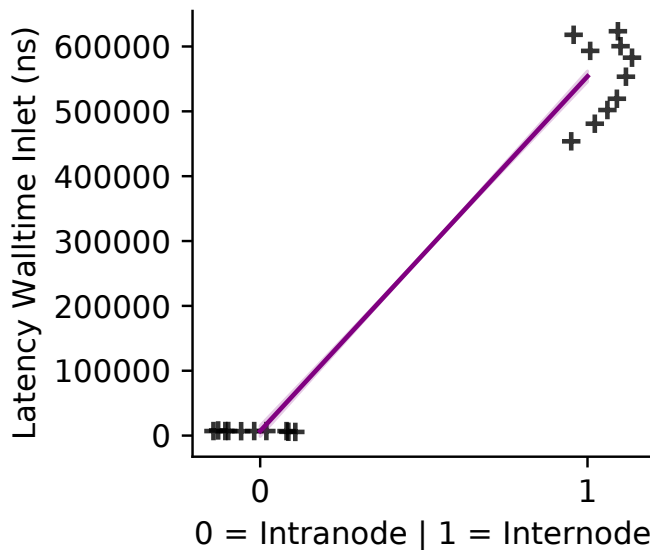


Estimated Statistic = Latency Walltime Inlet (ns) Mean

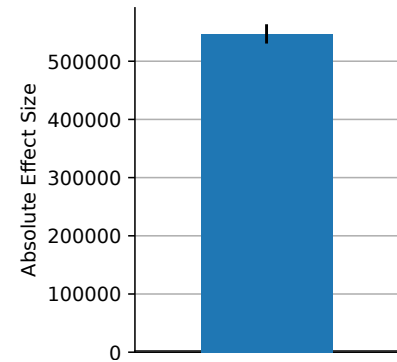


(a) Ordinary least squares regression plot. Observations are means per replicate. (b) Estimated regression coefficient for ordinary least squares regression. Zero corresponds to no effect.

## Quantile Regression



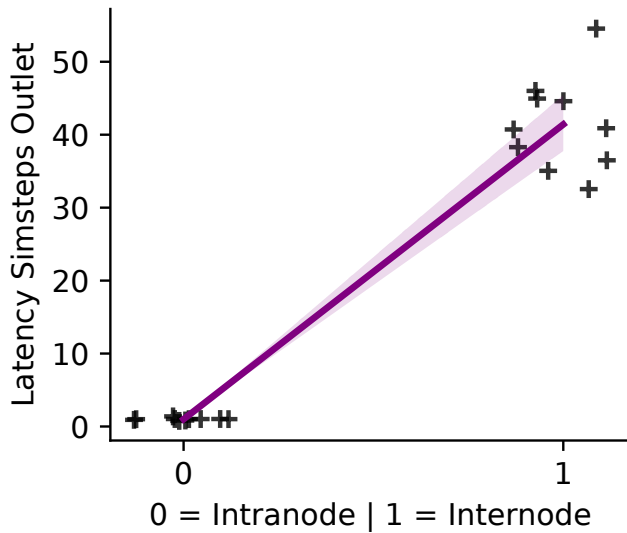
Estimated Statistic = Latency Walltime Inlet (ns) Median



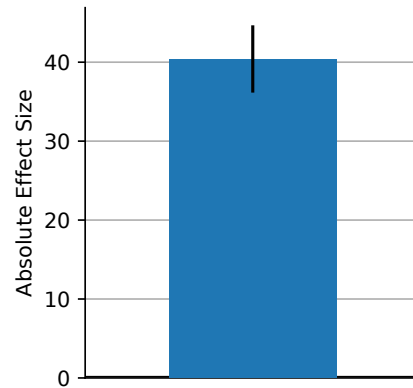
(c) Quantile regression plot. Observations are medians per replicate. (d) Estimated regression coefficient for quantile regression. Zero corresponds to no effect.

Fig. 52: Regressions of Latency Walltime Inlet (ns) against categorically coded treatment for intranode vs. internode experiment (Section III-D). Lower is better. Ordinary least squares regression (top row) estimates relationship between categorical dependent variable and mean of response variable. Quantile regression (bottom row) estimates relationship between categorical independent variable and median of response variable. Error bands and bars are 95% confidence intervals.

## Ordinary Least Squares Regression

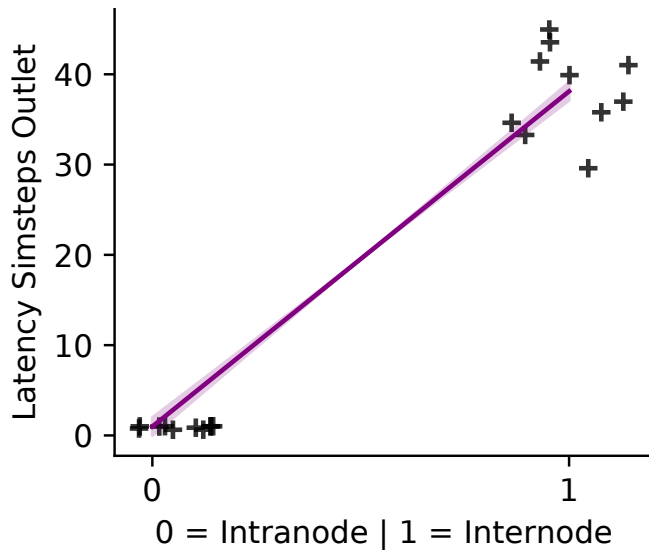


Estimated Statistic = Latency Simsteps Outlet Mean

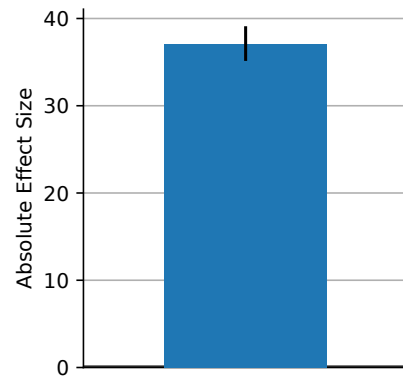


(a) Ordinary least squares regression plot. Observations are means per replicate. (b) Estimated regression coefficient for ordinary least squares regression. Zero corresponds to no effect.

## Quantile Regression



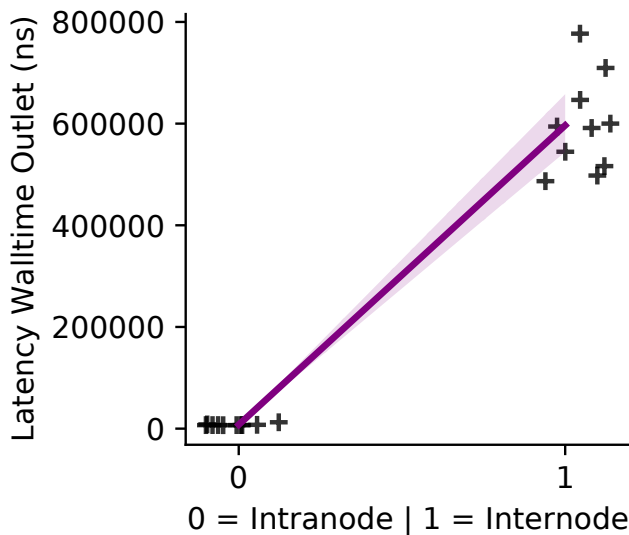
Estimated Statistic = Latency Simsteps Outlet Median



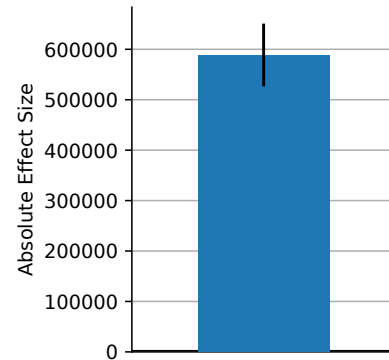
(c) Quantile regression plot. Observations are medians per replicate. (d) Estimated regression coefficient for quantile regression. Zero corresponds to no effect.

Fig. 53: Regressions of Latency Simsteps Outlet against categorically coded treatment for intranode vs. internode experiment (Section III-D). Lower is better. Ordinary least squares regression (top row) estimates relationship between categorical dependent variable and mean of response variable. Quantile regression (bottom row) estimates relationship between categorical independent variable and median of response variable. Error bands and bars are 95% confidence intervals.

## Ordinary Least Squares Regression

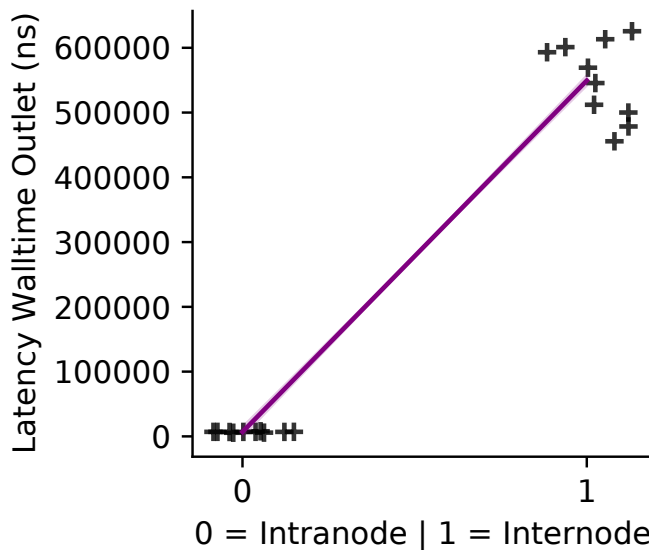


Estimated Statistic = Latency Walltime Outlet (ns) Mean

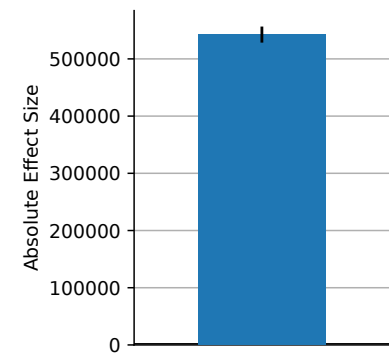


(a) Ordinary least squares regression plot. Observations are means per replicate. (b) Estimated regression coefficient for ordinary least squares regression. Zero corresponds to no effect.

## Quantile Regression



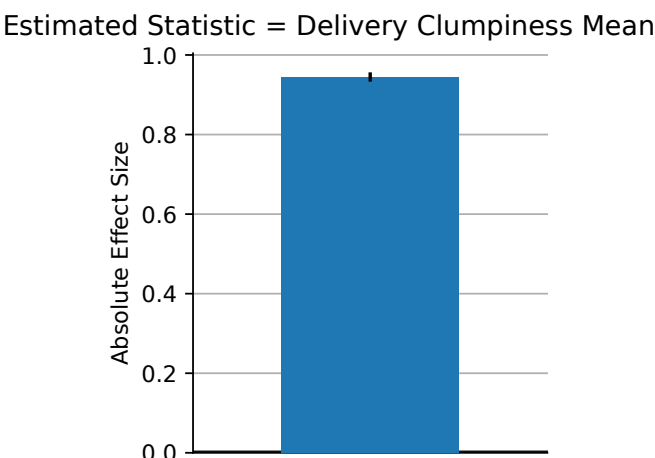
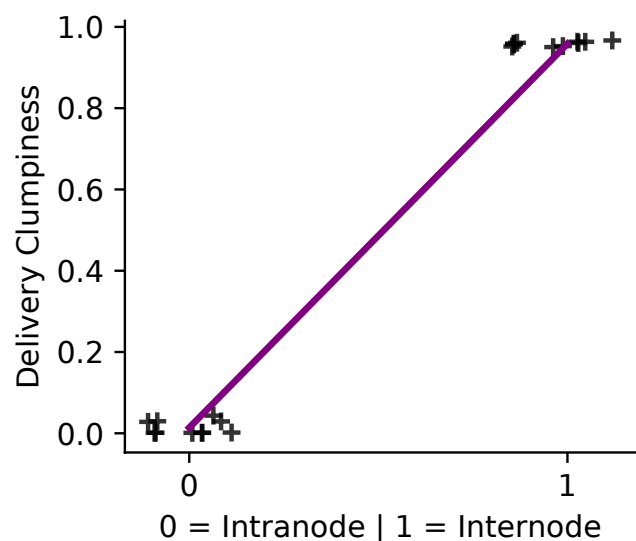
Estimated Statistic = Latency Walltime Outlet (ns) Median



(c) Quantile regression plot. Observations are medians per replicate. (d) Estimated regression coefficient for quantile regression. Zero corresponds to no effect.

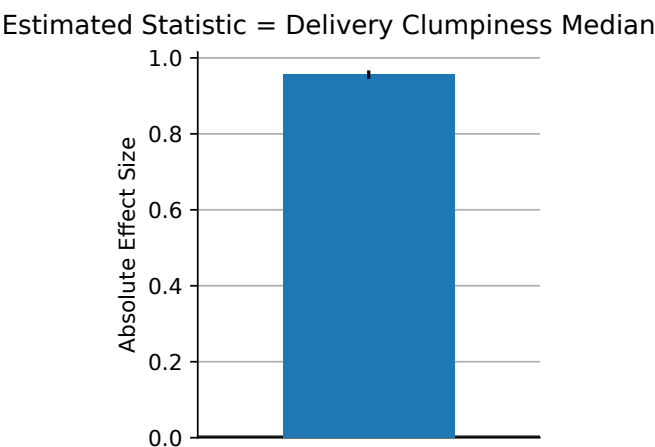
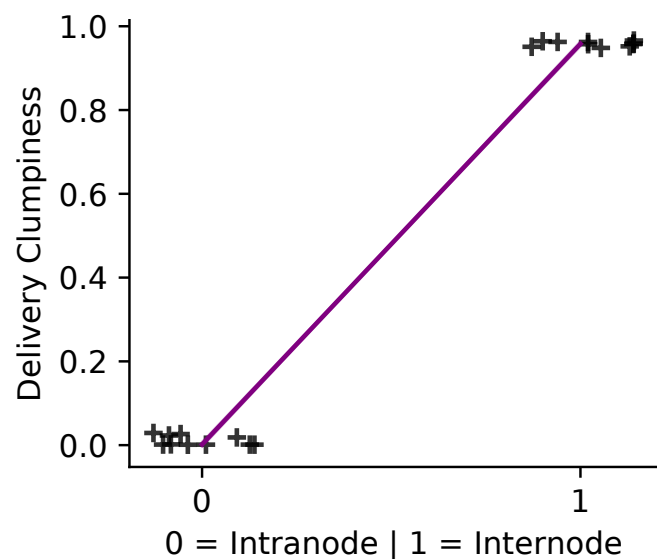
Fig. 54: Regressions of Latency Walltime Outlet (ns) against categorically coded treatment for intranode vs. internode experiment (Section III-D). Lower is better. Ordinary least squares regression (top row) estimates relationship between categorical dependent variable and mean of response variable. Quantile regression (bottom row) estimates relationship between categorical independent variable and median of response variable. Error bands and bars are 95% confidence intervals.

# Ordinary Least Squares Regression



(a) Ordinary least squares regression plot. Observations are means per replicate. (b) Estimated regression coefficient for ordinary least squares regression. Zero corresponds to no effect.

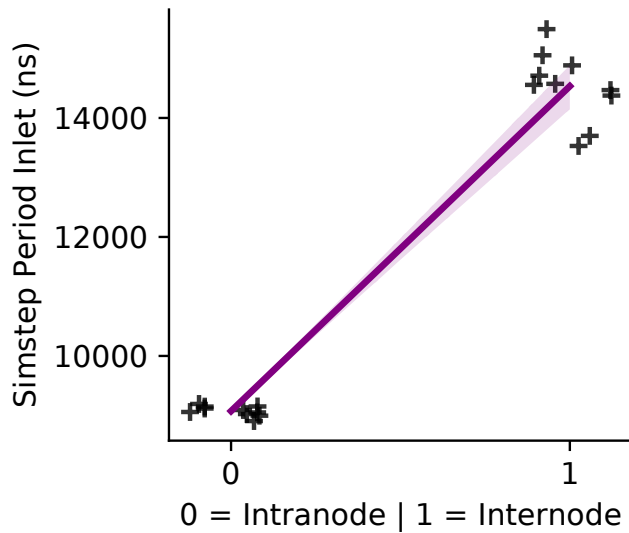
# Quantile Regression



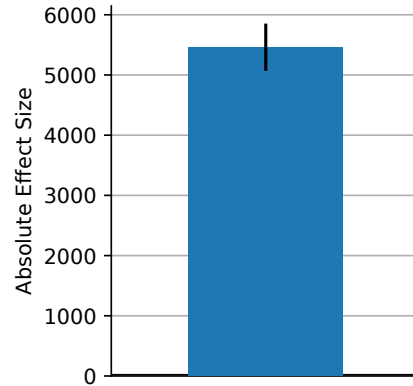
(c) Quantile regression plot. Observations are medians per replicate. (d) Estimated regression coefficient for quantile regression. Zero corresponds to no effect.

Fig. 55: Regressions of Delivery Clumpiness against categorically coded treatment for intranode vs. internode experiment (Section III-D). Lower is better. Ordinary least squares regression (top row) estimates relationship between categorical dependent variable and mean of response variable. Quantile regression (bottom row) estimates relationship between categorical independent variable and median of response variable. Error bands and bars are 95% confidence intervals.

## Ordinary Least Squares Regression

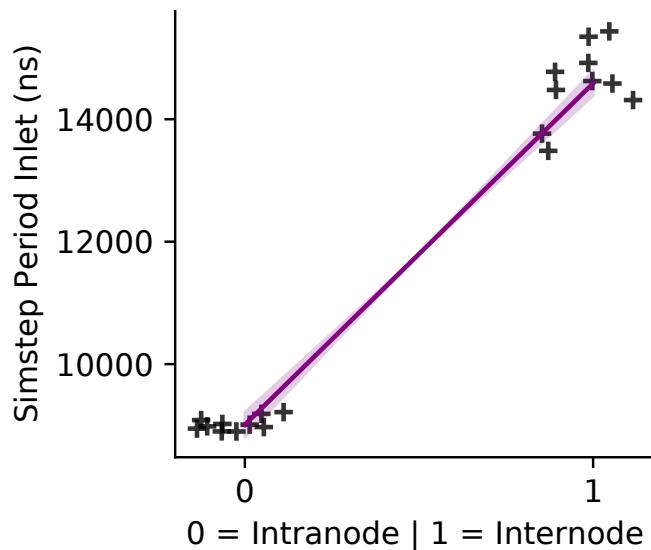


Estimated Statistic = Simstep Period Inlet (ns) Mean

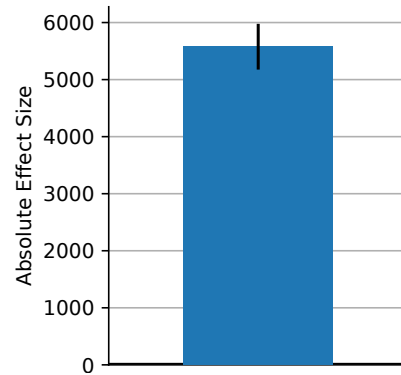


(a) Ordinary least squares regression plot. Observations are means per replicate. (b) Estimated regression coefficient for ordinary least squares regression. Zero corresponds to no effect.

## Quantile Regression



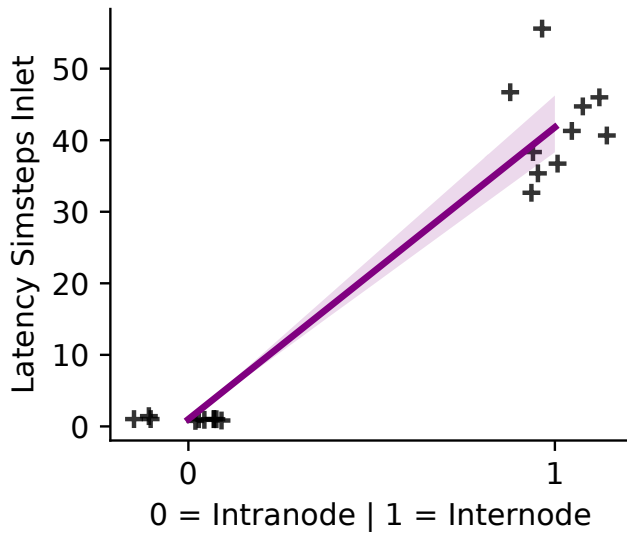
Estimated Statistic = Simstep Period Inlet (ns) Median



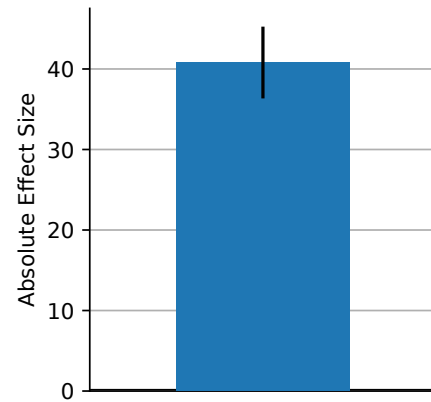
(c) Quantile regression plot. Observations are medians per replicate. (d) Estimated regression coefficient for quantile regression. Zero corresponds to no effect.

Fig. 56: Regressions of Simstep Period Inlet (ns) against categorically coded treatment for intranode vs. internode experiment (Section III-D). Lower is better. Ordinary least squares regression (top row) estimates relationship between categorical dependent variable and mean of response variable. Quantile regression (bottom row) estimates relationship between categorical independent variable and median of response variable. Error bands and bars are 95% confidence intervals.

## Ordinary Least Squares Regression

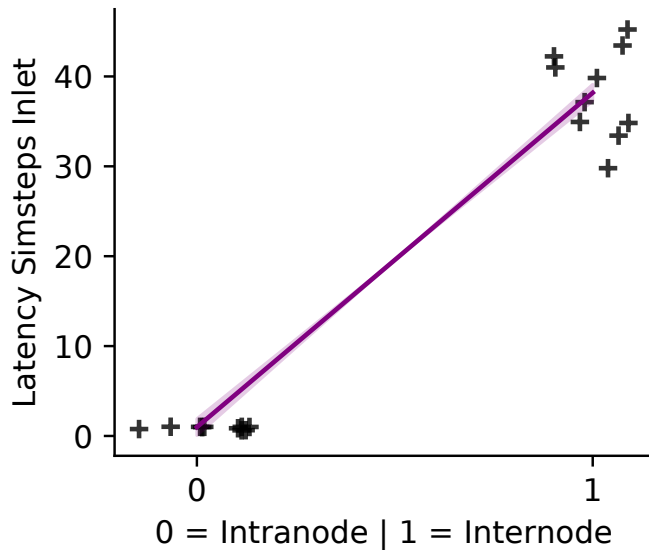


Estimated Statistic = Latency Simsteps Inlet Mean

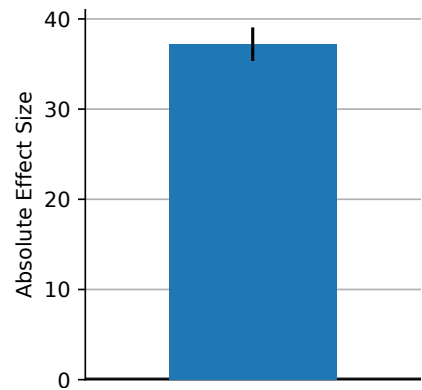


(a) Ordinary least squares regression plot. Observations are means per replicate. (b) Estimated regression coefficient for ordinary least squares regression. Zero corresponds to no effect.

## Quantile Regression



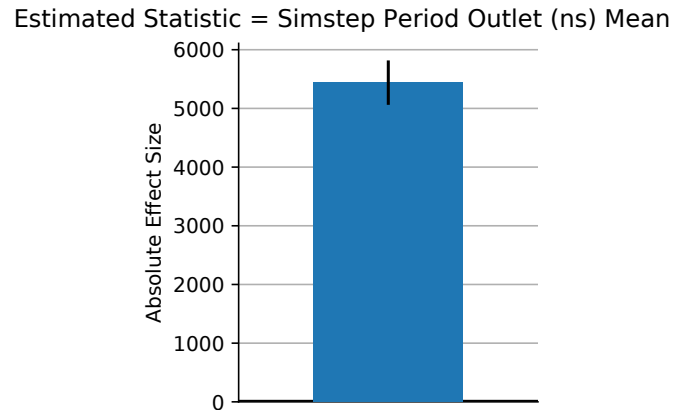
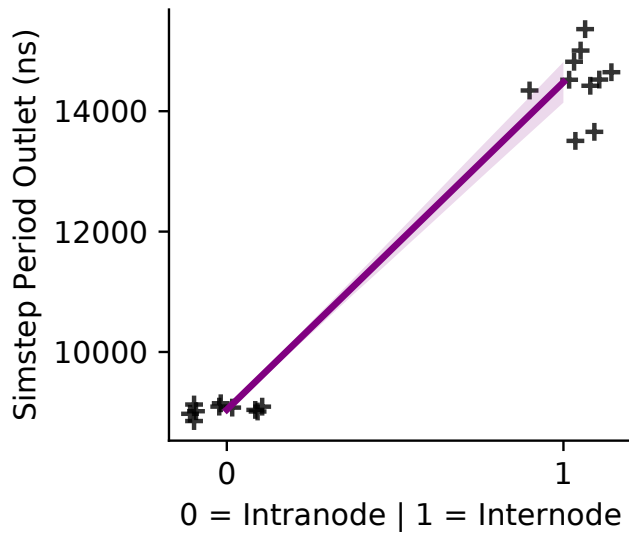
Estimated Statistic = Latency Simsteps Inlet Median



(c) Quantile regression plot. Observations are medians per replicate. (d) Estimated regression coefficient for quantile regression. Zero corresponds to no effect.

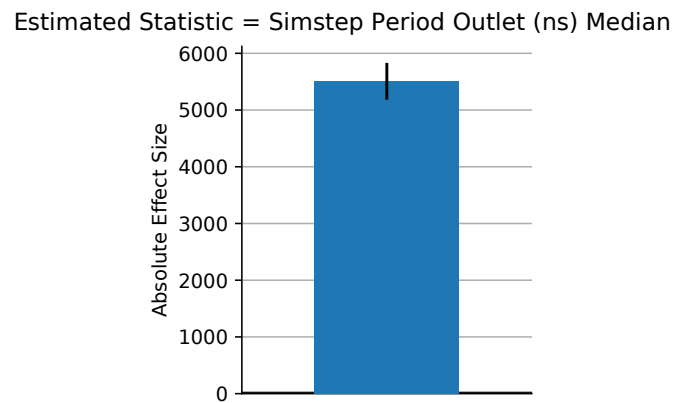
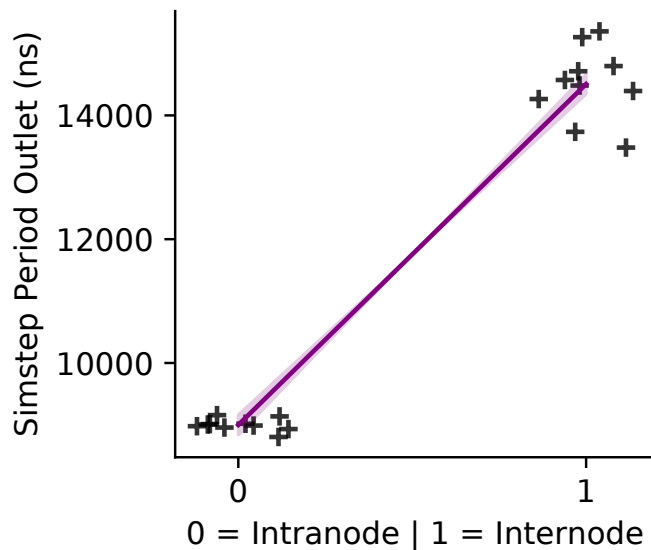
Fig. 57: Regressions of Latency Simsteps Inlet against categorically coded treatment for intranode vs. internode experiment (Section III-D). Lower is better. Ordinary least squares regression (top row) estimates relationship between categorical dependent variable and mean of response variable. Quantile regression (bottom row) estimates relationship between categorical independent variable and median of response variable. Error bands and bars are 95% confidence intervals.

## Ordinary Least Squares Regression



(a) Ordinary least squares regression plot. Observations are means per replicate. (b) Estimated regression coefficient for ordinary least squares regression. Zero corresponds to no effect.

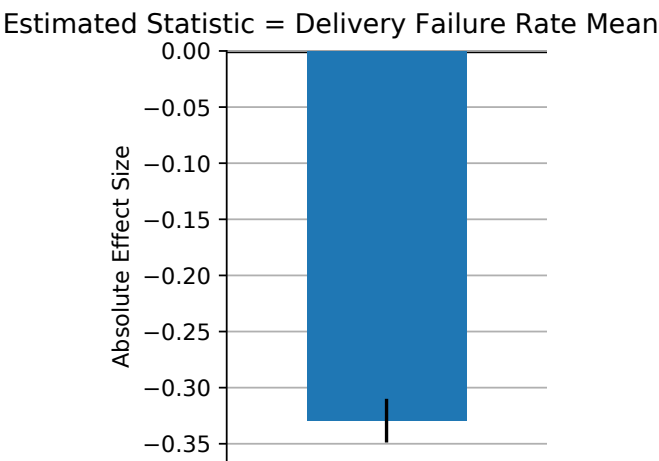
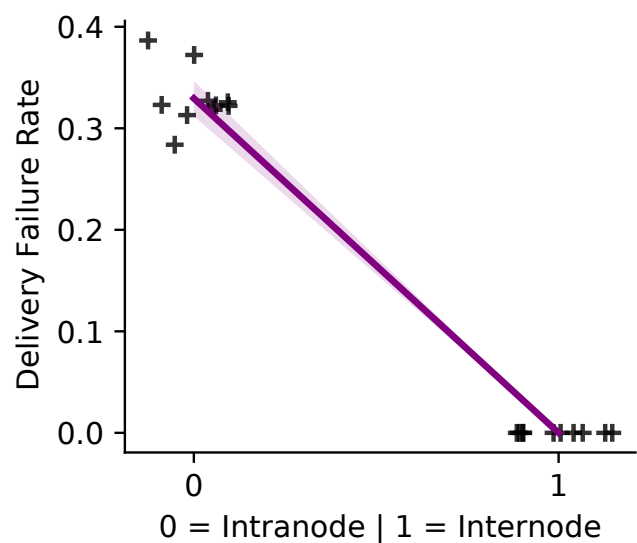
## Quantile Regression



(c) Quantile regression plot. Observations are medians per replicate. (d) Estimated regression coefficient for quantile regression. Zero corresponds to no effect.

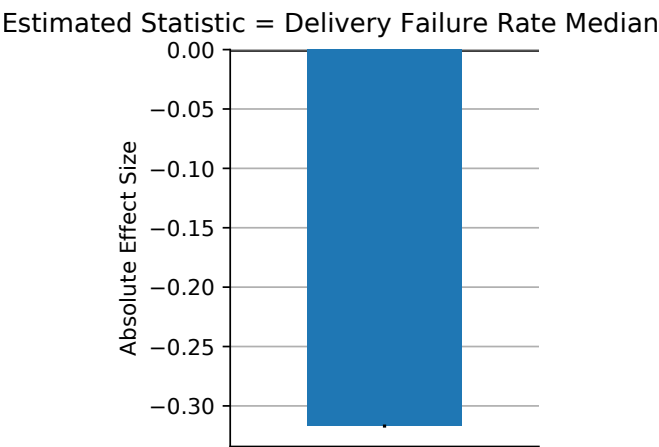
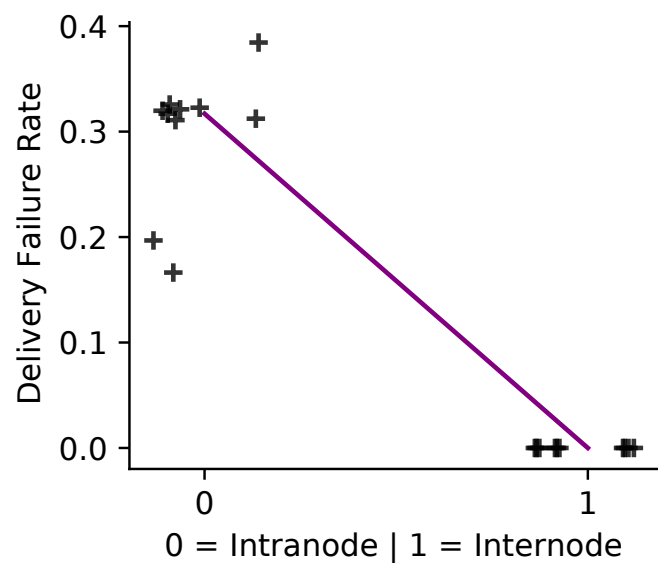
Fig. 58: Regressions of Simstep Period Outlet (ns) against categorically coded treatment for intranode vs. internode experiment (Section III-D). Lower is better. Ordinary least squares regression (top row) estimates relationship between categorical dependent variable and mean of response variable. Quantile regression (bottom row) estimates relationship between categorical independent variable and median of response variable. Error bands and bars are 95% confidence intervals.

# Ordinary Least Squares Regression



(a) Ordinary least squares regression plot. Observations are means per replicate. (b) Estimated regression coefficient for ordinary least squares regression. Zero corresponds to no effect.

# Quantile Regression



(c) Quantile regression plot. Observations are medians per replicate. (d) Estimated regression coefficient for quantile regression. Zero corresponds to no effect.

Fig. 59: Regressions of Delivery Failure Rate against categorically coded treatment for intranode vs. internode experiment (Section III-D). Lower is better. Ordinary least squares regression (top row) estimates relationship between categorical dependent variable and mean of response variable. Quantile regression (bottom row) estimates relationship between categorical independent variable and median of response variable. Error bands and bars are 95% confidence intervals.



TABLE XX: Full Ordinary Least Squares Regression results of quality of service metrics against log processor count for weak scaling experiment (Section III-F). Listed results include both piecewise and complete regression. Ordinary least squares regression estimates relationship between independent variable and mean of response variable. Quantile regression estimates relationship between independent variable and median of response variable. Significance level  $p < 0.05$  used. Inf or NaN values may occur due to multicollinearity or due to inf or NaN observations.

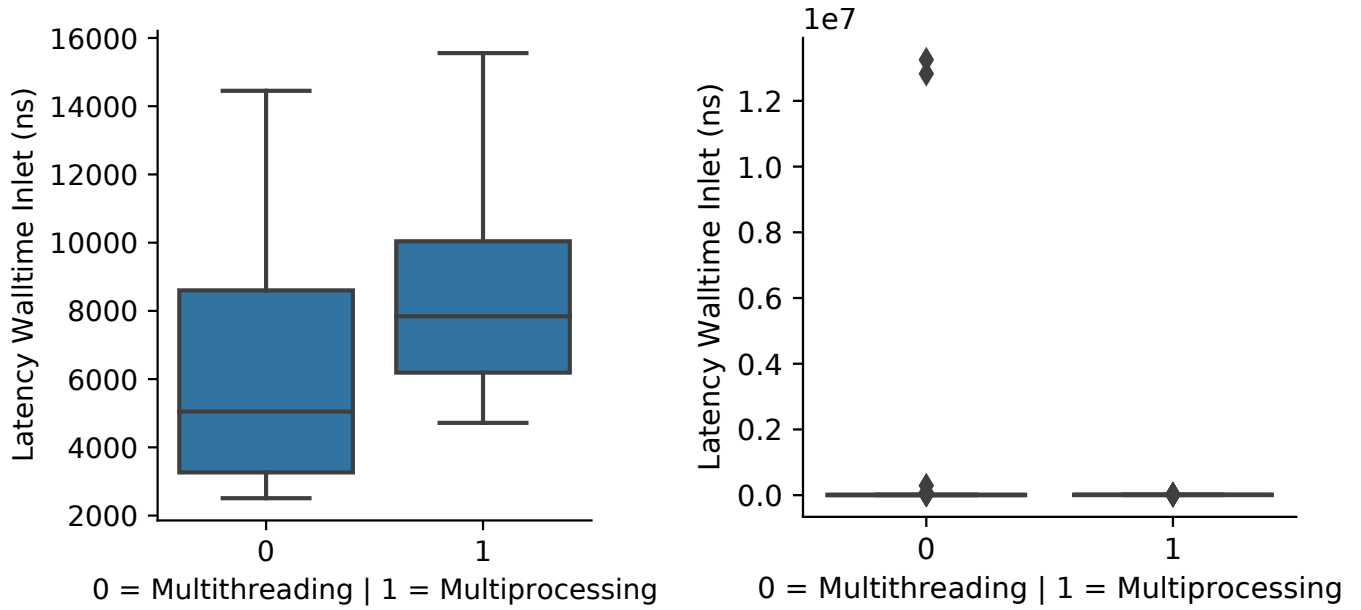
Metric	Statistic	Significant Effect Sign	Cpus Per Node	Num Simsels Per Cpu	Num Processes	Absolute Effect Size	Absolute Effect Size 95% CI Lower Bound		Relative Effect Size		Relative Effect Size 95% CI Lower Bound		Relative Effect Size 95% CI Upper Bound		n	p
							Absolute Effect Size	Upper Bound	Relative Effect Size	Upper Bound	Relative Effect Size	Upper Bound				
Latency Walltime Inlet (ns)	mean	+	1-2	1	2	600 000	530 000	660 000	77	68	85	20	2.1e-13			
Latency Walltime Outlet (ns)	mean	+	1-2	1	2	590 000	530 000	650 000	77	68	85	20	1.1e-13			
Latency Simssteps Inlet	mean	+	1-2	1	2	41	36	45	41	36	45	20	1.9e-13			
Latency Simssteps Outlet	mean	+	1-2	1	2	40	36	45	40	36	45	20	1e-13			
Delivery Failure Rate	mean	-	1-2	1	2	-0.33	-0.35	-0.31	-1	-1.1	-0.94	20	4e-18			
Delivery Clumpiness	mean	+	1-2	1	2	0.94	0.93	0.96	68	67	69	20	2.6e-30			
Simstep Period Inlet (ns)	mean	+	1-2	1	2	5 500	5 100	5 900	0.6	0.56	0.65	20	1.3e-16			
Simstep Period Outlet (ns)	mean	+	1-2	1	2	5 400	5 100	5 800	0.6	0.56	0.64	20	7.1e-17			

TABLE XXI: Full Quantile Regression results of quality of service metrics against log processor count for weak scaling experiment (Section III-F). Listed results include both piecewise and complete regression. Ordinary least squares regression estimates relationship between independent variable and mean of response variable. Quantile regression estimates relationship between independent variable and median of response variable. Significance level  $p < 0.05$  used. Inf or NaN values may occur due to multicollinearity or due to inf or NaN observations.

Metric	Statistic	Significant Effect Sign	Cpus Per Node	Num Simsels Per Cpu	Num Processes	Absolute Effect Size	Absolute Effect Size 95% CI Lower Bound	Absolute Effect Size 95% CI Upper Bound	Relative Effect Size	Relative Effect Size 95% CI Lower Bound	Relative Effect Size 95% CI Upper Bound	n	p
Latency Walltime Inlet (ns)	median	+	1-2	1	2	550 000	530 000	560 000	78	76	81	20	2.6e-23
Latency Walltime Outlet (ns)	median	+	1-2	1	2	540 000	530 000	560 000	78	76	80	20	1.5e-24
Latency Simsteps Inlet	median	+	1-2	1	2	37	35	39	38	36	39	20	2.1e-19
Latency Simsteps Outlet	median	+	1-2	1	2	37	35	39	37	35	39	20	6.7e-19
Delivery Failure Rate	median	-	1-2	1	2	-0.32	-0.32	-0.32	-1	-1	-0.99	20	5.7e-39
Delivery Clumpiness	median	+	1-2	1	2	0.96	0.95	0.97	610	600	620	20	4.6e-31
Simstep Period Inlet (ns)	median	+	1-2	1	2	5 600	5 200	6 000	0.62	0.58	0.66	20	1.3e-16
Simstep Period Outlet (ns)	median	+	1-2	1	2	5 500	5 200	5 800	0.61	0.58	0.65	20	3.7e-18

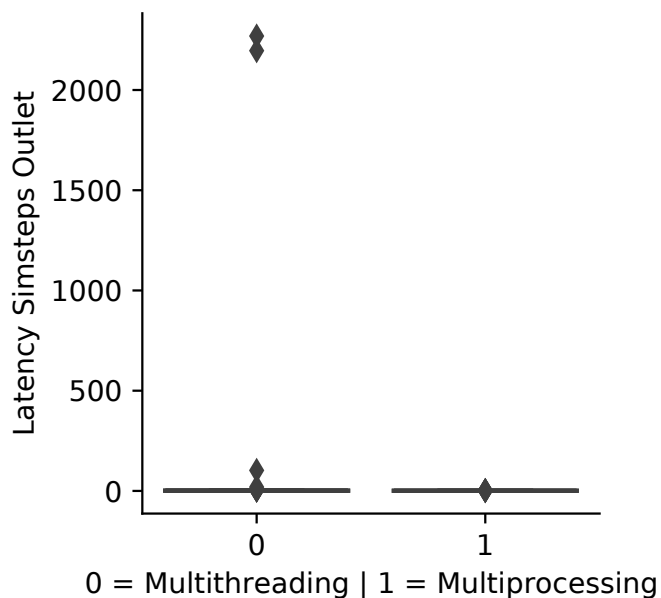
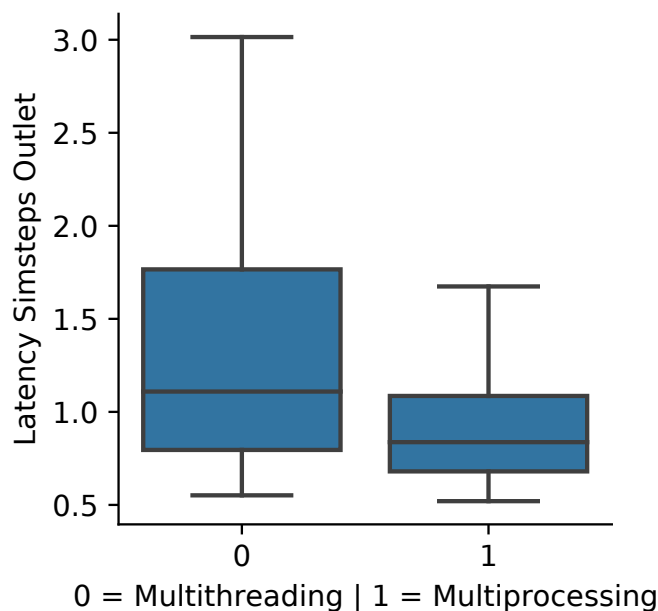
## VII. MULTITHREADING VS MULTIPROCESSING

This section provides full results from multithreading vs. multiprocessing experiments discussed in Section III-E.



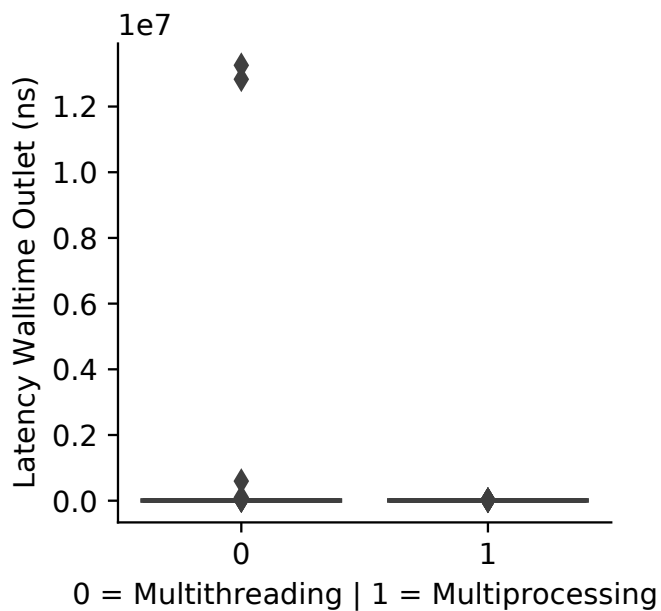
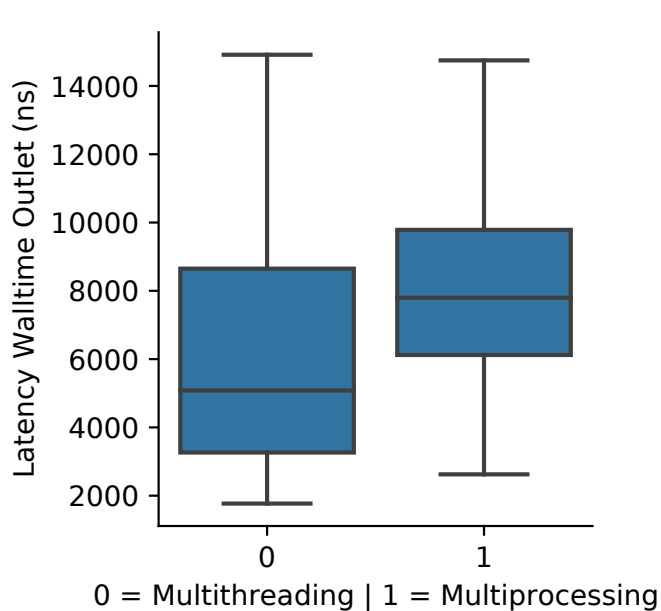
(a) Distribution of Latency Walltime Inlet (ns) for each snapshot, (b) Distribution of Latency Walltime Inlet (ns) for each snapshot, with outliers.

Fig. 60: Distribution of Latency Walltime Inlet (ns) for individual snapshot measurements for multithreading vs. multiprocessing experiment (Section III-E). Lower is better.



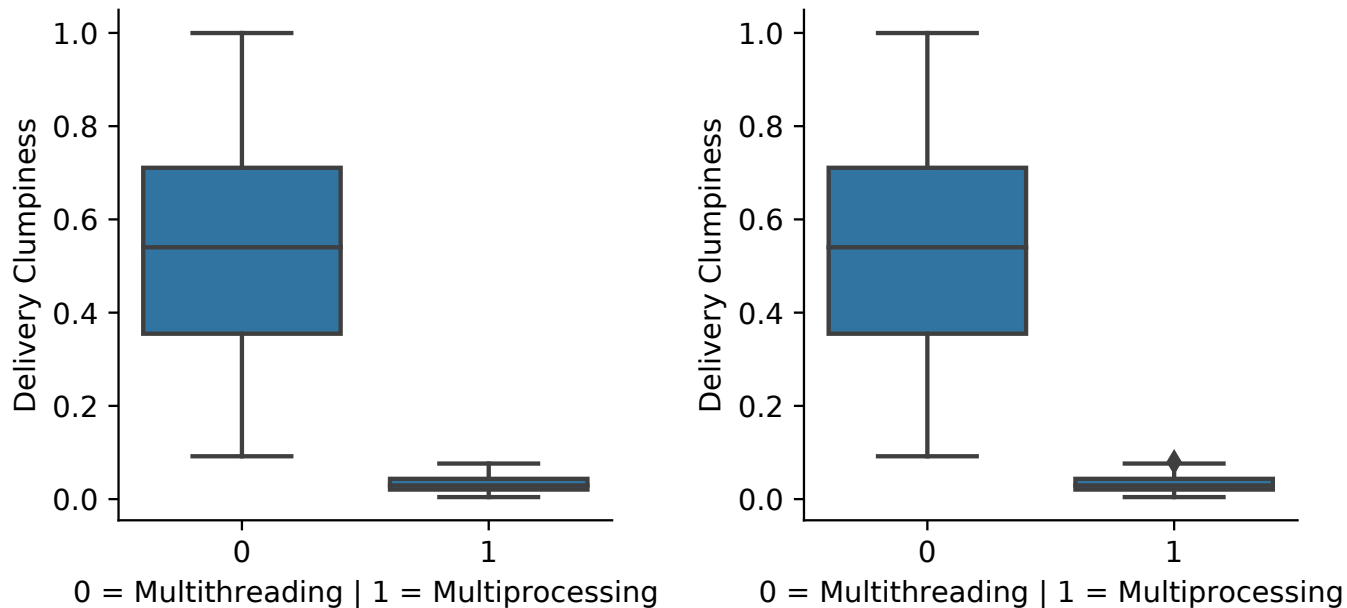
(a) Distribution of Latency Simsteps Outlet for each snapshot, without outliers. (b) Distribution of Latency Simsteps Outlet for each snapshot, with outliers.

Fig. 61: Distribution of Latency Simsteps Outlet for individual snapshot measurements for multithreading vs. multiprocessing experiment (Section III-E). Lower is better.



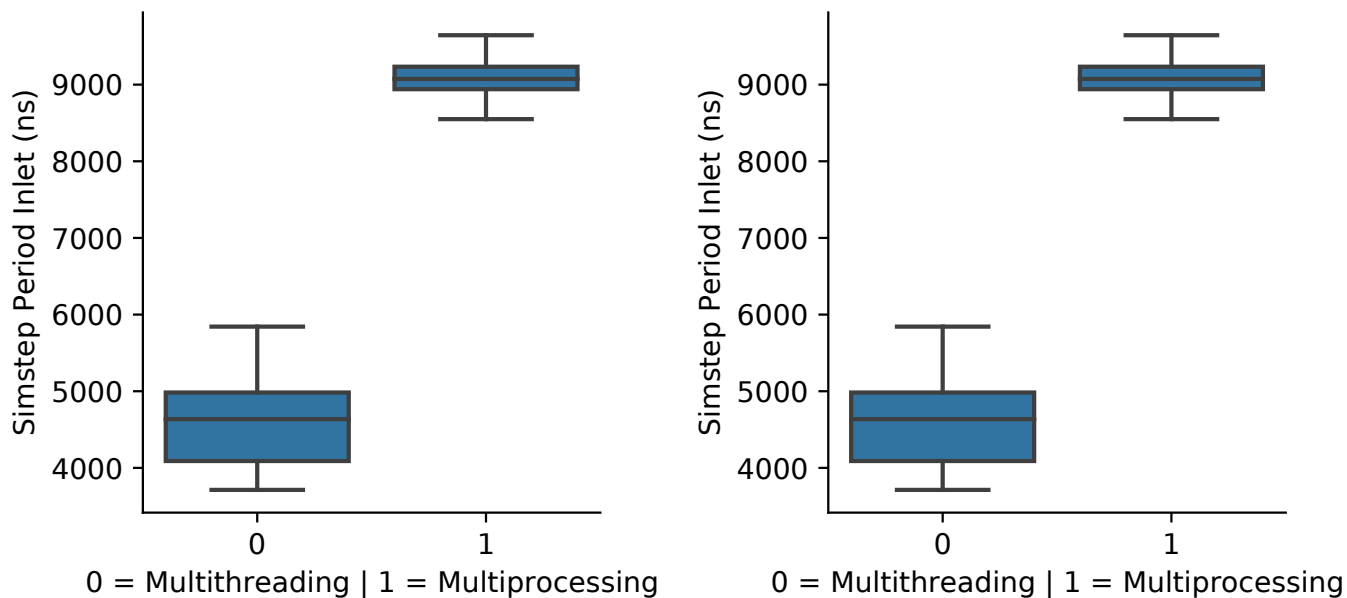
(a) Distribution of Latency Walltime Outlet (ns) for each snapshot, without outliers. (b) Distribution of Latency Walltime Outlet (ns) for each snapshot, with outliers.

Fig. 62: Distribution of Latency Walltime Outlet (ns) for individual snapshot measurements for multithreading vs. multiprocessing experiment (Section III-E). Lower is better.



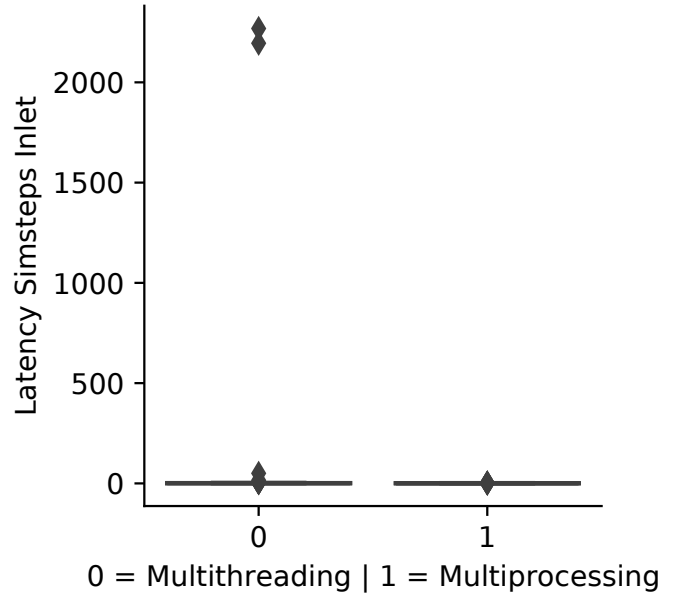
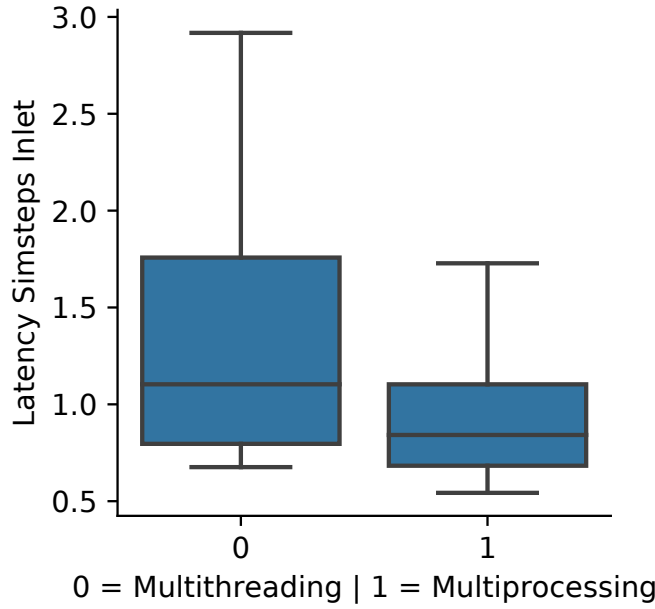
(a) Distribution of Delivery Clumpiness for each snapshot, without outliers. (b) Distribution of Delivery Clumpiness for each snapshot, with outliers.

Fig. 63: Distribution of Delivery Clumpiness for individual snapshot measurements for multithreading vs. multiprocessing experiment (Section III-E). Lower is better.



(a) Distribution of Simstep Period Inlet (ns) for each snapshot, without outliers. (b) Distribution of Simstep Period Inlet (ns) for each snapshot, with outliers.

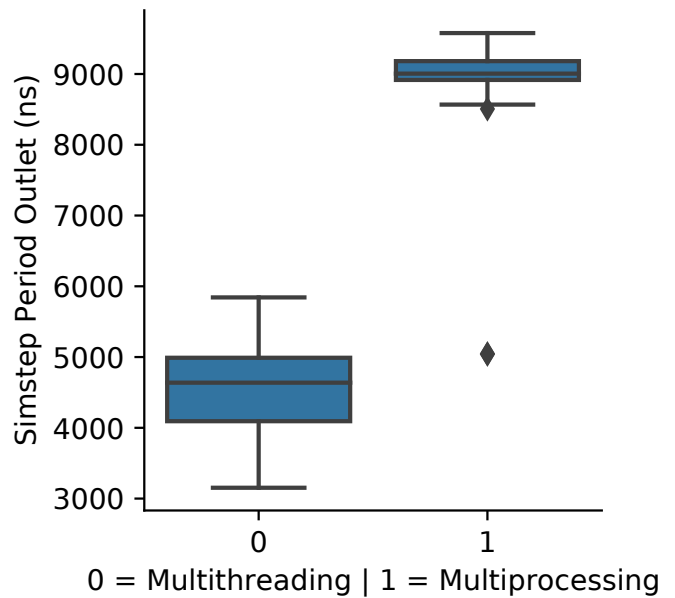
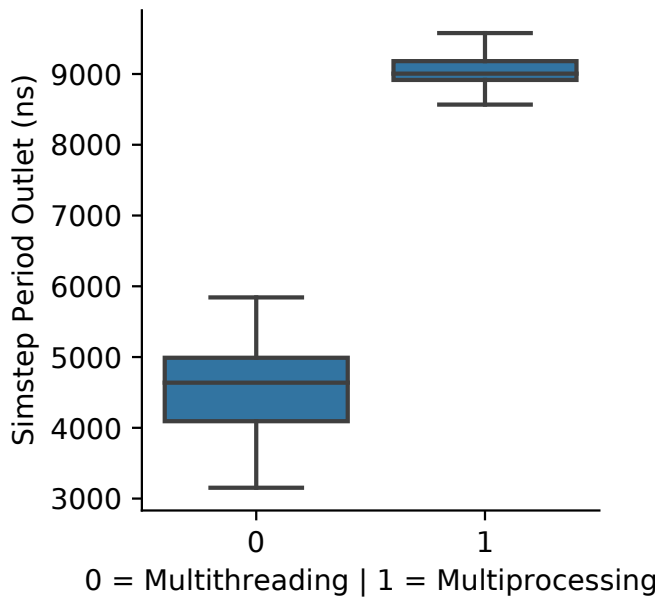
Fig. 64: Distribution of Simstep Period Inlet (ns) for individual snapshot measurements for multithreading vs. multiprocessing experiment (Section III-E). Lower is better.



(a) Distribution of Latency Simsteps Inlet for each snapshot, without outliers.

(b) Distribution of Latency Simsteps Inlet for each snapshot, with outliers.

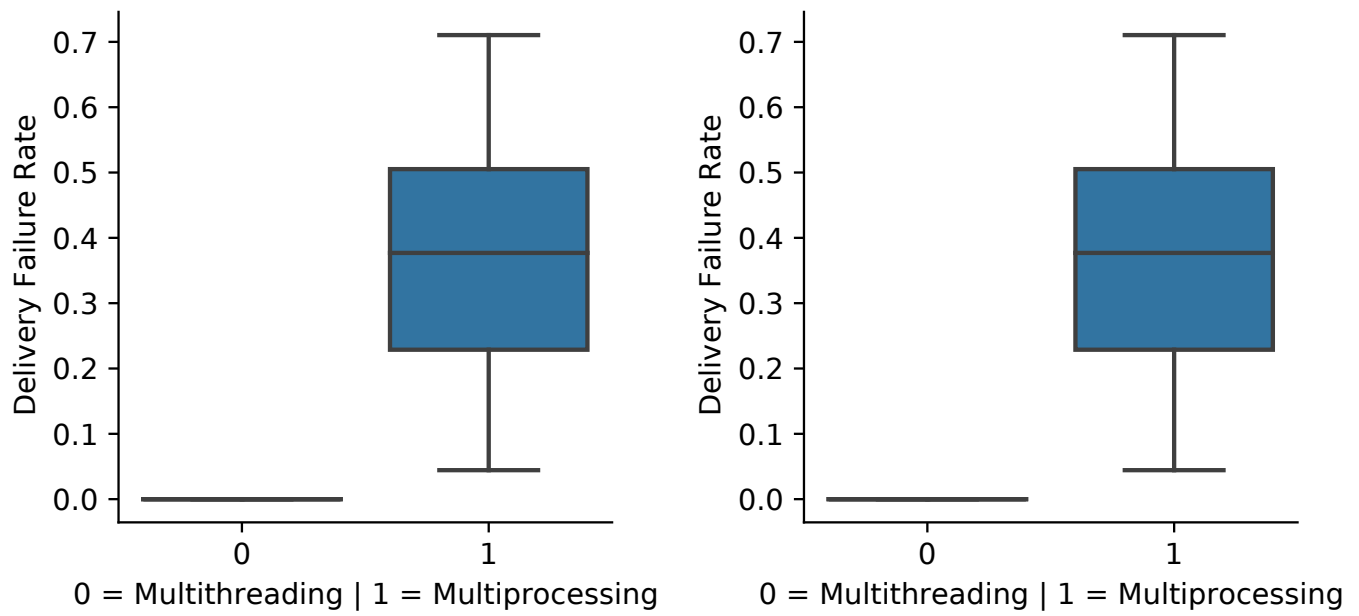
Fig. 65: Distribution of Latency Simsteps Inlet for individual snapshot measurements for multithreading vs. multiprocessing experiment (Section III-E). Lower is better.



(a) Distribution of Simstep Period Outlet (ns) for each snapshot, without outliers.

(b) Distribution of Simstep Period Outlet (ns) for each snapshot, with outliers.

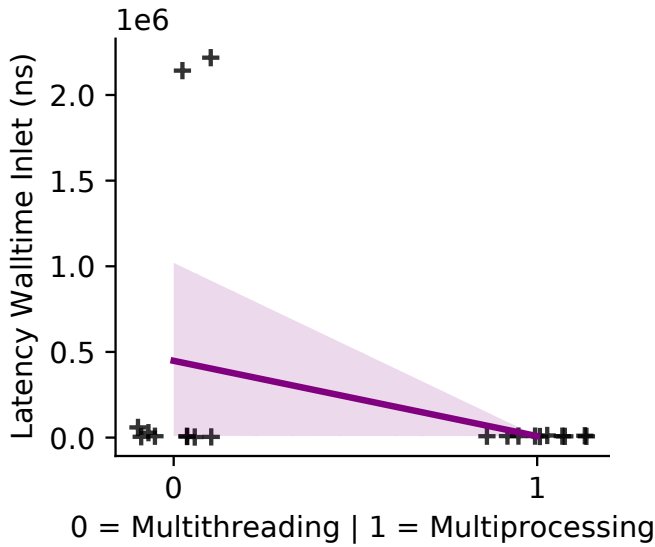
Fig. 66: Distribution of Simstep Period Outlet (ns) for individual snapshot measurements for multithreading vs. multiprocessing experiment (Section III-E). Lower is better.



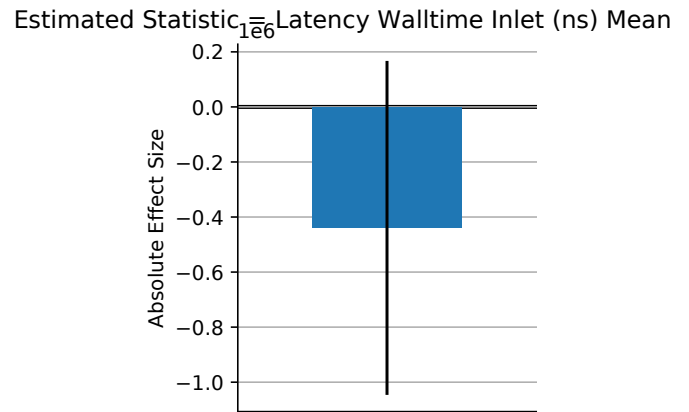
(a) Distribution of Delivery Failure Rate for each snapshot, without outliers. (b) Distribution of Delivery Failure Rate for each snapshot, with outliers.

Fig. 67: Distribution of Delivery Failure Rate for individual snapshot measurements for multithreading vs. multiprocessing experiment (Section III-E). Lower is better.

## Ordinary Least Squares Regression

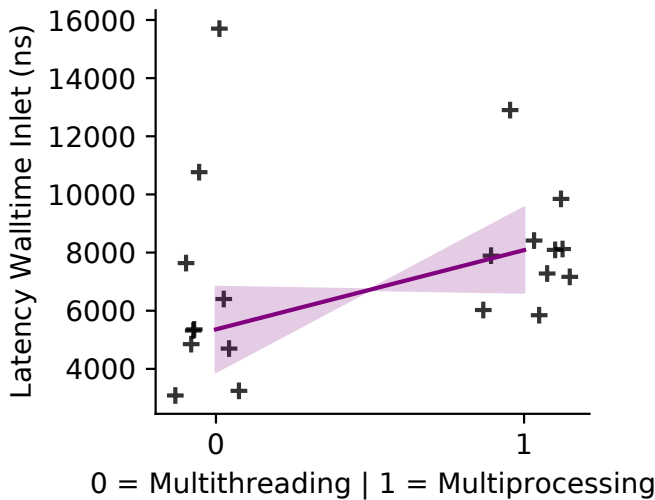


(a) Ordinary least squares regression plot. Observations are means per replicate.

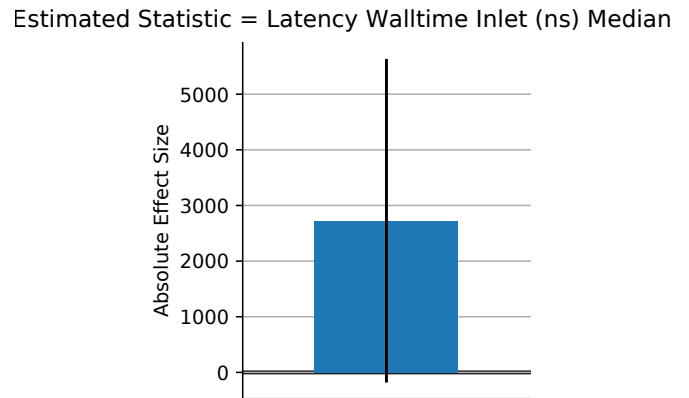


(b) Estimated regression coefficient for ordinary least squares regression. Zero corresponds to no effect.

## Quantile Regression



(c) Quantile regression plot. Observations are medians per replicate.

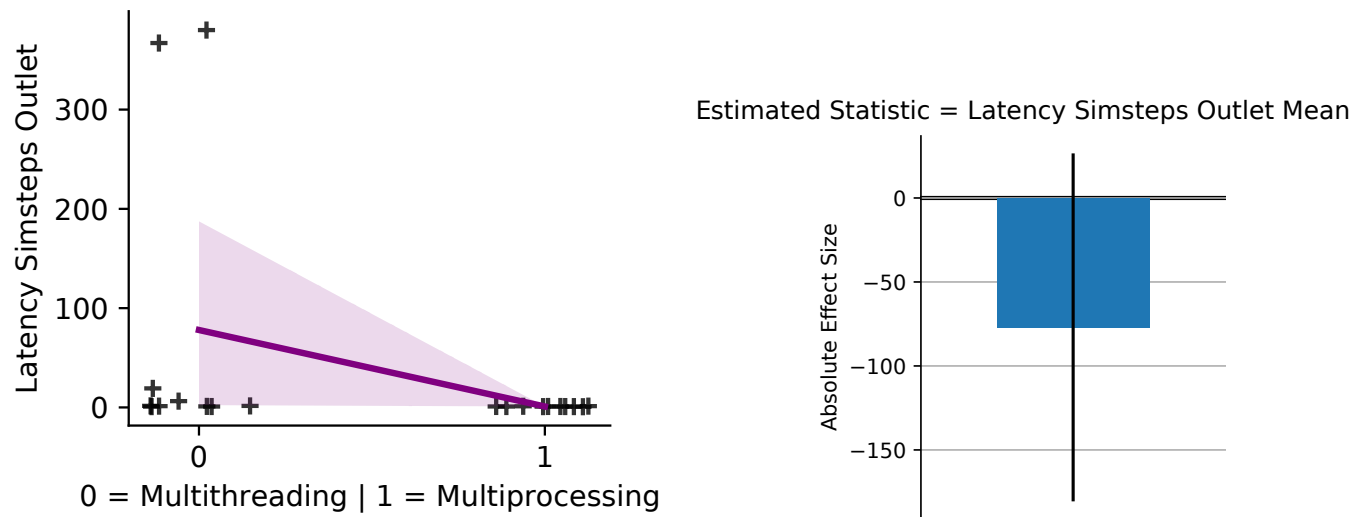


(d) Estimated regression coefficient for quantile regression. Zero corresponds to no effect.

Fig. 68: Regressions of Latency Walltime Inlet (ns) against categorically coded treatment for multithreading vs. multiprocessing experiment (Section III-E). Lower is better. Ordinary least squares regression (top row) estimates relationship between categorical dependent variable and mean of response variable. Quantile regression (bottom row) estimates relationship between categorical independent variable and median of response variable. Error bands and bars are 95% confidence intervals.

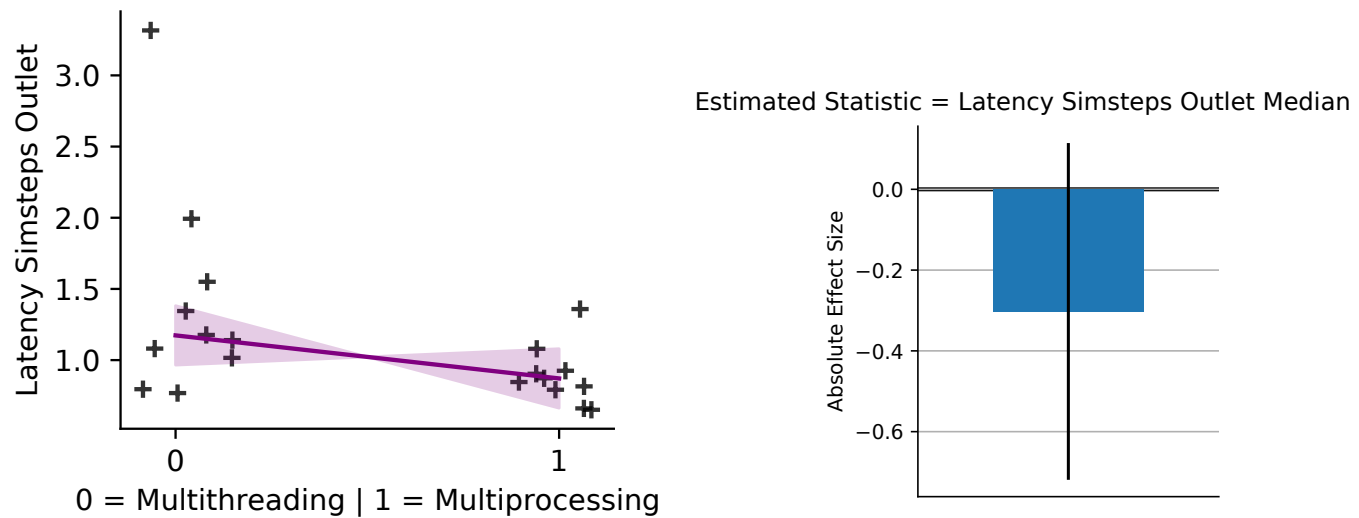


# Ordinary Least Squares Regression



(a) Ordinary least squares regression plot. Observations are means per replicate. (b) Estimated regression coefficient for ordinary least squares regression. Zero corresponds to no effect.

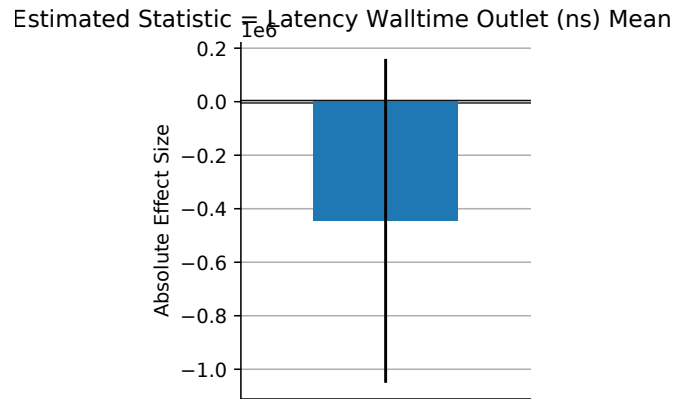
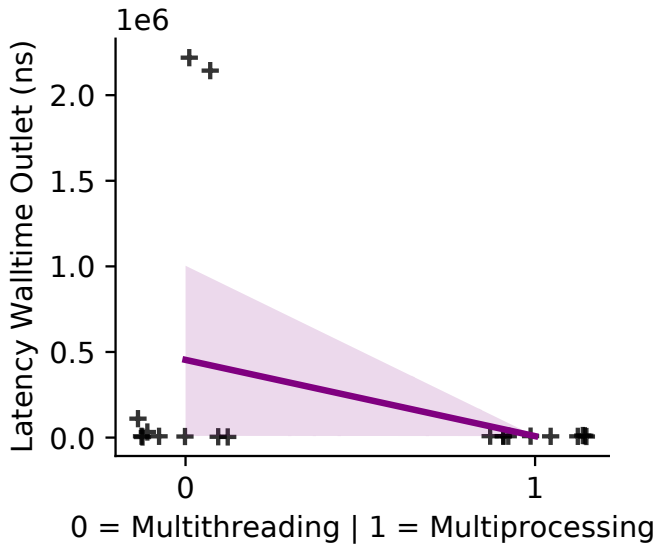
# Quantile Regression



(c) Quantile regression plot. Observations are medians per replicate. (d) Estimated regression coefficient for quantile regression. Zero corresponds to no effect.

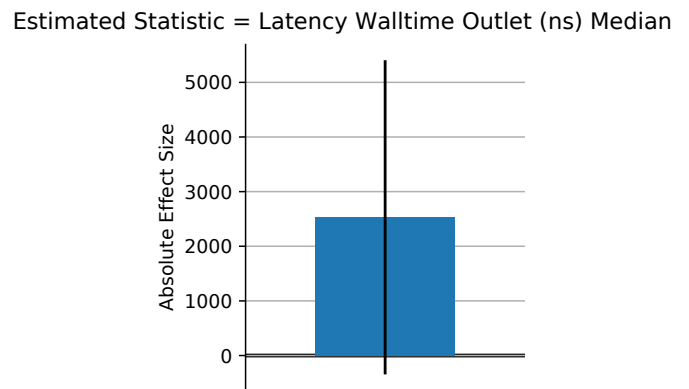
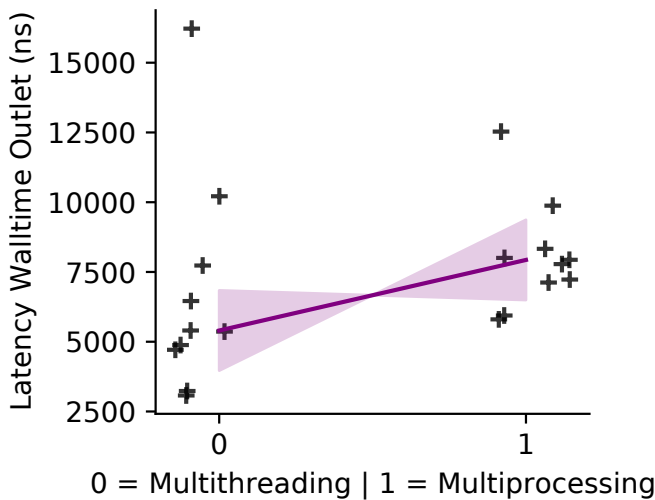
Fig. 69: Regressions of Latency Simsteps Outlet against categorically coded treatment for multithreading vs. multiprocessing experiment (Section III-E). Lower is better. Ordinary least squares regression (top row) estimates relationship between categorical dependent variable and mean of response variable. Quantile regression (bottom row) estimates relationship between categorical independent variable and median of response variable. Error bands and bars are 95% confidence intervals.

## Ordinary Least Squares Regression



(a) Ordinary least squares regression plot. Observations are means per replicate. (b) Estimated regression coefficient for ordinary least squares regression. Zero corresponds to no effect.

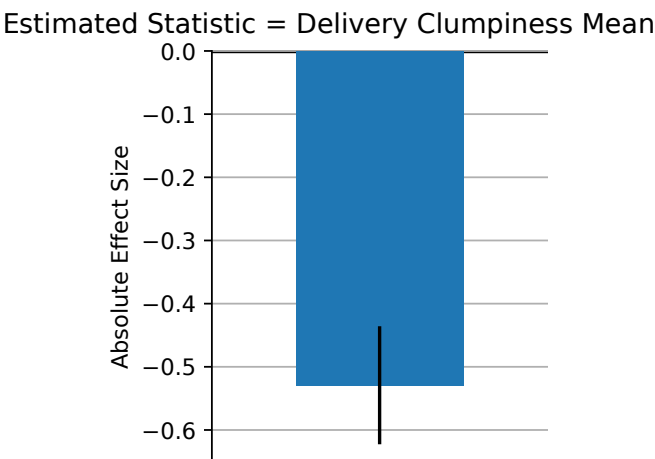
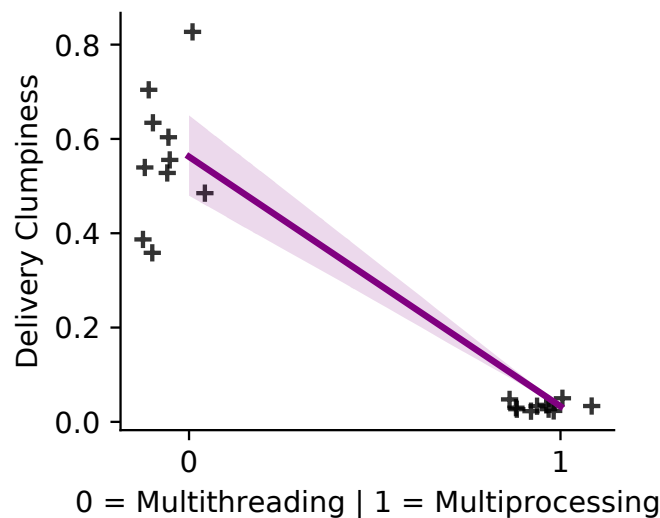
## Quantile Regression



(c) Quantile regression plot. Observations are medians per replicate. (d) Estimated regression coefficient for quantile regression. Zero corresponds to no effect.

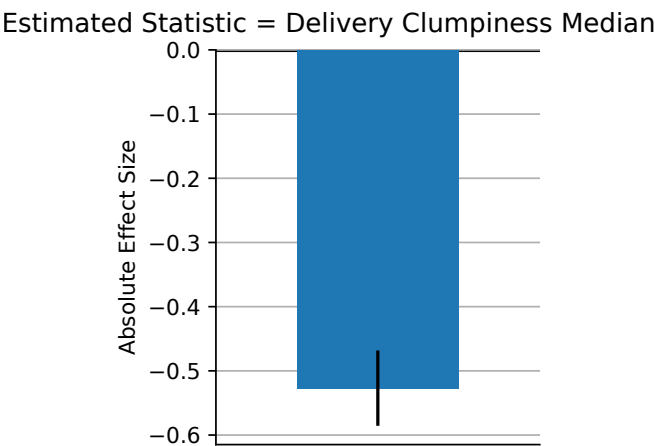
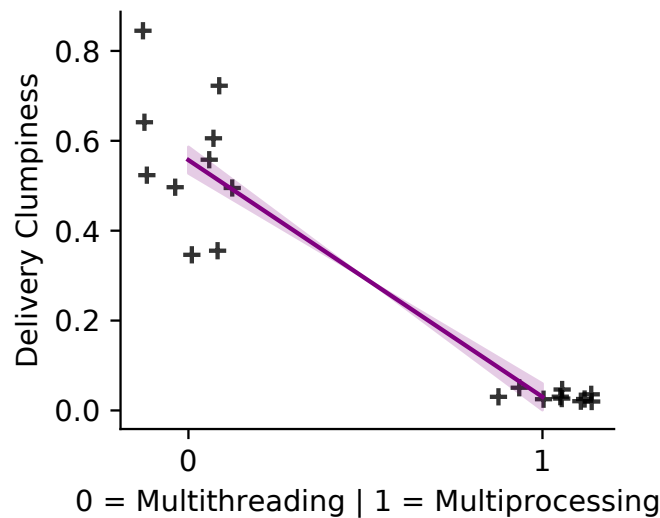
Fig. 70: Regressions of Latency Walltime Outlet (ns) against categorically coded treatment for multithreading vs. multiprocessing experiment (Section III-E). Lower is better. Ordinary least squares regression (top row) estimates relationship between categorical dependent variable and mean of response variable. Quantile regression (bottom row) estimates relationship between categorical independent variable and median of response variable. Error bands and bars are 95% confidence intervals.

# Ordinary Least Squares Regression



(a) Ordinary least squares regression plot. Observations are means per replicate. (b) Estimated regression coefficient for ordinary least squares regression. Zero corresponds to no effect.

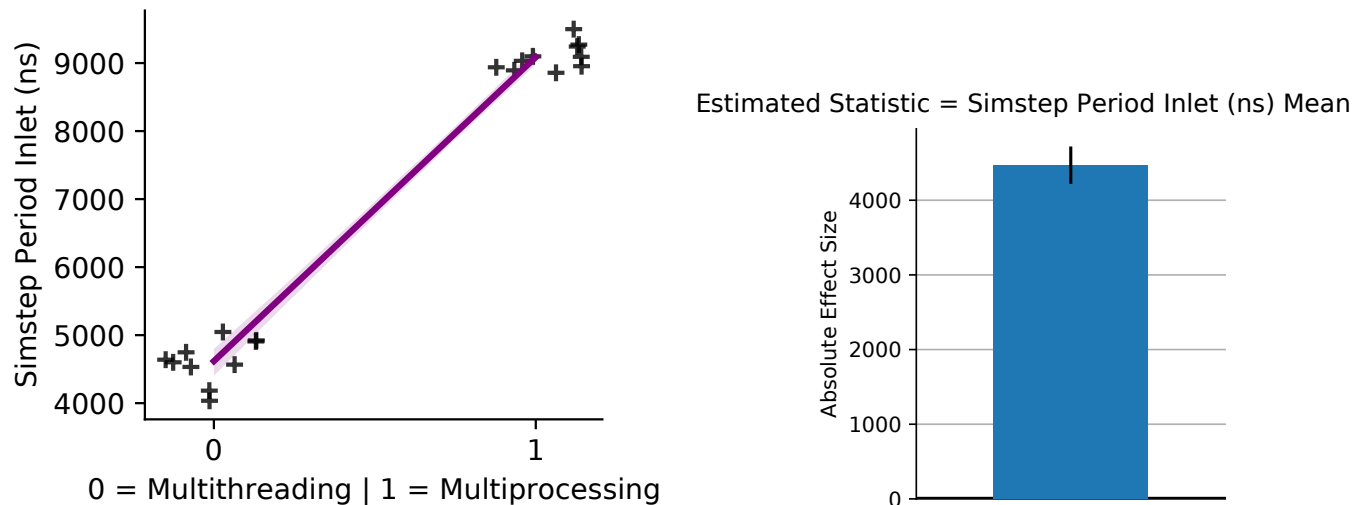
# Quantile Regression



(c) Quantile regression plot. Observations are medians per replicate. (d) Estimated regression coefficient for quantile regression. Zero corresponds to no effect.

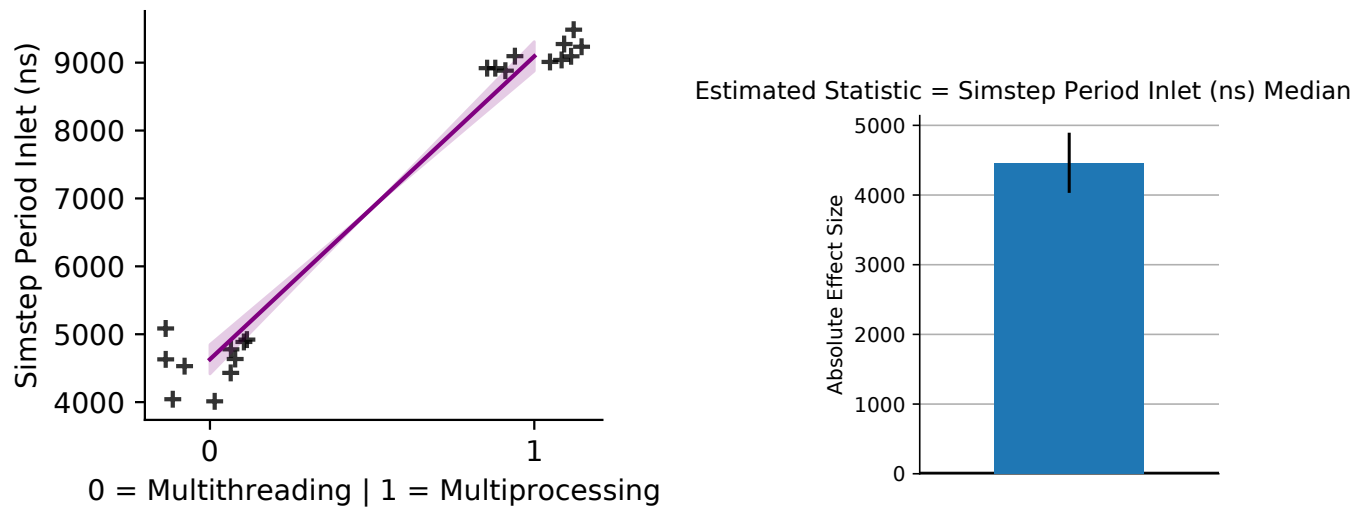
Fig. 71: Regressions of Delivery Clumpiness against categorically coded treatment for multithreading vs. multiprocessing experiment (Section III-E). Lower is better. Ordinary least squares regression (top row) estimates relationship between categorical dependent variable and mean of response variable. Quantile regression (bottom row) estimates relationship between categorical independent variable and median of response variable. Error bands and bars are 95% confidence intervals.

## Ordinary Least Squares Regression



(a) Ordinary least squares regression plot. Observations are means per replicate. (b) Estimated regression coefficient for ordinary least squares regression. Zero corresponds to no effect.

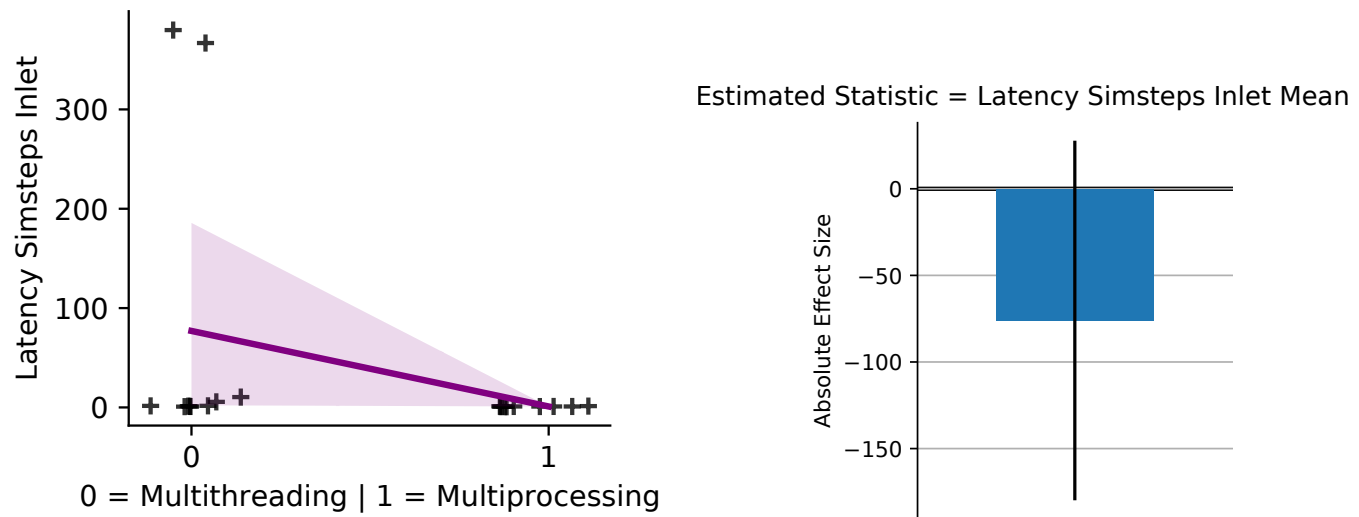
## Quantile Regression



(c) Quantile regression plot. Observations are medians per replicate. (d) Estimated regression coefficient for quantile regression. Zero corresponds to no effect.

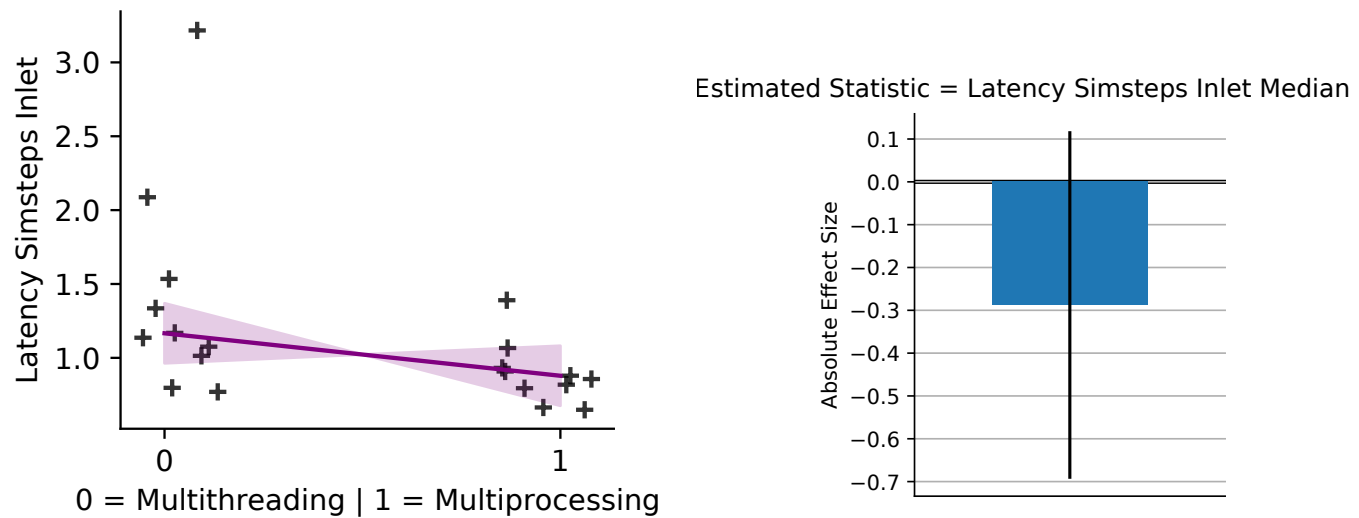
Fig. 72: Regressions of Simstep Period Inlet (ns) against categorically coded treatment for multithreading vs. multiprocessing experiment (Section III-E). Lower is better. Ordinary least squares regression (top row) estimates relationship between categorical dependent variable and mean of response variable. Quantile regression (bottom row) estimates relationship between categorical independent variable and median of response variable. Error bands and bars are 95% confidence intervals.

# Ordinary Least Squares Regression



(a) Ordinary least squares regression plot. Observations are means per replicate. (b) Estimated regression coefficient for ordinary least squares regression. Zero corresponds to no effect.

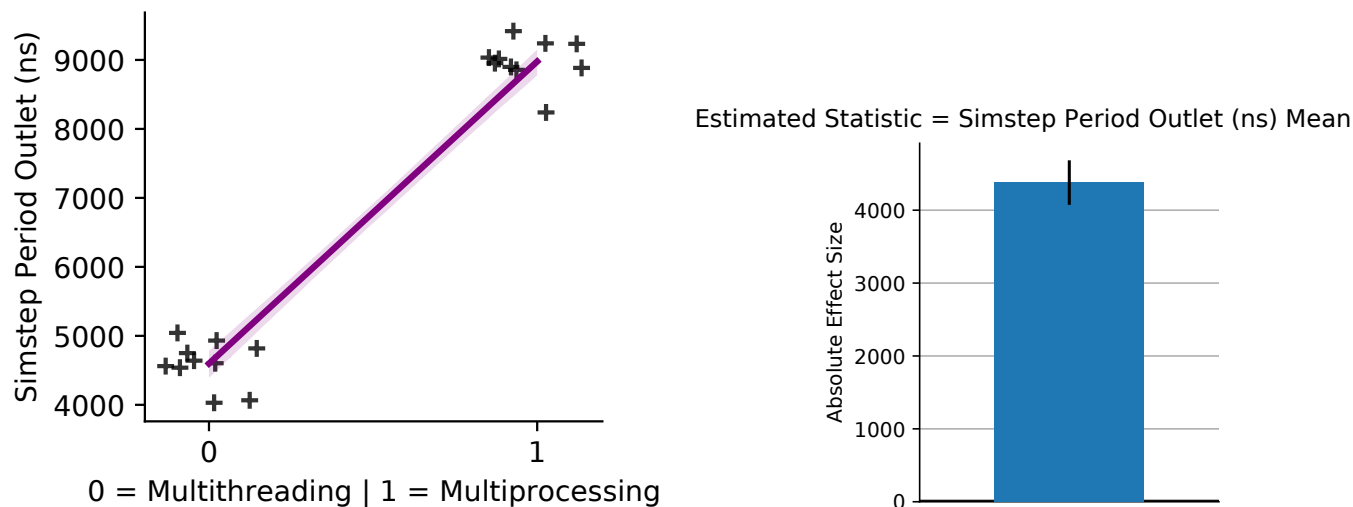
# Quantile Regression



(c) Quantile regression plot. Observations are medians per replicate. (d) Estimated regression coefficient for quantile regression. Zero corresponds to no effect.

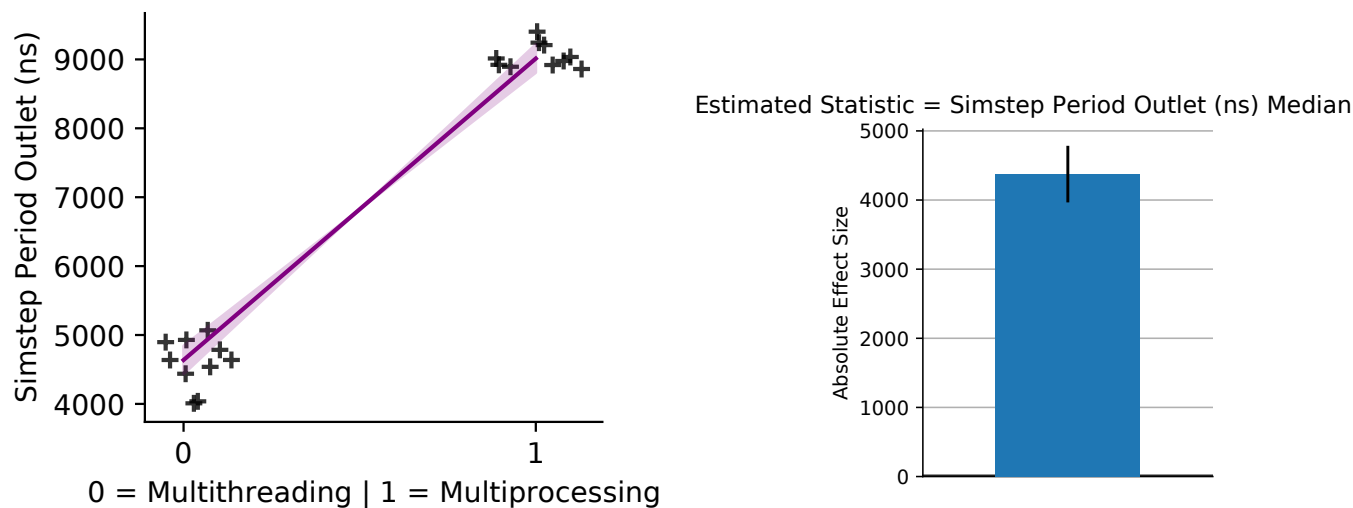
Fig. 73: Regressions of Latency Simsteps Inlet against categorically coded treatment for multithreading vs. multiprocessing experiment (Section III-E). Lower is better. Ordinary least squares regression (top row) estimates relationship between categorical dependent variable and mean of response variable. Quantile regression (bottom row) estimates relationship between categorical independent variable and median of response variable. Error bands and bars are 95% confidence intervals.

### Ordinary Least Squares Regression



(a) Ordinary least squares regression plot. Observations are means per replicate. (b) Estimated regression coefficient for ordinary least squares regression. Zero corresponds to no effect.

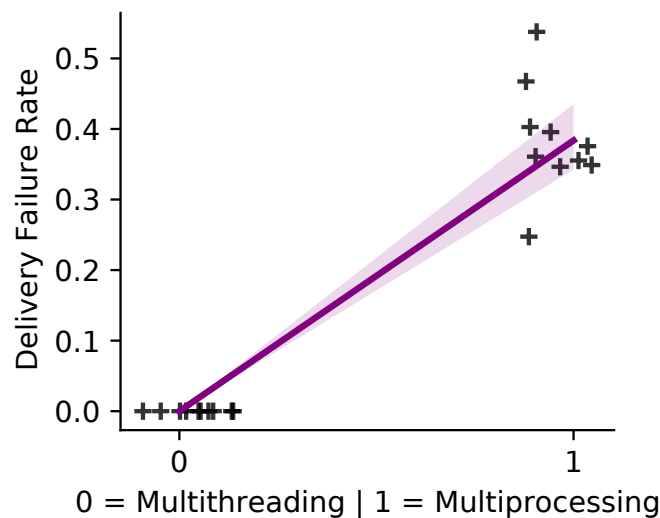
### Quantile Regression



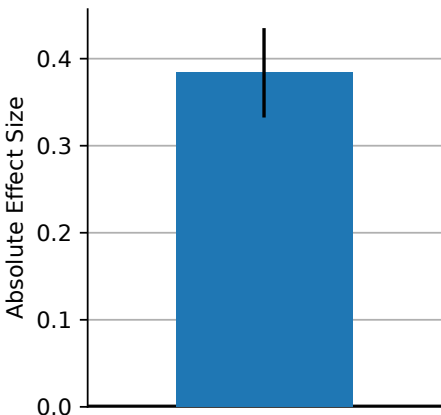
(c) Quantile regression plot. Observations are medians per replicate. (d) Estimated regression coefficient for quantile regression. Zero corresponds to no effect.

Fig. 74: Regressions of Simstep Period Outlet (ns) against categorically coded treatment for multithreading vs. multiprocessing experiment (Section III-E). Lower is better. Ordinary least squares regression (top row) estimates relationship between categorical dependent variable and mean of response variable. Quantile regression (bottom row) estimates relationship between categorical independent variable and median of response variable. Error bands and bars are 95% confidence intervals.

# Ordinary Least Squares Regression

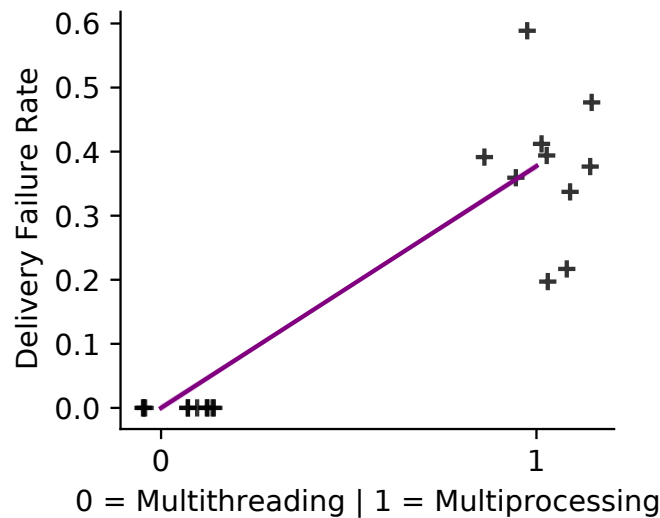


Estimated Statistic = Delivery Failure Rate Mean

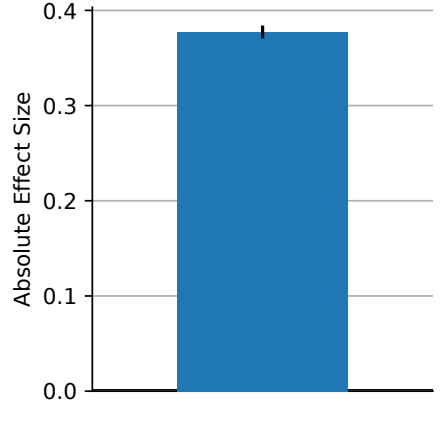


(a) Ordinary least squares regression plot. Observations are means per replicate. (b) Estimated regression coefficient for ordinary least squares regression. Zero corresponds to no effect.

# Quantile Regression



Estimated Statistic = Delivery Failure Rate Median



(c) Quantile regression plot. Observations are medians per replicate. (d) Estimated regression coefficient for quantile regression. Zero corresponds to no effect.

Fig. 75: Regressions of Delivery Failure Rate against categorically coded treatment for multithreading vs. multiprocessing experiment (Section III-E). Lower is better. Ordinary least squares regression (top row) estimates relationship between categorical dependent variable and mean of response variable. Quantile regression (bottom row) estimates relationship between categorical independent variable and median of response variable. Error bands and bars are 95% confidence intervals.

TABLE XXII: Full Ordinary Least Squares Regression results of quality of service metrics against categorically coded treatment for multithreading vs. multiprocessing experiment (Section III-E). Significance level  $p < 0.05$  used. Inf or NaN values may occur due to multicollinearity or due to inf or NaN observations.

Metric	Statistic	Significant Effect Sign	Cpus Per Node	Num Simsels Per Cpu	Num Processes	Absolute Effect Size	Absolute Effect Size 95% CI Lower Bound	Absolute Effect Size 95% CI Upper Bound	Relative Effect Size	Relative Effect Size 95% CI Lower Bound	Relative Effect Size 95% CI Upper Bound	n	p
Latency Walltime Inlet (ns)	mean	0	2	1	1/2	-440 000	-1e+06	170 000	-0.98	-2.3	0.37	20	0.15
Latency Walltime Outlet (ns)	mean	0	2	1	1/2	-450 000	-1.1e+06	160 000	-0.98	-2.3	0.35	20	0.14
Latency Simsteps Inlet	mean	0	2	1	1/2	-76	-180	28	-0.99	-2.3	0.36	20	0.14
Latency Simsteps Outlet	mean	0	2	1	1/2	-77	-180	27	-0.99	-2.3	0.34	20	0.14
Delivery Failure Rate	mean	+	2	1	1/2	0.38	0.33	0.44	-1.4e+06	-1.2e+06	-1.5e+06	20	6e-12
Delivery Clumpiness	mean	-	2	1	1/2	-0.53	-0.62	-0.44	-0.94	-1.1	-0.78	20	5.8e-10
Simstep Period Inlet (ns)	mean	+	2	1	1/2	4 500	4 200	4 700	0.97	0.91	1	20	1.5e-18
Simstep Period Outlet (ns)	mean	+	2	1	1/2	4 400	4 100	4 700	0.95	0.89	1	20	7.4e-17

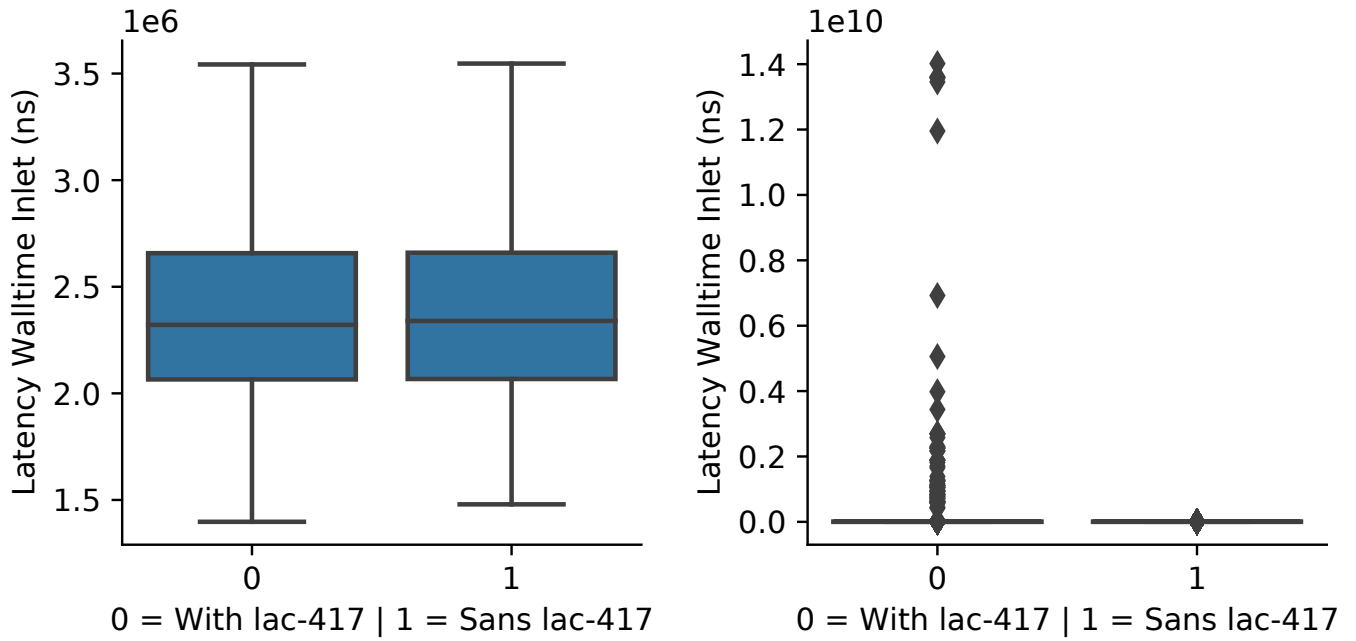


TABLE XXIII: Full Quantile Regression results of quality of service metrics against categorically coded treatment for multithreading vs. multiprocessing experiment (Section III-E). Significance level  $p < 0.05$  used. Inf or NaN values may occur due to multicollinearity or due to inf or NaN observations.

Metric	Statistic	Significant Effect Sign	Cpus Per Node	Num Simsels Per Cpu	Num Processes	Absolute Effect Size	Absolute Effect Size 95% CI Lower Bound		Absolute Effect Size 95% CI Upper Bound		Relative Effect Size	Relative Effect Size 95% CI Lower Bound		Relative Effect Size 95% CI Upper Bound		n	p
Latency Walltime Inlet (ns)	median	0	2	1	1/2	2700	-180	5600	0.51	-0.034	1.1	20	0.064				
Latency Walltime Outlet (ns)	median	0	2	1	1/2	2500	-350	5400	0.47	-0.064	1	20	0.081				
Latency Simsteps Inlet	median	0	2	1	1/2	-0.29	-0.69	0.12	-0.25	-0.6	0.1	20	0.15				
Latency Simsteps Outlet	median	0	2	1	1/2	-0.3	-0.72	0.11	-0.26	-0.62	0.099	20	0.14				
Delivery Failure Rate	median	+	2	1	1/2	0.38	0.37	0.38	inf	inf	inf	20	2e-27				
Delivery Clumpiness	median	-	2	1	1/2	-0.53	-0.59	-0.47	-0.97	-1.1	-0.87	20	2.6e-13				
Simstep Period Inlet (ns)	median	+	2	1	1/2	4500	4000	4900	0.96	0.87	1.1	20	2.3e-14				
Simstep Period Outlet (ns)	median	+	2	1	1/2	4400	4000	4800	0.94	0.86	1	20	1.3e-14				

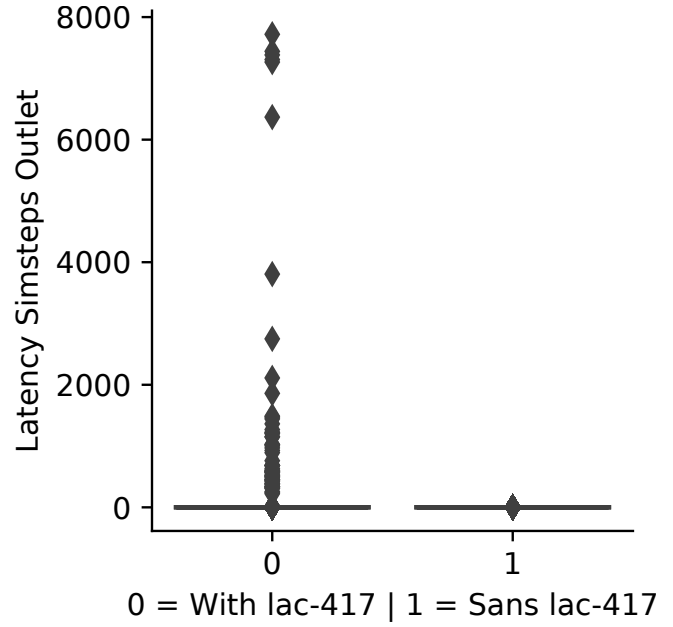
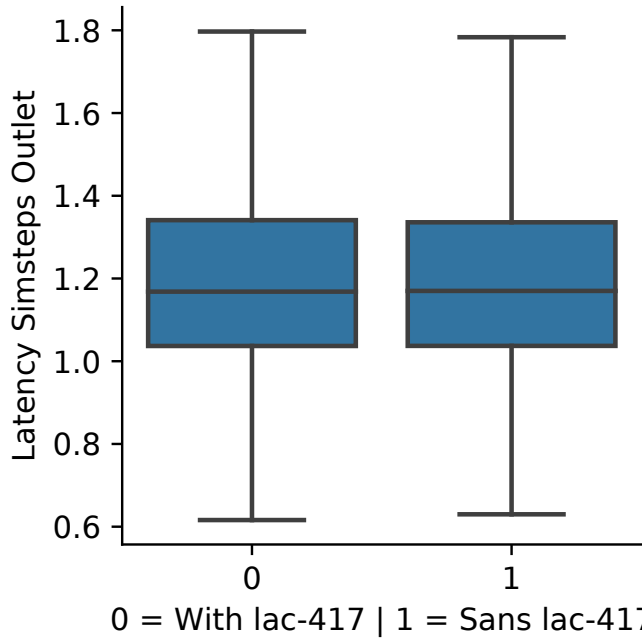
A. *With lac-417 vs. Sans lac-417*

This section provides full results from faulty hardware experiments discussed in Section III-G.



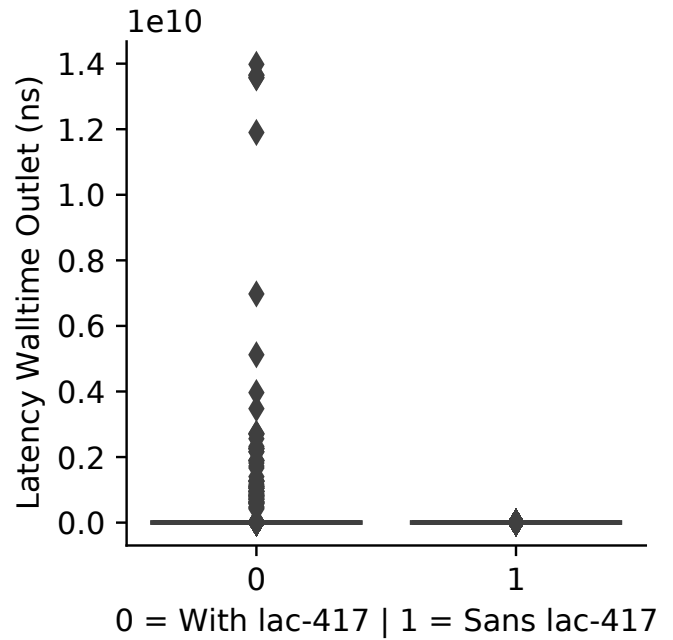
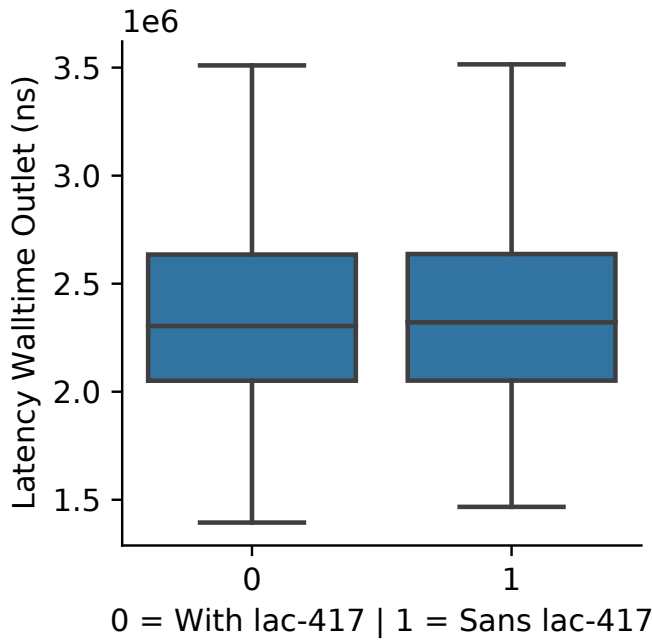
(a) Distribution of Latency Walltime Inlet (ns) for each snapshot, (b) Distribution of Latency Walltime Inlet (ns) for each snapshot, with outliers.

Fig. 76: Distribution of Latency Walltime Inlet (ns) for individual snapshot measurements for faulty hardware experiment (Section III-G). Lower is better.



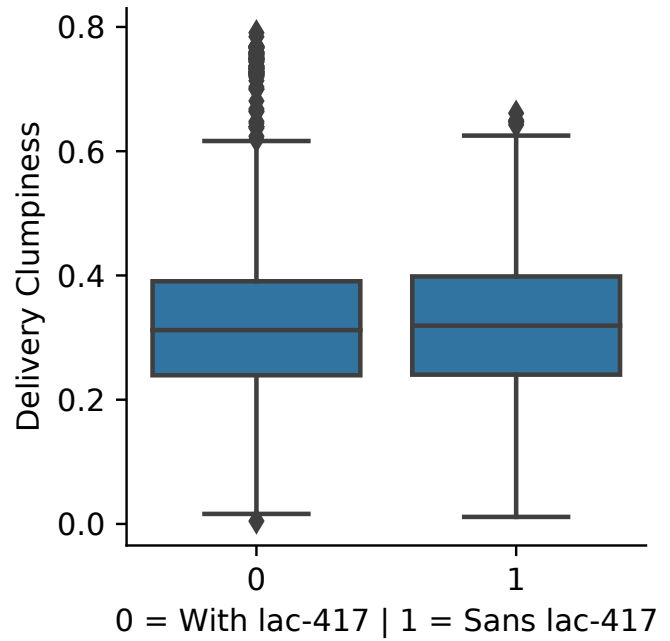
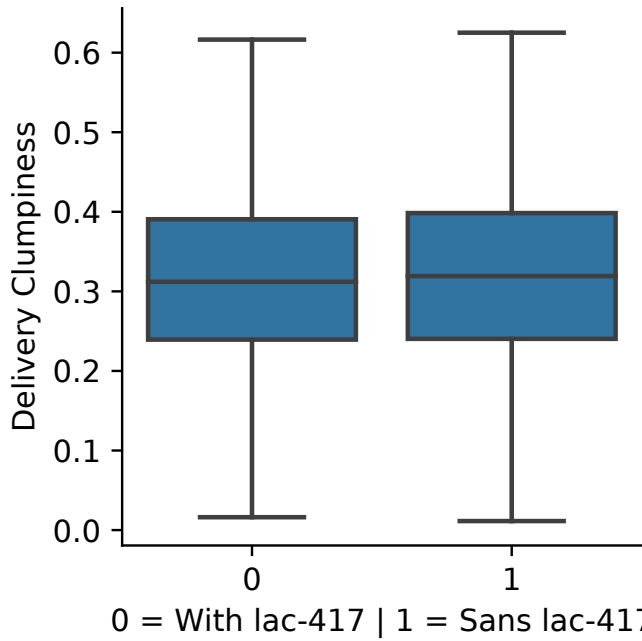
(a) Distribution of Latency Simsteps Outlet for each snapshot, without outliers. (b) Distribution of Latency Simsteps Outlet for each snapshot, with outliers.

Fig. 77: Distribution of Latency Simsteps Outlet for individual snapshot measurements for faulty hardware experiment (Section III-G). Lower is better.



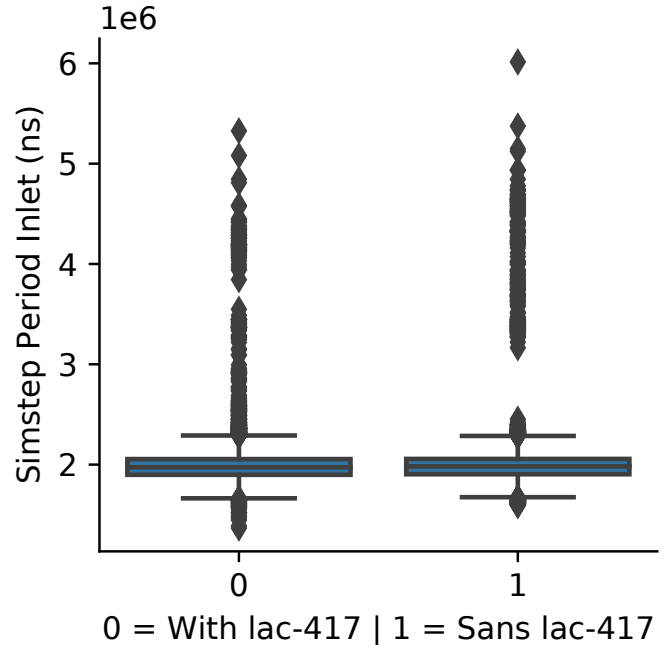
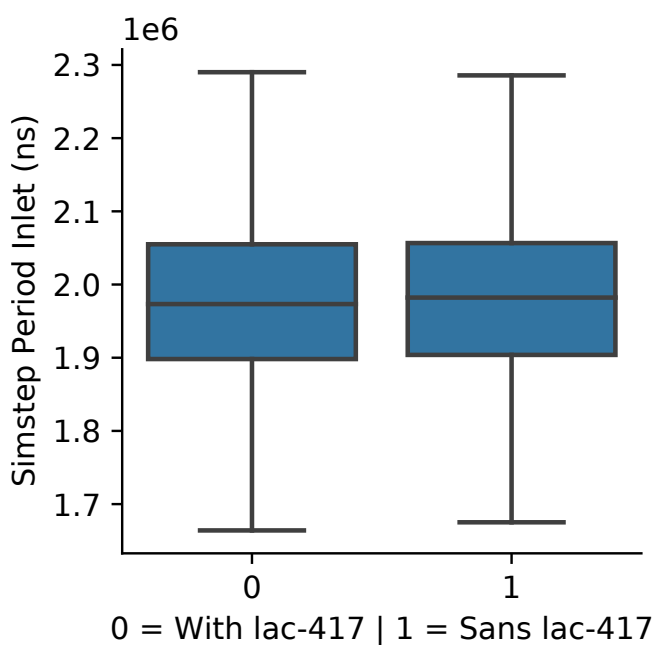
(a) Distribution of Latency Walltime Outlet (ns) for each snapshot, without outliers. (b) Distribution of Latency Walltime Outlet (ns) for each snapshot, with outliers.

Fig. 78: Distribution of Latency Walltime Outlet (ns) for individual snapshot measurements for faulty hardware experiment (Section III-G). Lower is better.



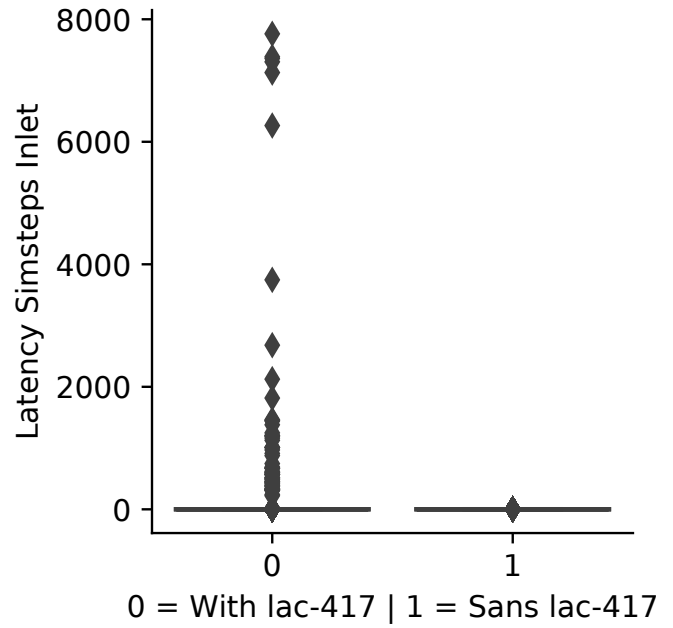
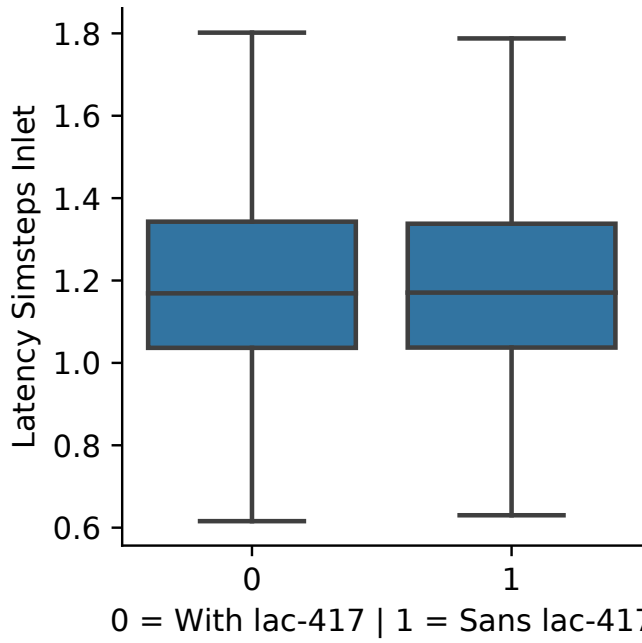
(a) Distribution of Delivery Clumpiness for each snapshot, without outliers. (b) Distribution of Delivery Clumpiness for each snapshot, with outliers.

Fig. 79: Distribution of Delivery Clumpiness for individual snapshot measurements for faulty hardware experiment (Section III-G). Lower is better.



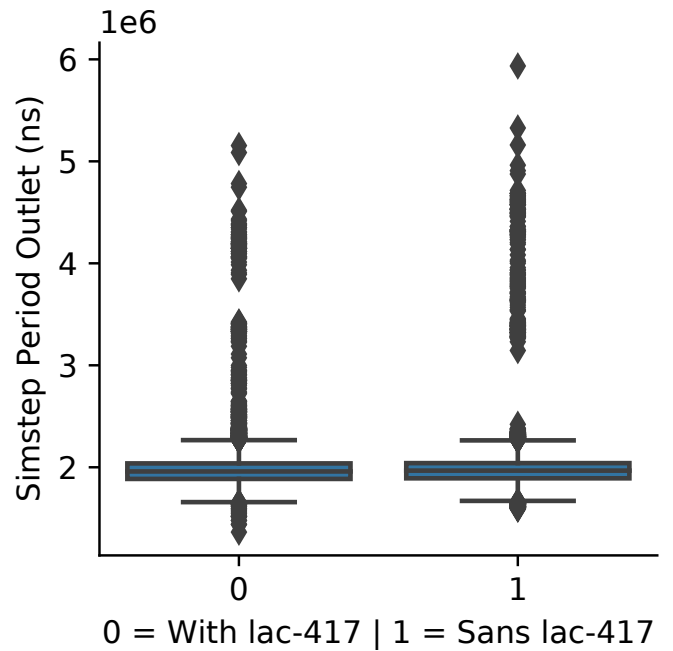
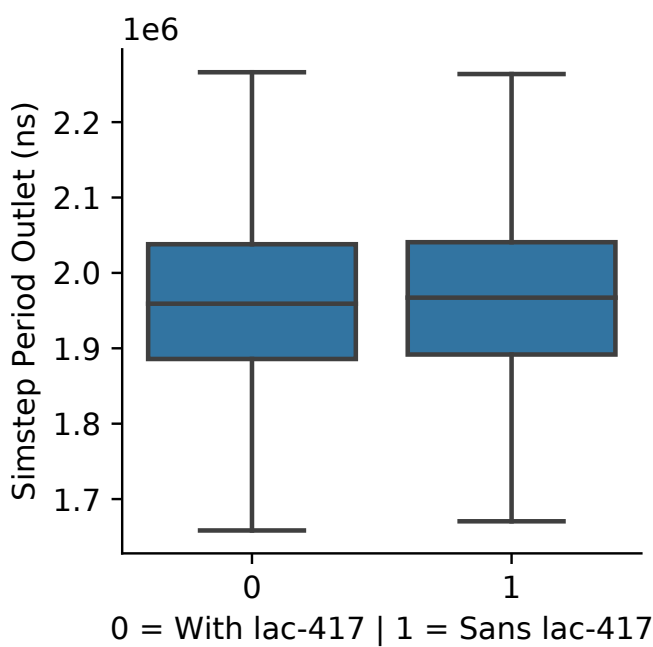
(a) Distribution of Simstep Period Inlet (ns) for each snapshot, without outliers. (b) Distribution of Simstep Period Inlet (ns) for each snapshot, with outliers.

Fig. 80: Distribution of Simstep Period Inlet (ns) for individual snapshot measurements for faulty hardware experiment (Section III-G). Lower is better.



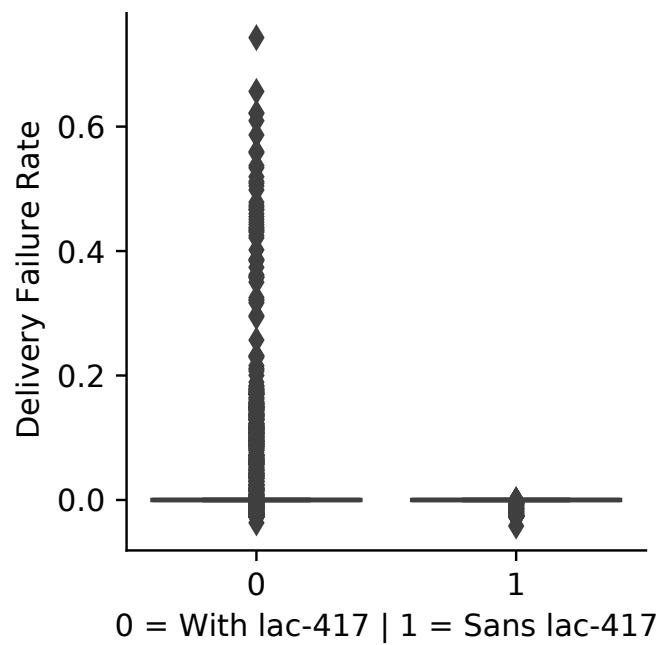
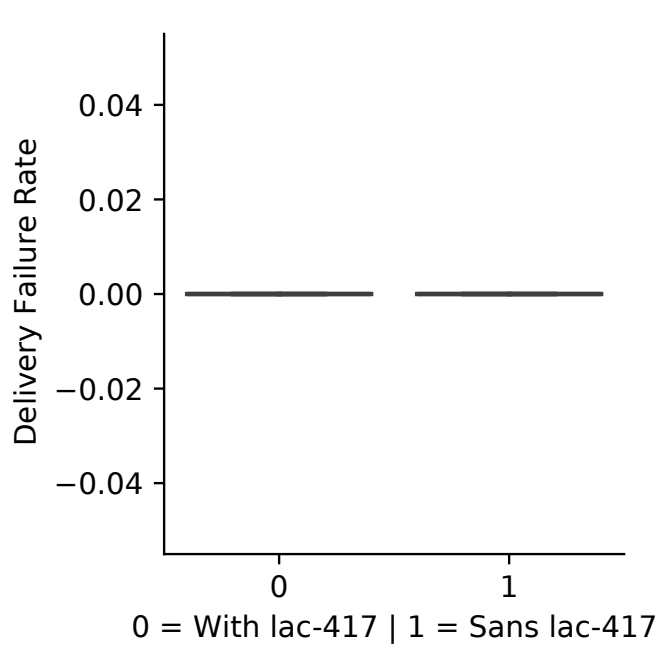
(a) Distribution of Latency Simsteps Inlet for each snapshot, without outliers. (b) Distribution of Latency Simsteps Inlet for each snapshot, with outliers.

Fig. 81: Distribution of Latency Simsteps Inlet for individual snapshot measurements for faulty hardware experiment (Section III-G). Lower is better.



(a) Distribution of Simstep Period Outlet (ns) for each snapshot, without outliers. (b) Distribution of Simstep Period Outlet (ns) for each snapshot, with outliers.

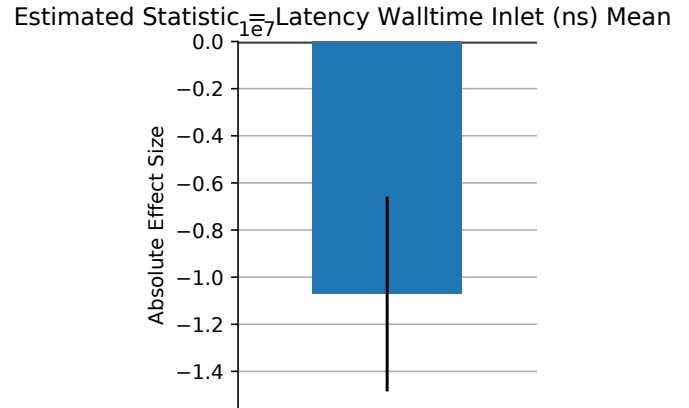
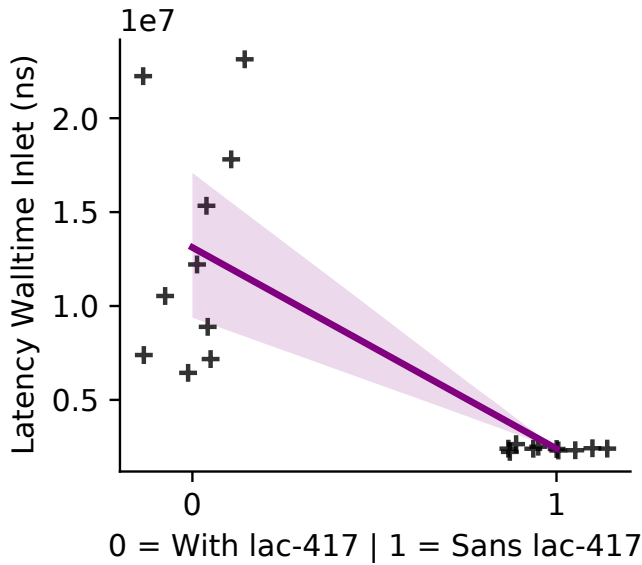
Fig. 82: Distribution of Simstep Period Outlet (ns) for individual snapshot measurements for faulty hardware experiment (Section III-G). Lower is better.



(a) Distribution of Delivery Failure Rate for each snapshot, without outliers. (b) Distribution of Delivery Failure Rate for each snapshot, with outliers.

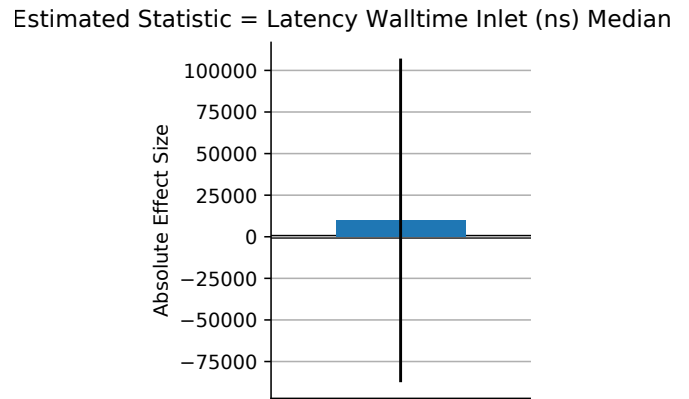
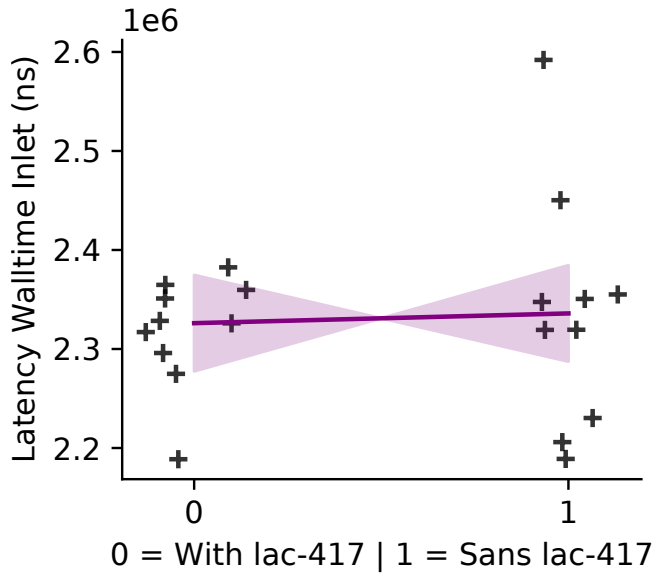
Fig. 83: Distribution of Delivery Failure Rate for individual snapshot measurements for faulty hardware experiment (Section III-G). Lower is better.

## Ordinary Least Squares Regression



(a) Ordinary least squares regression plot. Observations are means per replicate. (b) Estimated regression coefficient for ordinary least squares regression. Zero corresponds to no effect.

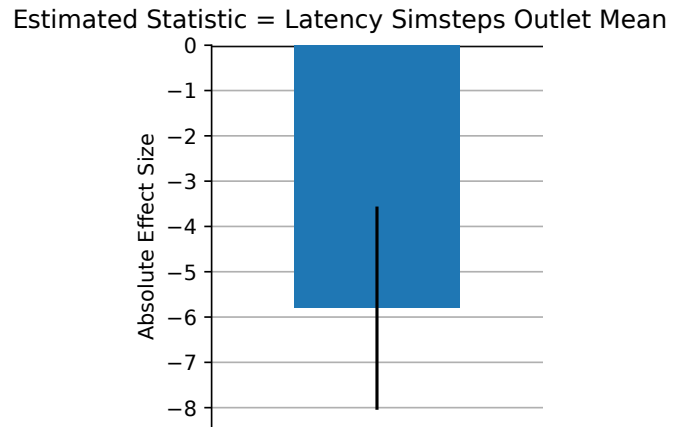
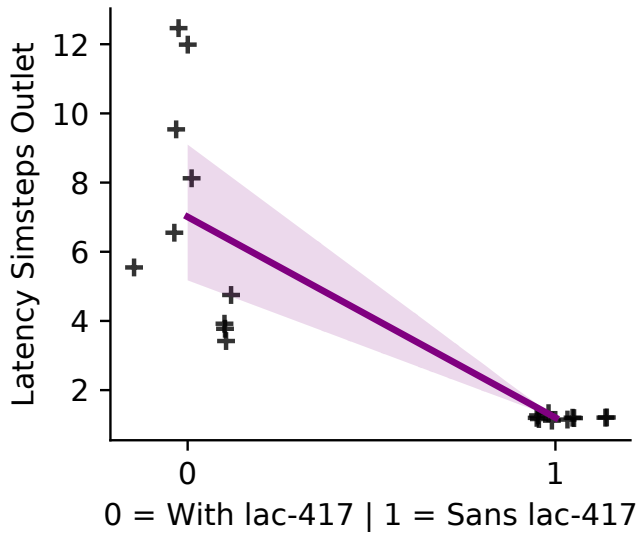
## Quantile Regression



(c) Quantile regression plot. Observations are medians per replicate. (d) Estimated regression coefficient for quantile regression. Zero corresponds to no effect.

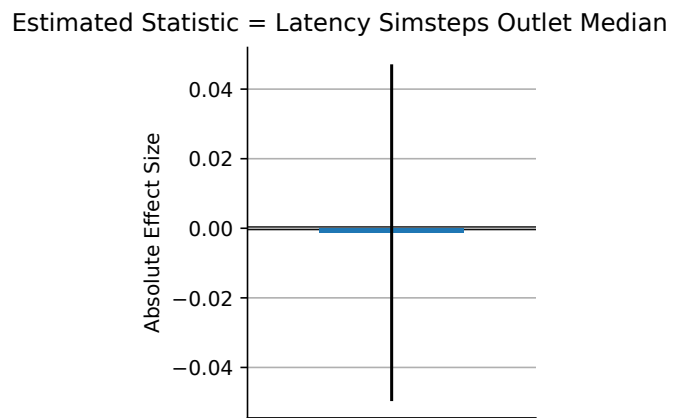
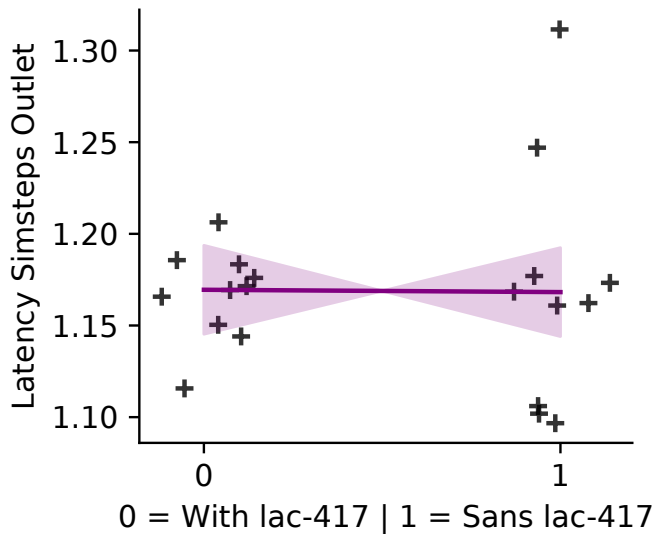
Fig. 84: Regressions of Latency Walltime Inlet (ns) against categorically coded treatment for faulty hardware experiment (Section III-G). Lower is better. Ordinary least squares regression (top row) estimates relationship between categorical independent variable and mean of response variable. Quantile regression (bottom row) estimates relationship between categorical independent variable and median of response variable. Error bands and bars are 95% confidence intervals.

## Ordinary Least Squares Regression



(a) Ordinary least squares regression plot. Observations are means per replicate. (b) Estimated regression coefficient for ordinary least squares regression. Zero corresponds to no effect.

## Quantile Regression

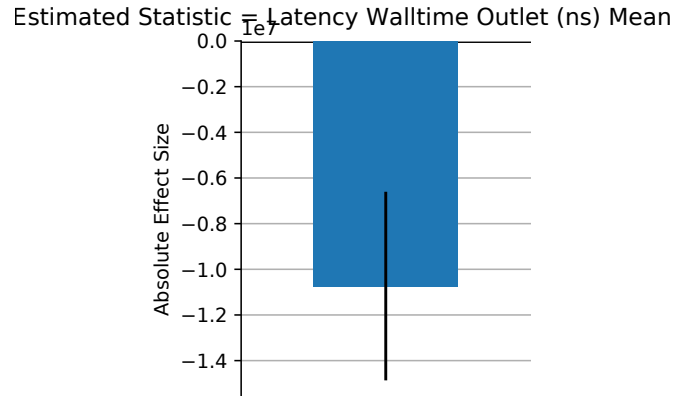
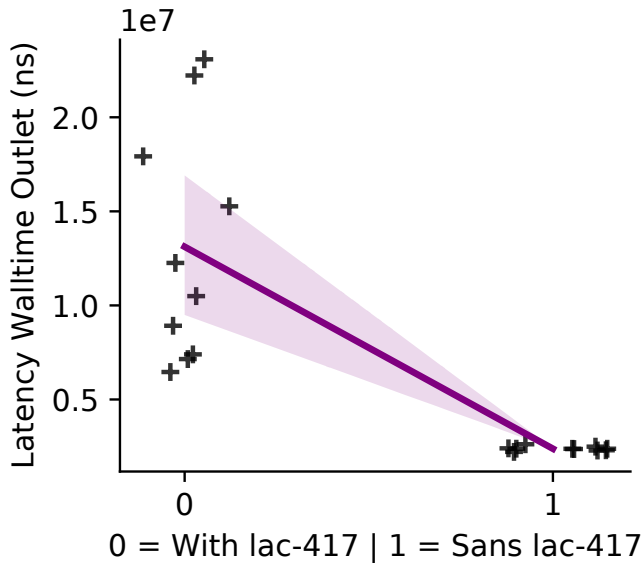


(c) Quantile regression plot. Observations are medians per replicate. (d) Estimated regression coefficient for quantile regression. Zero corresponds to no effect.

Fig. 85: Regressions of Latency Simsteps Outlet against categorically coded treatment for faulty hardware experiment (Section III-G). Lower is better. Ordinary least squares regression (top row) estimates relationship between categorical dependent variable and mean of response variable. Quantile regression (bottom row) estimates relationship between categorical independent variable and median of response variable. Error bands and bars are 95% confidence intervals.

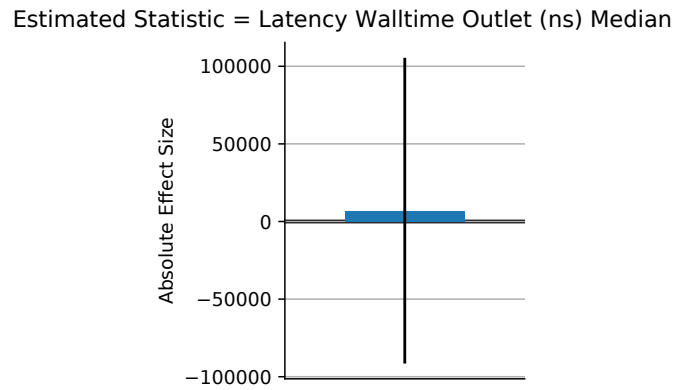
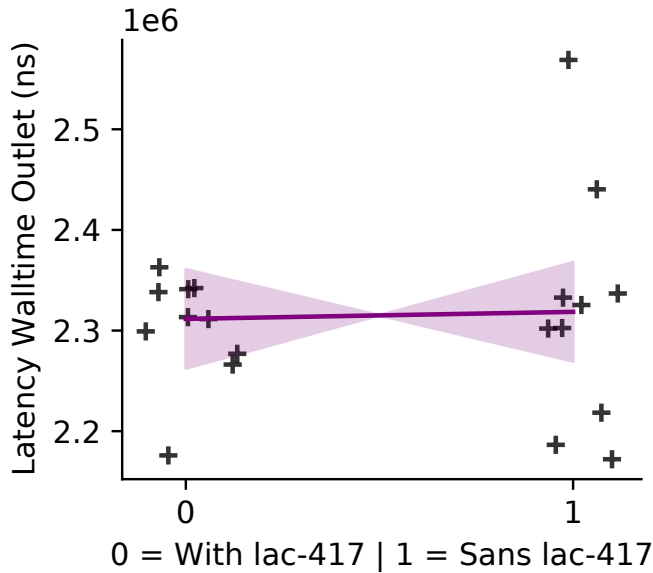


## Ordinary Least Squares Regression



(a) Ordinary least squares regression plot. Observations are means per replicate. (b) Estimated regression coefficient for ordinary least squares regression. Zero corresponds to no effect.

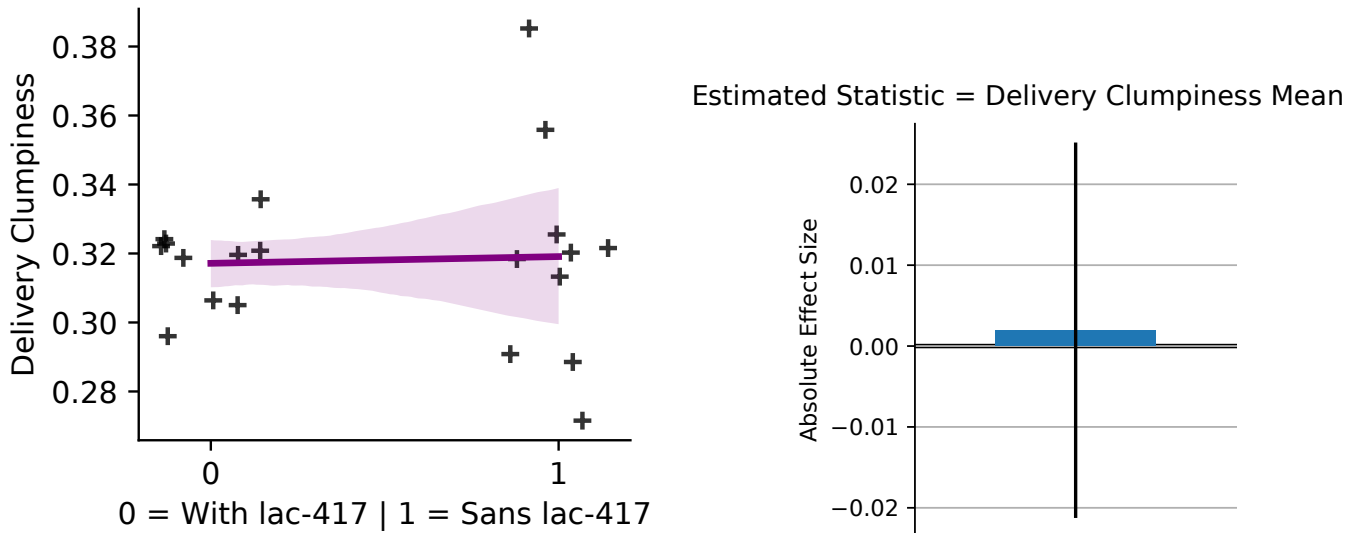
## Quantile Regression



(c) Quantile regression plot. Observations are medians per replicate. responds to no effect. (d) Estimated regression coefficient for quantile regression. Zero corresponds to no effect.

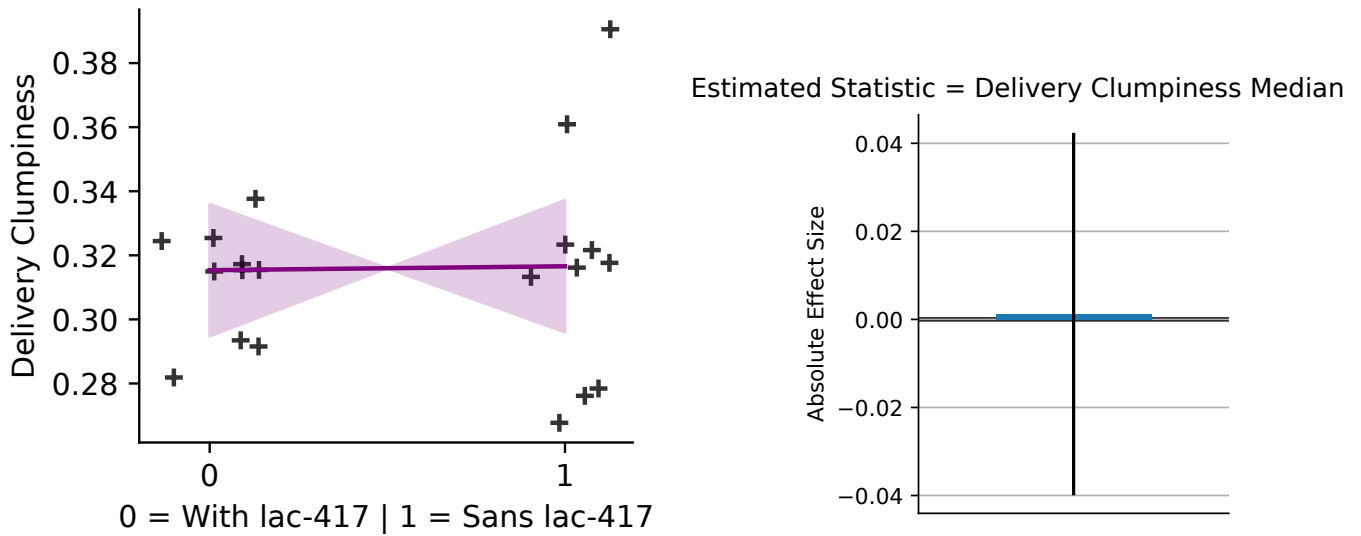
Fig. 86: Regressions of Latency Walltime Outlet (ns) against categorically coded treatment for faulty hardware experiment (Section III-G). Lower is better. Ordinary least squares regression (top row) estimates relationship between categorical dependent variable and mean of response variable. Quantile regression (bottom row) estimates relationship between categorical independent variable and median of response variable. Error bands and bars are 95% confidence intervals.

## Ordinary Least Squares Regression



(a) Ordinary least squares regression plot. Observations are means per replicate. (b) Estimated regression coefficient for ordinary least squares regression. Zero corresponds to no effect.

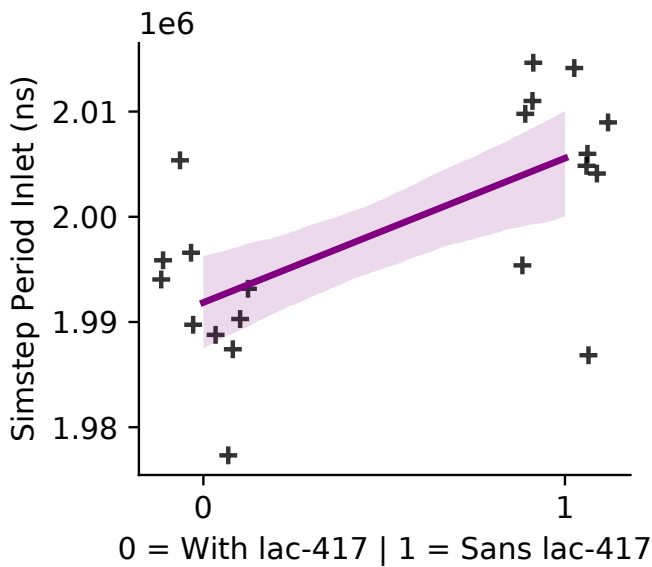
## Quantile Regression



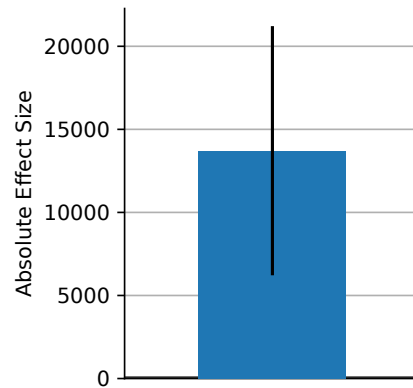
(c) Quantile regression plot. Observations are medians per replicate. (d) Estimated regression coefficient for quantile regression. Zero corresponds to no effect.

Fig. 87: Regressions of Delivery Clumpiness against categorically coded treatment for faulty hardware experiment (Section III-G). Lower is better. Ordinary least squares regression (top row) estimates relationship between categorical dependent variable and mean of response variable. Quantile regression (bottom row) estimates relationship between categorical independent variable and median of response variable. Error bands and bars are 95% confidence intervals.

## Ordinary Least Squares Regression

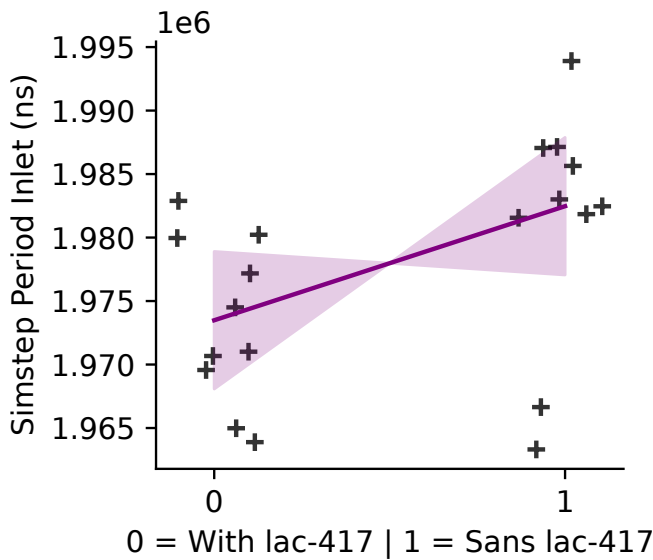


Estimated Statistic = Simstep Period Inlet (ns) Mean

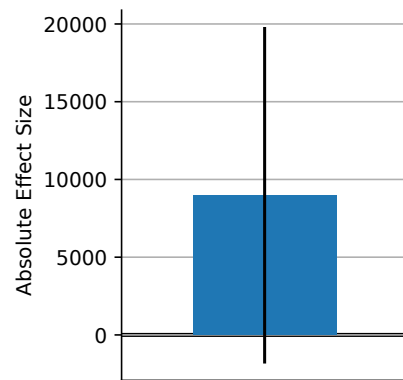


(a) Ordinary least squares regression plot. Observations are means per replicate. (b) Estimated regression coefficient for ordinary least squares regression. Zero corresponds to no effect.

## Quantile Regression



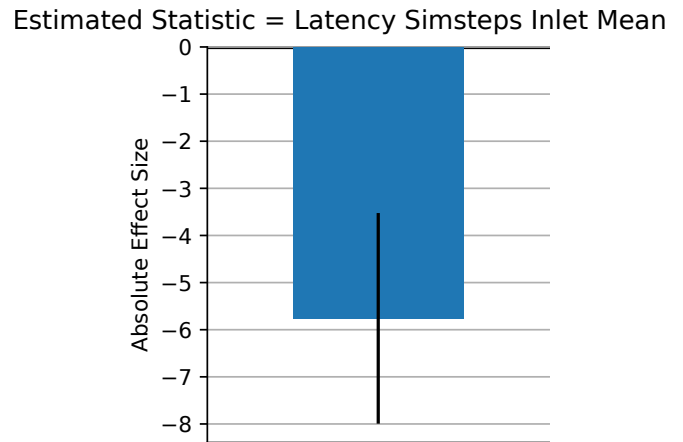
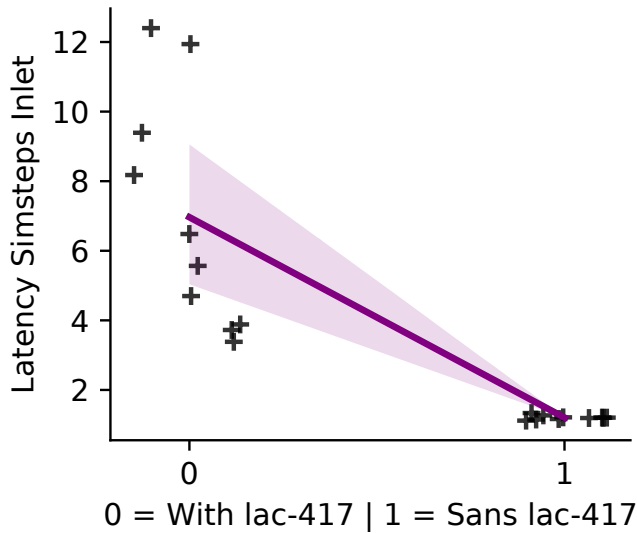
Estimated Statistic = Simstep Period Inlet (ns) Median



(c) Quantile regression plot. Observations are medians per replicate. (d) Estimated regression coefficient for quantile regression. Zero corresponds to no effect.

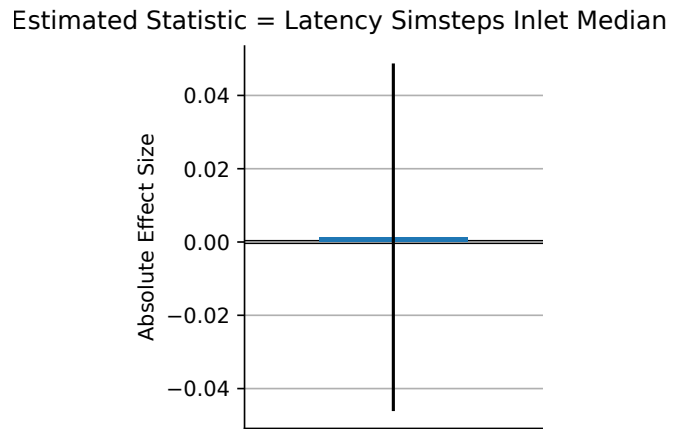
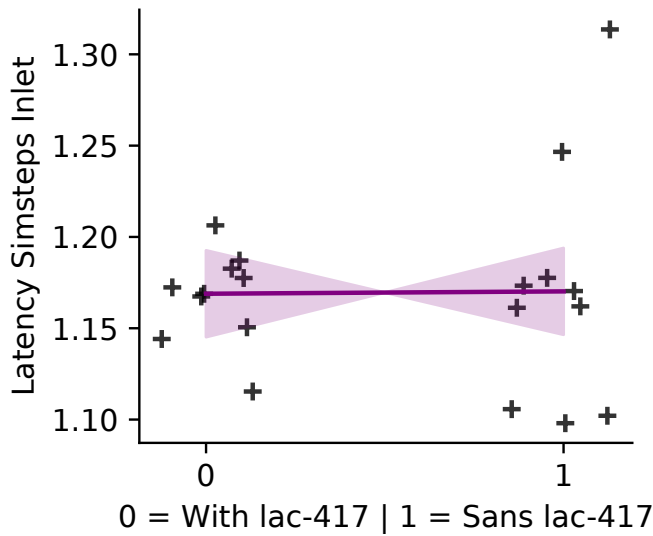
Fig. 88: Regressions of Simstep Period Inlet (ns) against categorically coded treatment for faulty hardware experiment (Section III-G). Lower is better. Ordinary least squares regression (top row) estimates relationship between categorical dependent variable and mean of response variable. Quantile regression (bottom row) estimates relationship between categorical independent variable and median of response variable. Error bands and bars are 95% confidence intervals.

## Ordinary Least Squares Regression



(a) Ordinary least squares regression plot. Observations are means per replicate. (b) Estimated regression coefficient for ordinary least squares regression. Zero corresponds to no effect.

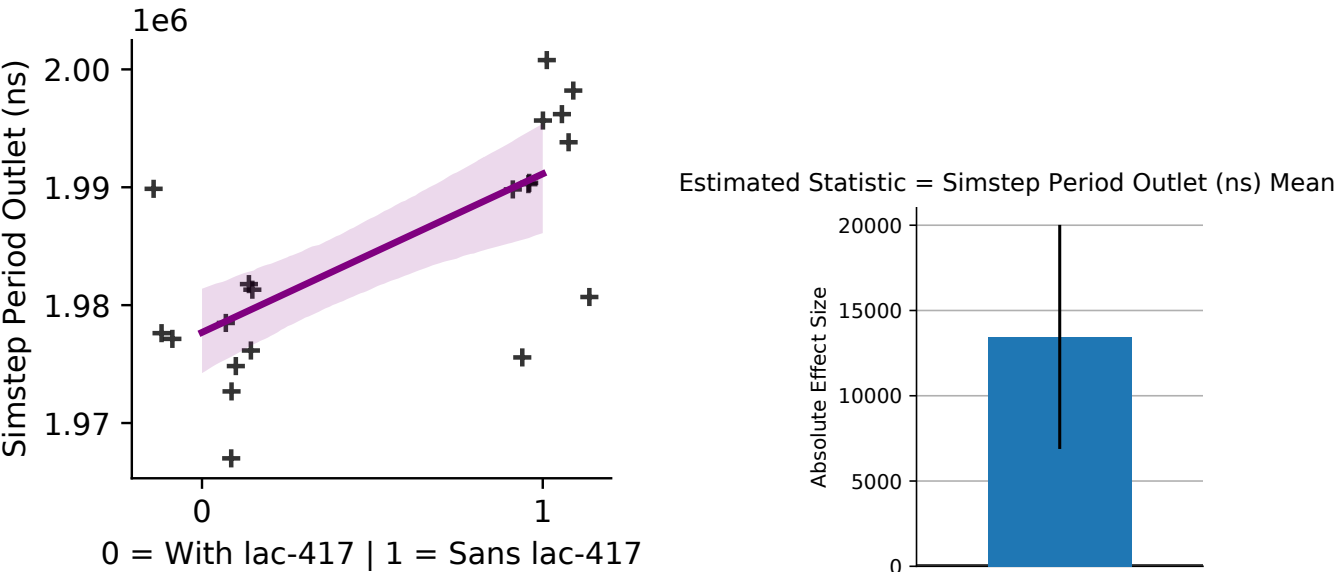
## Quantile Regression



(c) Quantile regression plot. Observations are medians per replicate. (d) Estimated regression coefficient for quantile regression. Zero corresponds to no effect.

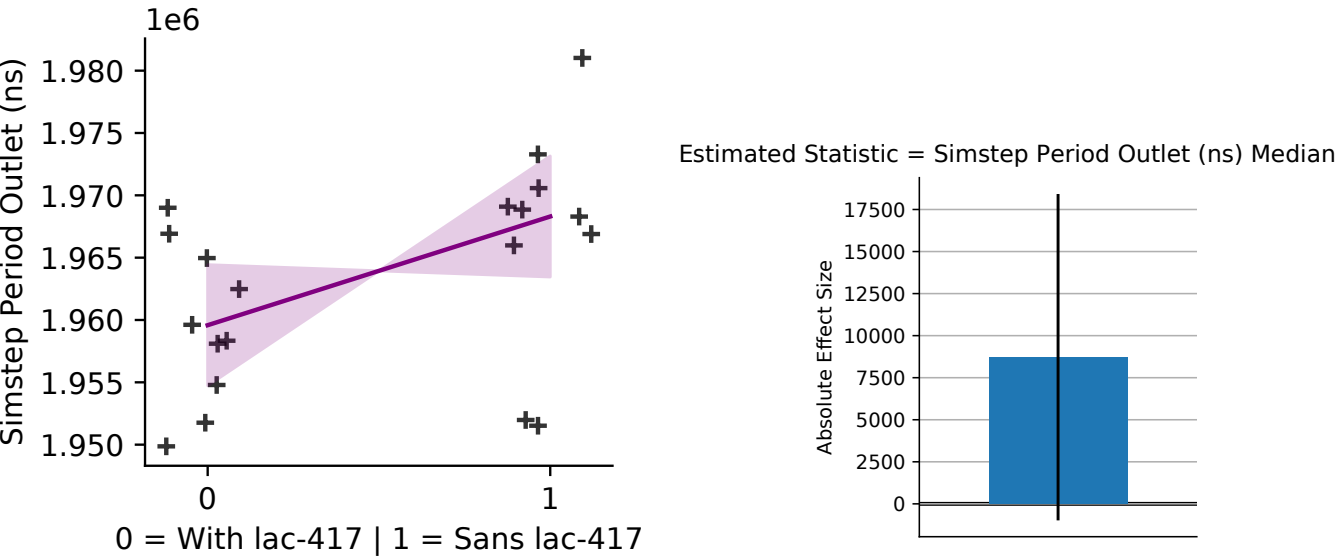
Fig. 89: Regressions of Latency Simsteps Inlet against categorically coded treatment for faulty hardware experiment (Section III-G). Lower is better. Ordinary least squares regression (top row) estimates relationship between categorical dependent variable and mean of response variable. Quantile regression (bottom row) estimates relationship between categorical independent variable and median of response variable. Error bands and bars are 95% confidence intervals.

# Ordinary Least Squares Regression



(a) Ordinary least squares regression plot. Observations are means per replicate. (b) Estimated regression coefficient for ordinary least squares regression. Zero corresponds to no effect.

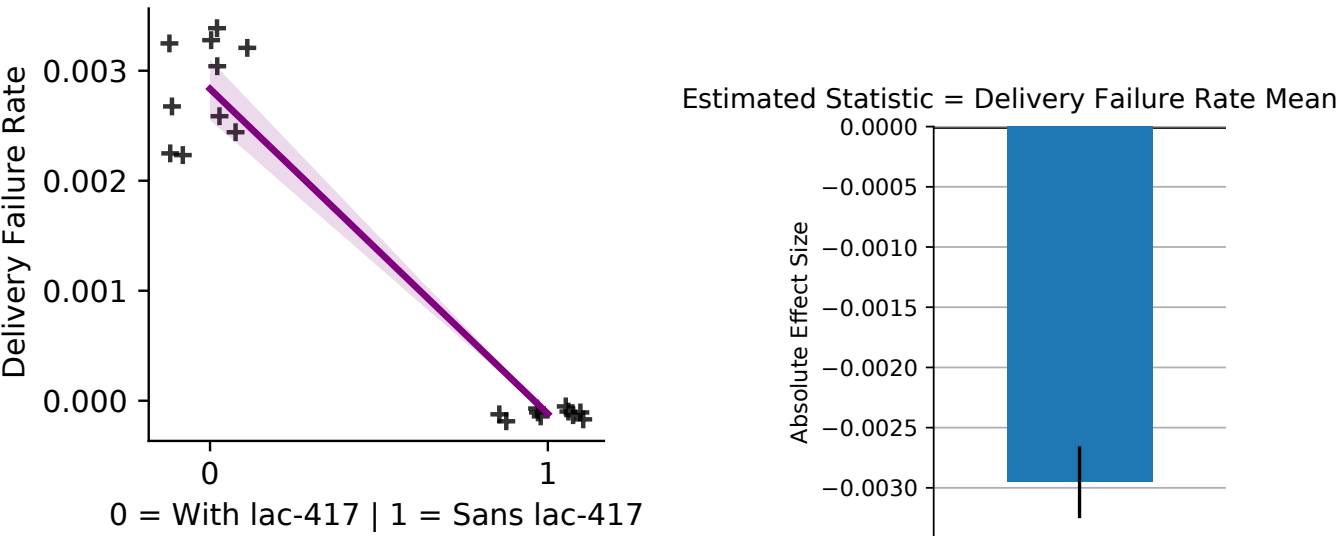
# Quantile Regression



(c) Quantile regression plot. Observations are medians per replicate. (d) Estimated regression coefficient for quantile regression. Zero corresponds to no effect.

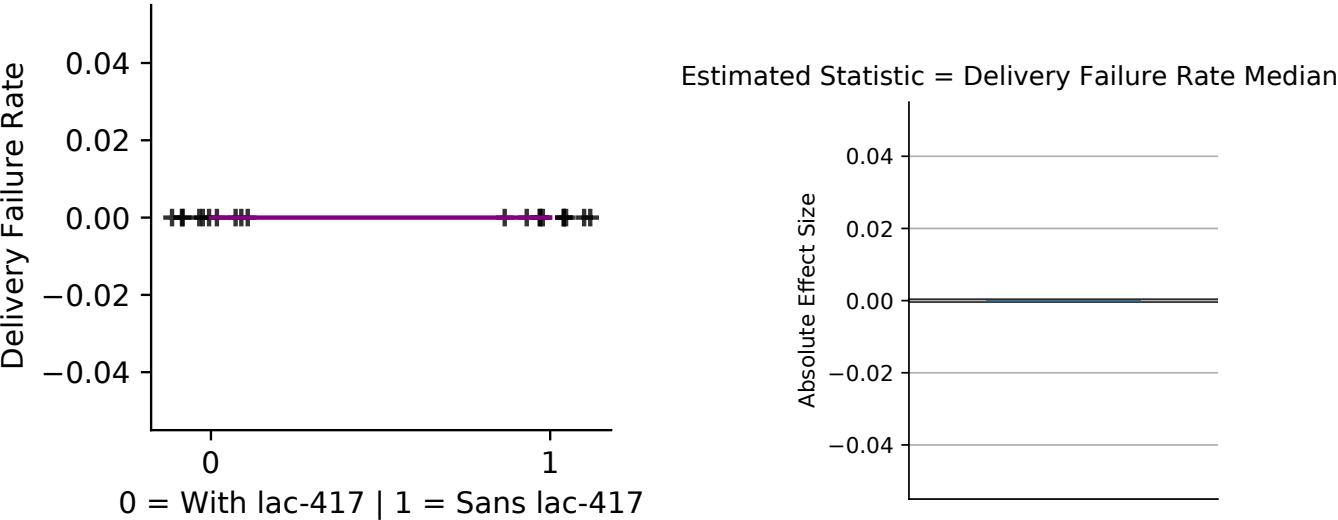
Fig. 90: Regressions of Simstep Period Outlet (ns) against categorically coded treatment for faulty hardware experiment (Section III-G). Lower is better. Ordinary least squares regression (top row) estimates relationship between categorical dependent variable and mean of response variable. Quantile regression (bottom row) estimates relationship between categorical independent variable and median of response variable. Error bands and bars are 95% confidence intervals.

# Ordinary Least Squares Regression



(a) Ordinary least squares regression plot. Observations are means per replicate. (b) Estimated regression coefficient for ordinary least squares regression. Zero corresponds to no effect.

# Quantile Regression



(c) Quantile regression plot. Observations are medians per replicate. (d) Estimated regression coefficient for quantile regression. Zero corresponds to no effect.

Fig. 91: Regressions of Delivery Failure Rate against categorically coded treatment for faulty hardware experiment (Section III-G). Lower is better. Ordinary least squares regression (top row) estimates relationship between categorical dependent variable and mean of response variable. Quantile regression (bottom row) estimates relationship between categorical independent variable and median of response variable. Error bands and bars are 95% confidence intervals.

TABLE XXIV: Full Ordinary Least Squares Regression results of quality of service metrics against categorically coded treatment for faulty hardware experiment (Section III-G). Significance level  $p < 0.05$  used. Inf or NaN values may occur due to multicollinearity or due to inf or NaN observations.

Metric	Statistic	Significant	Effect Sign	Cpus Per Node	Num Sineels Per Cpu	Num Processes	Absolute Effect Size	Absolute Effect Size 95% CI		Relative Effect Size	Relative Effect Size 95% CI		n	p
								Lower Bound	Upper Bound		Lower Bound	Upper Bound		
Latency Walltime Inlet (ns)	mean	-	1	2048	256	-1.1e+07	-1.5e+07	-6.6e+06	-0.82	-1.1	-0.5	20	3.6e-05	
Latency Walltime Outlet (ns)	mean	-	1	2048	256	-1.1e+07	-1.5e+07	-6.6e+06	-0.82	-1.1	-0.5	20	3.5e-05	
Latency Simsteps Inlet	mean	-	1	2048	256	-5.8	-8	-3.5	-0.83	-1.1	-0.51	20	3.8e-05	
Latency Simsteps Outlet	mean	-	1	2048	256	-5.8	-8	-3.6	-0.83	-1.1	-0.51	20	3.6e-05	
Delivery Failure Rate	mean	-	1	2048	256	-0.003	-0.0033	-0.0027	-1	-1.1	-0.94	20	4.9e-14	
Delivery Clumpiness	mean	0	1	2048	256	0.002	-0.021	0.025	0.0062	-0.067	0.079	20	0.86	
Simstep Period Inlet (ns)	mean	+	1	2048	256	14000	6200	21000	0.0069	0.0031	0.011	20	0.0012	
Simstep Period Outlet (ns)	mean	+	1	2048	256	13000	6900	20000	0.0068	0.0035	0.01	20	0.00043	

TABLE XXV: Full Quantile Regression results of quality of service metrics against categorically coded treatment for faulty hardware experiment (Section III-G). Significance level  $p < 0.05$  used. Inf or NaN values may occur due to multicollinearity or due to inf or NaN observations.

Metric	Statistic	Significant Effect Sign	Cpus Per Node	Num Simeks Per Cpu	Num Processes	Absolute Effect Size	Absolute Effect Size 95% CI Lower Bound	Absolute Effect Size 95% CI Upper Bound	Relative Effect Size	Relative Effect Size 95% CI Lower Bound	Relative Effect Size 95% CI Upper Bound	n	p
Latency Walltime Inlet (ns)	median	0	1	2048	256	9 800	-87 000	110 000	0.0042	-0.038	0.046	20	0.83
Latency Walltime Outlet (ns)	median	0	1	2048	256	7 000	-91 000	110 000	0.003	-0.04	0.046	20	0.88
Latency Simsteps Inlet	median	0	1	2048	256	0.0013	-0.046	0.049	0.0011	-0.039	0.042	20	0.95
Latency Simsteps Outlet	median	0	1	2048	256	-0.0013	-0.05	0.047	-0.0011	-0.042	0.04	20	0.96
Delivery Failure Rate	median	NaN	1	2048	256	0	nan	nan	nan	nan	nan	20	nan
Delivery Clumpiness	median	0	1	2048	256	0.0012	-0.04	0.042	0.0039	-0.13	0.13	20	0.95
Simstep Period Inlet (ns)	median	0	1	2048	256	9 000	-1 800	20 000	0.0046	-0.00093	0.01	20	0.098
Simstep Period Outlet (ns)	median	0	1	2048	256	8 700	-980	18 000	0.0045	-0.0005	0.0094	20	0.075